eISBN: 978-1-60805-739-9
ISBN: 978-1-60805-740-5

Towards a Unified Soil Mechanics Theory

The Use of Effective Stresses in Unsaturated Soils

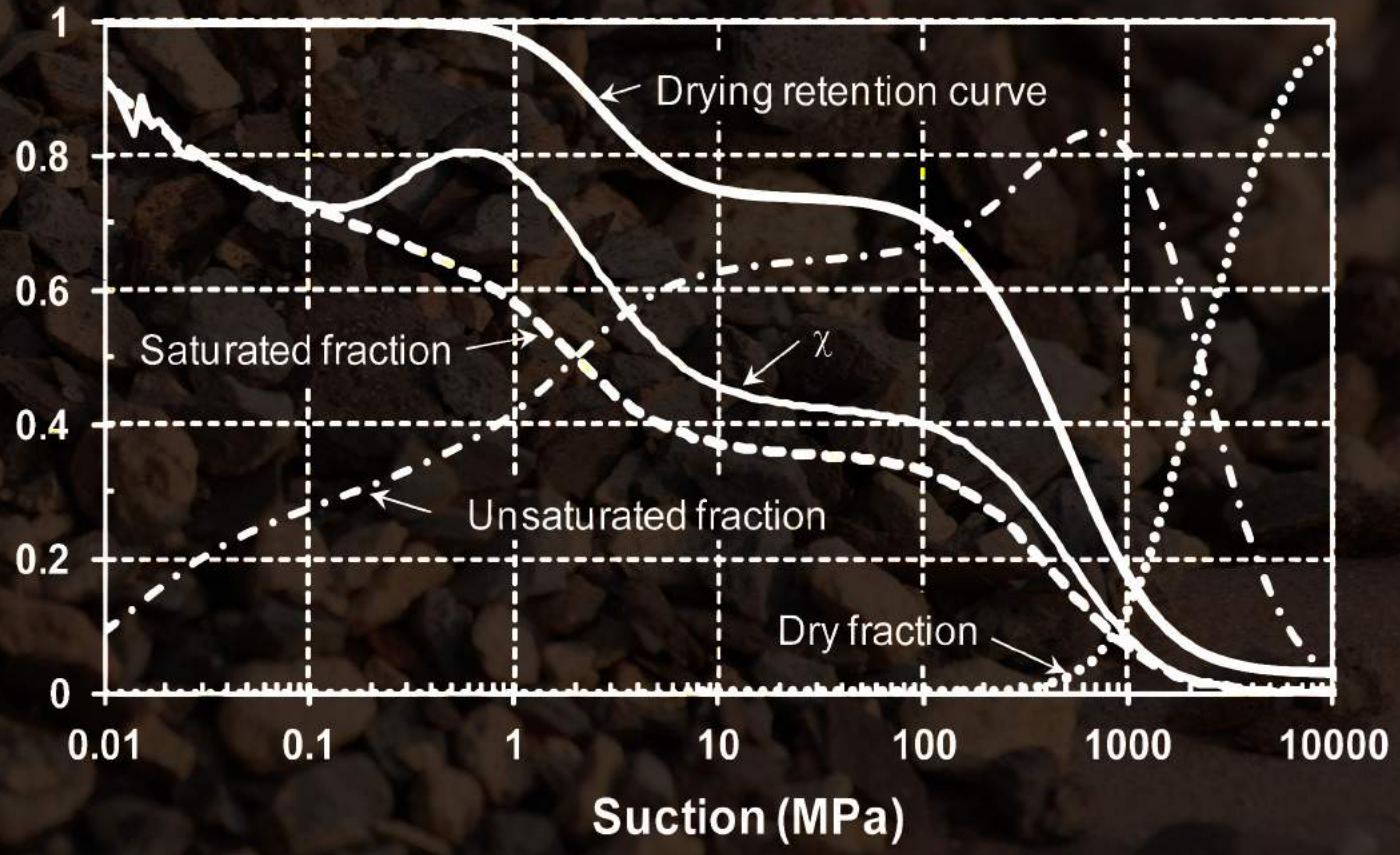

Eduardo Rojas

Bentham e Books

Towards a Unified Soil Mechanics Theory:
The Use of Effective Stresses in Unsaturated Soils

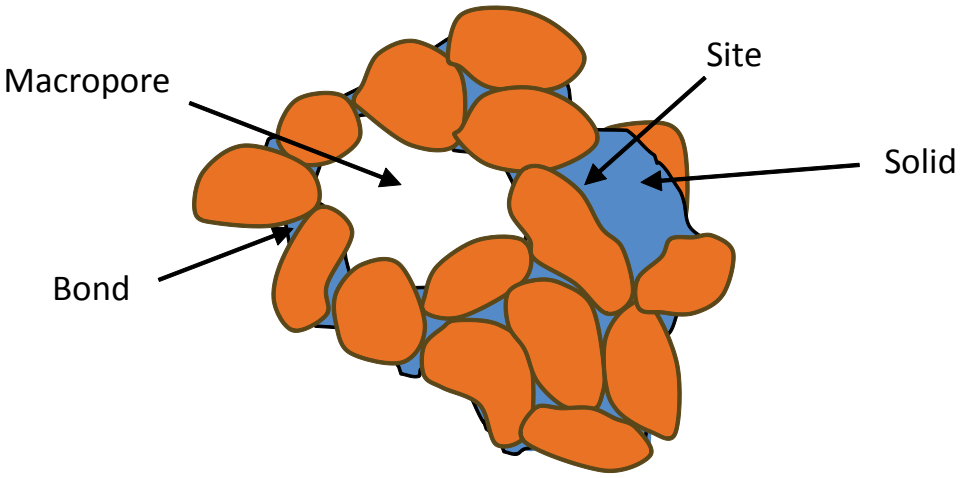

Authored By

Eduardo Rojas

Universidad Autónoma de Querétaro
México

DEDICATION

To Silvia, my loving wife, and to my son and daughter:
Carlos Javier and Sonia Itzel, who have showed me the
pleasure of shearing and enjoy each other.

CONTENTS

BIOGRAPHY

Eduardo Rojas graduated as Civil Engineer at the National Center of Technical and Industrial Education (CeNETI) in Mexico in 1980. He obtained his Master and PhD degrees in Soil Mechanics at the Institut de Mécanique de Grenoble (IMG), France, in 1981 and 1984, respectively.

He was associate researcher at the Institute of Engineering (II) in the Universidad Nacional Autónoma de México (UNAM) from 1984 to 1996 and chairman of the Department of Soil Mechanics in the Postgraduate Division of the Faculty of Engineering, UNAM, from 1993 to 1996. He has been research-professor at the Universidad Autónoma de Querétaro (UAQ) since 1996 where he teaches the courses of Geotechnical Engineering at undergraduate level and Unsaturated Soil Mechanics at postgraduate level. He was chairman of the Physics and Mathematics Research Center of the UAQ from 1998-2004. He has been granted twice the Alejandrina award in Science and Technology for the years 2002 and 2004. He is currently member of the National Research System (SNI). In combination with his academic activity at the university, he works as consultant engineer and has participated in different engineering projects covering several topics from the underpinning of tilted buildings, the analysis of the stability of slopes during heavy rain, to the design of deep and shallow foundation on different types of soils including expansive, collapsing, dispersive and highly compressive materials. He has published 9 books, 7 chapters of book, 32 papers in national and international Journals and 75 papers in national and international congresses.

FOREWORD

The choice of stress variables controlling the behavior of unsaturated soils has been a challenge for geotechnical engineers for more than half a century and in particular in the last two decades. Many researchers in the world are still working on this aspect and Professor Eduardo Rojas is one of them. There are two main approaches: the first one considers two stress variables, generally the net stress ($\sigma - u_a$) and matric suction ($u_a - u_w$); the other considers a single stress variable, generally called the effective stress. However, this latter approach generally shows deficiencies in reproducing the phenomenon of collapse under wetting.

In several technical papers and in this eBook, Professor Rojas has developed a porous-solid model that considers micropores, macropores and their connections, and the fact that they can be saturated, unsaturated or dry. This model is very powerful and allows the determination of the Soil-Water Retention Curves on both the drying and the wetting paths. This model is also the key for the determination of an equivalent effective stress that allows the analysis of the different aspects of the mechanical behavior of unsaturated soils: compression strength, tensional strength and volumetric behavior. Application of the model to experimental results published in the literature gives remarkable results.

Was it necessary to put all this information into one eBook? The answer is yes as it shows in one document the continuity from the physical model and the definition of an equivalent effective stress to their practical applications. Did the eBook provide a final response to the questions concerning representative stress variables for unsaturated soils? Probably not, but it gives a very consistent approach of the problem within the context of the existing literature and knowledge. It is a reference for all those interested to the behavior of unsaturated soils.

Professor Serge Leroueil
Laval University
Quebec
Canada

PREFACE

With the introduction of the effective stress concept, the behavior of saturated soils could be clearly understood and the basic principles of the saturated soil mechanics could be established. The effective stress principle states that the strength and volumetric behavior of saturated materials are exclusively controlled by effective stresses. Constitutive models for saturated materials of different types are all based on the effective stress principle. Later the Critical State theory combined the strength and volumetric behavior of saturated soils in a simple and powerful constitutive model. A great number of models for saturated soils are based on the critical state theory.

Things went not so smooth for unsaturated materials. More than fifty years ago Alan W. Bishop proposed an equation for the effective stresses of unsaturated soils. However, this equation was severely criticized because it could not explain by itself the phenomenon of collapse upon wetting of soils. In addition Bishop's effective stress parameter χ showed to be extremely elusive and difficult to be determined experimentally. Given these difficulties the use of the so called independent stress variables (mainly net stress and suction) became common in unsaturated soil mechanics. Different equations for the strength and volumetric behavior of soils were proposed and the theory for unsaturated soils became distant from that of saturated materials. The Barcelona Basic Model represents one of the most simple and completes models within this trend. The Barcelona Basic Model enhanced the Critical State theory to include unsaturated materials and give a plausible explanation to the phenomenon of collapse upon wetting. This model proved that this phenomenon could only be modeled if in addition to a volumetric equation, a proper elastoplastic framework was included. But then, the simulation of some particular phenomena related to the strength and volumetric behavior of unsaturated soils, appeal for the inclusion of the hysteresis of the soil-water retention curve and the hydro-mechanical coupling observed in unsaturated materials. The difficulties met in introducing these aspects into the independent stress variables models made it clear that a different approach should be considered. Then, quietly elastoplastic models based on Bishop's effective stress equation started to appear showing its superiority by including the hysteresis of

the soil-water retention curve and the hydromechanical coupling of unsaturated soils. And finally, the debate about the appropriateness of Bishop's equation to represent the effective stresses for unsaturated soils is slowly coming to an end. This transformation on the construction of constitutive models for unsaturated soils is also leading towards a unified soil mechanics theory.

This eBook shows how the effective stress principle can be applied to simulate the strength and volumetric behavior of unsaturated soils employing the same equations commonly used for saturated materials. The eBook initiates with an analysis of the stresses transmitted to the different phases of an unsaturated soil when it is loaded. This analysis results in an expression for the stresses carried by the solid skeleton of the material. This expression can be written in the same terms as Bishop´s effective stress equation and leads to an analytical expression for Bishop's effective stress parameter χ. However, the variables required to obtain χ cannot be experimentally determined. For that purpose, a network porous-solid model is developed able to approximately reproduce the structure of soils based on the grain and pore size distributions of the material. This porous-solid model is able to determine the allocation of water in the pores of the soil and thus simulate the soil-water retention curves of the material including the scanning curves. It is also possible to obtain the required parameters to determine the value of Bishop's parameter χ and therefore compute the current effective stress. Nevertheless, the use of a network solid-porous model requires large memory storage capacity that cannot be presently found in common computers and thus the solid-porous model computer program becomes very slow. For that reason, a probabilistic solid-porous model is developed that reduces the storage requirements and speeds the simulations. Finally an elastoplastic framework is developed to account for the volumetric behavior of unsaturated soils including compacted materials. This framework allows the simulation of the collapse upon wetting phenomenon and explains some other phenomena that could not be explained using the independent stress variables approach. All these developments lead to a general framework for the strength and volumetric behavior of soils including saturated, unsaturated and compacted materials. In that sense, a unified soil mechanics theory is presently on its way.

ACKNOWLEDGEMENTS

All graphic material contained in this eBook was carefully prepared by María de la Luz Pérez-Rea and Hiram Arroyo Contreras, Researcher and PhD student at the School of Engineering of the University of Querétaro, Mexico, respectively. Their help is greatly appreciated.

CONFLICT OF INTEREST

The author(s) confirm that the eBook content has no conflict of interest.

Eduardo Rojas
University of Queretaro
Mexico
E-mail: erg@uaq.mx

List of Abreviations

BBM	=	Barcelona Basic Model
GSD	=	Grain Size Distribution
LCYS	=	Loading Collapse Yield Surface
MIP	=	Mercury Intrusion Porosimetry Tests
PSD	=	Pore Size Distribution
SDYS	=	Suction Decrease Yield Surface
SEM	=	Scanning Electron Micrographs
SIYS	=	Suction Increase Yield Surface
SWRC	=	Soil Water Retention Curve
VCL	=	Virgin Consolidation Line
WP	=	Wetting Path
2D	=	Bi-Dimensional
3D	=	Three-Dimensional

Send Orders of Reprints at reprints@benthamscience.net
Towards a Unified Soil Mechanics Theory, **2013, 3-11**

CHAPTER 1

Introduction

Abstract: The use of the effective stress principle led to a general theory for the strength and volumetric behavior of saturated soils. Presently, all constitutive models for saturated soils are based on this principle. In 1959 Bishop proposed an equation for the effective stress of unsaturated soils. However, it was severely criticized because it could not explain by itself the phenomenon of collapse upon wetting. Moreover, an analytical expression for the determination of its main parameter χ was not provided and in addition, its value could not be easily determined in the laboratory. Since then several equations to determine the value of parameter χ have been proposed and fifty years later it is acknowledge that Bishop's effective stress equation can be employed to simulate the behavior of unsaturated soils when it is complemented with a proper elastoplastic framework.

Keywords: Saturated soil, unsaturated soil, effective stress, total stress, pore water pressure, air pressure, suction, constitutive model, volumetric behavior, shear strength, collapse, elastoplastic framework, state surface, independent stress variables, effective stress parameter.

1.1. DIFFERENT APPROACHES FOR UNSATURATED SOILS

Even though the idea of using effective stresses in the study of unsaturated materials is old, the incapacity to provide an explanation to the phenomenon of collapse upon wetting (among other reasons) made this approach to be abandoned for about forty years. During that time some other approaches to study the behavior of unsaturated soils were used. The state or constitutive surfaces [1], as the one represented in Fig. **1**, were used for some time. In these plots, the behavior of a certain state variable, as for example the void ratio, is plotted as a function of two independent stress variables mainly the mean net stress ($\bar{p} = p - u_a$) and suction ($s = u_a - u_w$), where p represents the total mean stress and u_a and u_w represent the air and water pressures, respectively. This procedure aimed to establish general mathematical relationships between the void ratio or the degree of saturation with the independent stress variables as Hung, Fredlund and Pereira [2] have done. This method represented to some researchers the acceptance of the inexistence of an effective stress equation for unsaturated materials (see for example [3]). However, state surfaces soon showed their limitations. For example, unicity could only be ensured

Eduardo Rojas

under certain conditions especially because of the hysteresis of the Soil-Water Retention Curve (SWRC) and could not explain complex stress-path dependency. In any case, this task would have been formidable complex because the behavior of unsaturated materials depends not only on the mean net stress and suction but also on the degree of saturation and the structure of soils. Recently Zhang and Lytton [4] proposed a modified state-surface approach under isotropic stress conditions that can be applied to the study of the volumetric behavior of unsaturated soils including collapsing and expansive soils.

Sometime later the independent stress variables approach was employed to study the behavior of unsaturated soils. The independent stress state variables were defined as those stresses controlling the strength and volumetric behavior of soils. By performing the analysis of the equilibrium of an elemental volume of unsaturated soil, Fredlund and Morgenstern [5] proved that the use of two out of three possible combinations of the stress variables represented by the total stress (σ), the air pressure and the water pressure, were sufficient to completely define the state of stresses of an unsaturated sample. The three possible combinations are: $(\sigma - u_w)$ with $(u_a - u_w)$; $(\sigma - u_a)$ with $(\sigma - u_w)$; and $(\sigma - u_a)$ with $(u_a - u_w)$. Being the last combination, net stress $(\bar{\sigma} = \sigma - u_a)$ and suction, the most employed to study the behavior of unsaturated soils.

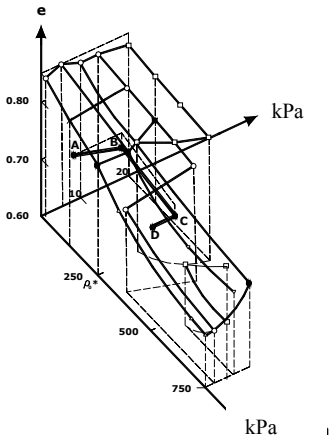

Figure 1: State surface for the void ratio (after Matyas and Radhakrishna [1]).

This theoretical analysis co-validated the experimental observations made by Bishop and Donald [6] in 1961. These researchers performed a series of triaxial tests where the confining stress (σ_3), the air and the water pressures were all independently controlled during the loading of the sample. In this way the values of the net confining stress $(\sigma_3 - u_a)$ and suction could be maintained constant throughout the test while the independent pressures could change. These results showed that the independent variations of σ_3, u_a and u_w had no effect on the stress-strain curve whenever the confining net stress and suction remained constant. However, a variation on these values resulted in marked changes in the stress-strain curve of the sample.

With the use of the independent stress variables, the representation of the failure surface for unsaturated soils required, additional to the normal net stress $(\sigma_n - u_a)$ and the shear stress (τ) axes, the inclusion of the suction axis as indicated in Fig. **2**. This figure shows the failure lines for a saturated material (indicated by the friction angle φ) and for an unsaturated one (indicated by the friction angle φ_s) where for the later, the cohesion (c) appears as a strength parameter.

Following this tendency, Alonso, Gens and Josa [7] proposed a constitutive model for unsaturated soils based on the Modified Critical State Model developed by Roscoe and Burland [8]. This model, known as the Barcelona Basic Model (BBM), is one of the most simple and complete models to simulate the behavior of unsaturated soils including collapsing and expansive soils. One of the main contributions attributed to the BBM is that it clearly explains the phenomenon of collapse upon wetting by introducing the Loading Collapse Yield Surface (LCYS) as illustrated in Fig. **3**. This phenomenon occurs when a saturated sample is dried (path AB in Fig. **3**), then loaded by increasing the net stress (path BC) and finally wetted up to saturation (path CD).

This behavior can be explained in the following terms: when a soil dries, it stiffens because additional contact stresses between solids particles develop and the soil behaves as a preconsolidated material. Therefore, when the sample is loaded by increasing the net stress, it slightly deforms. Subsequently, when the soil wets, the stiffness of the material vanishes as the additional contact stresses between solid particles disappears and at this stage, the volumetric deformation

that did not occur during the loading stage when the soil was dry, takes place suddenly during the wetting of the sample. This means that the sample returns to the saturated compression line of the material. The inability of Bishop's equation to explain this behavior was one of the major reasons for its abandon during several decades.

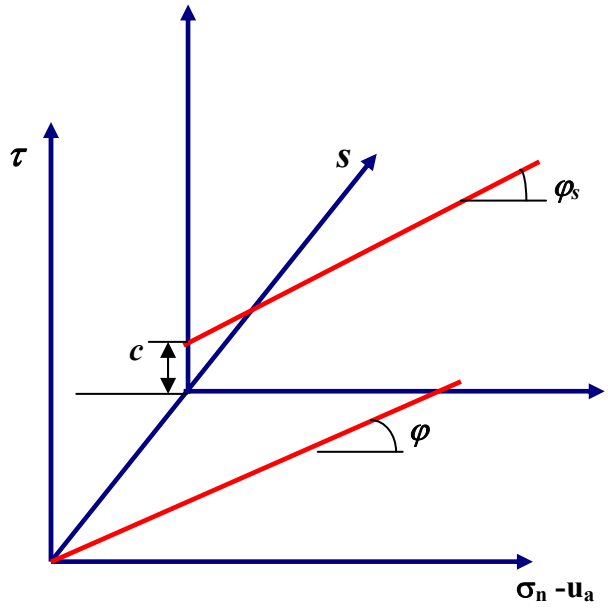

Figure 2: Failure lines for the saturated and unsaturated conditions.

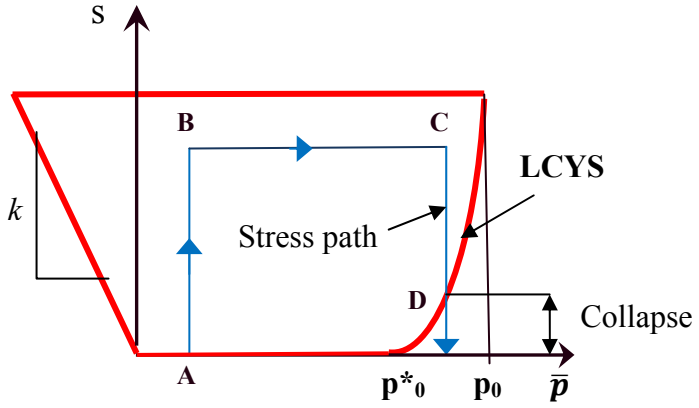

Figure 3: Simulation of the phenomenon of collapse upon wetting by the inclusion of the LCYS (after Alonso, Gens and Josa [7]).

1.2. EFFECTIVE STRESS

In 1936 Terzaghi [9] stated the principle of effective stress for saturated soils leading to the equation:

$$\sigma' = \sigma - u_w$$

where σ' represents the effective stress. This equation implicitly considers the following two hypotheses:

a) The solid particles and water are incompressible.

b) The contact area between two particles is independent of the confining pressure and can be neglected.

If one of these hypotheses is missing, then different equations can be obtained. For example, if the contact area between particles is considered, the stress regulating the shear strength of soils [10] can be written as:

$$\sigma' = \sigma - k\,u_w$$

where,

$$k = \left(1 - a\tan\psi/\tan\phi\right)$$

In the above expression a represents the contact area between particles per unit area, ψ is the friction angle of the mineral comprising the solid particles and φ is the internal friction angle of the granular media.

On the other hand, according to Lade and De Boer [11], if the compressibility of the solid particles is considered, the value of parameter k for the volumetric behavior of saturated porous media is:

$$k = \left(1 - \left(1 - n\right)C_s/C_e\right)$$

where n represents the soil porosity, C_s is the compressibility of the solid material comprising the solid particles and C_e is the compressibility of the soil structure.

The above expressions show that an effective stress does not represent a physical measurable quantity but it is an artificial stress used to simplify the relations for volumetric and strength behavior of materials and may include mechanical properties or state variables. That is to say, it represents a constitutive variable. However, for the range of stresses frequently used in geotechnical engineering, the variation of parameter k is so small that it is very difficult to determine, even with sophisticated laboratory equipment. Therefore, it can be said that Terzaghi's effective stress equation represents an excellent approximation for both the shear strength and the volumetric behavior of saturated soils.

Because of this simplification, when researchers were looking for an effective stress equation for unsaturated soils, it was assumed that such equation should be written as a function of stress variables only and this assumption gave rise to a great deal of confusion.

In the late 50's some researchers focused on the behavior of unsaturated soils and proposed different equations for the effective stress: Jennings [12], Croney, Coleman and Black [13], Bishop [14] and Aitchison [15] among others. However, only that proposed by Bishop [14] prevailed. This equation writes,

$$\sigma' = \sigma - u_a + \chi\left(u_a - u_w\right) = \overline{\sigma} + \chi\, s \ldots \tag{1.1}$$

where χ is a parameter mainly related to the degree of saturation $\left(S_w\right)$ of the material.

Different expressions have been proposed for the value of parameter χ. For example Aitchinson [15] proposed the following relationship:

$$\chi = S_w + \frac{1}{s}\sum_{i=0}^{s} 0.3\, s_i\, \Delta S_{wi}$$

This equation considers that parameter χ is a function of the addition of the product of the increment of the degree of saturation (ΔS_{wi}) multiplied by the value of suction (s_i) along the SWRC from suction cero to the current suction of the soil. This means that parameter χ is not only related to the degree of saturation

of the material but also to the way water intrudes the pores of soil. In other words, the structure of soil also plays a role in the value of χ. A similar conclusion was reached by Jennings and Burland in 1962 when they reported that the void ratio also affects the value of parameter χ.

Later Blight [16] proposed two different methods to determine the value of parameter χ: the first one is based on the comparison of the results of two triaxial tests, one performed on a saturated sample and the other on an unsaturated one. The second one, results from the analysis of contact forces between two solid particles linked by a meniscus of water. However, the author concludes that it is not possible to decide which method is the more convenient.

Recently, Khalili and Khabbaz [17] proposed the following equation to determine the value of parameter χ :

$$\chi = \left[\frac{s}{s_{ae}}\right]^{-0.55}$$

where s_{ae} represents the air entry value. For suctions below the air entry value, it is considered that air is only present in the form of air bubbles, therefore $u_a = u_w$ and, Bishop's equation reduces to Terzaghi's effective stress equation. One important aspect of this equation is that it includes a parameter from the SWRC. The SWRC represents a relationship between the water content or the degree of saturation of the sample with suction. This trend, where significant parameters of the SWRC are used to obtain the value of χ, has been followed by other researchers with fair results as shown below.

Based on experimental evidence Öberg and Sällfors [18] proposed that, for granular materials and degrees of saturation over 50%, parameter χ may adopt the value of the degree of saturation ($\chi = S_w$). In this way, the simplified version of Bishop's equation appeared. Some researchers have proposed other empirical expressions for parameter χ based on the results of tests made on sand, silt and clay. Amongst the most successful are those shown in Table **1**. It is interesting to observe that all these expressions are closely related to the SWRC. These expressions along with some others were confronted with the experimental results

of different soils collected by Garven and Vanapalli [19]. The results of this exercise showed that equation T1 was the most appropriate with 70% of success followed by equations T2 and T3 with only 25% and 17%, respectively. Even though equation T1 had a good rate of success, its major drawback is that it cannot account for the behavior of all types of soils as stated by Garven and Vanapalli [19].

Additional experimental results showed that the value of parameter χ was affected by different factors such as the wetting-drying history, the voids ratio and the structure of the soil [6, 20].

Table1: Some relationships for the value of parameter χ

Number	Equation	Author
T1	$\chi = (S_w)^{\kappa}$ κ = fitting parameter	Vanapalli, Fredlund, Pufahl and Clifton [21]
T2	$\chi = (S_w - S_r)/(1 - S_r)$ S_r = residual degree of saturation	Vanapalli Fredlund, Pufahl and Clifton [21]
T3	$\chi = S_w$	Öberg and Sällfours [18]

Added to the problem of the determination of parameter χ, the validity of Bishop's equation was questioned because it could not predict by itself the phenomenon of collapse upon wetting [20]. During this phenomenon, the volume of a soil sample suddenly reduces while the mean net stress remains constant. Therefore, intuitively, this phenomenon was interpreted as the result of an increment of the effective stress applied to the soil sample, while Bishop's equation predicts the reduction of these stresses at wetting because suction decreases and becomes nil at saturation.

However, it is now accepted that, because collapse represents a plastic volumetric response of the soil, it can only be explained when an elastoplastic framework similar to that proposed by Alonso, Gens and Josa [7] is added to a constitutive model based on the independent state variables approach. Similarly, collapse cannot be explained using a single constitutive variable as that represented by Bishop's effective stress equation without an elastoplastic framework.

Only recently Bishop´s equation has reappeared on the constitutive modeling for unsaturated soils as it has proven major efficiency in coupling the hydraulic and mechanical behavior of unsaturated materials (see for example [22-25]).

Although some attempts to obtain Bishop's effective stress equation have been done over the years (see for example [1, 18, 26]) none of them have prevailed. In the next chapter, a procedure to obtain an analytical expression for parameter χ is presented.

CHAPTER 2

The Effective Stress Equation

Abstract: Based on the analysis of the equilibrium of solid particles of an unsaturated sample subject to certain suction it is possible to establish an analytical expression for Bishop´s parameter χ. The resulting stress can be used to predict the shear strength and volumetric behavior of unsaturated soils. This equation clarifies some features of the strength of unsaturated soils that up to now had no apparent explanation. The effective stress parameter χ is written as a function of three quantities: the saturated fraction, the unsaturated fraction and the degree of saturation of the unsaturated fraction of the sample. A drawback to this expression is that the determination of these three parameters cannot be made from current experimental procedures.

Keywords: Equilibrium, total stress, effective stress, suction, volumetric behavior, shear strength, effective stress parameter, saturated fraction, unsaturated fraction, dry fraction, degree of saturation of the unsaturated fraction, microstructure, macrostructure, water menisci, homogeneous material.

2.1. INTRODUCTION

Most natural soils show a bimodal structure consisting in a microstructure and a macrostructure [27]. The microstructure can be formed by packets of fine particles that flocculate and remain attached. These packets or aggregates contain the intra-aggregate pores which are pores of small size. On the other hand, the macrostructure is the arrangement of packets of fine particles alone or mixed with solid grains that show the inter-aggregate and inter-particle (when solid grains are present) pores which are pores of larger size. In such a case, the size of pores usually ranges from 500μm to 0.01μm. The smallest pore size being close to the thickness of the adsorbed water layer which means that these pores never dry. This phenomenon accounts for the difference in the consistency of fine and coarse materials when dry. When the suction applied to a soil is low, great part of the macrostructure and the totality of the microstructure remain saturated. When suction increases, the saturated soil volume decreases in such a way that some solids are now completely surrounded by dry pores while others are only partially surrounded by saturated pores. Instead most of the microstructure is still saturated. Finally, for very high suction, the saturated soil volume tends to disappear while

Eduardo Rojas

the dry fraction increases. In the case of coarse materials the saturated fraction may completely disappear while for clayey soils this never happens because of the existence of intra-aggregated voids filled with layers of adsorbed water. Therefore it can be said that, in general, an unsaturated soil consists of a saturated fraction, where soil particles are completely surrounded by water, an unsaturated fraction, where solid particles are linked together by water menisci and a dry fraction where solids are completely surrounded by air. In some cases the bimodal structure may not appear for example in homogeneous dense sands. In that case the transit from the saturated to the dry condition happens very fast and the saturated fraction completely disappears at small values of suction while the dry fraction increases rapidly. This behavior is reflected on the SWRCs of every material as will be shown later.

If a soil sample is confined in a closed environment at a constant temperature during an appropriate period of time, then it can be admitted that the relative humidity is the same everywhere in the sample and therefore, the value of suction is constant throughout the sample. Thus, air and water pressures in the saturated zones are the same as for the unsaturated. This implies that all saturated zones are surrounded by menisci of water showing the same radius of curvature as the unsaturated zones.

2.2. EFFECTIVE STRESS EQUATION

Consider a homogenous and isotropic soil showing a bimodal structure where pores are randomly distributed as shown in Fig. **1**. The term homogenous means that a representative elementary volume can be used to model the whole material as this volume adequately reflects both the microstructure and macrostructure of the system. The term isotropic means that the mechanical and geometrical properties are the same in all three directions, including the spatial distribution of menisci.

The solid particles constituting both the macro and the microstructure can be observed in Fig. **1**. Also the water menisci and gas phase are included. In general, it is considered that the solid particles of the microstructure are grouped in the form of packets. In this case, the influence of the contractile skin is ignored as

both Haines [28] and Murray [29] demonstrated that its influence could be ignored for practical purposes. Also the water vapor, adsorbed water and dissolved air are disregarded as Murray [29] has proved that their influence is also minimal. Finally, the contact areas between solids will be neglected as implicitly considered in Terzaghi's effective stress equation. Based on a Disturbed State Model, Desai and Wang [30] performed an analysis of the effective stress on saturated soils which includes the effect of the variation of the contact area of solids. A similar procedure could be used herein if the contact area of solids was not neglected.

For this analysis, the following notation is used: a superscript indicates the fraction being referred: *s* for the saturated, *u* for the unsaturated and *d* for the dry fraction of the soil. A subscript indicates the phase being referred: $\tilde{s}$ for solids, *w* for water and *a* for air. A double subindex indicates the influence of one phase to another; for example, $A_{\tilde{s}a}$ and $A_{\tilde{s}w}$ represents the area of solids subjected to air and water pressure, respectively.

Considering a unitary thickness of the soil section shown in Fig. **1**, it can be established that the total area (*A*) of the cross section B-B', results from the addition of the saturated $\left(A^s\right)$, the unsaturated $\left(A^u\right)$ and the dry fractions (A^d) of the sample, that is to say $A = A^s + A^u + A^u$. Also, the total area of the saturated fraction results from the addition of the area where water directly reacts (A_w^s) plus that occupied by solids ($A_{\tilde{s}}^s$), in the form $A^s = A_w^s + A_{\tilde{s}}^s$. Moreover, the solid particles on the saturated fraction are only in contact with water and other solids. If the contact area between solids is neglected, then all the horizontal projection of the area of solids represented in section B-B' is subject to the water pressure; that is $A_{\tilde{s}}^s = A_{\tilde{s}w}^s$. Therefore the total area of the saturated fraction can be written as the addition of the areas where water directly reacts plus the horizontal projection of solids pushed by water in the form:

$$A^s = A_w^s + A_{\tilde{s}w}^s \ldots \tag{2.1}$$

On the other hand, the total area of the unsaturated fraction results from the sum of the areas where the solid ($A_{\tilde{s}}^u$), liquid (A_w^u) and gas (A_a^u) phases react, that is $A^u = A_{\tilde{s}}^u + A_w^u + A_a^u$. Additionally, the solids also are in contact with the three

phases. If the contact area between solids is ignored, then the horizontal projection of the solids on section B-B' results from the sum of the areas of solids where the pressures of liquid ($A^u_{\tilde{s}w} = \left(A^u_{\tilde{s}w}\right)_1 + \left(A^u_{\tilde{s}w}\right)_2$) and air ($A^u_{\tilde{s}a}$) react:

$$A^u_{\tilde{s}} = A^u_{\tilde{s}w} + A^u_{\tilde{s}a} \ldots \tag{2.2}$$

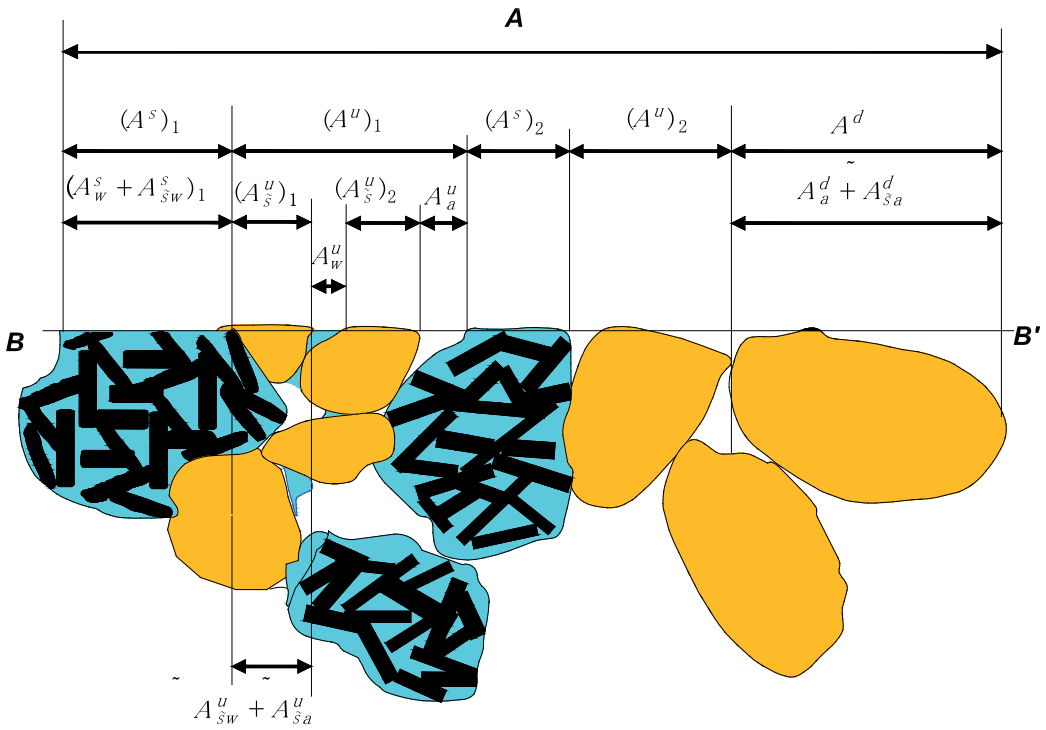

Figure 1: Section of an unsaturated soil showing the contact areas of the different phases.

Finally, in the dry fraction all particles are surrounded by air and also they are in contact with other particles. Again, if the contact area between particles is neglected then the total area of the dry fraction results from the addition of the area where air directly reacts plus the area of solids cut by line B-B', in the form:

$$A^d = A^d_a + A^d_{\tilde{s}a}$$

In this way, the total area for both the saturated and unsaturated fractions where the liquid phase reacts can be written as:

$$A_w = A_w^s + A_{\tilde{s}w}^s + A_w^u + A_{\tilde{s}w}^u \ldots \tag{2.3}$$

and the total area where the air pressure reacts is:

$$A_a = A_a^u + A_{\tilde{s}a}^u + A_a^d + A_{\tilde{s}a}^d = A - A_w \ldots \tag{2.4}$$

If a vertical force F is applied on the plane B-B', the equilibrium of the system is ensured by the reaction of each phase, resulting in the following equation:

$$F = \sigma_1 A = \sigma_{\tilde{s}1} A_{\tilde{s}} + u_a A_a + u_w A_w \ldots \tag{2.5}$$

where σ_1 is the total vertical stress and $\sigma_{\tilde{s}1}$ is the vertical stress transmitted by the solid particles. The term $\sigma_{\tilde{s}1} A_{\tilde{s}}$ can also be written as $\sigma_{\tilde{s}1} A_{\tilde{s}} = \sigma_1' A$, where σ'_1 represents the effective vertical stress which is related to the stress supported by the solid skeleton and therefore, it also can be related to the shear strength and the volumetric behavior of the material. Therefore, Equation (2.5) can be rewritten as:

$$\sigma_1 A = \sigma_1' A + u_a A_a + u_w A_w \ldots \tag{2.6}$$

Manipulating Equations (2.4) and (2.6), the following relationship is obtained:

$$\sigma_1' = \left(\sigma_1 - u_a\right) + \left(u_a - u_w\right)\left(\frac{A_w}{A}\right) \ldots \tag{2.7}$$

where the term A_w/A represents Bishop's parameter χ. Similar equations to the one shown above have been proposed by Matyas and Radhakrishna [1] and Öberg and Sällfors [18]. On one side, Matyas and Radhakrishna [1] stated that A_w/A represents a measure of the saturated pore space and therefore this quantity depends mainly on the degree of saturation of the material. On the other side, Öberg [31] analyzed the value of the ratio A_w/A for a three dimensional ideal soil made of spheres in open and close packing. He observed that the value of this parameter was close to the degree of saturation (S_w) for both cases, especially when $S_w \geq 50\%$. He also reported that within this range, the difference between A_w/A and S_w was not larger than 20%. Accordingly, these authors concluded that, under certain conditions, the ratio A_w/A can be approximated to the degree of saturation of the soil, as its exact value is difficult to obtain in practice.

A more convenient way to write the quantity A_w/A is using common soil mechanics volumetric relationships. According to Equations (2.1) and (2.3), the ratio A_w/A can be expressed as:

$$\frac{A_w}{A} = \frac{A^s}{A} + \frac{A_w^u + A_{\tilde{s}w}^u}{A} \ldots \tag{2.8}$$

The term A^s/A represents the ratio of the saturated area (A^s) to the total area of the section (A). If pores are randomly distributed in a homogeneous isotropic material it can be proven that the areas of water, air and solids appearing in a cross section of a representative elementary volume of the material, adequately represent the volumetric distribution of the phases [32]. Therefore, the areas corresponding to each phase can be related to their respective volumes, in the form:

$$\frac{A^s}{A} = \frac{V^s}{V} = f^s \ldots \tag{2.9}$$

where V^s and V represent the volume of the saturated fraction and the total volume of the material, respectively. In that sense, f^s is called the saturated fraction of the soil. Therefore, according to Equation (2.1), the volume of the saturated fraction is obtained by adding the volume of solids completely surrounded by pores filled with water with the volume of those pores. The solids surrounded by water are called saturated solids. The saturated fraction is then obtained by dividing the saturated volume by the total volume of the material.

On the other hand, Equation (2.2) can be rewritten as

$$A_{\tilde{s}}^u = A_{\tilde{s}w}^u + A_{\tilde{s}a}^u = A_{\tilde{s}}^u \frac{A_v^u}{A_v^u} = A_{\tilde{s}}^u \frac{A_w^u + A_a^u}{A_v^u} = A_{\tilde{s}}^u \frac{A_w^u}{A_v^u} + A_{\tilde{s}}^u \frac{A_a^u}{A_v^u}$$

where A_v^u represents the area of voids of the unsaturated fraction. Gathering together the terms involving air pressure on one side, and the terms involving water pressure on the other, the following relationships can be found: $A_{\tilde{s}w}^u = A_{\tilde{s}}^u \left(A_w^u / A_v^u \right)$ and $A_{\tilde{s}a}^u = A_{\tilde{s}}^u \left(A_a^u / A_v^u \right)$. Then, using the relationship

$A^u = A^u_{\tilde{s}} + A^u_w + A^u_a = A^u_{\tilde{s}} + A^u_v$, the term $\left(A^u_w + A^u_{\tilde{s}w}\right)\big/A$ in Equation (2.8) can be written as:

$$\frac{\left(A^u_w + A^u_{\tilde{s}w}\right)}{A} = \frac{A^u_w\left(1 + A^u_{\tilde{s}}\big/A^u_v\right)}{A} = \frac{A^u_w}{A^u_v}\frac{A^u}{A}\ldots \tag{2.10}$$

Again, by considering the pores randomly distributed into a homogeneous isotropic material, areas and volumes can be related. Therefore, the above equation transforms into:

$$\frac{A^u_w}{A^u_v}\frac{A^u}{A} = \frac{V^u_w}{V^u_v}\frac{V^u}{V} = S^u_w\left(f^u\right)\ldots \tag{2.11}$$

where V^u_w and V^u_v represent the volume of water and voids of the unsaturated fraction, respectively while V^u is the total volume of the unsaturated fraction, $S^u_w = V^u_w\big/V^u_v$ represents the degree of saturation of the unsaturated fraction and $f^u = V^u\big/V$ represents the unsaturated fraction of the soil. Therefore, the volume of the unsaturated fraction results from the addition of the volume of all solids surrounded by a combination of saturated and dry pores plus the volume of these pores. These solids are called unsaturated solids. Those pores filled with water but in contact with both saturated and unsaturated solids are considered part of the saturated fraction. This is so because they are part of the pores that surrounds a saturated solid. The unsaturated fraction of the soil is then represented by the unsaturated volume divided by the total volume of the material. Additionally, there may be a dry fraction represented by the volume of dry elements divided by the total volume of the sample. The volume of dry elements is obtained by adding the volume of dry solids with the volume of pores surrounding these solids. The dry solids are those particles exclusively surrounded by dry pores. The addition of the saturated, unsaturated and dry fractions results in unity:

$$f^s + f^u + f^d = 1\ldots \tag{2.12}$$

Finally, the degree of saturation of the unsaturated fraction is represented by the volume of water of the unsaturated fraction divided by the volume of voids of this same fraction.

Finally, by using Equations (2.7), (2.8), (2.9), (2.10) and (2.11), the effective vertical stress can be written as:

$$\sigma_1' = \overline{\sigma}_1 + s\left[f^s + S_w^u f^u \right] \ldots \tag{2.13}$$

where $\overline{\sigma}_1$ represents the net stress in the vertical direction. Accordingly, the tensorial form of the effective stress can be expressed as:

$$\sigma_{ij}' = \sigma_{ij} - u_a \delta_{ij} + s\left[f^s + S_w^u f^u \right] \delta_{ij}$$

where δ_{ij} represents the delta of Kronecker. By multiplying the above relation by δ_{ij}, it becomes:

$$p' = p - u_a + s\left[f^s + S_w^u f^u \right] = \overline{p} + \chi s \ldots \tag{2.14}$$

where p', p and $\overline{p}$ represent the mean effective stress, the mean total stress and the mean net stress, respectively. By comparing Equations (2.13) and (1.1), the value of Bishop's parameter χ can be found:

$$\chi = \frac{A_w}{A} = f^s + S_w^u f^u \ldots \tag{2.15}$$

The variables f^s and S_w^u can also be written as a function of the global degree of saturation (S_w) and the void ratio (e) of the soil in combination with the variables $r_v^s = V_v^s / V_v$ and $r_{\tilde{s}}^s = V_{\tilde{s}}^s / V_{\tilde{s}}$, which represent the ratio of the volume of voids of the saturated fraction (V_v^s) to the total volume of voids of the soil sample (V_v) and the ratio of the volume of solids of the saturated fraction ($V_{\tilde{s}}^s$) to the total volume of solids of the soil sample ($V_{\tilde{s}}$), respectively,

$$S_w^u = \frac{V_w^u}{V_v^u} = \frac{V_w - V_v^s}{V_v - V_v^s} = \left(S_w - r_v^s\right) \Big/ \left(1 - r_v^s\right)$$

$$f^s = \frac{V^s}{V} = \frac{V_v^s + V_{\tilde{s}}^s}{V} = \frac{V_v^s / V_{\tilde{s}} + V_{\tilde{s}}^s / V_{\tilde{s}}}{1+e} = \frac{e r_v^s + r_{\tilde{s}}^s}{1+e}$$

where V_w represent the total volume of water of the sample. Then, Bishop's parameter χ can also be expressed as:

$$\chi = f^s + S_w^u\left(1 - f^{\tilde{s}}\right) = \frac{er_v^s + r_{\tilde{s}}^s}{1+e} + \left(\frac{S_w - r_v^s}{1 - r_v^s}\right)\left(1 - \frac{er_v^s + r_{\tilde{s}}^s}{1+e}\right)\ldots \tag{2.16}$$

That is to say, Bishop's parameter χ not only depends on the global degree of saturation of the soil but also on the global void ratio and the volume of voids and solids of the saturated fraction.

By applying the principles of thermodynamics and specifically that of enthalpy, Murray [29] proposed a coupled stress p_c' to normalize the shear strength of unsaturated soils subject to different suctions. The comparison with experimental results, however, showed some scatter and the results of saturated tests could not be included into the formulation. In his study, Murray [29] obtained the value of Bishop's parameter as $\chi = \left(1 + eS_w\right)/\left(1+e\right)$, which is somehow similar to Equation (2.16). The difference comes from the fact that Murray neglected the effect of air pressure on the solid particles.

Equation (2.13) can also be written as:

$$\sigma_1' = \overline{\sigma}_1 + \sigma_s^* = \sigma_1 - u_a + s\chi \ldots \tag{2.17}$$

where $\sigma_s^* = s\chi = s\left[f^s + S_w^u f^u\right]$ is called the matric suction stress and represents that part of the effective stress generated by matric suction. In the case of saturated soils $\left(f^s = 1, f^u = 0,\ \chi = 1\right)$, the effective stress becomes Terzaghi's effective stress. For a completely dry soil, as for example clean sand, ($f^s = 0$ and $S_w^u = S_w = 0$) the effective stress becomes the net stress. Finally, for the case of a soil with no saturated fraction, for example a poorly graded clean sand subject to a small suction where all water appears in the form of menisci ($f^s = 0, S_w^u = S_w$), the effective stress becomes Bishop's stress with $\chi = S_w$.

According to the principle of effective stress, the equation for the shear strength of unsaturated soils can be written as:

$$\tau = \sigma_n' \tan\phi = \left(\overline{\sigma}_n + \sigma_s^*\right)\tan\phi \ldots \tag{2.18}$$

where σ'_n and $\bar{\sigma}_n$ represent the effective and the net normal stress, respectively. A similar equation has been proposed by Vanapalli, Fredlund, Pufahl and Clifton [21], even though the matric suction stress was written solely as a function of the degree of saturation and the residual degree of saturation. This equation states that the effect of suction on the strength of soil is simply the increment of the contact stress between particles produced by the presence of menisci of water, as assumed by Haines [33].

If the shear strength equation for unsaturated soils (Equation (2.18)) is derived with respect to soil suction, then the following relation is obtained:

$$\frac{\partial \tau}{\partial s} = \tan\phi \left\{ \left[f^s + S_w^u f^u \right] + s \left[\frac{\partial f^s}{\partial s}\left(1 - S_w^u\right) + \frac{\partial S_w^u}{\partial s} f^u \right] \right\}$$

with

$$\frac{\partial f^s}{\partial s} = \frac{\left(1+e\right)\left[\frac{\partial r_{\tilde{s}}^s}{\partial s} + r_v^s \frac{\partial e}{\partial s} + e \frac{\partial r_v^s}{\partial s} \right] - \left(r_{\tilde{s}}^s + e r_v^s \right) \frac{\partial e}{\partial s}}{\left(1+e\right)^2}$$

$$\frac{\partial S_w^u}{\partial s} = \frac{\left(1 - r_v^s\right)\left[\frac{\partial S_w}{\partial s} - \frac{\partial r_v^s}{\partial s} \right] + \left(S_w - r_v^s \right)\left(\frac{\partial r_v^s}{\partial s} \right)}{\left(1 - r_v^s\right)^2}$$

Then, the slope at the origin ($s = 0$ and $f^s = 1$), has the value:

$$\left(\frac{\partial \tau}{\partial s} \right)_{s=0} = \tan\phi$$

In other words, the initial slope of the increment of the shear strength with soil suction equals the internal friction angle. This result has also been experimentally observed by different researchers, for example: Escario, Jucá and Coppe [34] and Gan and Fredlund [35]. However, none of them attempted to explain this finding.

The equation of the failure surface on the plane of mean effective stress *versus* deviator stress can be written in the same form as for saturated soils:

$$q = Mp' \ldots \quad (2.19)$$

where q represents the deviator stress and the slope of the failure surface M is given by:

$$M = \frac{6 \sin \varphi}{3 - \sin \varphi}$$

Because of the hysteresis of the loading-unloading and drying-wetting curves, the behavior of unsaturated soils is influenced by the wetting-drying history of the soil. This influence has been observed by experiments carried out by Bishop and Blight [36], Allan and Sridharan [37], Nishimura, Hirabayashi, Fredlund and Gan [38] and Sivakumar and Wheeler [39]).

If the functions defining parameters f^s, f^u and S_w^u were known, then the matric suction stress could be expressed solely as a function of suction. That is why some of the equations proposed for parameter χ based exclusively on the value of suction or the degree of saturation and some properties of the SWRC, show certain convergence with the experimental results [17, 21].

The main drawback of the analysis shown above is that parameters f^s, f^u, and S_w^u cannot be obtained from direct experimental procedures. For example, Klubertanz, Laloui, Vulliet and Gachet [40] have been using the neutron tomography procedure and the image processing to study the flow of water and the strains of unsaturated materials. These images discriminate the solid, the water and the air phases in different sections of the material and the porous and solid structures of the sample can be observed using an image processor. Nevertheless, the resolution of this equipment is around 0.125 mm which means that this method cannot be used for silty or clayey soils and, only the images of coarse and medium sands have been generated using this technique. This inconvenient has been overcome by combining this method with the X ray tomography which allows a resolution of the order of microns. It can be expected that in the next future the combination of these techniques could provide experimental values for parameters f^s, f^u, and S_w^u required to compute the effective stress of unsaturated soils.

In the meanwhile an alternative procedure for obtaining the values of these parameters is throughout a porous-solid model. A model of this type should be able to represent the structure of real soils by considering the pore and grain size distributions. Additionally, it should be able to reproduce the phenomenon of hydraulic hysteresis during wetting-drying cycles. A model of this type is described in the next chapter.

CHAPTER 3

The Porous-Solid Model

Abstract: In the previous chapter, an analytical expression based on the equilibrium of the solid particles of an unsaturated soil sample subjected to loading was established in order to determine Bishop´s parameter χ. This parameter can be written as a function of the saturated fraction, the unsaturated fraction and the degree of saturation of the unsaturated fraction of the sample. However, the determination of these three parameters cannot be made from current experimental procedures. In order to quantify these parameters, a porous-solid model capable of simulating the structure of real soils is proposed herein. The data required to build the porous-solid model are the grain and pore size distributions in addition to the void ratio of the material.

Keywords: Porous-solid model, soil structure, macropores, mesopores, micropores, sites, cavities, bonds, network porous models, random models, distinct element method, pore size distribution, grain size distribution, soil-water retention curves, pore shrinkage.

3.1. INTRODUCTION

Only recently it has been acknowledge that Bishop´s effective stress equation ($\sigma' = \bar{\sigma} + \chi s$) may lead to more realistic and simple constitutive models for unsaturated soils (see for example [22, 24, 25]). However, the problem of a proper determination of parameter χ still subsists as it has been experimentally recognized that the approximation $\chi \approx S_w$ is not satisfactory for most soils.

In the previous chapter, the analysis of stresses in the skeleton of an unsaturated soil showing a bimodal structure resulted in an effective stress equation for unsaturated materials (Equation (2.13)). Unfortunately, parameters f^s, f^u and S_w^u required for the determination of the effective stress cannot be obtained from current laboratory techniques.

An alternative procedure for the determination of parameters f^s, f^u and S_w^u is the use of a porous model able to simulate the distribution of water in the pores of soils and hence reproduce the SWRCs.

Some simplified porous models have been already developed to study different phenomena such as capillary condensation and evaporation [41] or activated

chemical absorption in heterogeneous surfaces [42]. Also, Fredlund and Xing [43] proposed an equation that defines the SWRC based on the Pore Size Distribution (PSD) of the material. More recently Simms and Yanful [44] proposed a porous network that correctly simulates the SWRC, relative hydraulic conductivity, volume change and PSD. However, these latter models do not account for hysteresis. One way to include hysteresis and observe in detail the influence of water menisci on the deformation and volumetric behavior of unsaturated soils is by mean of a micromechanical model. This type of models is more complex than simple porous models because, besides simulating the porous structure, it also simulates the solid skeleton of the material and may include the phenomenon of shrinkage of macropores at drying. A model with these characteristics can be used to determine the values of parameters f^s, f^u and S_w^u required to compute the effective stress for unsaturated soils. Three of these models are described below.

3.2. DIFFERENT TYPES OF POROUS-SOLID MODELS

The accurate description of real porous media, such as soils, is quite a complicated task, if only because they have millions or billions of pores per gram which sizes ranges from 0.01 to 500 micrometers. Another problem is the phenomenon of hysteresis. Already in 1929, Haines [28] postulated that the main drainage SWRC occurs at higher suctions than the main wetting curve, because the latter is controlled by the largest pores while the former, is controlled by the smallest. Additionally, when load or suction increases there is a reduction in the size of the largest pores. Simms and Yanful [45] studied the shrinkage of pores by analyzing the changes in the PSD of a glacial till during suction increases. They noticed that the PSD of this material exhibits two crests, as shows Fig. **1**. The first of these crests, the one located at approximately 0.1μm, corresponds to the mesopores, *i.e.,* those that maintain their size when suction increases. The other crest (located at approximately 5μm) corresponds to the macropores, which shrink with increasing suction. Simms and Yanful [45] observed that for this particular soil, practically all macropores experienced a progressive shrinkage as suction increased. For suctions of the order of 2.5MPa, practically all macropores had shrunk, and their size diminished to approximately the size of mesopores. The same type of behavior was observed for other soils. Additionally, there is the shrinkage of pores with loading. Simms and Yanful [46] performed a series of

PSD tests on different soils subject to different confining stresses. These results show a general trend for both macropores and mesopores to reduce their size with increasing confining stresses although, macropores reduce their size largely more than mesopores.

Accordingly, a simplified description of the structure of soils that captures the phenomena described above can be made with four elements: the macropores, the mesopores, the connectors and the solids. Both macropores and mesopores represent the cavities or sites of the porous media. These elements contain most of the volume of voids. The mesopores are those pores from medium to small size. The macropores are the largest pores in the soil and differ from the mesopores in that the former shrink with increasing suction or load. The connectors or bonds are the elements that link together the cavities. These pores are the smallest in the porous media and can also be called micropores. The volume contained by bonds is negligible compared to that of cavities. Finally, solids are included in the spaces left by pores and form the skeleton of the material. If an analogy is made between the porous structure of a soil and a building, then the rooms and corridors of the building represent the cavities while the doors and windows represent the bonds. Additionally, the solid structure of the building represents the skeleton of the soil.

Each one of these elements (macropores, mesopores, bonds and solids) posses its own size distribution however, its spatial distribution is strongly correlated given the geometrical restrictions to be fulfilled. These correlations allow reproducing in a simplified manner the structure of soils. Therefore, a porous-solid model built with these elements can simulate the most important aspects of the wetting-drying phenomena, as for example the hydraulic hysteresis of the SWRC and the shrinkage of macropores. For this purpose, the model must comply with certain conditions that allow it to correctly describe the main phenomena of real soils. These conditions are:

a) Heterogeneity of sizes. Meaning that all elements (macropores, mesopores bonds and solids) have their own size distribution.

b) Compressibility of the network. This can be accomplished by allowing the shrinkage of macropores when suction or load increases.

c) Geometrical restrictions, in order to guarantee that the bonds connecting to one site do not intersect one another.

d) Size correlation between neighbors. Meaning that there is a statistical correlation between the sizes of the different elements meeting at a certain place such as cavities with bonds and cavities with solids. This correlation naturally appears during the construction of the model given the geometrical restrictions to be fulfilled.

e) Non-uniform connectivity, as the number of bonds converging at one site may change from site to site.

f) Segregation between fine and coarse particles, as fine particles join together and appear in the form of packets of different sizes.

g) Isolated clusters, as some pores remain inaccessible at wetting or drying.

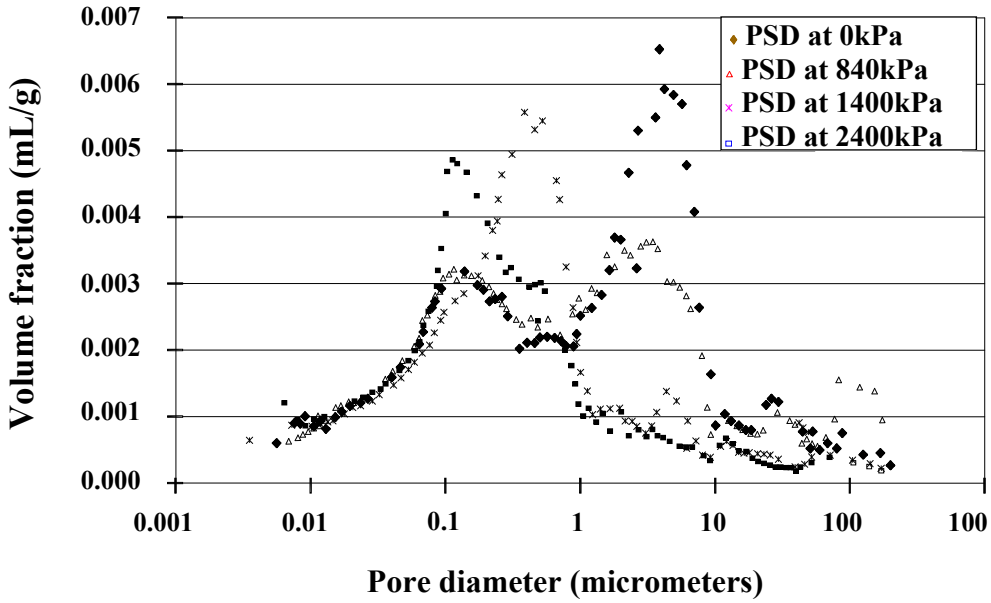

Figure 1: PSD for a glacial till (after Simms and Yanful [45]).

The presence of isolated clusters is confirmed by the existence of the primary and secondary boundary curves. The primary boundary curves at wetting or drying are

obtained from independent tests beginning with completely dry ($S_w = 0$) or fully saturated ($S_w = 1$) materials, respectively. However, when drying-wetting cycles are applied, the degree of saturation never reaches these limits and the secondary boundary curves appear (see Fig. **2**). With further cycling, these curves remain unchanged [47]. It is clear that a real soil exposed to wetting-drying cycles behaves according to the secondary boundary curves. This phenomenon has been called permanent hysteresis, and means that the relationship between the capillary pressure and the degree of saturation is not unique but depends on the history of the wetting-drying cycles [48]. The secondary boundary wetting and drying curves develop when free water intrudes or withdraws, respectively, from the pores of the material. Moreover, free water is responsible for most of the capillary phenomenon in unsaturated soils and therefore, the influence of adsorbed water can be neglected. In that sense, a porous model intending to take account of the capillary phenomenon will only consider the influence of free water in the form of an effective degree of saturation as will be shown later.

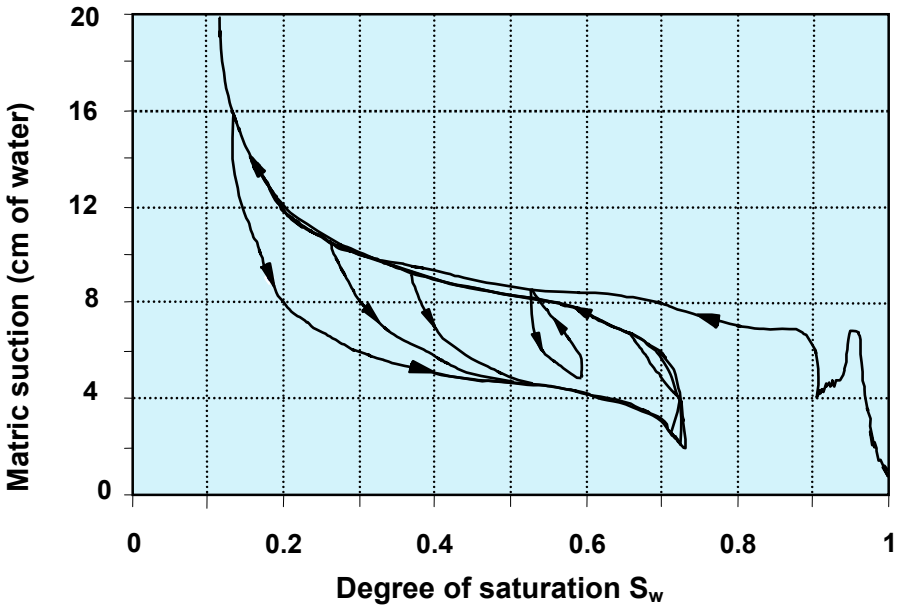

Figure 2: Experimental SWRCs (after Ray and Morris, [49]).

In the following sections three different types of models are presented which comply in a major or minor degree with some of the conditions stated above.

3.2.1. Distinct Element Models

One of the first attempts to develop micromechanical models is due to Cundall and Strack [50] who developed the Distinct Element Method (DEM). These authors consider the solids as disc shaped particles of different sizes. Knowing the spatial distribution (structure) of the solids and the external loads, contact stresses and deformations can be determined. Since these models first appear they have been evolving and presently they can deal with the micromechanics of unsaturated soils, among other applications. A model of this type has been developed by Gili and Alonso [51] which correctly simulates different phenomena of unsaturated materials. This model is briefly described below.

To properly simulate the behavior of unsaturated materials through a micromechanical model, menisci have to be added as new elements and the forces they introduce at the contact between solids need to be considered. In general, simple geometrical shapes as discs or spheres of different sizes are considered for solid particles (see Fig. **3**). Then, the shape of the menisci and therefore the additional stresses on the solids solely depend on the arrangement or structure of the solids and the current water content (or suction). When a boundary condition is modified, the water content may change as a result of water transfer in the form of liquid or vapor. This transfer may occur along the surface of solids or through the pores. When this happens a new distribution of forces occurs and the spatial distribution of solids changes. Therefore the micromechanical model should include three different elements: the solid particles, the pores and the menisci of water. A model of this type can be very helpful in understanding the mechanisms involving the volumetric response of the material produced by a combination of load and suction. Also the effect of suction on the strength of unsaturated soils can be studied. In addition, micromechanical modeling can be used to verify some hypothesis made in elastoplastic constitutive modeling. The model can be two-dimensional (2D) or three-dimensional (3D). They require reproducing realistically the forces induced by water menisci. This type of models is applicable mainly to sands and silts although it can also explain some features of the behavior of fine soils showing a structure made of aggregates or packets of particles. This type of structure can be obtained by compaction on the dry side.

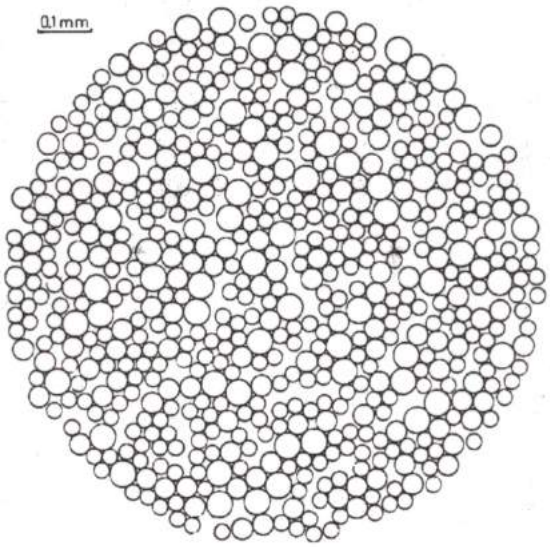

Figure 3: DEM model considering 592 spherical particles.

In the micromechanical model, capillary forces are computed from the Laplace equation for double capillary radii:

$$s = T_s \left(\frac{1}{r_1} + \frac{1}{r_2}\right) \ldots \tag{3.1}$$

where r_1 and r_2 represent the radii of the meniscus and T_s is the air-water interfacial tension. The contact force between two spherical grains of radii r linked by a meniscus of water covering the surface of the grain with an angle 4θ measured from the center to the surface of the particle is according to Haines [33].

$$\Delta\sigma_n = \frac{\pi\, T_s(1 - 2\tan\theta)}{r(1 + \tan\theta)}$$

The current position of solids, pores and menisci is followed by three connectivity matrices: particle-menisci matrix, pore-menisci matrix and menisci-particle/pore matrix. The first two specify the menisci located on the periphery of a solid and the third identifies the two solids linked by a specific water meniscus. All three matrices are required to establish the flow equations amongst different elements. Moreover, all the transfer processes are described by a linear mass-flow rate equation of the type:

$$\frac{\Delta M_{ij}}{\Delta t} = K_{ij}(p_j - p_i)$$

where ΔM_{ij} is the mass of a given species interchanged in a time increment Δt between entities i and j. p_i defines the pressure or concentration of a given species at entity i and K_{ij} is a generalized transfer coefficient which includes geometrical terms and constitutive flow parameters such as permeability and diffusivity. The types of flow considered by the model are: air-air, vapor-vapor, air (gas)-air (dissolved), water (vapor)-water-liquid, liquid-liquid, water-dissolved air. The first two occur exclusively in the pores, the following two occur between pores and menisci and the last two occur exclusively in the water menisci.

The equilibrium force and particle displacements are computed according to the procedure described by Cundall and Strack [50]. A 2D rheological model considering elastic, plastic and viscous units is used to simulate the contact between particles (see Fig. **4**). All individual particles must remain in equilibrium. At any contact between particles both normal (N) and shear stresses (T) are considered. The forces exerted by the menisci are considered to be normal to the tangent plane. The limiting shear force between particles is given by the condition $T \leq \mu N$, where μ is the contact friction coefficient.

This micromechanical model has been applied to the simulation of different stress paths, for example: isotropic loading at constant suction, collapse test including the effect of deviator stress, loading-wetting tests, loading-drying tests and wetting-drying cycles.

The simulation of the collapse test included the loading stage by increasing the mean net stress in several steps; from 2kPa to 4kPa, then to 6kPa and finally to 10kPa. Fig. **5** shows the distribution of forces at contacts between particles at 2kPa and 10kPa. Observe that not only the distribution and intensity of the total forces change but also the shape of the sample modifies with loading. To simulate the collapse of the structure, suction has been reduced in two steps; initiating at 90kPa it has been reduced to 10kPa and finally to 0kPa. Fig. **6** shows the distribution of the total force at contacts when suction reaches 10kPa. The sample reacts by reducing its volume and modifying its shape.

These type of simulations show in detail some important aspects of the behavior of soils for example: when loading is applied, the associated volumetric reduction is mainly the result of the destruction of larger pores giving rise to new smaller pores. Also the reduction of the potential of collapse with the increase in the intensity of confining stress can be reproduced on loose soils. This phenomenon occurs because the increase on the confining stress already causes an important volumetric reduction of the material.

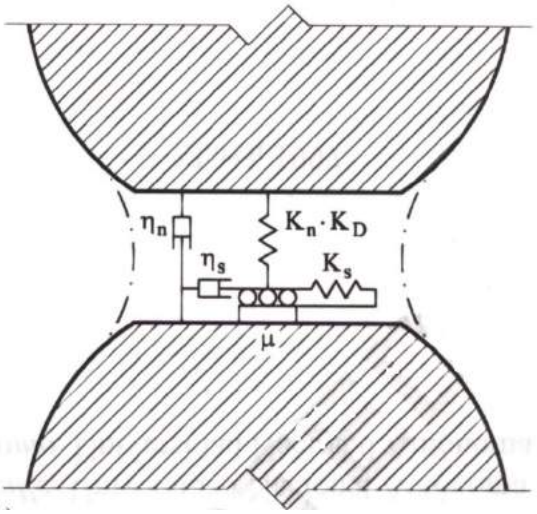

Figure 4: Rheological model at particle contact (from Alonso, Rojas and Pinyol [52] with permission from SMIG).

Also, the change in suction produced by an instantaneous loading as well as the volumetric response during drying-wetting cycles can be studied with these simulations. Specially, the reduction of irreversible deformation with the number of drying-wetting cycles.

Due to computational constraints this type of models uses a limited number of solids, ranging between 1,000 to 10,000. The Grain Size Distribution (GSD) and the water content are introduced as data whereas the PSD in the model is obtained by quantifying the number and size of the voids left by the solids when the initial target void ratio is reached. This procedure constitutes in fact one of the main disadvantages of this type of models because they cannot reproduce a particular PSD as it emerges from the random distribution of solids. Still solids can be

arranged differently depending on the nature and formation process of the soil [53]. This means that, depending on the fabric process, a soil sample may show different PSDs even if both the GSD and the void ratio remain the same as is shown in Fig. **7**. And because the SWRCs depend on the PSD of the material, a different set of SWRCs can be obtained for each fabric.

3.2.2. Random Models

Another type of model that has been recently developed to include both the GSD and the PSD of the material [54] are the random models. These models are built in a bi-dimensional or three-dimensional grid made of squares or cubes. With the GSD, the PSD and the void ratio (e) of the material it is possible to define the number of solids and cavities of each size that need to be placed within a certain area or volume.

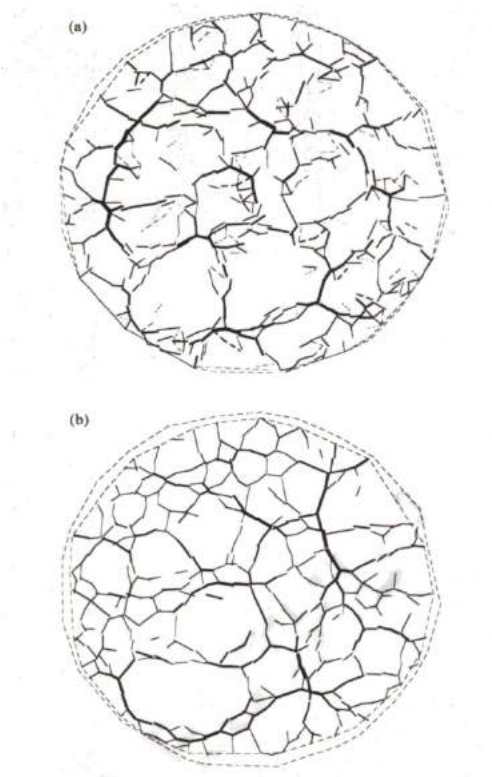

Figure 5: Distribution of total forces at different net stress (a) 2kPa, (b) 10kPa (from Alonso, Rojas and Pinyol [52] with permission from SMIG).

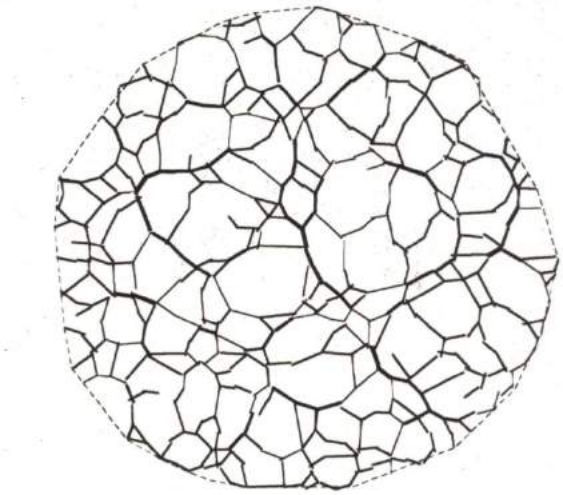

Figure 6: Total force distribution when suction is reduced from 90kPa to 10kPa (from Alonso, Rojas and Pinyol [52] with permission from SMIG).

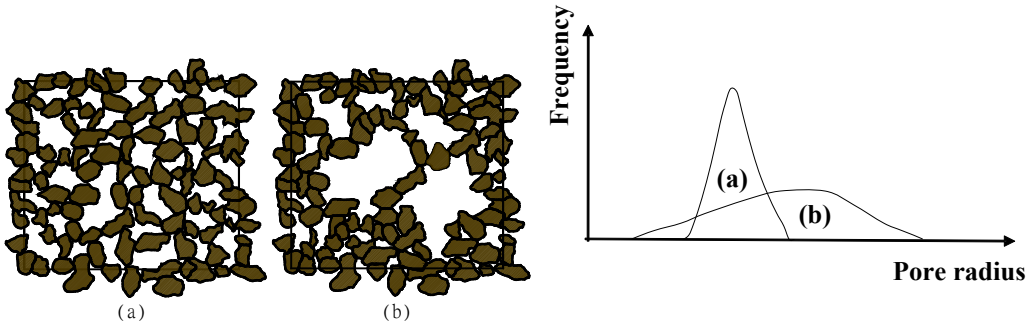

Figure 7: Two different PSDs for the same GSD and void ratio (after Leonards, Alarcon, Frost, Mohamedzein, Santamarina, Thevanayagam, Tomaz and Tyree, [53]).

For the case of a bi-dimensional model a rectangular area with dimensions L in length and H in height is considered. In order to create an area with a number of elements that can be processed with ease by a common PC, the dimensions of this area are established by the following conditions: $20\ D_{max} < L < 250\ D_{min}$ and $H < 150\ D_{min}$ where D_{min} and D_{max} represent the diameter of the smallest pore and the largest solid to be placed on the rectangular area, respectively. These conditions were established in order to have an adequate number (not too small and not too large) of both the largest solids and the smallest pores. Once the area of the model has been defined, it is fully covered with squares whose sides represent $\sqrt{\pi}/2$

times the diameter of the smallest element in the model (D_{min}) equivalent to one pixel. Therefore, a total of $N = [L/D_{min}]x[H/D_{min}](4/\pi)$ pixels are placed within this area. These squares are called basic units and are used as a pattern to place the solids and cavities of the model. The number of basic units occupied by a solid or pore of certain size is established in such a way that all sizes are multiples of the basic unit. In the case of soils, the GSD usually shows larger sizes than the PSD although they may have some overlap. This means that the basic units represent the smallest cavities of the material.

The number of solids and cavities of each size are obtained from the GSD and the PSD of the soil, respectively, when plotted in the axis of volume fraction *versus* size. The volume fraction is defined as the ratio of the volume of solids (or cavities) which size ranges between certain limits to the total volume of solids (or cavities). To each volume fraction, the mean size of its range is assigned. The range of sizes for each volume fraction is selected in such a way that all mean sizes are multiples of the basic unit. As the void ratio represents the proportion between pores and solids, the product of the factor $e/(1+e)$ by the volume fraction of cavities divided by the volume of a single cavity corresponding to that size, results in the number of cavities of a specific size. In the same way, the product of the factor $1/(1+e)$ by the volume fraction of solids divided by the volume of a single solid corresponding to that size, represents the number of solids of that specific size.

Once the number of cavities and solids of each size has been determined, they are located in the model's area. In order to include all the required elements into the model's area, solids and cavities are placed at random following a size strategy which consists of placing these elements from the largest to the smallest. The location of solids and cavities initiates by randomly selecting a basic unit within the model's area where one of the largest solids is to be placed. Then, the basic units needed to represent the size of this solid are found using a polar searching procedure. This procedure consists of placing an origin of polar coordinates at the center of the selected basic unit and then turning around this origin with a constant radius to locate the closer adjacent elements that are available to generate the solid. The angle of rotation is gradually increased until a complete turn is made. If the required number of basic units is still not completed, the radius is

increased. This process continues until the required number of basic units is found. All new elements formed during this process, in addition to complying with the established number of basic units, must also comply with a continuity condition. This condition establishes that a basic unit which is part of an element should have contact at least on one of their faces with another basic unit of this element. This condition allows the existence of different shapes for solids and cavities, but does not permit the generation of "strangled" elements *i.e.,* elements with basic units that have contact solely at one corner. Once all basic units constituting an element have been identified, they are assembled in a single element using a Boolean function. Additionally, all the basic units contained by this element are deleted from the list of available basic units. This procedure avoids the overlap between neighboring elements although they may have contact at the corners or sides of other elements. Once all the largest elements have been formed, the next smaller size elements (whether they are solids or cavities) are generated. This procedure continues until all solids and cavities have been located into the model's area. If at any location, the required number of basic units forming a continuous solid or pore cannot be found then another site is randomly selected until both conditions are fulfilled. Fig. **8** shows the flow diagram to locate and generate the solids and pores on the model´s area.

With this procedure, the largest elements show more regular shapes than the smaller which tend to show irregular shapes. This occurs because the former are the first to be placed and have no restrictions in gathering adjacent basic units whereas the later are formed with the basic units left by larger elements. This process ends with the elements one size larger than the basic unit as these last do not require the random location procedure.

In most cases, not all elements of the smaller sizes can be located in the network because not enough groups with the required number of continuous basic units can be found. This usually happens with the elements one size larger than the basic unit because they are the last ones to be randomly placed in the network. These elements usually require groups of four or more basic units to be formed. To solve this problem, the following procedure has been adopted. First, the program identifies the groups with the larger number of basic units still available

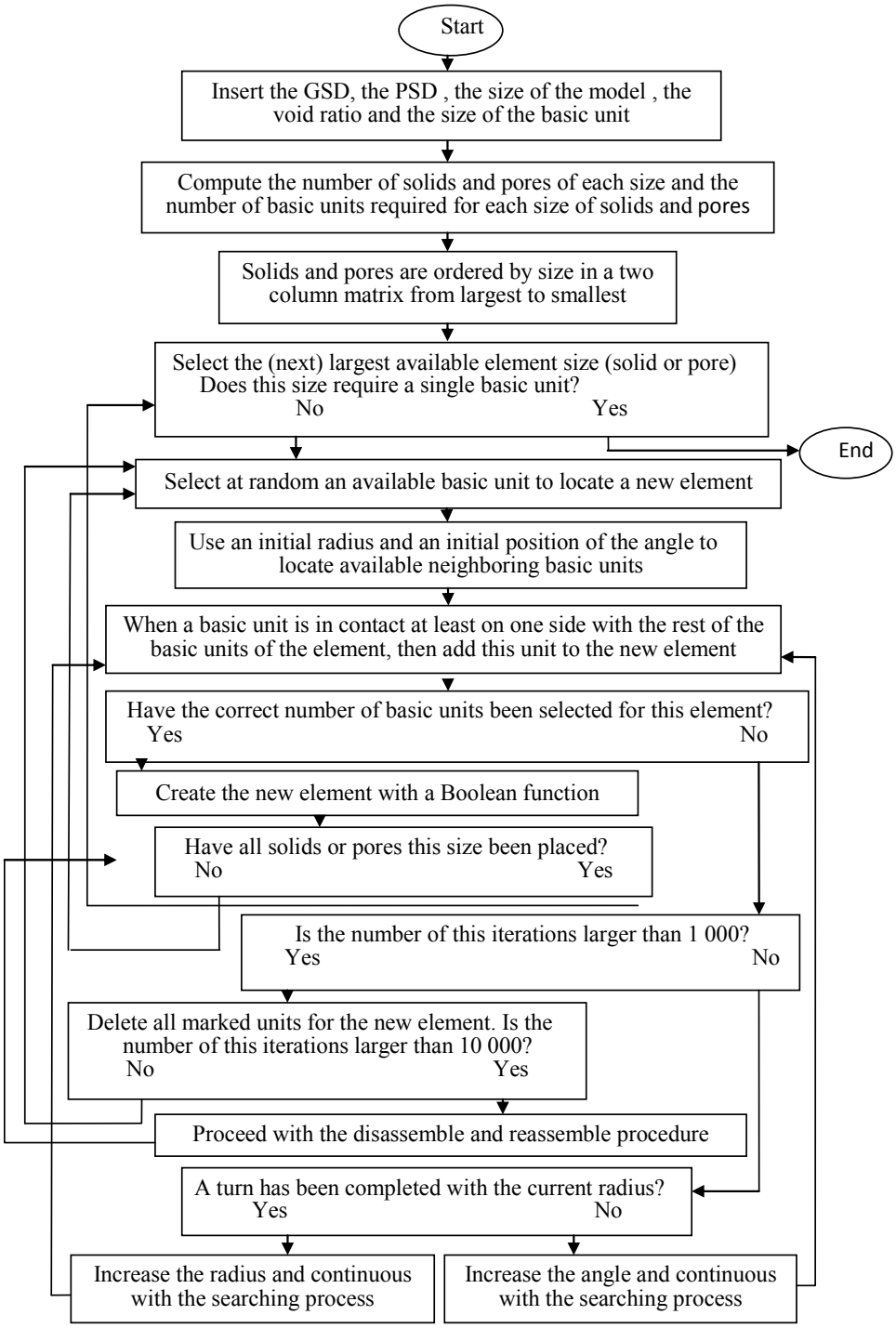

Figure 8: Flow diagram for the construction of the random porous-solid model.

in the model and verifies if any of the neighboring solids or cavities around this group has additional adjacent basic units still available at their boundaries. If the program identifies the required number of basic units along the boundaries of these elements then it proceeds to rearrange them. To this purpose, the identified elements are disassembled into their basic units and then, the basic units required to increase the size of the group for the new element are liberated and substituted by the available basic units located at their boundaries. Finally all these elements are reassembled with their new basic units.

This process is illustrated in Fig. **9**. Suppose that pores made of four basic units constitute the elements one size larger than the smallest size represented by the basic unit. Consider that some of these pores have already been generated but still some more are required. However, no more continuous groups of four basic units can be found in the model's area. Consider also that at a certain location a continuous group of two basic units is found (pore P_4). Then the neighboring elements to this pore (Solid S_1, Solid S_2, Solid S_4 and Pore P_3) are analyzed to identify the basic units that are still available at their boundaries. In this case, elements S_2 and P_3 are selected as they are in contact with the basic units B_1 and B_2 still available. Next, S_2 and P_3 are disassembled to liberate two basic units that are in contact with pore P_4. Then S_2 and P_3 are reassembled by including the available basic units found at their boundaries. Finally, Pore P_4 is generated using the liberated units from its neighbors. With this procedure all cavities and solids can be inserted into the model's area.

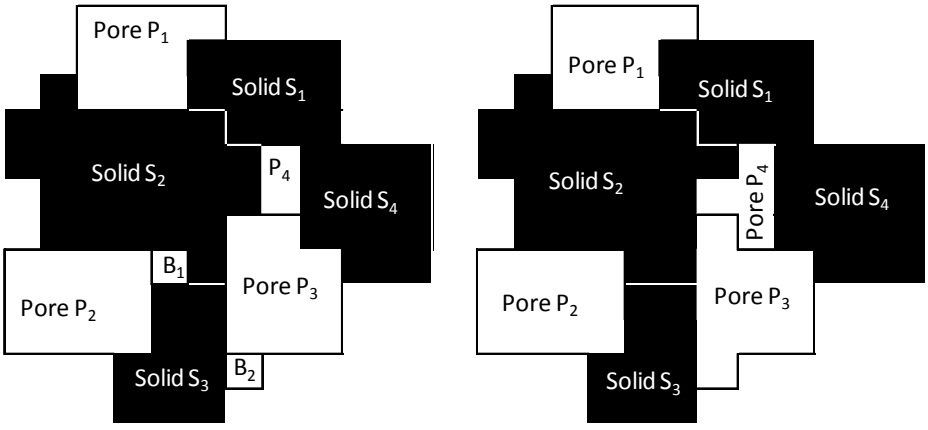

Figure 9: Generating Pore P_4 by disassembling and reassembling Solid S_2 and Pore P_3.

When all solids and cavities have been located (see Fig. **10**), the bonds or connectors are included in the porous structure by linking neighboring cavities. A maximum and a minimum connectivity number are established for the model. This means that the number of bonds connected to each cavity can vary between these limits. These values can be established from the experimental results obtained by Dullien [55] on a sandstone sample. Dullien [55] reported a connectivity varying from 2 to 10 with a mean value of 2.9 and very low frequencies for connectivity ranging between 7 and 10. By extrapolating these results to the case of soils, it can be said that their connectivity may vary from 2 to 6.

The connectivity of pores in the model can be established by using the aforementioned polar search procedure. The search for the neighboring sites of a cavity starts with a radius slightly larger than the equivalent radius of the cavity being considered and is performed by increments of the polar angle. If the minimum connectivity number is not reached at the end of a complete turn, then the searching radius is slightly increased and the procedure continues until the connectivity reaches at least its minimum value at the end of a complete turn. This process can also be stopped when the number of connecting elements reaches the maximum established value. For the model discussed herein, a minimum connectivity of 2 and a maximum of 6 were considered according to the discussion above. When this process is concluded for all cavities, a size is randomly assigned for each bond or connector. This size is obtained from the bond size distribution of the material. Because bonds are always smaller than the cavities they are connect to, the size of a bond is selected exclusively from those sizes smaller than the smallest cavity to which the bond is connected to.

If the size distribution for both cavities and connectors could be experimentally determined, then the porous model could predict both branches of the SWRC. Unfortunately at present, the experimental determination of the PSD for porous materials includes solely the size distribution of cavities because the volume of bonds or connectors is, in general, negligible compared with that of cavities. Therefore, to overcome this lack of information, the shape of the curve of the size distribution of connectors is considered to be similar to that of cavities while the size of connectors is obtained by adjusting the numerical drying SWRC with the experimental one. This is equivalent to horizontally displace the size distribution

curve of connectors in the axis of pore size until the best fit between the numerical and the experimental drying curve is obtained. The drying curve is the one to be fitted because it is mainly dependent on the size distribution of bonds or connectors as aforementioned. The adjustment of the size of bonds practically does not affect the wetting curve which is mainly dependent on the size distribution of cavities. In addition, as connectors are the last elements to be placed in the model, their size can be modified once solids and cavities have been located. This facilitates the fitting process for the drying curve. The necessity of fitting the drying SWRC represents an important drawback to the model which could only be avoided by supposing a value for the ratio between the size of cavities and bonds as both curves are considered to show similar shapes.

Once all cavities, connectors and solids have been distributed in the model, it is possible to simulate the main wetting SWRC as well as the scanning curves. To achieve this, each site is transformed into a circle of the same area and placed at the centroid of the irregular pore.

To simulate the main drying curve it is assumed that all pores are initially saturated and that suction equals zero. Then suction is increased by steps and the critical radius (R_c) determined. This radius represents the lower limit of the size of pores able to drain during a drying process, and is given by the Lapace equation in the form of:

$$R_C = \frac{2\,T_S \cos\theta}{s} \ldots \tag{3.2}$$

where θ is the water-soil mineral contact angle. In general, for the case of most soil minerals in contact with water it is considered that $\theta = 0$. According to Equation (3.2), all pores with radius R complying with the condition $R \geq R_C$ will be able to dry. Therefore the model can identify all pores able to dry at the current value of suction.

Once all pores which size is larger or equal to the critical radius have been identified, they are considered as potentially active, meaning that they can dry if they comply with the continuous path principle. This principle states that a pore can dry only if it is connected to a continuous path of previously dried pores that

reaches the boundary of the model where the bulk of gas is present. This type of pores is called active pores. This means that all boundary elements connected to the bulk of fluid (air or water) are already active pores whereas those elements located at the interior of the porous model need to be tested for this condition.

The same procedure can be followed to determine the main wetting curve except that in this case, all pores are initially dry, suction has a very large initial value which reduces by steps and the potentially active pores are those complying with the condition $R < R_C$.

For the scanning curves, the initial drying or wetting stage is the same up to the point where the inversion takes place. When inversion occurs, only those pores that have been activated will be able to deactivate. This means that solely those pores that have been dried during a drying process are able to saturate when inversion takes place. Correspondingly, only those pores that saturate during a wetting process are able to dry after the inversion.

The procedure to build the porous-solid model allows the generation of different solid structures for the same material meaning that even if the GSD and the void ratio are maintained constant, different PSDs can be generated. This characteristic is not considered by the porous models based on the DEM described earlier. With this model it is possible to study the effect of the structure of soils on the SWRCs. At its present stage this model can only roughly simulate the structure of soils. Refinements including a 3D version with larger number of elements and size ranges may result in better predictions. It is also possible to isolate the solids from the porous structure of the soil and include rheological models at the contacts between solids. This may allow simulating different phenomena as for example the volumetric deformation of the solid skeleton by loading or suction increase and the resulting variation of the PSD. Also the strength of the material at different suctions can be simulated in the same way as DEM models do.

One of the main restrictions to this type of models is the number of elements that a common computer can handle efficiently. In its present version, the model can deal with 40,000 basic units. The size of the scratch memory of the computer is the main constraint to increase the number of elements in the model. This constraint imposes

additional restrictions related to the range of pore and solid sizes that the model is able to include. For example, if the model considers a large range of sizes for solids and pores, the number of basic units required to build the largest elements will be so big and the number of these elements will be so small that the SWRCs may show abrupt changes. Therefore, the range of sizes that the model is able to consider is of about one order of magnitude for both the GSD and the PSD. This also restricts the type of materials that can be considered by the model. For example, at present only the structure of clean sands or clean silts can be simulated.

The computing time of the model greatly depends on the number of basic units and the number of elements of the porous-solid structure. A model made of 10,000 basic units with six different ranges of sizes for solids and pores takes around three hours of processing in a common PC to simulate the main SWRCs.

In order to verify the capabilities of the random model to simulate the SWRC of porous materials using its PSD as data, some experimental results for Vycor glass were used. Figs. **10** and **11** represent the solid and porous structure of the Vycor glass obtained from its PSD. The squares in Fig. **11** represent the cavities and the lines represent the bonds. In this case a minimum of 2 and a maximum of 6 bonds were assigned to each cavity. Fig. **12** shows a three-dimensional view of the porous structure of Vycor glass.

Figure 10: Solid skeleton of the Vycor glass (in black).

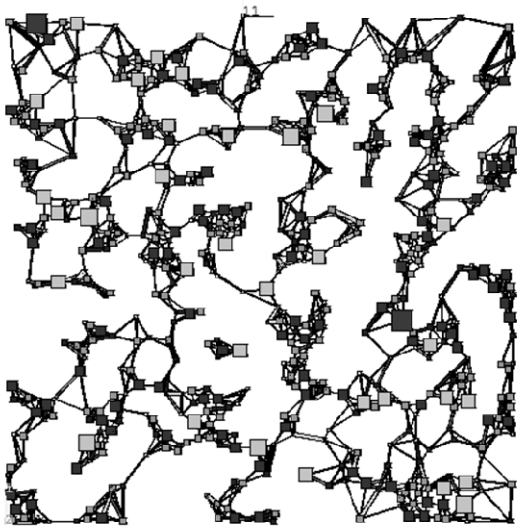

Figure 11: Porous structure of the Vycor glass.

Fig. **13** shows the numerical and experimental main SWRCs as well as the numerical and experimental results for two wetting scanning curves. From this figure it can be observed that the model simulates with fair accuracy the SWRC of the material. Improved results can be expected if the number of size ranges for pores and solids could be increased.

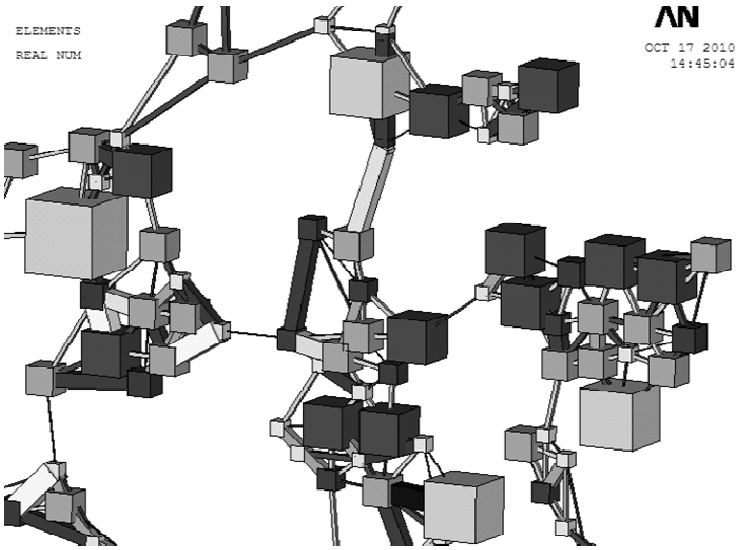

Figure 12: 3D view of the porous structure of the Vycor glass.

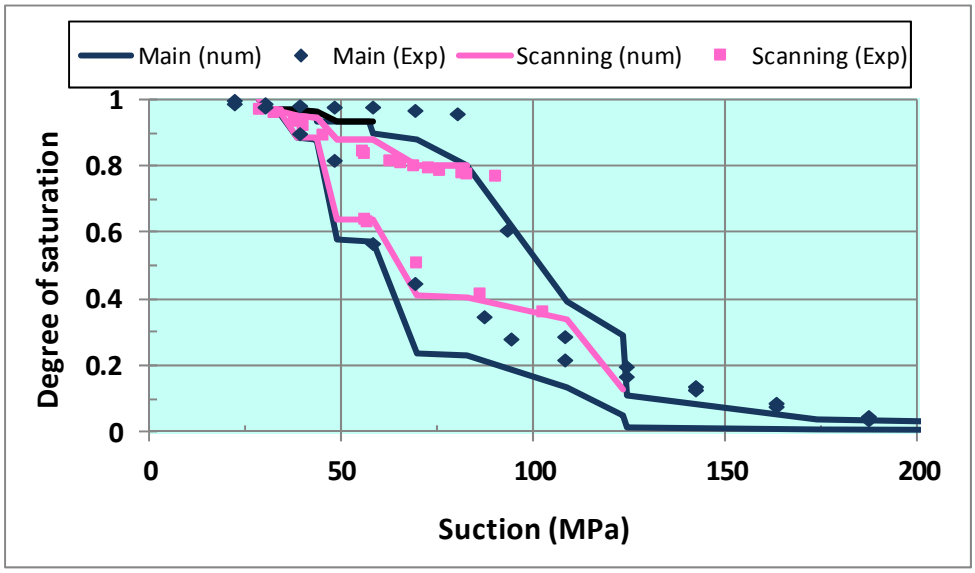

Figure 13: Numerical and experimental main SWRCs and two drying scanning curves.

3.2.3. Network Models

Another type of porous-solid models recently developed is that made of nodes and connectors using regular networks. The nodes represent the sites or cavities and the connectors are the bonds or throats. The cavities are subdivided in macropores and mesopores. Solids are included in the spaces between these elements. The simplest porous-solid network models are those built on the plane where the cavities are represented by circles and the bonds or connectors by rectangles. In a three-dimensional configuration, the cavities are represented by spheres and the bonds or connectors by cylinders. The connectivity (C) represents the number of connectors meeting at a certain cavity and may have a constant value or it may vary from site to site. In this last case, it is sufficient to consider a certain number of connectors of size zero.

Due to the presence of elements of different sizes that need to be arranged in a certain way, the model has to comply with a constructive principle that emerges from geometrical restrictions. This principle ensures that the porous network is physically possible. This principle states that in order to avoid the intersection of two adjacent connectors (*i.e.,* those that meet at an angle of 90^{o} with the concurrent site) with radii r_{B1} and r_{B2}, the following condition should be fulfilled

$$\sqrt{{r_{B1}}^2 + {r_{B2}}^2} \leq r_S$$

An important parameter that affects the morphology of porous networks is the overlap between the size distributions of connectors and sites. The larger the overlap, the more complex the generation of the network becomes. In fact there is a limit on the value of the overlap that allows the generation of networks without violating the constructive principle. In general, when there is a considerable overlap and a small but well differentiated number of sizes, the phenomenon of segregation appears. This phenomenon groups together elements of the same size in different zones of the network. In this way, small cavities gather around and are surrounded by bigger ones. This property allows the modeling of the structure of soils in a simplified way. A model of this type is described in the next section.

3.3. THE NETWORK MODEL

Similar to random models, network models include all four elements (macropores, mesopores, connectors and solids) distributed on a regular network. The porous-solid network is generated following the Monte Carlo procedure. Positions for mesopores and connectors are initially assigned at random to completely fill the network. Thereafter the constructive principle is verified at every node. If the principle is violated at a certain location, an exchange between mesopores and/or bonds from another location (also determined at random) is simulated. If the number of infractions decreases with this exchange, then it is granted. This process continues till no infraction of the constructive principle subsists.

Once this process is completed, then macropores are placed by substituting the required number of mesopores. Macropores are also placed at random, merely verifying that the site to be replaced is smaller than the substituting macropore. If this is not the case, then another site is selected at random until this condition is fulfilled. This procedure ensures the observance of the constructive principle.

In the same way, solids are also placed at random but following a size strategy. This strategy ensures that the size of solids is related to the mean size of its surrounding pores. For example, according to Taylor [56], the pore size d between three spheres of the same size D in close arrangement is $d = D/6.5$; hence, here it

is considered that the size of a solid showing the size of gravel or sand that needs to be placed in a certain position of the network must be larger than three times the mean size of their surrounding pores, that is to say $3d \leq D$. On the other hand, clay particles exhibit a flat shape and, consequently, the aggregation of several particles may generate pores larger than their equivalent radii. Therefore, considering that fine particles associate in structures of four or more elements, with a void ratio larger or equal to two, it can be established that the maximum pore size *d* should be smaller than $D_e \leq 0.5d$, where D_e represents the equivalent diameter of clay particles. Silt particles lay between sand and clay, and therefore, their size lie between the limits $0.5d \leq D \leq 3d$.

The distribution of solids in the pore network starts by specifying the size of the solid (gravel-sand, silt or clay) to be set in a particular place. This can be accomplished by retrieving the maximum and minimum sizes of pores surrounding that specific place. In general, when the constructive principle is being observed, pores of the same size can be found in different zones of the network. Then a solid the size of the specific group to be placed (gravel-sand, silt or clay) is picked up at random. If it does not comply with the required size range, another solid is picked up. If no more solids of the required size are available, then the range of possible sizes is enlarged until a solid can be found. A certain percentage of infractions among the total number of solids is accepted since, at the borders between fine and coarse materials, the presence of pores of very different sizes may lead to geometrical restrictions that no solid can satisfy. By observing these rules it is possible to build a network that approximately simulates both the solid and porous structure of soils.

This model considers that the size distribution of all elements of the network (macropores, mesopores, connectors and solids) follow a logarithmic normal distribution, meaning that only two data are required to define each one of these distributions: the mean size ($\bar{R}$) and the standard deviation (δ). These parameters are obtained from the PSD and the GSD of the material (both parameters for each distribution). It is also possible to use double or triple logarithmic normal distributions to better reproduce the PSD and GSD of mixed soils. In such a case, additional parameters relating the proportion between the volumes of the different distributions are required. One additional parameter is required for a double

normal distribution and two additional parameters are needed for a triple normal distribution. This parameter is called here the proportional volume factor, P_{vf}.

The model can be built in two or three dimensions and in different sizes. However, as all elements in the network are placed at random, it implies that different networks could be built with the same data and hence, the principle of uniqueness of results could not be respected. This problem can be overcome when sufficiently large networks are used. In fact, this is a problem also faced during experimental procedures as the soil sample should be large enough to represent the properties of a specific mass of soil. Therefore, large networks are preferred to small ones as they lead to more realistic and consistent results especially when the overlap between bonds and cavities is large. In opposition, this type of networks increases significantly the required memory size and the computing time. In fact, an important restriction for the development of random networks is the requirements in memory size. For example, the biggest network that a common PC can manage with ease is a 1000 x 1000 plane network or a 100 x 100 x 100 three-dimensional network. If an important overlap exists between cavities and bonds, the required computing time to construct the network is around 8 hours.

Fig. **14** shows a portion of a network built according to the procedure described above. It sketches the four different elements included in the network: macropores, mesopores, bonds and solids. The upper left-hand corner of the network represents a portion of soil tending towards the coarse fraction where sand particles are accommodated. The lower right-hand corner represents a portion of soil tending towards the fine fraction where clay particles are set. Between these two groups a transition of silt is present and fills most of the network. Notice that the distribution of solids and pores is made on a regular grid for practical purpose, however the size of solids is not directly linked to the size of the space between the pores but rather to the pores size, as mentioned before. The length of connectors or bonds is considered as constant throughout the network. Because bonds are basically windows connecting two cavities they are considered to be very thin, therefore their length is considered to be similar to the size of the smallest cavities. In any case this parameter seldom affects the results provided by the porous model as the volume of connectors is negligible compared with that of cavities as aforementioned.

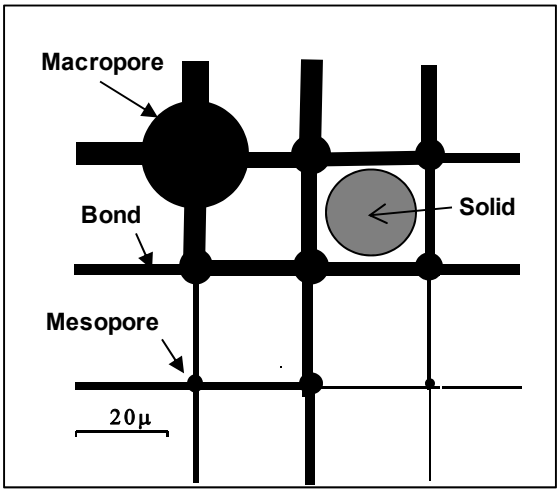

Figure 14: The elements of the porous-solid network: macropores, mesopores, bonds and solids.

In addition, when the distribution of all elements is completed, it is necessary to verify that the ratio between the volume of voids and the volume of solids corresponds to the void ratio of the material. Because clay particles generally show a flat shape and the hydrometer technique reports equivalent radii that have little rapport with their volume, a parameter called shape factor S_f is introduced in order to adjust the solid volume to its real value. This parameter tends towards unity for clean rounded sand but decreases dramatically when the fine fraction of the soil increases, especially for clays with high specific surface.

The model described above seems to be more appropriate for coarse materials where solids and pores show more or less spheroid shapes. In the specific case of clays, the solid particles are rather flat and the shape of pores largely varies from spheroids to slots [57]. In this last case, the size of bonds may be of the same order as that of cavities and therefore the model proposed herein is probably not the most appropriate. In addition, in the case of clays subject to small water contents, interparticle forces are dominated by the van der Wals interactions [58] which are not considered in this model. In any case, only the comparison between experimental and theoretical results would give light on this issue.

3.4. MECHANISMS OF WETTING AND DRAINAGE

Consider a porous network where the size distributions of cavities and connectors show a certain overlap. Consider also that no isolated clusters develop during the

wetting and drainage phenomena. Therefore, in the first stage of its development, the proposed model only attempts to simulate the primary boundary curves. Finally, assume that pores fill and empty according to Laplace's equation given by relationship (3.2).

Hence, when all pores are filled with water (*i.e.,* suction is nil) and gas is forced into them by small increments of suction, the first elements to drain are the largest, while the smaller only drain when suction is further increased. This means that bonds control the drainage process. In contrast, when a dry soil is subject to wetting by small decrements of suction, the first elements to fill in with liquid are the smallest, while the larger only fill with further decrements of suction. This means that cavities control the wetting process. Under these considerations, the conditions for the drainage and imbibition of pores can be stated and the primary boundary curves obtained.

3.4.1. Main Drying Curve

Consider that a soil sample is undergoing a drainage process where some cavities and bonds still remain saturated. The required conditions for a bond to dry are the following: a) gas has penetrated at least one of the bonds surrounding the two sites linked by the bond being considered (given that sites are always larger than bonds, the former do not show any restriction regarding drainage, once one of their connecting bonds has been invaded) and b) gas should be able to penetrate the bond under consideration, meaning that the bond is larger or equal to the critical radius given by Equation (3.2).

On the other hand, the conditions for a site to be filled with gas are as follows: a) at least one bond of the contiguous sites has already been drained. This means that at least one site contiguous to the one under consideration has been already filled with gas as sites show no opposition to be drained once one of their bonds has been drained. b) Gas should be able to fill the bond that links the site already filled with gas with the one being considered. In other words, this bond should be smaller or equal to the critical size.

3.4.2. Main Wetting Curve

Consider now that the soil is undergoing a wetting process with some sites and bonds already saturated. For a bond to be saturated, the following conditions

should be met a) at least one bond contiguous to the one being considered has to be saturated and b) water must be able to penetrate the site linking the saturated bond with the one under consideration, that is to say this adjacent site has to be smaller than the critical size.

For a site to be liquid filled, the following conditions must be fulfilled: a) at least one site contiguous to the one being considered is already saturated and, because bonds are always smaller that sites, all bonds connected to this saturated site are also saturated and b) the site under consideration can be invaded by water; in other words, it should be smaller than the critical size.

The degree of saturation can be easily obtained by dividing the current volume of sites and bonds filled with water by the total volume of pores.

3.4.3. Secondary and Scanning Curves

Once the primary boundary curves have been defined, the secondary curves can be easily obtained by considering that a certain number of elements remain inaccessible. This is readily done with the aid of a cluster coefficient C_c, defined as the ratio of the volume of pores belonging to closed clusters to the total volume of pores. One value is required for the maximum degree of saturation reached during wetting and another for the residual degree of saturation attained during drying. In this way, maximum and minimum values for the degree of saturation are given to the primary curves so they become the secondary boundary curves. This is equivalent to exclusively consider the effect of free water in the porous model as it is the main responsible for the capillary phenomenon that affects the volumetric and strength behavior of unsaturated soils.

In case of inversions during a wetting or drying path, the conditions required for the wetting or drainage of sites and bonds remain the same as for the boundary curves. The only change results from the number of sites and bonds able to saturate or drain. For example, consider that an inversion arises during a wetting path and that the distribution of sites and bonds already saturated is that shown in Fig. **15**(a). Therefore, at the inversion to drying, only those sites and bonds that have already been filled with water will be able to drain. Additionally, Fig. **15**(b) shows the distribution of sites and bonds filled with gas during a drying path.

Hence, when an inversion occurs, only those sites and bonds already filled with gas can saturate. With these considerations it is possible to generate the scanning curves during wetting-drying cycles. A flow diagram to build a computational network model is shown in Fig. **16**.

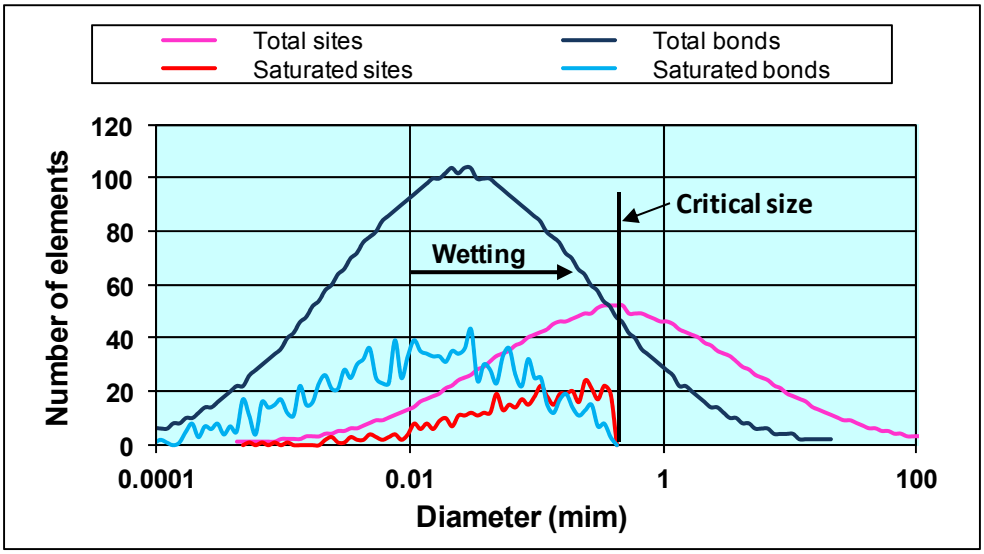

(a)

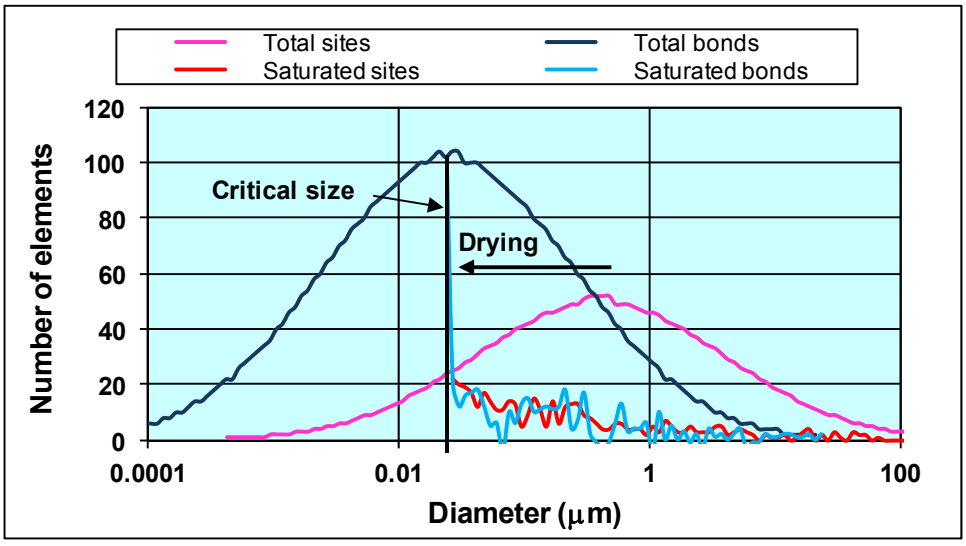

(b)

Figure 15: Comparison between the saturated and the total distributions for sites and bonds during a (a) wetting path and (b) drying path.

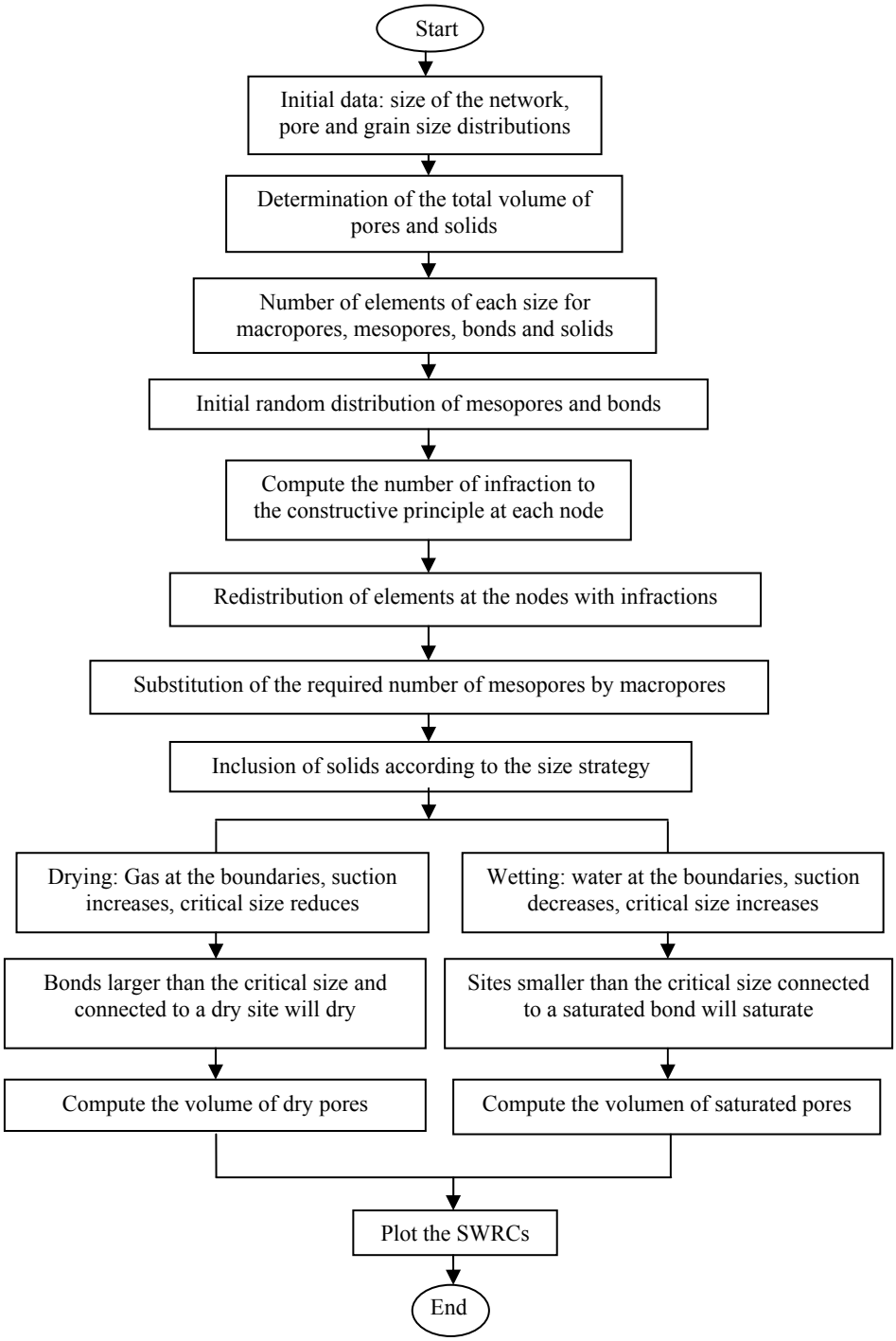

Figure 16: Flow diagram to build a computational network model.

Fig. **17** shows the wetting and drying boundary curves as well as some scanning curves obtained with the computational network porous model. These numerical results are similar to the experimental curves shown in Fig. **2**. One of the main differences between Figs. **2** and **17** is that the numerical scanning curves become asymptotic to the secondary boundary curves, while the experimental results show that the scanning curves reach the boundary curves at a point not far from the inversion point. This behavior needs to be studied further to improve the results of the model.

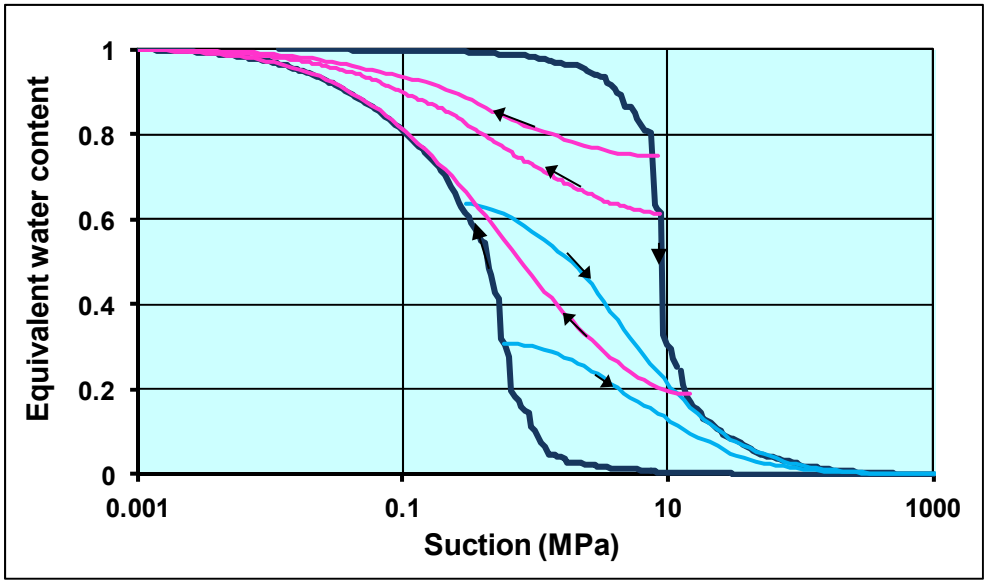

Figure 17: Boundary and scanning curves obtained from the computational network porous model.

An option to overcome the constraints related to memory size and computing time in network models is the use of probabilistic network models [59]. In that case, the boundary curves can be established from the probability of a pore of a certain size to be drained or filled with water when subjected to a certain suction. A model of this type is developed in the next chapter.

Send Orders of Reprints at reprints@benthamscience.net

CHAPTER 4

The Probabilistic Porous-Solid Model

Abstract: In the previous chapter, a computational network porous model was developed to simulate the hydraulic behavior of unsaturated soils. However, important computational constraints make this model unpractical. In this chapter a probabilistic porous-solid model is developed to overcome these constraints. The probabilistic model is an alternative to the use of computational network models and shows important advantages. This model was built by analyzing the probability of a certain pore to be filled or remain filled with water during a wetting or drying process, respectively. The numerical results of the probabilistic model are compared with those of the computational network model showing only slight differences. Then the model is validated by doing some numerical and experimental comparisons. Finally a parametric analysis is presented.

Keywords: Probabilistic model, network models, basic unit, hydro-mechanical coupling, solids, cavities, bonds, saturated fraction, unsaturated fraction, dry fraction, degree of saturation of the unsaturated fraction, retention curves, Bishop's parameter, relative volume, porosimetry tests, macropores, mesopores, micropores.

4.1. INTRODUCTION

Recently, Bishop's stress equation has been used for the development of simpler and more realistic constitutive models for unsaturated soils [22, 24, 25] not only because it can estimate approximately the strength of soils but also because it takes into account the hydro-mechanical coupling observed in unsaturated soils. This phenomenon becomes evident by the fact that the degree of saturation affects the stiffness and strength of soil samples subject to the same suction. Part of this phenomenon can be related to the hysteresis of the SWRCs as, for a single value of suction, a large range of values for the degree of saturation is possible. Another part can be related to the volumetric deformation of the sample during loading or suction increase as this in turn affects the SWRCs.

The analysis presented in Chapter 2 shows that Bishop´s effective stress equation for unsaturated soils (Equation (1.1)) can be expressed as Equation (2.13) with parameter χ defined by Equation (2.15). According to this last equation,

Eduardo Rojas

parameter χ depends not only on the degree of saturation (S_w) of the sample, but also on the void ratio and the structure of the soil as experimentally observed by Bishop and Donald [6]. The main problem with the use of Bishop's equation lies precisely on the determination of parameter χ. In this chapter, a probabilistic porous-solid model is developed for the determination of this parameter using both branches of the SWRC as data.

4.2. THE PROBABILISTIC MODEL

Based on the framework of the computational network model presented in the previous chapter, it is possible to develop a probabilistic porous-solid model [59]. The model is based on the concept of basic units which allows the introduction of the solid phase resulting in a porous-solid model that can be used to determine the current effective stress in an unsaturated material. Initially, basic units for sites and bonds are defined and the equations for the main boundary curves at wetting and drying are obtained.

The procedure to develop the probabilistic model is as follows: first, an infinite bi- or three-dimensional network made of macropores, mesopores, bonds and solids is considered. Thereafter, the conditions for a pore (cavity or bond) to drain or saturate during a drying or wetting process are established. Then, based on the size distribution of each element, it is possible to write the above conditions in the form of probability equations. These equations can then be simultaneously solved and the probability for a pore of a certain size to drain or saturate during a drying or wetting process can be determined. Subsequently, it is possible to establish a ratio between the dried and saturated pores and thus obtain the degree of saturation of the material to finally plot the SWRCs in wetting and drying.

This process requires knowledge on the distributions of the relative volumes of cavities $\left(V_{RS}\right)$ and bonds $\left(V_{RB}\right)$ as a function of their size. The relative volume is defined as the volume of the elements of certain size, divided by their total volume. These distributions can be obtained from the results of porosimetry tests. Once these distributions are known, it is possible to define the relative volume of cavities (macropores and mesopores) $S\left(R_C\right)$ and bonds or connectors $B\left(R_C\right)$ smaller or equal to the critical radius R_C in the form,

$$S(R_C) = \int_0^{R_C} V_{RS}(R)\,dR \ldots \tag{4.1}$$

$$B(R_C) = \int_0^{R_C} V_{RB}(R)\,dR \ldots \tag{4.2}$$

When these integrals are solved for the full range of sizes the result is unity, which means that these functions in fact represent the distribution of probabilities for sites and bonds, respectively. These functions are represented in Fig. **1**(a) and (b) for the wetting and drying path, respectively.

Using the above equations it is possible to determine the volume of pores of a certain size. For example, if V_S represents the total volume of cavities, the product $V_S\,S(R_C) = V_S \int_0^{R_C} V_{RS}(R)\,dR$ represents the volume of cavities from size zero to R_C.

(a)

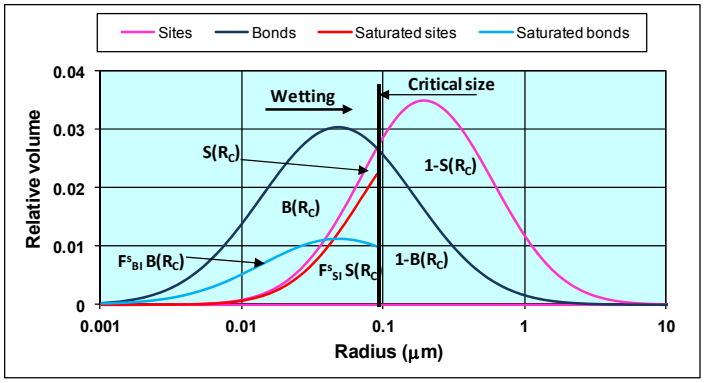

(b)

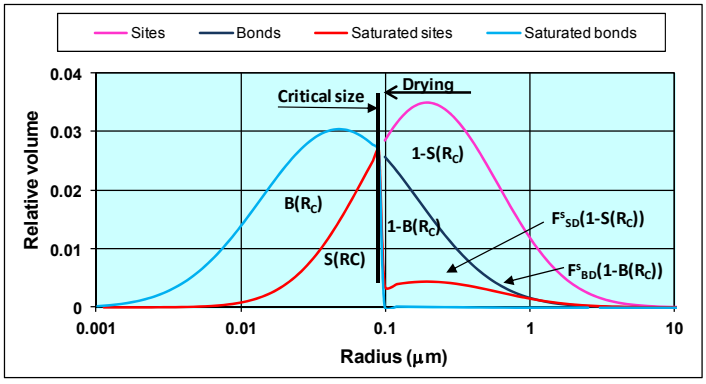

Figure 1: Relative volume distribution for saturated cavities and bonds at (a) wetting and (b) drying.

4.3. MAIN WETTING CURVE

Consider a dry soil subject to a wetting path under controlled suction. During this process, some air bubbles may remain trapped within the irregularities of solid grains. Additionally, some pores may remain dry because, for example, all bonds connecting to a cavity may saturate before the cavity can fill with water because it is larger than the current critical size. However, for simplicity it is initially considered that all pores can saturate. This means that the equations for the primary SWRC at wetting and drying are initially developed and later the secondary curves are obtained.

Fig. **2**(a) shows the basic unit for cavities in a bi-dimensional porous network. It consists of a central cavity connected to four concurrent bonds each of which is connected to an external cavity. Consider that this basic unit is initially dry and subject to a wetting process. By inspecting this unit it can be established that the central cavity can saturate only if the following two conditions are simultaneously fulfilled: a) its radius is smaller than the current critical radius meaning that water can intrude the cavity and b) at least one bond connected to this cavity is already saturated and linked to the bulk of water.

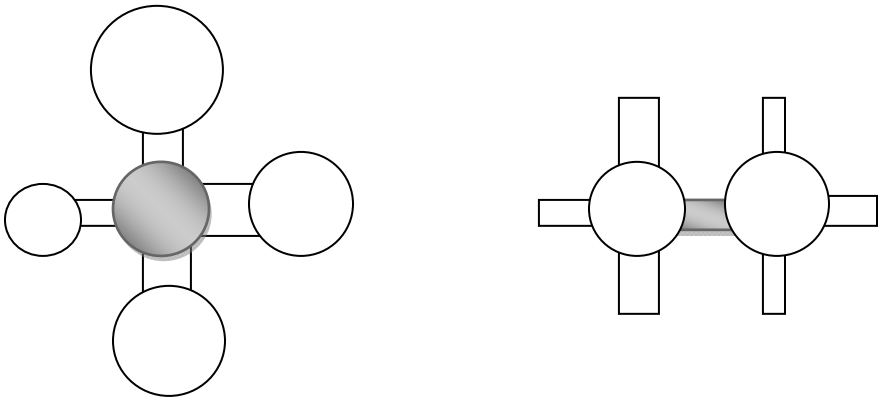

(a) (b)

Figure 2: Basic units for (a) cavities and (b) bonds.

The first condition is expressed as $S(R_C)$ according to Equation (4.1). The second condition implies that the cavity cannot saturate if all concurrent bonds remain filled with gas. This last condition can be expressed as $(1-L_{BI})^C$ where C

is the connectivity of the network and L_{BI} represents the probability for a bond to be saturated and linked to the bulk of water. As pores can only exhibit one of two possible states: saturated or dry, then $1-L_{BI}=G_{BI}$ represents the probability of the bond to be filled with gas. Accordingly, the condition that at least one bond concurrent to the considered cavity is saturated and linked to the bulk of water can be expressed as $\left[1-\left(1-L_{BI}\right)^{C}\right]$. Therefore, if L_{SI} represents the probability for a cavity to saturate during a wetting process, its value is given by the product of the two conditions listed above as they must occur simultaneously, in the form:

$$L_{SI}=S(R_C)\left[1-\left(1-L_{BI}\right)^{C}\right]\ldots \tag{4.3}$$

Additionally, Fig. **2**(b) shows the basic unit for bonds. This unit can be used to establish the conditions for bonds to saturate or dry. It consists of a central bond connecting two cavities each one connected to *C-1* additional bonds. Based on this unit, it can be said that a bond can saturate during a wetting process only when the two following conditions are simultaneously fulfilled: a) Its size is smaller than the critical radius and therefore it can be invaded by water and b) at least one of its two connected sites is already saturated and linked to the bulk of water. The first condition can be represented by $B\left(R_C\right)$ according to Equation (4.2). The second condition can be expressed as $\left[1-\left(1-L_{SI}\right)^{2}\right]$, where $\left(1-L_{SI}\right)^{2}={G_{SI}}^{2}$ represents the probability of the two connected sites to be filled with gas at the same time. Therefore, if L_{BI} represents the probability for a bond to saturate during a wetting process, its value is given by the product of the two aforementioned conditions as they must occur simultaneously:

$$L_{BI}=B\left(R_C\right)\left[1-\left(1-L_{SI}\right)^{2}\right]\ldots \tag{4.4}$$

By substituting the above relationship in Equation (4.3), it results in:

$$L_{SI}=S(R_C)\left\{1-\left[1-B\left(R_C\right)L_{SI}\right]^{C}\right\}=S\left(R_C\right)F_{SI}^{s}\left(R_C\right)\ldots \tag{4.5}$$

Note that the exponent *2* in Equation (4.4) has been replaced by *1* in Equation (4.5). This is so because in Equation (4.5), L_{SI} represents the probability of a cavity to be filled with water. Therefore, its C converging bonds have only one additional cavity to which they are connected to and this cavity must comply with

the condition of being saturated (white cavities in Fig. **2**(a)). Therefore, equation (4.4) transforms into $L_{BI} = B\left(R_C\right) L_{SI}$.

In addition, parameter $F_{SI}^{s}\left(R_C\right)$ represents the proportion of cavities filled with water with respect to the total number of cavities during a wetting process, in other words, it represents a saturation factor at wetting for the function $S\left(R_C\right)$ (see Fig. **1**(a)). Therefore, the volume of saturated cavities during a wetting process at the critical radius R_C ($V_{SI}^{s}(R_C)$) can be found by multiplying the reduction factor by the volume of cavities which sizes range from zero to R_C, in the form:

$$V_{SI}^{s}\left(R_C\right) = F_{SI}^{s}\left(R_C\right) \sum_{R=0}^{R_C} V_{SR}\left(R\right)$$

where $V_{SR}\left(R\right)$ represents the volume of all sites of size *R*. This equation implies that there is a proportion of $F_{SI}^{s}\left(R_C\right)$ of the total volume of sites which size ranges from zero to R_C that saturate at wetting (see Fig. **1**(a)).On the other hand, by substituting Equation (4.3) into Equation (4.4), it results:

$$L_{BI} = B\left(R_C\right)\left\{1-\left\{1-S\left(R_C\right)\left[1-\left(1-L_{BI}\right)^{C-1}\right]\right\}^{2}\right\} = B\left(R_C\right) F_{BI}^{s}\left(R_C\right) \ldots \qquad (4.6)$$

Note that the exponent *C* in Equation (4.3) has been replaced by *C-1* in Equation (4.6). This is so because in Equation (4.6), L_{BI} represents the probability of a bond to be filled with water. Therefore its two connected sites have only *C-1* additional bonds that must comply with the condition that at least one of them should be filled with water (white bonds in Fig. **2**(b)).

The parameter $F_{BI}^{s}\left(R_C\right)$ in the above relationship represents the proportion of bonds filled with water with respect to the total number of bonds which sizes range from zero to R_C, *i.e.,* it represents the saturation factor at wetting for the function $B\left(R_C\right)$ (see Fig. **1**(a)).

In the same manner as for cavities, the volume of saturated bonds can be found with the product of the reduction factor by the volume of bonds of a certain size, in the form:

$$V_{BI}^{s}\left(R_C\right)=F_{BI}^{s}\left(R_C\right)\sum_{R=0}^{R_C}V_{BR}\left(R\right)$$

where $V_{BR}\left(R\right)$ represents the volume of all bonds of size R.

It can be proved that Equations (4.5) and (4.6) are consistent as L_{SI} and L_{BI} are equal to zero and one when both $S(R_C)$ and $B\left(R_C\right)$ reach these same values. These equations can be solved by any iterative method and, in general, the convergence to the solution occurs in two or maximum three iterations with a tolerance of a thousandth.

Accordingly, the degree of saturation at wetting (S_{wI}) for a certain value of the critical radius (R_C) is given by:

$$S_{wI}\left(R_C\right)=\frac{V_{SI}^{s}\left(R_C\right)+V_{BI}^{s}\left(R_C\right)}{V_S+V_B}\ldots \tag{4.7}$$

where V_S and V_B represent the total volume of sites and bonds. And because the critical radius is dependent on the value of suction according to Equation (3.2), it is possible to plot the wetting SWRC in the axes of suction *vs.* degree of saturation.

Because the probabilistic model considers a network of infinite size, the effect of the borders is not taken into account. Either way, for very large networks this effect becomes negligible. For example, if it is assumed that at the borders of the network only solids and bonds can be found, then all bonds at the borders are connected to a single site. In a cubic network made of n sites by side, the proportion of bonds at the borders with respect to the total is approximately *3/n* which represents a very small value if it is acknowledged that n is of the order of several thousands to several millions per gram of material depending on the type of soil.

4.4. MAIN DRYING CURVE

Consider now a drying process (see Fig. **1**(b)). By inspecting the basic unit in Fig. **2**(a), it can established that a cavity should comply with one of the following two

conditions to remain saturated during a drying process: a) its radius is smaller than the critical size and therefore it cannot be drained or b) it is larger or equal to the critical size but at the same time, all its concurrent bonds are saturated. The first condition is represented by $S(R_C)$ according to Equation (4.1). The second condition can be expressed as $\left[1-S\left(R_C\right)\right]{L_{BD}}^{C}$, where L_{BD} represents the probability for a bond to be saturated during a drying process. Then, if L_{SD} represents the probability of a cavity to remain saturated and connected to the bulk of water during a drying process, its value is obtained by the addition of the two above conditions because they are complementary:

$$L_{SD} = S\left(R_C\right)+\left[1-S\left(R_C\right)\right]{L_{BD}}^{C} \ldots \tag{4.8}$$

Consider now the basic unit for bonds shown in Fig. **2**(b). According to this figure, it can be established that a bond requires complying with one of the following two conditions in order to remain saturated during a drying process: a) its size is smaller than the critical radius and therefore, water cannot be displaced by gas or b) it can be invaded by gas but its two connected sites are saturated. The first condition can be written as $B\left(R_C\right)$ according to Equation (4.2). The second condition states that the bond is able to drain (condition represented by $\left[1-B\left(R_C\right)\right]$) but it remains filled with water because its two connected sites are saturated (condition represented by ${L_{SD}}^{2}$). Then, this second condition can be expressed as $\left[1-B\left(R_C\right)\right]{L_{SD}}^{2}$. Therefore, if L_{BD} represents the probability for a bond to be saturated, its value is represented by the addition of these two conditions as they are complementary, resulting in:

$$L_{BD} = B\left(R_C\right)+\left[1-B\left(R_C\right)\right]{L_{SD}}^{2} \ldots \tag{4.9}$$

And by substituting Equation (4.9) into (4.8), it becomes:

$$L_{SD} = S\left(R_C\right)+\left[1-S\left(R_C\right)\right]\left\{B\left(R_C\right)+\left[1-B\left(R_C\right)\right]L_{SD}\right\}^{C} = S\left(R_C\right)+\left[1-S\left(R_C\right)\right]F_{SD}^{s}\left(R_C\right) \ldots \tag{4.10}$$

Notice that the exponent *2* in Equation (4.9) has been reduced to *1* in Equation (4.10) because this last equation represents the probability of a cavity to be saturated and therefore, its *C* concurrent bonds are only linked to an additional cavity (blank cavities in Fig. **2**(a)).

Also notice that in this case the reduction factor for the term $S(R_C)$ is unity, meaning that in spite of the size of adjacent elements, all cavities whose size is smaller than the critical size remain saturated at this stage. In contrast, those cavities larger or equal to the critical size have a proportion of $F_{SD}^{s} = \left\{B(R_C) + \left[1 - B(R_C)\right] L_{SD}\right\}^{C}$ saturated elements (see Fig. **1**(b)).

Furthermore, note that the element $\left[1 - S(R_C)\right] F_{SD}$ involves the product $\left[1 - S(R_C)\right]\left[1 - B(R_C)\right]$. This product is performed numerically in the model by discretizing the size distributions of cavities and bonds in the form $\left\{\Delta\left[1 - S(R_C)\right]\right\}\left\{\Delta\left[1 - B(R_C)\right]\right\}$. Because the constructive principle establishes that two adjacent bonds should not intersect each other then, all products where the size of bonds divided by a factor $\sqrt{2}$ (considering that the two adjacent bonds have the same size) is larger than the size of cavities, are discarded. This consideration has to be applied to all factors involving the product between the size distribution of cavities and bonds.

On the other hand, by substituting Equations (4.8) in (4.9) it results in:

$$L_{BD} = B(R_C) + \left[1 - B(R_C)\right]\left\{\left[1 - S(R_C)\right] {L_{BD}}^{C-1}\right\}^{2} = B(R_C) + \left[1 - B(R_C)\right] F_{BD}^{s}(R_C) \quad \ldots (4.11)$$

Notice that the exponent *C* in Equation (4.8) has been reduced to C-*1* in Equation (4.11) because this last equation represents the probability of a bond to be saturated and therefore, the sites connected to this bond only have *C-1* additional bonds that require to be liquid filled (bonds in white in Fig. **2**(b)). Also notice that the product $\left[1 - B(R_C)\right] S(R_C)$ has been removed from Equation (4.11). This is so because it involves the product of bonds of larger size ($1 - B(R_C)$) than the size of sites ($S(R_C)$), as it can be verified in Fig. **1**(b). And, because the constructive principle states that sites must be larger than the bonds they are connected to, this product becomes null. Finally, it can be verified that Equations (4.10) and (4.14) are consistent because L_{SD} as well as L_{BD} become zero and one when both $B(R_C)$ and $S(R_C)$ reach these same values.

With the above equations it is possible to determine the volume of bonds and sites that remain saturated during a drying process when the critical radius reaches the value R_C, as shown below:

$$V_{SD}^{s}\left(R_C\right)=\sum_{R=0}^{R_C}V_{SR}\left(R\right)+F_{SD}^{s}\left(R_C\right)\sum_{R=R_C}^{\infty}V_{SR}\left(R\right)$$

$$V_{BD}^{s}\left(R_C\right)=\sum_{R=0}^{R_C}V_{BR}\left(R\right)+F_{BD}^{s}\left(R_C\right)\sum_{R=R_C}^{\infty}V_{BR}\left(R\right)$$

These equations indicate that during a drying process all pores smaller than the critical size remain saturated as suction is not large enough to dry them whereas those bonds and sites larger or equal to the critical size have a proportion of F_{BD}^{s} and F_{SD}^{s} of saturated elements, respectively (see Fig. **1**(b)).

Accordingly, the degree of saturation of a sample subject to drying ($S_{wD}\left(R_C\right)$) is given by the relationship:

$$S_{wD}\left(R_C\right)=\frac{V_{SD}^{s}\left(R_C\right)+V_{BD}^{s}\left(R_C\right)}{V_S+V_B}\ldots \tag{4.12}$$

And because the value of R_C depends on suction (Equation (3.2)), then it is possible to plot the drying SWRC in the axes of degree of saturation *vs.* suction.

The degree of saturation given by Equations (4.12) and (4.7) varies from 1 to 0, however real soils subject to wetting-drying cycles never reach these values. Because of this, these equations are affected by two reduction factors: one representing the maximum and the other the residual degree of saturation of the soil as explained before.

It can be verified that these equations obtained by means of the basic unit concept are the same as those derived from a purely analytical procedure [59], although in this case they have been obtained in a simpler and more rational way. In addition, this procedure allows introducing the solid phase into the model as shown below.

4.5. SATURATED AND DRY VOLUMES

Once the volumes of cavities and bonds filled with water have been defined, it is possible to determine the saturated and the dry volumes during a wetting or drying

process. For this purpose it is convenient to consider the basic solid unit depicted in Fig. **3**. It represents the bi-dimensional case where a solid is encircled by four cavities and four bonds. These elements are called the surrounding pores and are shown in gray tones. In addition to these elements there are the external elements (shown in white) consisting in eight bonds and eight cavities. To these elements follow the farther external sites and bonds (not shown in the figure). Table **1** shows the number of surrounding, external and farther external sites and bonds in a bi- and tri-dimensional network. It also shows the equations defining the number of elements for each case. These equations are used to determine the probability of surrounding pores to be saturated or dry.

Consider that a soil sample undergoes a wetting process. Initially all pores are dry and suction is very large. Then, suction reduces by steps and the smallest pores are the first to saturate. By inspecting Fig. **3** it can be established that all pores surrounding a solid saturate when the following two conditions are fulfilled: a) all bonds and cavities surrounding the solid are smaller than the critical size, *i.e.,* they can be intruded by water and, b) simultaneously at least one external bond is already saturated and connected to the bulk of water.

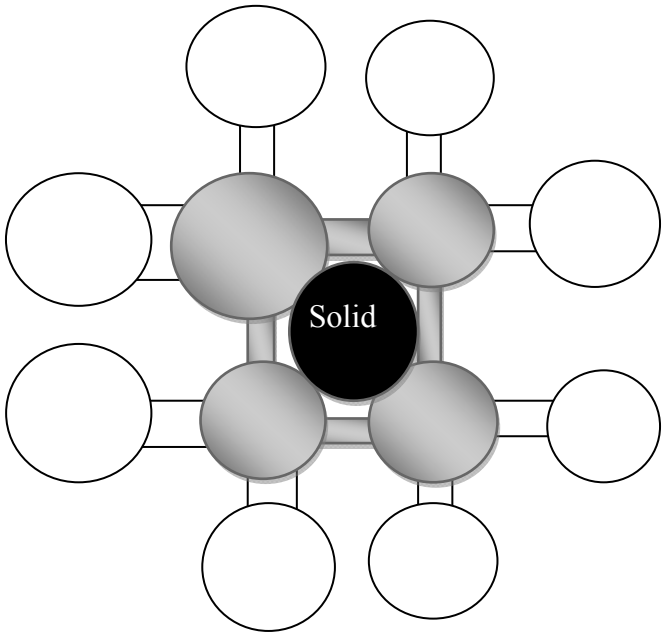

Figure 3: Basic unit for solids.

Table 1: Number of surrounding, external and farther external elements in a basic solid unit

Type	Element	Bi-dimensional	Tri-dimensional	Equation
Surrounding	Cavities	4	8	2(C-2)
	Bonds	4	12	4(C-3)
External	Cavities	8	24	C(C-2)
	Bonds	8	24	C(C-2)
Farther external	Cavities	12	72	6(C-2)(C-3)
	Bonds	20	96	$C(C-2)^2+2(6-C)$

The first condition can be written as $\left[S\left(R_C\right)\right]^{2(C-2)}\left[B\left(R_C\right)\right]^{4(C-3)}$ where the exponents *2(C-2)* and *4(C-3)* represent the number of surrounding cavities and bonds, respectively (refer to Table **1**). The second condition can be expressed as $1-\left[1-L_{BI_1}\right]^{C(C-2)}$ where the exponent *C(C-2)* represents the number of external bonds (see Table **1**) and L_{BI_1} represents the probability of an external bond to be liquid filled. When all the surrounding pores of a solid are saturated, they form a saturated unit. Therefore, the probability of having a saturated unit at wetting ($L_{\tilde{s}I}$) results from the product of the two aforementioned conditions (as they must be fulfilled simultaneously), in the form:

$$L_{\tilde{s}I}=\left[S\left(R_C\right)\right]^{2(C-2)}\left[B\left(R_C\right)\right]^{4(C-3)}\left\{1-\left[1-L_{BI_1}\right]^{C(C-2)}\right\}\ldots \tag{4.13}$$

Parameter L_{BI_1} can be obtained from Equations (4.3) and (4.4) but with different exponents as the number of connected elements in this case change. For example, exponent C in Equation (4.4), representing the number of bonds connected to a single cavity in the basic cavity unit, transforms into $\dfrac{C\left(C-2\right)^2+2\left(6-C\right)}{C\left(C-2\right)}$ which represents the number of farther external bonds connected to a single external cavity. This value is obtained by dividing the corresponding equations indicated in Table **1**. Also, exponent 2 in Equation (4.6) transforms into 1 as all external bonds are connected to a single external site (refer to Table **1**). Therefore, the expression for L_{BI_1} results in:

$$L_{BI_1} = B(R_C)\,S(R_C)\left[1-\left[1-L_{BI_1}\right]^{\frac{C(C-2)^2+2(6-C)}{C(C-2)}}\right]$$

A similar procedure can be applied to determine the probability that a solid is completely surrounded by pores filled with gas and thus appertains to the dry fraction. Consider again the basic unit shown in Fig. **3**. By inspecting this figure it can be concluded that all pores (cavities and bonds) around a solid remain dry as long as all surrounding cavities keep dry. Therefore, if $G_{\tilde{s}I}$ represents the probability of a solid to be surrounded by pores filled with gas and, G_{SI} is the probability of a cavity to be filled with gas, the above condition writes:

$$G_{\tilde{s}I} = G_{SI}{}^{2(C-2)} = \left(1-L_{SI_1}\right)^{2(C-2)} \ldots \tag{4.14}$$

where the exponent *2(C-2)* represents the number of surrounding cavities and L_{SI_1} represents the probability of a surrounding site to be liquid filled. The value of parameter L_{SI_1} can be obtained from a relationship similar to Equation (4.5) except that exponent C is substituted by *C*/2 which represents the number of external bonds connected to a single surrounding site, according to Table **1**. By doing this substitution, Equation (4.5) transforms into:

$$L_{SI_1} = S(R_C)\left\{1-\left[1-B(R_C)\,L_{SI_1}\right]^{C/2}\right\}$$

By solving this equation, the value of $G_{\tilde{s}I}$ can be obtained from Equation (4.14).

Consider now a drying process. Initially all pores are saturated and suction is equal to zero. Then, suction increases by steps and the largest pores start to dry. By inspecting Fig. **3** it can be concluded that all surrounding bonds remain saturated as long as all surrounding sites also do so. Therefore, the probability that all pores surrounding a solid are saturated during a drying process ($L_{\tilde{s}D}$) is equal to the probability that all surrounding cavities remain saturated:

$$L_{\tilde{s}D} = L_{SD_1}{}^{2(c-2)} \ldots \tag{4.15}$$

where the exponent $2(C-2)$ is the number of sites surrounding a solid and L_{SD_1} represents the probability of surrounding sites to be liquid filled during a drying process. The relationship to determine L_{SD_1} is similar to Equation (4.10) except that exponent C transforms into C/2 which represents the number of external bonds connected to a single surrounding site according to Table **1**. Therefore, by doing this substitution, Equation (4.10) transforms into:

$$L_{SD_1} = S(R_C) + \left[1 - S(R_C)\right]\left\{B(R_C) + \left[1 - B(R_C)\right] L_{SD_1}\right\}^{C/2} \ldots \quad (4.16)$$

By solving Equation (4.16) it is possible to obtain the value of $L_{\tilde{s}D}$ from Equation (4.15).

Moreover, the conditions required for all surrounding pores of a solid to dry during a drying process are the following: a) all surrounding cavities and bonds must be able to dry and b) at least one external bond should already be dry and connected to the bulk of gas. The first condition writes $\left[1 - S(R_C)\right]^{2(C-2)}\left[1 - B(R_C)\right]^{4(C-3)}$. The second condition can be expressed as $1 - \left(1 - G_{BD_1}\right)^{C(C-2)} = 1 - L_{BD_1}{}^{C(C-2)}$ where G_{BD_1} and L_{BD_1} represent the probability of an external bond to be filled with gas and liquid, respectively. Then, if $G_{\tilde{s}D}$ represents the probability of having a dry solid unit during a drying process, its value is given by the product of the two aforementioned conditions as they must happen simultaneously:

$$G_{\tilde{s}D} = \left[1 - S(R_C)\right]^{2(C-2)}\left[1 - B(R_C)\right]^{4(C-3)}\left(1 - L_{BD_1}{}^{C(C-2)}\right) \ldots \quad (4.17)$$

The value of L_{BD_1} can be obtained from the combination of Equations (4.8) and (4.9) but with different exponents according to the number of connected elements. According to Table **1**, exponent C in Equation (4.8) transforms into $\dfrac{C(C-2)^2 + 2(6-C)}{C(C-2)}$ which represent the number of farther external bonds connected to a single external cavity while exponent 2 in Equation (4.9) transforms into 1 because it represents the number of external bonds connected to a single external cavity (refer to Table **1**). By combining the resulting equations, it becomes:

$$L_{BD_1} = B\left(R_C\right) + \left[1 - B\left(R_C\right)\right]\left\{\left[1 - S\left(R_C\right)\right] L_{BD_1}^{\frac{C(C-2)^2 + 2(6-C)}{C(C-2)}}\right\}$$

By solving the relationship above, the value of $G_{\tilde{s}D}$ can be obtained with Equation (4.17).

With these relationships it is now possible to define the distribution of saturated cavities and bonds as a function of their size. For example, in the case of sites, Equation (4.13) can be rewritten in the following form:

$$L_{\tilde{s}I} = S\left(R_C\right) S\left(R_C\right)^{2C-5} B\left(R_C\right)^{4(C-3)} \left\{1 - \left[1 - L_{BI_1}\right]^{C(C-2)}\right\} = F_{SI}^s S\left(R_C\right) = F_{SI}^s \int_0^{R_C} V_{RS}\left(R\right) dR$$

where F_{SI}^s represents the saturation factor for cavities in a solid unit. Then, the volume of saturated cavities of size R is represented by:

$$dV_S^s = F_{SI}^s V_S V_{RS}\left(R\right) dR$$

And the total volume of saturated cavities (V_S^s) is:

$$V_S^s = F_{SI}^s V_S \int_0^{R_C} V_{RS}\left(R\right) dR = F_{SI}^s S\left(R_C\right) V_S = L_{\tilde{s}I} V_S$$

In the same way the distribution of the volume of saturated bonds V_B^s as a function of their size can be obtained. In that case, the saturation factor for the relative volume of bonds $\left(F_{BI}^s\right)$ results from Equation (4.13) rewritten in the following form:

$$L_{\tilde{s}I} = B\left(R_C\right) B\left(R_C\right)^{4C-13} S\left(R_C\right)^{2(C-2)} \left\{1 - \left[1 - L_{BI_1}\right]^{C(C-2)}\right\} = F_{BI}^s B\left(R_C\right)$$

Then, the volume of saturated bonds of size R is given by $dV_B^s = F_{BI}^s V_B V_{RB}\left(R\right) dR$ and, the total volume of saturated bonds (V_B^s) is:

$$V_B^s = F_{BI}^s V_B \int_0^{R_C} V_{RB}\left(R\right) dR = F_{BI}^s B\left(R_C\right) V_B = L_{\tilde{s}I} V_B$$

Finally, because there is a correlation in sizes between cavities and solids as explained before, the volume of saturated solids ($V_{\tilde{s}I}^{s}$) can be determined as $V_{\tilde{s}I}^{s} = L_{\tilde{s}I}\ V_{\tilde{s}}$. Once the volume of saturated cavities, bonds and solids have been defined, it is possible to define the volume of the saturated fraction:

$$f^{s} = \frac{V^{s}}{V} = \frac{V_{S}^{s} + V_{B}^{s} + V_{\tilde{s}}^{s}}{V}$$

The same procedure can be applied to define the dry fraction of the soil. For example, in the case of a drying process, Equation (4.17) can be rewritten as:

$$G_{\tilde{s}D} = \left(1 - L_{BD_1}{}^{C(C-2)}\right)\left[1 - B\left(R_C\right)\right]^{4(C-3)}\left[1 - S\left(R_C\right)\right]^{2C-5}\left[1 - S\left(R_C\right)\right] = F_{SD}^{d}\left[1 - S\left(R_C\right)\right]$$

where F_{SD}^{d} represents the dry factor for cavities in the solid unit during a drying process. Then, the volume of dry cavities of a certain size ($dV_{S}^{d}\left(R\right)$) can be found by multiplying the dry factor F_{SD}^{d} by the volume of cavities of that specific size. Finally, the total volume of saturated cavities is obtained by the addition of all saturated cavities from size R_C to the maximum size R_{max}, that is to say $V_{S}^{d} = \int_{R_C}^{R_{\max}} dV_{S}^{d}\left(R\right) = F_{SD}^{d} V_{S} \int_{R_C}^{R_{\max}} V_{RS}\left(R\right)$. By applying the same procedure, the volume of dry bonds V_{B}^{d} can be obtained. Moreover, the volume of solids of the dry fraction is given by $V_{\tilde{s}}^{d} = G_{\tilde{s}D}\ V_{\tilde{s}}$ and finally, the dry fraction is:

$$f^{d} = \frac{V^{d}}{V} = \frac{V_{S}^{d} + V_{B}^{d} + V_{\tilde{s}}^{d}}{V}$$

Once f^{s} and f^{d} have been established, it is possible to define the value of the unsaturated fraction f^{u} using Equation (2.12). Furthermore, the degree of saturation of the unsaturated fraction can be obtained by dividing the volume of water by the volume of voids both belonging to the unsaturated fraction. The volume of water of the unsaturated fraction is obtained by subtracting the volume of bonds and cavities belonging to the saturated fraction from the volume of pores filled with water. On the other hand, the volume of voids of the unsaturated

fraction can be obtained by subtracting the saturated and dry volumes of bonds and cavities from the total volume of voids, that is to say:

$$S_w^u = \frac{V_w^u}{V_v^u} = \frac{V_w - V_w^s}{V_v - V_v^s - V_v^d} = \frac{V_w - V_S^s - V_B^s}{V_v - V_S^s - V_B^s - V_S^d - V_B^d}$$

Once parameters f^s, f^u and S_w^u have been established, it is possible to determine the mean effective stress (Equation (2.14)) and the shear strength (Equation (2.18)) of a soil subject to any value of suction during a wetting or drying path.

In principle, the parameters required by the porous-solid model are the PSD and the GSD, the voids ratio, the connectivity and a shape parameter for the fine fraction. All these parameters are discussed below.

When the PSD is obtained from porosimetry tests, it is possible to discriminate the volume of mesopores and macropores because usually porosimetry tests performed on soils show a bimodal distribution: the one with smaller sizes corresponds to the mesopores and the other with larger sizes corresponds to the macropores [45]. However, these tests do not permit the determination of the size distribution of bonds mainly because the volume of these elements is negligible compared to that of cavities. Therefore, in order to define the size distribution for bonds, use can be made of two properties of SWRCs: the first one establishes that there is a unique relationship between the PSD and the SWRCs [60]. The second is that the drying branch depends mainly on the size distribution of bonds while the wetting branch is dependent mainly on the size distribution of cavities [28]. In this way, by fitting the numerical drying curve with the experimental results, it is possible to define the size distribution for bonds. This process begins by proposing a size distribution for these elements while the size distribution for cavities is obtained from a porosimetry test. Then the numerical drying SWRC is compared with the experimental one and the size distribution for bonds is subsequently adjusted until the best fit is obtained. If porosimetry data is not available, then both SWRCs are required and the adjusting process includes the size distributions for macropores, mesopores and bonds. The PSD and GSD of the material can be introduced directly into the model in the form of tables or they can

be adjusted using proper mathematical functions. Presently, the model uses single, double or triple logarithmic normal distributions to adjust the experimental data. These functions have proven to be sufficiently flexible in order to accurately simulate the pore and GSDs for different types of soils. Direct porosimetry tests such as image analysis of micrographs or indirect methods such as Mercury Intrusion Porosimetry (MIP) or nitrogen adsorption can be used to determine the PSD of a soil.

The connectivity of a two- and a three-dimensional network is 4 and 6, respectively. However, direct determination techniques indicate that real soils show connectivity values between 2 and 6 as mention before [55]. In the case of the probabilistic porous-solid model, the connectivity (which in fact represents the value of the mean connectivity of the sample) can take integer or fractional values to better reflect the structural characteristics of a particular soil.

Finally, as the size distribution of solids plays a main role in the determination of the volume of saturated solids, it is important to take into account the hypothesis considered to obtain this distribution. For example, one of the most widely used methods to obtain the GSD of fine soils is the hydrometer test. However, this method assumes that solid particles have rounded shapes. This hypothesis may be adequate for the grains of sands but not for fine particles and especially not for clays which in general show flat shapes. For this reason, a shape factor (S_f) needs to be introduced into the porous-solid model, as explained before. This parameter adjusts the real volume of fine material ensuring that the numerical voids ratio corresponds to the experimental one. The shape factor comes close to unity for rounded sands but reduces drastically in the case of plastic clays.

4.6. SCANNING CURVES

When an inversion during a wetting or drying process takes place, the resulting paths are called scanning curves. The mechanisms of wetting or drying for sites and bonds in this case are exactly the same as those described for the boundary curves, except that the initial conditions change, as it is explained below.

4.6.1. Drying-Wetting Cycle

Fig. **1**(b) shows the proportion of pores filled with gas at a certain stage of a drying process. In the case of a drying-wetting cycle, only those bonds and sites already invaded by gas during the drying stage (G_{BDR} and G_{SDR}, respectively) can be replenished with water, and therefore the values of L_{SI} and L_{BI} in Equations (4.5) and (4.6) should be substituted by the terms $\left(L_{SDI}-L_{SDR}\right)/G_{SDR}$ and $\left(L_{BDI}-L_{BDR}\right)/G_{BDR}$, where L_{SDI} and L_{BDI} represent the probability for a site or a bond, respectively, to be liquid-filled after an inversion in drying and L_{SDR} and L_{BDR} represent the probability for a site and a bond to be liquid-filled at the moment of inversion, respectively. Additionally, the probability functions $S\left(R_C\right)$ and $B\left(R_C\right)$, should also be scaled according to the following equations:

$$S_A\left(R_C\right)=\frac{S\left(R_C\right)-S_R\left(R_C\right)}{1-S_R\left(R_C\right)}, \qquad B_A\left(R_C\right)=\frac{B\left(R_C\right)-B_R\left(R_C\right)}{1-B_R\left(R_C\right)}$$

where $S_A\left(R_C\right)$ and $B_A\left(R_C\right)$ are the adjusted probability functions for sites and bonds, respectively. Finally, knowing that $G_{BDR}=1-L_{BDR}$ and $G_{SDR}=1-L_{SDR}$ Equations (4.5) and (4.6) transform into:

$$L_{SDI}=\left(1-L_{SDR}\right)S_A\left(R_c\right)\left[1-\left(1-\frac{L_{SDI}-L_{SDR}}{1-L_{SDR}}B_A\left(R_C\right)\right)^C\right]+L_{SDR} \quad \ldots \quad (4.18)$$
$$=\left(1-L_{SDR}\right)S_A\left(R_c\right)F_{SDI}^s\left(R_C\right)+L_{SDR}$$

$$L_{BDI}=\left(1-L_{BDR}\right)B_A\left(R_C\right)\left\{1-\left\{1-S_A\left(R_C\right)\left[1-\left(1-\frac{L_{BDI}-L_{BDR}}{1-L_{BDR}}\right)^{C-1}\right]\right\}^2\right\}+L_{BDR} \quad \ldots (4.19)$$
$$=\left(1-L_{BDR}\right)B_A\left(R_C\right)F_{BDI}^s\left(R_C\right)+L_{BDR}$$

The above equations ensure that the adjusted probability functions for sites and bonds ($S_A\left(R_C\right)$ and $B_A\left(R_C\right)$) continue varying from one to zero and thus the equations describing L_{BDI} and L_{SDI} remain auto-consistent.

With the above equations it is possible to determine the volume of bonds and sites that remain saturated once the inversion in the wetting process initiates:

$$V_{SDI}^{s}\left(R_C\right)=\sum_{R=0}^{R_R}V_{SR}\left(R\right)+\frac{1-L_{SDR}}{1-S\left(R_R\right)}\left[F_{SDI}^{s}\left(R_C\right)\sum_{R=R_R}^{\infty}V_{SR}\left(R\right)\right]$$

$$V_{BDI}^{s}\left(R_C\right)=\sum_{R=0}^{R_R}V_{BR}\left(R\right)+\frac{1-L_{BDR}}{1-B\left(R_R\right)}\left[F_{BDI}^{s}\left(R_C\right)\sum_{R=R_R}^{\infty}V_{BR}\left(R\right)\right]$$

where R_R and R_C represent the critical radius at the moment of inversion and the critical radius during the wetting stage, respectively. Parameters $F_{SDI}^{s}(R_C)$ and $F_{BDI}^{s}(R_C)$ can be obtained from Equations (4.18) and (4.19) in the form:

$$F_{SDI}^{s}\left(R_C\right)=\left[1-\left(1-\frac{L_{SDI}-L_{SDR}}{G_{SDR}}B_A\left(R_C\right)\right)^{C}\right]$$

$$F_{BDI}^{s}(R_C)=\left\{1-\left\{1-S_A\left(R_C\right)\left[1-\left(1-\frac{L_{BDI}-L_{BDR}}{G_{BDR}}\right)^{C-1}\right]\right\}^{2}\right\}$$

The degree of saturation of the system is obtained as expressed in Equation (4.7), except that $V_{SI}^{s}\left(R_c\right)$ and $V_{BI}^{s}\left(R_c\right)$ are substituted by $V_{SDI}^{s}\left(R_c\right)$ and $V_{BDI}^{s}\left(R_c\right)$, respectively.

4.6.2. Wetting-Drying Cycle

When an inversion occurs at a certain stage of a wetting path, the distribution of sites and bonds invaded by water is, approximately, that shown in Fig. **1**(a). Therefore, during the drying stage, only those sites and bonds already invaded by fluid during the wetting phase are able to drain. Consequently, the limits of the probability for a site or a bond to dry during the drying process goes from their value at the moment of inversion (L_{SIR} and L_{BIR}, respectively) to zero for a completely dry soil. Therefore, the values of L_{BD} and L_{SD} in Equations (4.9) and (4.10), should be scaled in the form of L_{BID}/L_{BIR} and L_{SID}/L_{SIR}, respectively, where L_{BID} and L_{SID} represent

the probability for a bond and a site to be liquid-filled at drying after being subjected to wetting, respectively. The probability functions $S(R_C)$ and $B(R_C)$, should also be scaled according to the following equations:

$$S_A(R_C) = \frac{S(R_C)}{S_R(R_C)}, \qquad B_A(R_C) = \frac{B(R_C)}{B_R(R_C)}$$

where $S_A(R_C)$ and $B_A(R_C)$ represent the adjusted values of the probability functions for sites ($S(R_C)$) and bonds ($B(R_C)$), while $S_R(R_C)$ and $B_R(R_C)$ represent the probability values for sites and bonds at the moment of inversion, respectively.

With these considerations, Equations (4.10) and (4.11) transform into:

$$L_{SID} = \left\{ S_A(R_C) + \left[1 - S_A(R_C)\right] \left\{ B_A(R_C) + \left[1 - B_A(R_C)\right] \left(L_{SID}/L_{SIR}\right) \right\}^C \right\} L_{SIR}$$

$$= \left\{ S_A(R_C) + \left[1 - S_A(R_C)\right] F_{SID}^s \right\} L_{SIR} \qquad \ldots \quad (4.20)$$

$$L_{BID} = \left\{ B_A(R_C) + \left(1 - B_A(R_C)\right) \left\{ \left[1 - S_A(R_C)\right] \left(L_{BID}/L_{BIR}\right)^{C-1} \right\}^2 \right\} L_{BIR}$$

$$\ldots \quad (4.21)$$

$$= \left\{ B_A(R_C) + \left(1 - B_A(R_C)\right) F_{BID}^s \right\} L_{BIR}$$

The above equations ensure that the adjusted probability functions for sites ($S_A(R_C)$) and bonds ($B_A(R_C)$) remain varying from one to zero, and thus the equations defining L_{BID} and L_{SID} remain auto-consistent. In this form, when an inversion takes place, the sign of the increment of the probability functions $S(R_C)$ or $B(R_C)$ change, and they continue increasing or reducing until a new inversion takes place.

With the above equations it is possible to determine the volume of bonds and sites that remain saturated once the wetting of the sample stops and the drying process initiates:

$$V_{SID}^{s}\left(R_C\right)=\frac{L_{SIR}}{S\left(R_R\right)}\left[\sum_{R=0}^{R_{CR}}V_{SR}\left(R\right)+F_{SID}^{s}\left(R_C\right)\sum_{R=R_{CR}}^{R_R}V_{SR}\left(R\right)\right]$$

$$V_{BID}^{s}\left(R_C\right)=\frac{L_{BIR}}{B\left(R_R\right)}\left[\sum_{R=0}^{R_{CR}}V_{BR}\left(R\right)+F_{BID}^{s}\left(R_C\right)\sum_{R=R_{CR}}^{R_R}V_{BR}\left(R\right)\right]$$

where R_R and R_C represent the critical radius at the moment of inversion and the critical radius during the drying stage, respectively. Parameters F_{SID}^{s} and F_{BID}^{s} can be obtained from Equations (4.20) and (4.21) in the form:

$$F_{SID}^{s}\left(R_C\right)=\left\{B_A\left(R_C\right)+\left[1-B_A\left(R_C\right)\right]\left(L_{SID}/L_{SIR}\right)\right\}^{C}$$

$$F_{BID}^{s}(R_C)=\{[1-S_A(R_C)](L_{BID}/L_{BIR})^{C-1}\}^{2}$$

The degree of saturation of the system is obtained as expressed in Equation (4.12), except that $V_{SD}^{s}\left(R_C\right)$ and $V_{BD}^{s}\left(R_C\right)$ are substituted by $V_{SID}^{s}\left(R_C\right)$ and $V_{BID}^{s}\left(R_C\right)$, respectively.

The above equations can be used to simulate the secondary boundary curves as well as the scanning curves when they are plotted either on the axes of equivalent volumetric water content or degree of saturation *versus* suction. The equivalent volumetric water content Θ, was defined by van Genuchten [61] in the form $\Theta=\left(\theta-\theta_r\right)/\left(\theta_s-\theta_r\right)$, where θ_r and θ_s represent the residual and saturated volumetric water content, respectively, and θ is the current volumetric water content of the sample. At its present stage, the probabilistic porous-solid model does not consider the collapse of pores experienced by the material during loading or drying [45].

With the above equations, a very simple computer program can be created to produce results in seconds. This model offers important advantages when compared with computational network models. Usually these last models require heavy programs that are difficult to manipulate and require several hours to produce results for large networks. Another advantage of the probabilistic model is that all pore and solid sizes are well-represented, no matter if their size

distribution curves involve several orders of magnitude, which is certainly not the case for computational network models. This has important consequences regarding the influence of the size of the network on the results especially for materials with large size distributions. While the probabilistic model considers an infinite network, computational models require defining the size of the network and it is possible that the largest network that a PC can handle may not be sufficient to nullify the size effect. Additionally the computer code of the probabilistic model can be easily adapted to other computer programs to develop a general constitutive model for soils.

4.7. VALIDATION OF THE PROBABILISTIC MODEL

The probabilistic model can be evaluated by comparing its results with those produced by a computational network model using a simple normal distribution with low standard deviation for the sizes of sites and bonds. Fig. **4** shows this comparison for the following data R_S = 1.0 μm, δ_S = 2.5, R_B = 0.2 μm and δ_B = 2.0, where R_S and R_B represent the mean size for sites an bonds whereas δ_S and δ_B are the standard deviation for sites and bonds, respectively. The connectivity in the probabilistic model was taken as four (bi-dimensional case) and the size of the network in the computational network model was 500 x 500. Notice that the results produced by both models regarding the SWRC are practically the same.

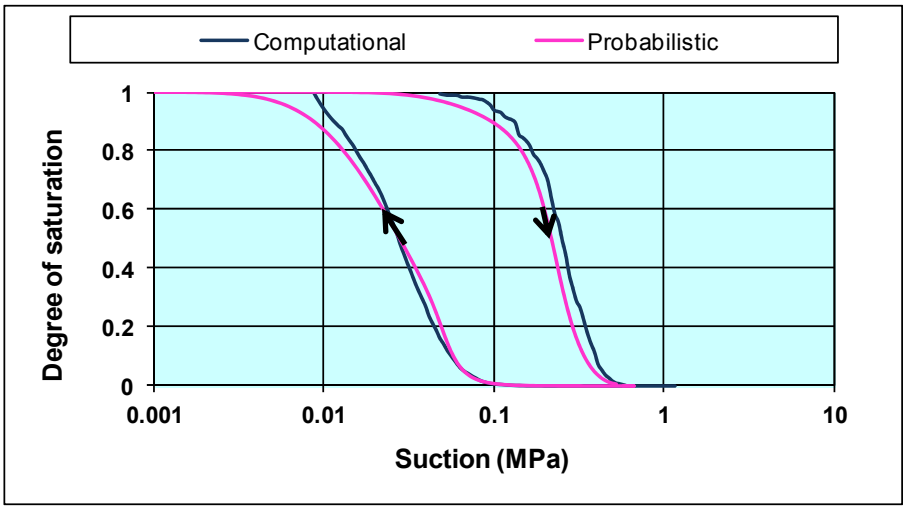

Figure 4: Results comparison between the computational and probabilistic model.

The most important difference is that the drying curve generated by the probabilistic model is slightly displaced to the left when compared to that produced by the computational model. Also, the wetting curve of the probabilistic model shows a more gradual variation close to saturation than that of the computational model. This last detail is linked to the small number of pores of the largest size that results during the determination of the number of pores of each size in the computational network model.

To validate the porous model described above, the experimental results reported by Brown [62] and Enustun and Enuysal [63] are used. Brown [62] reported the main hysteresis loop and some scanning curves for a sample of Vycor glass using gas xenon in isothermal conditions. His experimental results are reported in Fig. **5** in the axes of equivalent volumetric water content *versus* suction. Additionally, Enustun and Enuysal [63] determined the size distribution of this same material by filling the pores with metal, leaching away the glass and imaging the residue in an electron microscope. Their results are presented in Fig. **6** in the axes of frequency *vs.* pore radius.

Fig. **5** also shows the comparison between numerical and experimental results for the main wetting and drying curves as well as for various scanning curves at wetting and drying. In this case, the main numerical adsorption and desorption curves were fitted with the experimental results by means of the iterative PSD method earlier described. For this case a normal distribution for mesopores and bonds was sufficient to properly describe the wetting and drying SWRC. Given the uniform porosity of the Vycor glass, the use of macropores to simulate the SWRC was not necessary. The size distribution parameters used to elaborate these figures were: $\overline{R}_S = 0.0020\mu m$, $\delta_S = 0.001\mu m$, $\overline{R}_B = 0.0013$ μm, $\delta_B = 0.0003$ μm. The numerical scanning curves were obtained by defining the water content at which the inversion from drying to wetting takes place. A good general agreement between experimental and numerical results can be observed.

Fig. **6** also presents the numerical size distribution obtained from the iterative procedure to obtain the main drying and wetting curves shown in Fig. **5**. It can be observed that the numerical size distribution for sites shows approximately the

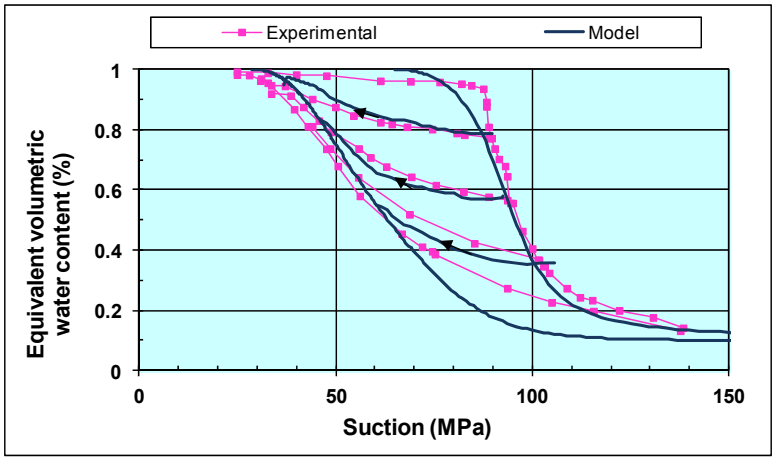

(a)

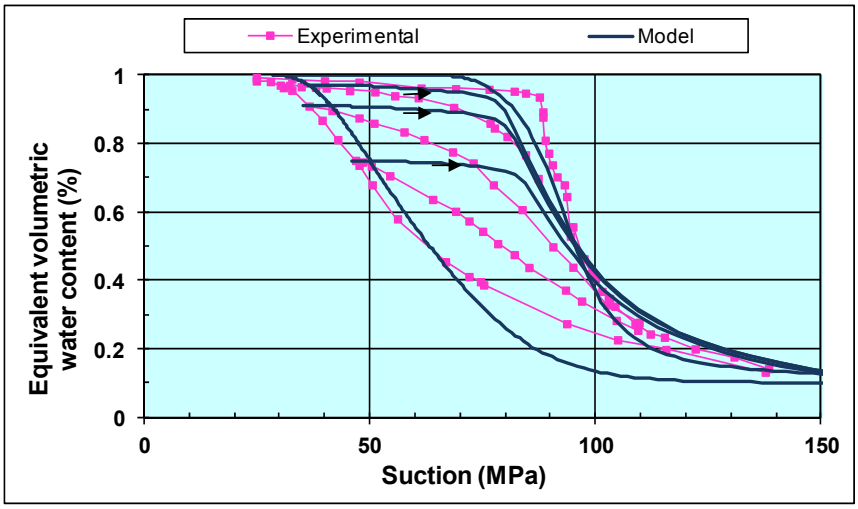

(b)

Figure 5: Numerical and experimental main retention curves and scanning curves for (a) drying-wetting and (b) wetting-drying cycles. Experimental results by Brown [62].

same shape than the experimental data. However, a horizontal displacement of approximately 1nm is observed between both curves. A similar result was obtained by Mason [64] when he applied the percolation theory to reproduce the main hysteresis loops of the Vycor glass. Mason [64] attributes this difference to the reduction in the thickness of the adsorbed water layer when casting the metal into the pores. In any case, this difference is rather small and shows the degree of precision that the model can reach when simulating wetting-drying processes.

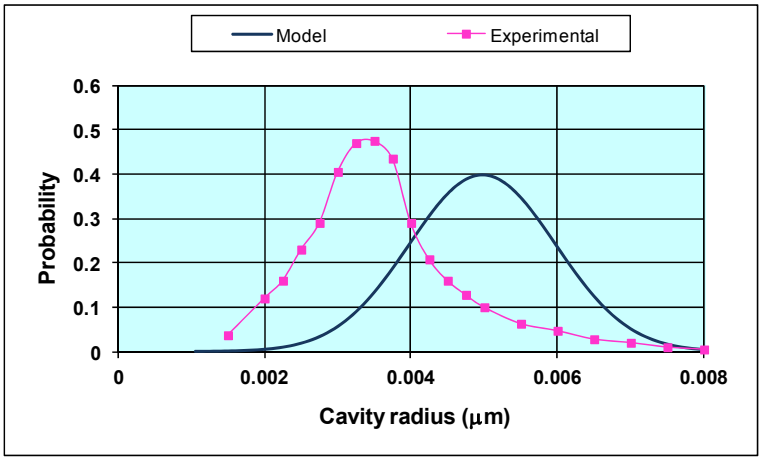

Figure 6: Numerical and experimental size distribution for cavities (experimental results after Enustun and Enuysal, [63]).

4.8. PARAMETRIC ANALYSIS

Figs. **7-9** show the influence of the porosimetry on the wetting and drying SWRC. For simplicity, a logarithmic normal distribution for bonds and sites has been used. In a logarithmic normal distribution the only parameters required are the mean size ($\overline{R}$) and the standard deviation (δ) for each element. In addition, it is necessary to define the length of the bonds.

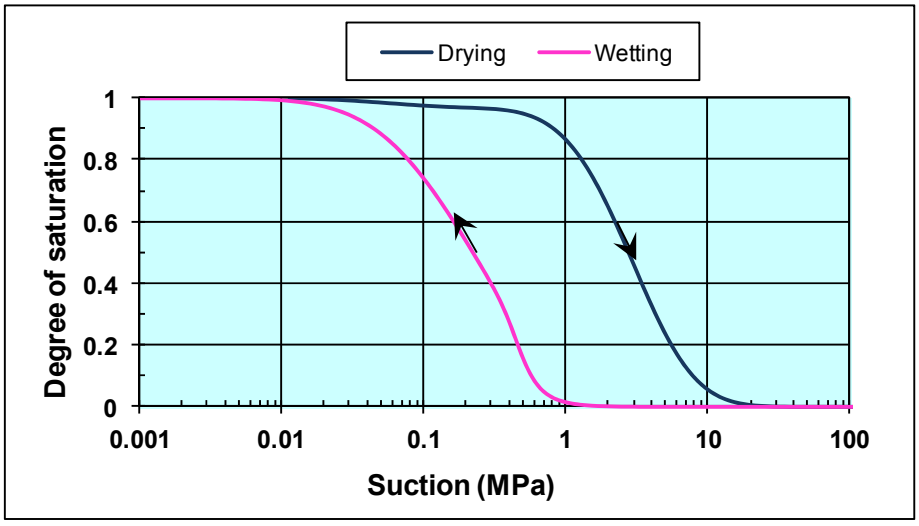

Figure 7: Model results with $\overline{R}_S$ =.03 μm, $\overline{R}_B$ =.003 μm, δ_S =3.5 and δ_B =3.5.

The wetting and drying curves in Fig. **7** were obtained using the following parameters: $\overline{R}_S$=.03μm, $\overline{R}_B$=.003μm, δ_S=3.5 and δ_B=3.5. In Fig. **8** the following parameters were used: $\overline{R}_S$=.03μm, $\overline{R}_B$=.003μm, δ_S=2.5 and δ_B=2.5. Finally, Fig. **9** was obtained using $\overline{R}_S$=.1μm. $\overline{R}_B$=.03μm, δ_S=3.5 and δ_B=3.5. The considered length of the bonds was 0.001μm.

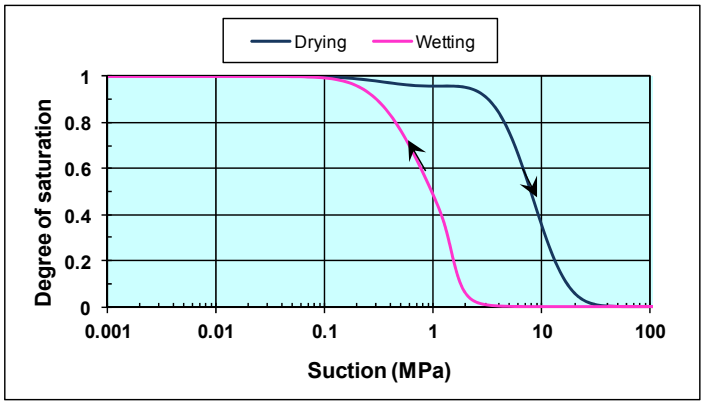

Figure 8: Model results with $\overline{R}_S$=.03μm, $\overline{R}_B$=.003μm, δ_S=2.5 and δ_B=2.5.

When these figures are compared, the influence of each parameter can be determined. For example, when comparing Figs. **7** and **8**, the effect of the standard deviation on bonds and sites can be observed. When comparing Figs. **7** and **9**, the effect of the mean size on bonds and sites is observed and finally when comparing Figs. **8** and **9**, the combined effect of mean size and standard deviation is noticed. According to these comparisons, it can be concluded that the standard deviation of mesopores (δ_S) and bonds (δ_B) defines the extension of the curves on the axis of suction. This is so because this parameter defines the range of values of the pores for each element. Then, large standard deviations represent well graded materials with many different sizes of pores and the SWRC extends along the suction axis. In contrast, small standard deviations represent poorly graded materials with uniform pore sizes and therefore, the SWRC appears more vertical.

On the other hand, the mean size of sites ($\overline{R}_S$) and bonds ($\overline{R}_B$) defines the position of the wetting and drying curves in the axis of suction, respectively. For example, small mean sizes indicate the presence of fine soils and the curves are

located at the zone of large suctions. On the contrary, large mean values indicate the presence of granular soils and the curves appear in the zone of small suctions. Also, as pointed out before, the parameters for sites affect mainly the wetting curve while those for bonds affect the drying curve. Finally, when the mean values for sites and bonds approach each other, the curves also get closer and *vice versa*. The length of bonds modifies the volume occupied by these elements but has no major influence on these curves.

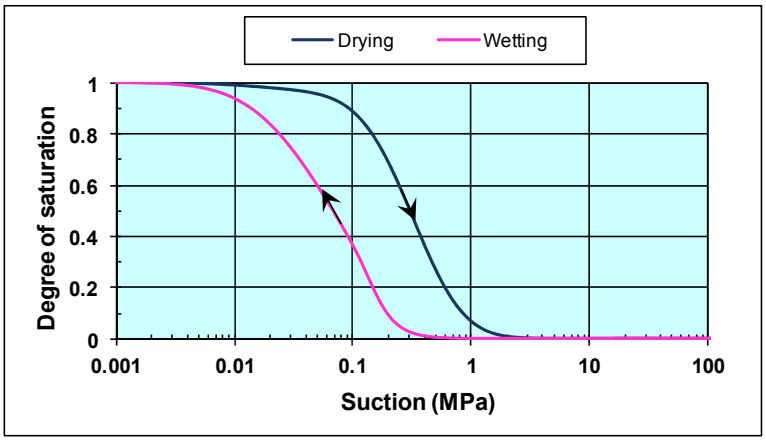

Figure 9: Model results with $\overline{R}_S$=.1μm, $\overline{R}_B$=.03μm, δ_S=3.5 and δ_B=3.5.

CHAPTER 5

Applications of the Porous-Solid Model

Abstract: In the previous chapter, a probabilistic porous-solid model adequate for the simulation of soil-water retention curves of soils was developed. In this chapter, the model is used to interpret more realistically the results of mercury intrusion porosimetry experiments. Moreover, it is used to obtain the pore size distribution of different soils while using both boundary branches of the retention curve as data. The numerical and experimental comparisons for different soils show that the model approximately reproduces the pore size distribution obtained from mercury intrusion porosimetry tests. Finally, the procedure to adjust the numerical and experimental soil-water retention curves in order to obtain the pore size distribution of soils is presented herein.

Keywords: Mercury intrusion porosimetry tests, scanning electron micrographs, pore size distribution, grain size distribution, superficial tension, contact angle, soil-water retention curve, critical radius, relative volume, macropores, mesopores, micropores, hydro-mechanical coupling, soil mixtures, logarithmic normal distribution, mean size, standard deviation.

5.1. INTRODUCTION

One of the most popular methods to obtain the PSD of soils is Mercury Intrusion Porosimetry (MIP). MIP tests are made in pressure chambers filled with mercury (which is a non-wetting fluid) where a moisture-free soil sample is immersed. Then, the pressure in the chamber is progressively increased while the volume of intruded mercury in the pores of soil is recorded. The diameter of the intruded pores at certain pressure is obtained from the Laplace equation (Equation (3.2)), *via* the appropriate parameters of surface tension for the air-mercury interface and the contact angle between mercury and solid particles. Finally, a graph of the relative intruded volume *vs.* the size of the pores is generated. With these results, the sizes of both macropores and mesopores can be established. However, the unrealistic hypotheses made to determine the pore sizes, together with the impossibility of measuring the whole range of sizes [46], as well as doubts related to the deleterious effect of high mercury pressures on the size of pores for loose soils [65], and some inconsistencies on the application of data to correctly reproduce the SWRCs [66], require these results to be taken with caution and to be considered only as an approximation to the real PSD of the material.

Eduardo Rojas

5.2. MERCURY INTRUSION POROSIMETRY TESTS

Recently, the use of the MIP test to ascertain the PSD of soils has become quite popular in unsaturated soil mechanics, primarily because of its simplicity. To perform this test, a sample of around 1cm^3 is introduced into a cell filled with mercury. The sample has been previously dried by means of different techniques, being two of them the most frequently used: oven-drying and freeze-drying. In general, the freeze-drying method is preferred as it is associated with a smaller affectation to the original structure of the soil due to the rapid rate of freezing. Once the sample has been placed in the cell, the pressure of mercury is increased gradually and the volume of intruding mercury is measured. The radii of the intruded pores are obtained from the Laplace equation involving the superficial tension of mercury and the contact angle between mercury and soil. The main hypothesis employed to interpret these results is to assume that only those pores the size of the critical radius (determined from the Laplace equation for the current mercury pressure) are intruded at each increment of the mercury pressure. Then, a graph showing the relative volume of pores (in cm^3 per gram) for each pore size is produced. More details of the equipment and procedure required to obtain the PSD of soils by MIP is reported by Simms and Yanful [45].

However, the hypothesis made to interpret MIP tests is clearly unrealistic. It is equivalent to supposing that only equally sized pores are interconnected, while there is no interconnection between pores of different sizes. In fact, it has been acknowledged that the results of MIP tests exaggerate the frequency of small pores while underestimating that of large pores [67]. This is a result of the intrusion of mercury in the bonds, matching that of the cavity connected to this bond. This is explained by the fact that larger pores are the first ones to be intruded when mercury pressure increases.

Considering a network porous model as the one described in Chapter 3, it is possible to give a better interpretation of the results of MIP tests. The invasion of mercury (which is a non wetting fluid) is similar to a drying process where pores are invaded by air (which is also a non wetting fluid), forcing the water to drain out of the sample. In both cases, the largest pores are the first ones to be filled in with fluid as indicated in Fig. **1**.

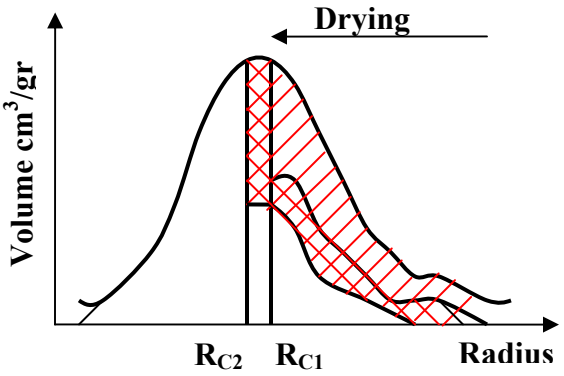

Figure 1: Pores invaded by mercury (shaded zone) during a MIP test.

When mercury pressure increases only a fraction of pores with an equal or larger size regarding the critical radius will saturate while the rest will remain blocked by smaller bonds. This occurs because of the interconnection of pores of all sizes. Some larger pores saturate during this increase of mercury pressure because at least one of their interconnected bonds belongs to those that saturate with this increment.

The mechanism of mercury invasion is sketched in Fig. **1**. Considering that the critical radius reduces from R_{C1} to R_{C2} due to the increase in mercury pressure, the blank zone in the figure represents the volume of pores that still have not yet been invaded by mercury. The single shadow zone represents the volume of pores already invaded by mercury before the new pressure increment. Finally, the double shadow zone represents the volume of pores occupied during the new pressure increment.

For MIP tests, the appropriate values of the contact angle and surface tension have to be taken into consideration. According to Equation (3.2), the ratio between the suctions in a pore filled with water (s_w) and with mercury $\left(s_m\right)$ is given by the relation:

$$\frac{s_w}{s_m} = \frac{T_{sw}\cos\theta_w}{T_{sm}\cos\theta_m} \quad \ldots \tag{5.1}$$

where T_{sw} and T_{sm} represent the surface tension for water and mercury, respectively and θ_w and θ_m are the contact angles for water and mercury with the soil minerals, respectively.

Therefore, the porous model can be used to simulate MIP tests if considering that the sample is subjected to a drying process, in which the air volume represents the intruded mercury and the critical radius is computed by means of Equation (3.2).

As stated previously, the employment of MIP tests on plastic soil has been questioned [65], and for that reason the evaluation of the capabilities of the porous model to interpret MIP tests has been carried out with respect to the results reported by Roels, Elsen, Cermeliet and Hens [68] on a rigid calcareous sedimentary rock from Savonnières, France. These authors reported the porosimetry study of this material by using two different techniques: image analysis and mercury intrusion. For the image analysis, they obtained a series of micrographs of a cross-section of the rock by means of a Scanning Electron Micrographs (SEM). Then, by applying the spherical pore segment model, the authors could define the relative volume for each pore. Fig. **2** shows the results from both tests, where a marked difference between these two techniques can be observed. It is worth noting that MIP tests may report pore sizes up to two orders of magnitude smaller than the image analysis technique. Similar results have been reported when comparing the MIP method with other techniques [67].

Fig. **3** shows the wetting and drying SWRC of the limestone obtained from a pressure membrane apparatus. In this case, the material is stiff enough to avoid appreciable volume changes during wetting-drying cycles and therefore its void ratio remains approximately constant, meaning that, the phenomenon of progressive collapse of pores is not required in these simulations. Hence, it has been possible to relate the water content of the sample with its degree of saturation. On the other hand, it has been assumed that the PSD obtained from the image analysis technique reflects the real PSD of the rock and consequently was adopted as the distribution of cavities (macropores and mesopores) existing in the porous model. Subsequently, a size distribution for bonds was proposed and the SWRC in wetting and drying were simulated and compared with the experimental results. The proposed distribution for bonds was then modified until the best fit for both curves was obtained. During the fitting process it was considered that the size distribution of bonds affects mainly the drying curve while it shows a minor effect on the wetting curve, as aforementioned. In contrast, the size distribution of sites affects mainly the wetting curve while it shows a minor effect on the drying

curve. On a later section of this chapter, the procedure to fit numerical with experimental SWRCs is explained.

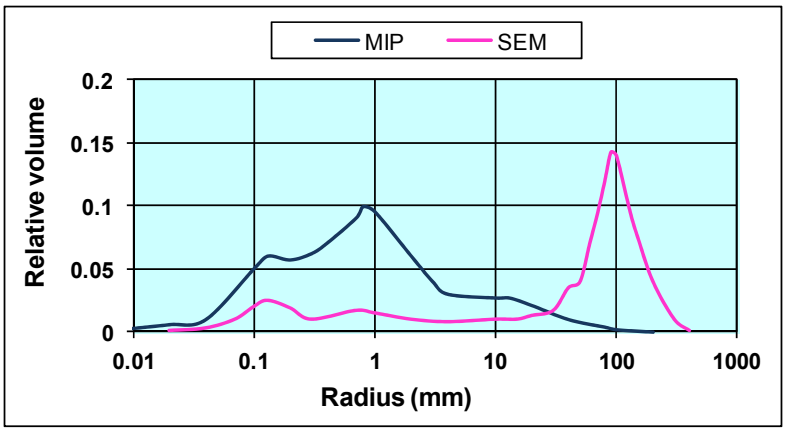

Figure 2: Porosimetry results by MIP and SEM (data from Roels, Elsen, Cermeliet and Hens [68]).

The best fit for both curves is shown in Fig. **4**. To reach this result a triple logarithmic normal size distribution was adopted for bonds. The pore size density function for sites and bonds is shown in Fig. **5**. The data for the adopted distribution for bonds is: $\overline{R}_{B1} = 0.007\mu m$, $\overline{R}_{B2} = 0.05\mu m$, $\overline{R}_{B3} = 1.0\mu m$, $\delta_{B1} = 4$, $\delta_{B2} = 5.3$, $\delta_{B3} = 3$, P_{vf1}=.025, P_{vf2}=.0015.

Once the size distribution for bonds has been established, it is possible to simulate MIP tests using the considerations previously mentioned. The parameters required to simulate this test were reported by Roels, Elsen, Cermeliet, and Hens [68] which include: $T_{sw} = 0.073$ N/m, $T_{sm} = 0.485$ N/m $\theta_w = 0$ and $\theta_m = 140^o$. According to these parameters and Equation (5.1), the equivalent water suction for this test is $s_w = 0.2\, s_m$. With this value, Fig. **6** was obtained. This figure shows the comparison between the experimental results of the MIP test with those obtained from the porous model. This figure also shows the numerical PSD resulting from the density functions shown in Fig. **5**. Even if some differences between the numerical and experimental MIP curves subsist, especially those related to the relative volume of small pores, the shape of both curves is very similar. It can also be verified that the size distribution of pores obtained from the simulation of the MIP test reduces by two orders of magnitude the original PSD of the soil as it is observed in the experimental results shown in Fig. **2**.

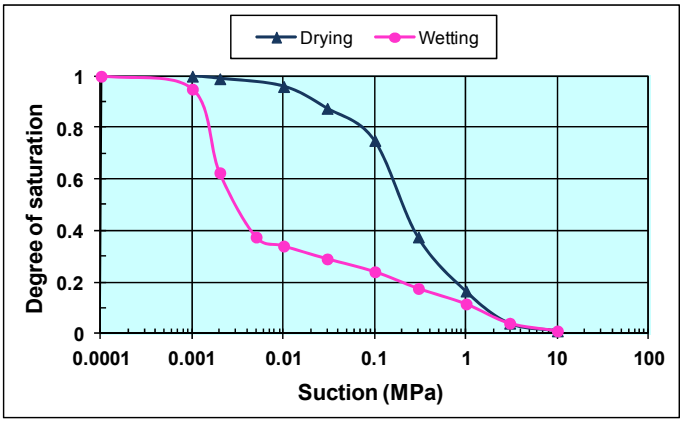

Figure 3: Wetting and drying SWRC (data from Roels, Elsen, Cermeliet and Hens [68]).

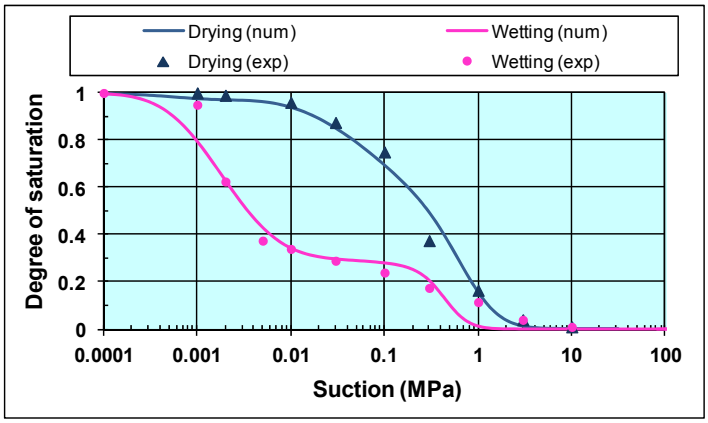

Figure 4: Numerical and experimental wetting and drying SWRC (experimental data from Roels, Elsen, Cermeliet and Hens [68]).

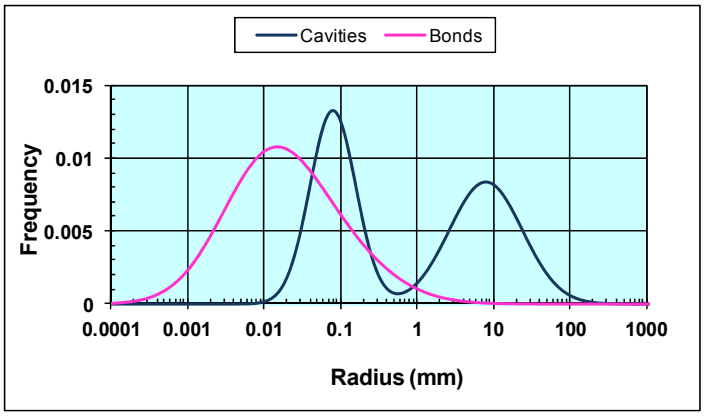

Figure 5: Frequency function adopted for bonds and comparison with sites.

This result has serious implications regarding some procedures recently developed to define the SWRC or the hydraulic conductivity of unsaturated soils based on the PSD obtained from MIP tests. Finally, another important remark is that the PSD obtained from a single MIP test provides insufficient information to define the size distribution of the two different porous elements, namely the cavities and the bonds, of the model adopted herein. Therefore, additional information is needed. For example, the results of intrusion tests require to be complemented with retraction tests as is currently performed in the nitrogen adsorption-desorption method.

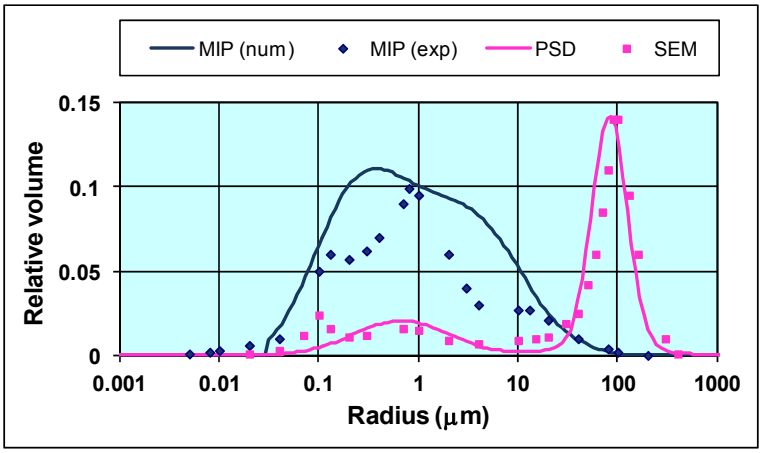

Figure 6: Numerical and experimental comparison for a MIP test on a Savonnières rock (experimental data from Roels, Elsen, Cermeliet and Hens [68]).

5.3. SOIL-WATER RETENTION CURVES

The SWRC is the relationship between suction and water content or degree of saturation of soils as explained before. The relevance of the SWRC in the study of unsaturated soils behavior has increased since the hydro-mechanical coupling phenomenon in these materials was identified. Evidence of the hydro-mechanical coupling can be seen in the influence of the degree of saturation on the strength of unsaturated soils when identical samples are subjected to the same suction. This means that a sample subject to wetting shows different strength than one following a drying path, even if suction is the same for both samples. Another evidence of this coupling is the influence of volumetric deformations (induced by mechanical actions on the soil sample) on the SWRC. Recent constitutive models

for unsaturated soils involve the modeling of the SWRC to induce this hydro-mechanical coupling [22, 24, 25]. Besides, recent developments in the design of pavements require using the SWRC [69]. Even the tensional strength of soils can be related to the SWRC [70].

Different methods and empirical relationships have been proposed to model the SWRC. Some of these equations use parameters related to the air entry value, the residual water content and the main slope of the curve [61, 71]. Other methods are based on the GSD in addition to other soil properties, and use a statistical correlation between soil data and water content [72-74]. The degree of confidence of these models depends largely on the quality and quantity of the data used for the statistical correlation. Other methods use the PSD which, in some cases, is estimated from the GSD [75-77]. Otherwise, it is directly obtained from porosimetry tests [78, 79]. As the SWRC depends on the PSD of the material then, the precision in the PSD measurements affects the results derived from these models.

Likewise, different network models have been proposed to simulate the SWRC. For example, Androutsopoulos and Man [80] proposed a bidimensional square network model made of randomly distributed cylinders of different sizes. The Laplace equation was used to determine which pores can drain or saturate according to their size and current suction. Saturation or drainage starts at the borders and continues through the porous network in a quasi-static flow where suction monotonically reduces or increases. Considering a logarithmic normal distribution for the diameter of the cylindrical pores, these researchers were able to approximately reproduce the intrusion and retraction of mercury in a cobalt/molybdenum porous sample. However, the experimental PSD for this material was not reported and the differences with the numerical PSD used for the simulations rested unknown.

Simms and Yanful [79] used a similar network model that included the pore shrinkage phenomenon due to suction increase. With this model they tried to reproduce the experimental SWRC of different soils using the PSD obtained from MIP tests. Nevertheless, the comparison between numerical and experimental SWRCs for different materials was not very successful [78]. Similar results were reported by Zhang and Li [81]. The main reason for these poor results lies on the main hypothesis made to interpret MIP tests as discussed before.

Zhang and Li [81] performed a series of tests on five different mixtures of completely decomposed granite with sizes varying from gravel to clay. These tests included the GSD, the PSD and the drying SWRC. The PSD was obtained from MIP tests. The SWRC was achieved using a pressure plate apparatus for suctions up to 0.5 MPa. In some cases this method was complemented with the psychrometer technique reaching suctions up to 50 MPa. The basic parameters for the five mixtures of soil are shown in Table **1**.

Table 1: Basic parameters for the five different soils

Soil Type	Max. Dry Dens. (g/cm^3)	Op. water Content (%)	Clay (%)	Silt (%)	Sand (%)	Gravel (%)	ASTM D2487
1	1.97	9	3.9	3.1	16.7	76.3	GP
2	1.96	11	5.9	18.7	17.9	57.5	GW
3	1.90	13	7.9	34.3	19.1	38.7	SP
4	1.71	18	9.9	49.9	20.3	19.9	SW
5	1.55	21	11.9	65.5	21.5	1.1	SM

The SWRCs for all five soils are presented in Fig. **7**. Notice that the more the proportion of coarse material of the soil increases, the more the SWRC displaces to lower degrees of saturation for the same suction. The only material that does not follow this tendency is the poorly graded sand (SP) which shows degrees of saturation similar to silty sand (SM).

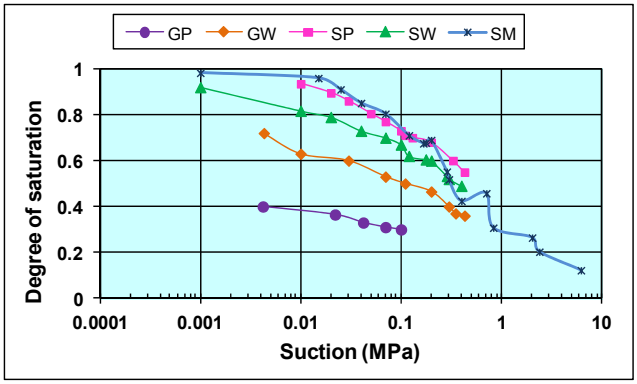

Figure 7: Experimental SWRCs for the five soils tested (data from Zhang and Li [81]).

The numerical PSD was obtained by fitting the numerical with the experimental SWRC of each material. The procedure used to fit the numerical with the

experimental results is presented as an example in the next section of this chapter. The PSD resulting from this procedure is considered to be the porous-solid model PSD. Similarly, the GSD was obtained from the simulation of the cumulative finer by weight gradation of each soil employing a single, double or triple logarithmic normal distribution depending on the material.

Once the SWRC was correctly reproduced, the resulting PSD of the soil was used to simulate a MIP test according to the principles outlined in the previous section of this chapter. Finally, the results of the simulated MIP tests were compared with the experimental results.

Figs. **8**(a)-**12**(a) show the simulation of the SWRC for GP, GW, SP, SW and SM soils from which the numerical PSD of each material was established. The parameters adopted for the PSD and the GSD for all soils are presented in Table **2**.

Table 2: Mean size and standard deviation for the normal distributions for sites, bonds and solids of the materials described in Table **1**

Soil		S_1	S_2	B_1	B_2	B_3	Sol_1	Sol_2	Sol_3	e_0	S_f
GP	$\bar{R}$(μm)	0.15	40	.04	25	0.0	7	320	0.0	0.705	.00015
	δ	2.5	2.5	5.0	3.0	0.0	3.0	3.0	0.0		
	P_{vf}		1.5E-5		.008			3E-3			
GW	$\bar{R}$(μm)	0.15	15	.001	.005	0.0	0.4	700	0.0	0.61	0.061
	δ	2.5	2.5	1.5	3.0	0.0	3.6	2.5	0.0		
	P_{vf}		9E-6		.0005			3.3E-6			
SP	$\bar{R}$(μm)	0.15	10.0	.015	1.0	0.0	0.5	550	800	0.62	0.017
	δ	2.0	2.0	3.0	3.0	0.0	3.4	2.8	2.0		
	P_{vf}		1.5E-4		6E-3			1.6E-6	1E-7		
SW	$\bar{R}$(μm)	0.3	90	.001	.02	18	0.2	100	2000	0.63	0.0385
	δ	2.5	2.5	3.0	3.0	3.0	4.0	2.5	2.0		
	P_{vf}		3E-6		1E-2	1.5E-5		6E-6	4E-8		
SM	$\bar{R}$(μm)	0.3	1.6	.01	1.0	0.0	0.4	13.0	0.0	1.02	0.144
	δ	2.0	2.0	3.0	3.0	0.0	3.0	2.5	0.0		
	P_{vf}		2E-2		3E-3			8E-4			

Notes: $\bar{R}$ = mean size, σ = standard deviation, S = sites (S), B = bonds, Sol = solids, sub-scripts from 1 to 3 indicate the three different logarithmic normal distributions, P_{vf} = Proportional volume factor, e_0= initial voids ratio, S_f = shape factor.

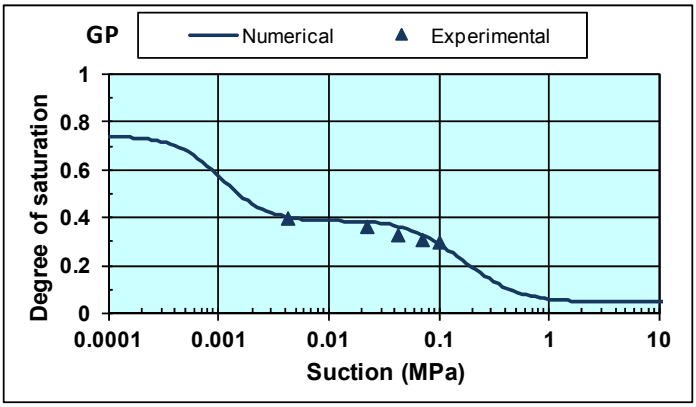

(a)

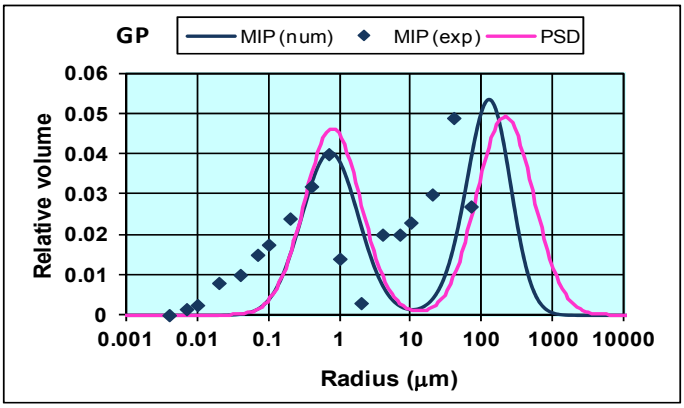

(b)

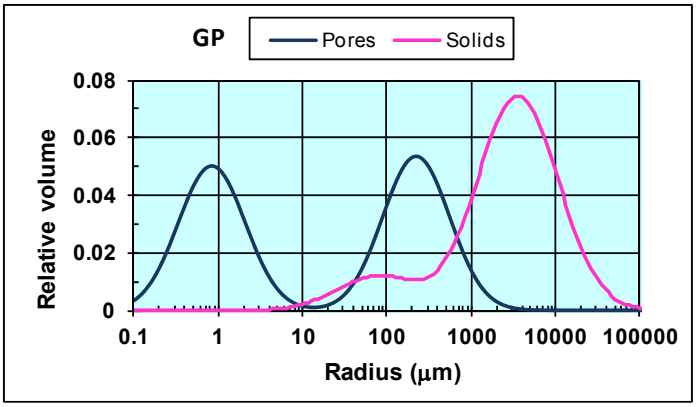

(c)

Figure 8: Numerical and experimental results for (a) the drying curve,(b) the PSD and (c) numerical PSD with experimental GSD for soil GP (experimental data by Zhang and Li [81]).

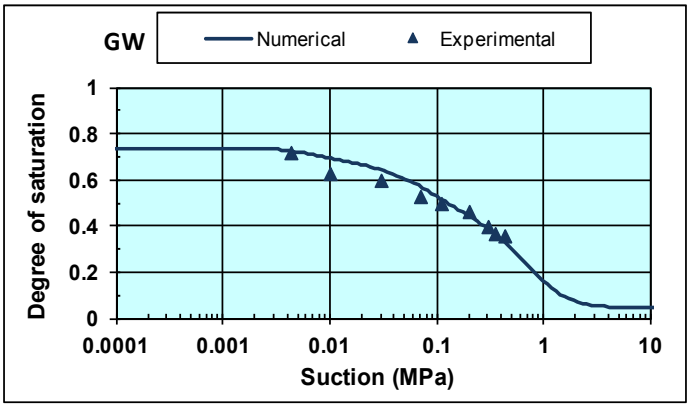

(a)

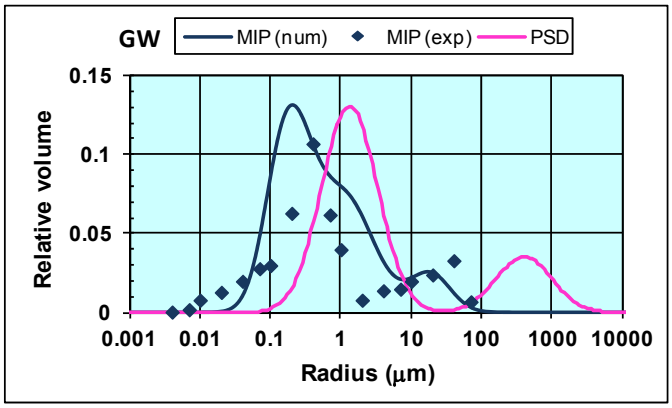

(b)

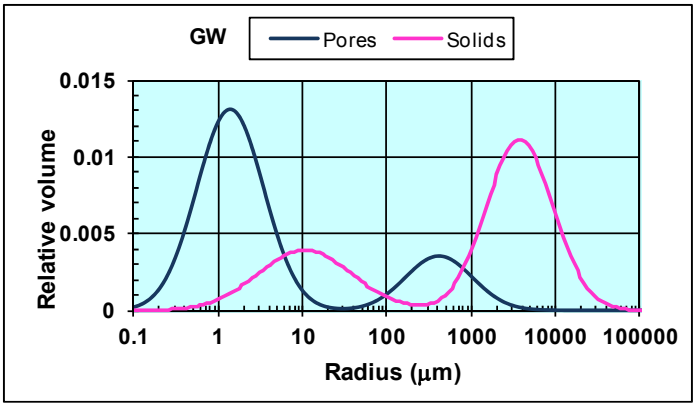

(c)

Figure 9: Numerical and experimental results for (a) the drying curve, (b) PSD and (c) numerical PSD with experimental GSD for GW soil (experimental data by Zhang and Li [81]).

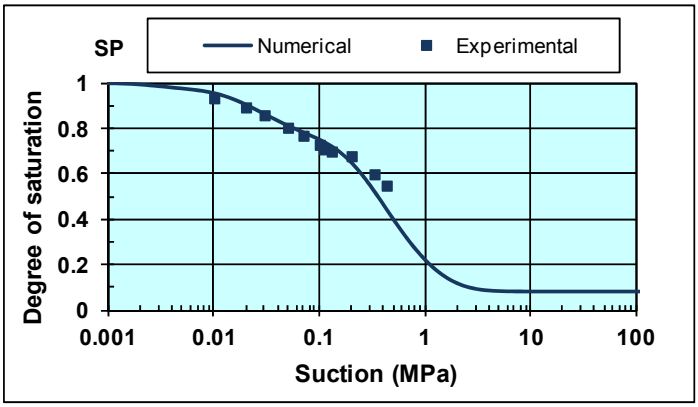

(a)

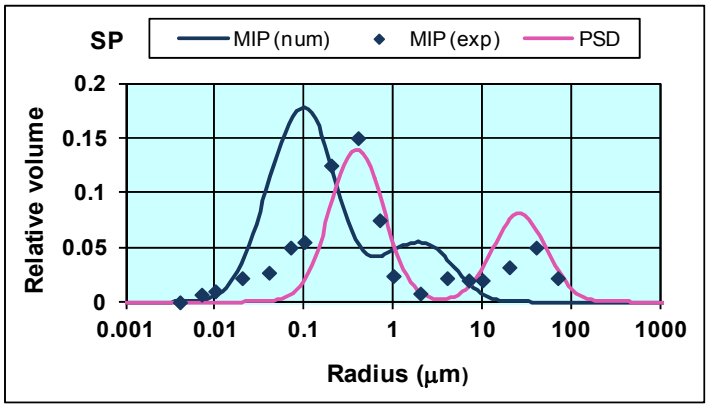

(b)

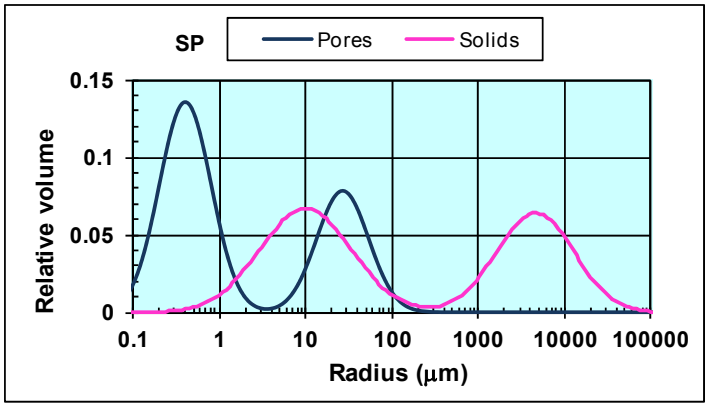

(c)

Figure 10: Numerical and experimental results for (a) the drying curve, (b) PSD and (c) numerical PSD with experimental GSD for SP soil (experimental data by Zhang and Li [81]).

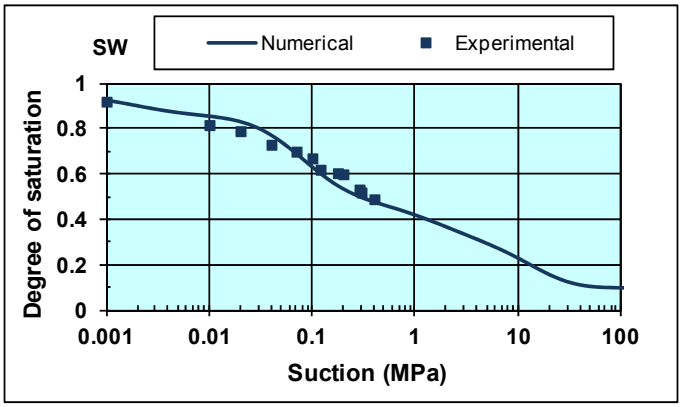

(a)

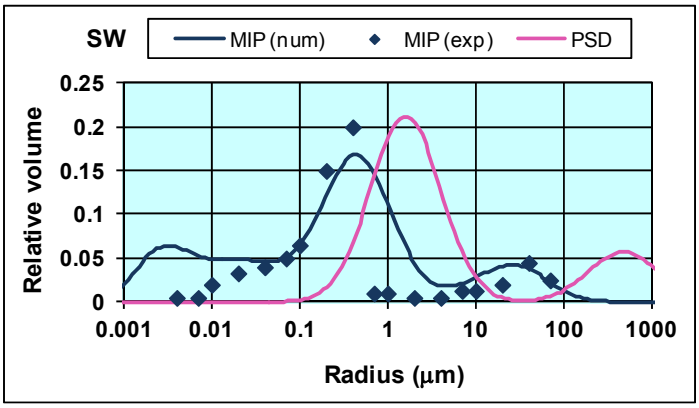

(b)

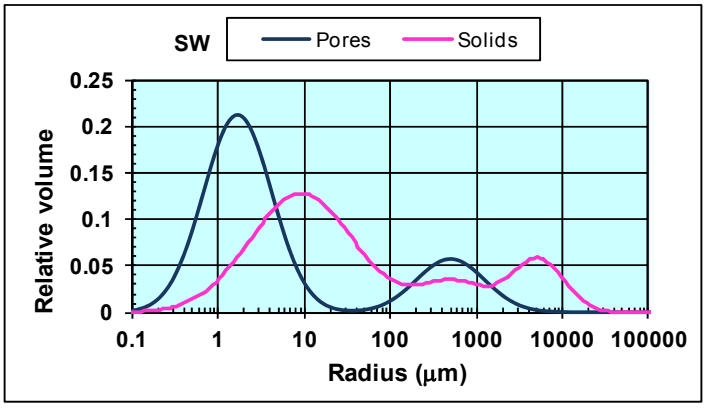

(c)

Figure 11: Numerical and experimental results for (a) the drying curve, (b) PSD and (c) numerical PSD with experimental GSD for SW soil (experimental data by Zhang and Li [81]).

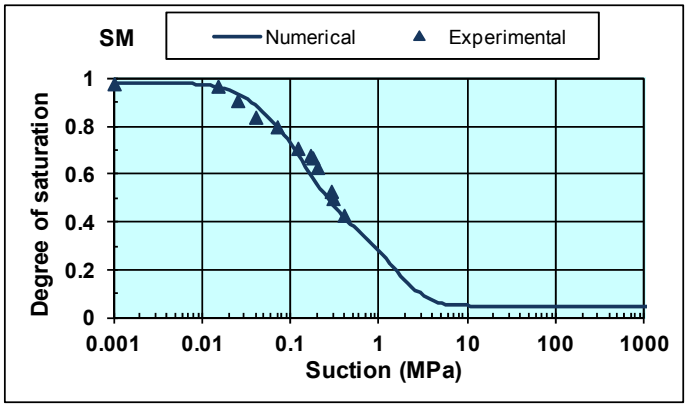

(a)

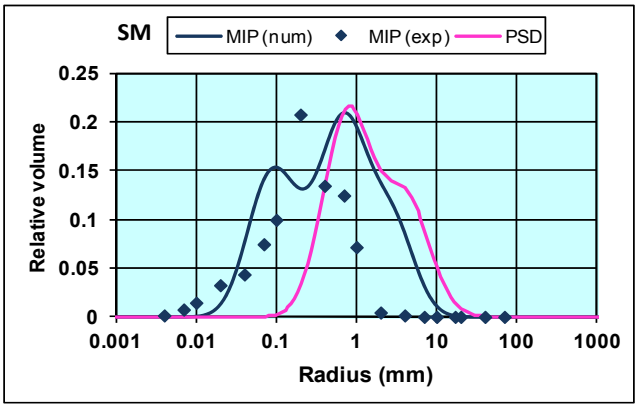

(b)

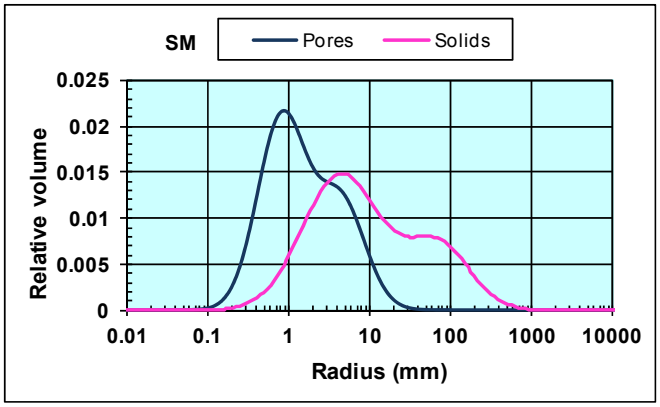

(c)

Figure 12: Numerical and experimental results for (a) the drying curve, (b) PSD and (c) numerical PSD with experimental GSD for SM soil (experimental data by Zhang and Li [81]).

As can be observed in Figs. **8**(b)-**12**(b), the difference between the porous model PSD and that obtained from the simulation of the MIP test is about one order of magnitude. This difference explains the failure of those network models that intend to reproduce the SWRC directly from the PSD obtained from MIP tests, and this arises from the fact that SWRCs are simulated by using the network model while MIP tests are interpreted according to the capillary tubes bundle model.

The experimental PSD matches with the numerical results for all soils (see Figs. **8**(b), **9**(b), **11**(b) and **12**(b)) except for SP soil (Fig. **10**(b)) whose experimental points are closer to the porous network PSD. This result is caused by the fact that the experimental SWRC obtained for this material is very close to that of SM soil (see Fig. **7**), despite the fact that their experimental PSD are quite different (compare Figs. **10**(b) and **12**(b)). In other words, the experimental results for SP soil cannot be correctly reproduced by the model because they show some inconsistencies with respect to the other soils.

It can also be observed in these figures that the numerical PSD of soils GP, GW, SW and SM -obtained from the simulation of MIP tests- consistently show slightly smaller pore sizes than those experimentally determined. This is also the case of the example presented in the previous section of this chapter. The differences in the value of the contact angle when water or mercury intrudes or retracts from pores ([82], [55]) may explain this result, as the advancing angle has been found to be significantly larger than the receding one. Instead the model considers the same value for both cases. In spite of this, it can be concluded that the probabilistic model is able to approximately define the PSD of the soil based on the SWRC or *vice versa*.

It can also be noticed that all soils show a significant correlation between their numerical PSD and their GSD (see Figs. **8**(c)-**12**(c)) as it was experimentally observed by Alonso *et al*. (2008) for different soils. This result explains why some methods based on the GSD of the material have had relative success in predicting the SWRC for soils (see for example [72, 75, 77]).

5.4. OBTAINING THE PORE SIZE DISTRIBUTION

The procedure to fit the numerical with the experimental SWRCs is shown in this section. At the end of this fitting process, the PSD of the soil is determined

because, as stated before, there is a one to one relationship between the PSD and the SWRCs of porous materials.

The data published by Roels, Elsen, Cermeliet and Hens [68], used previously in the example presented in section 2 of this chapter, is also employed for this case. These researchers reported both the wetting and the drying SWRCs, the results of MIP tests and the PSD obtained from SEM analysis. For this instance, it is considered that the only available data are the main SWRCs of the soil. Therefore, numerical and experimental PSD are used here merely to show how they approach each other during the fitting process.

The first step to adjust the numerical and the experimental SWRCs of a soil is to arbitrarily choose the initial values for the mean size and the standard deviation of pores. The larger pores (cavities) regulate the wetting curves while the smaller (bonds) regulate the drying curve. When the SWRC shows a development, where suction varies in several orders of magnitude or when the PSD shows two or three peaks, then a double or triple logarithmic normal distribution is required. Suppose that the drying SWRC has already been fitted using a triple logarithmic normal distribution. This distribution was chosen because the SWRCs show a development in the suction axis of several orders of magnitude. Usually both the wetting and the drying branches require the same order of size distribution (single, double or triple). In that sense, a triple logarithmic normal distribution is also proposed to fit the wetting curve. The results obtained with the initially proposed values for this distribution (Table **3**) are shown in Fig. **13**. Fig. **13**(a) shows the comparison between the numerical and experimental SWRCs while Fig. **13**(b) shows the proposed PSD compared with the SEM analysis as well as the numerical and experimental PSD obtained from a MIP test.

Fig. **13**(a) shows important differences in the slope for the numerical and experimental wetting curve. When the numerical curves display steep slopes with regards to the experimental results, then the standard deviation needs to be increased. If the slopes are too smooth with respect to experimental results then the standard deviation needs to be reduced. In this case, the slopes of the numerical curve are too steep compared to experimental results, especially for large values of suction. This means that the standard deviation for the small cavities (Cavities 1 and 2) needs to be increased as indicated in Table **4**.

Table 3: Initial proposed values for parameters of cavities considering a triple logarithmic normal distribution

Element	Cavities 1	Cavities 2	Cavities 3
$\bar{R}$ (μm)	0.15	15	150
δ	1.5	1.5	1.5
P_{vf}		2E-5	2.5E-5

Table 4: Second try for the values of parameters for cavities

Element	Cavities 1	Cavities 2	Cavities 3
$\bar{R}$ (μm)	0.15	15	150
δ	3.0	3.0	1.5
P_{vf}		2E-5	2.5E-5

Fig. **14** shows the results obtained with the values indicated in Table **4**. A better correlation of slopes for the numerical and experimental SWRCs can now be observed in Fig. **14**(a). However, the curves look displaced to the right hand side. This implies that the mean size of cavities needs to be reduced in order to increase the suction required to intrude the pores. Therefore, the pore sizes of cavities are reduced as indicated in Table **5**.

The results obtained with the values of Table **5** can be observed in Fig. **15**. A final adjustment of parameters for the best fit of the wetting curve is shown in Table **6**. These parameters result in the curves shown in Figs. **4** and **5** of this chapter. This same process can be applied to fit the drying curve. At this point it can be observed that the numerical PSD, obtained with the fitting process of the SWRCs, is well correlated to the experimental PSD obtained from the SEM analysis. Besides the numerical and experimental PSD for a MIP test show good agreement (Fig. **6**).

Table 5: Third try for the values of parameters for cavities

Element	Cavities 1	Cavities 2	Cavities 3
$\bar{R}$ (μm)	0.06	6	60
δ	3.0	3.0	1.5
P_{vf}		2E-5	2.5E-5

Table 6: Final values of the parameters for cavities

Element	Cavities 1	Cavities 2	Cavities 3
$\bar{R}$ (μm)	0.06	6	73
δ	3.0	3.0	1.4
P_{vf}		2E-5	2.5E-5

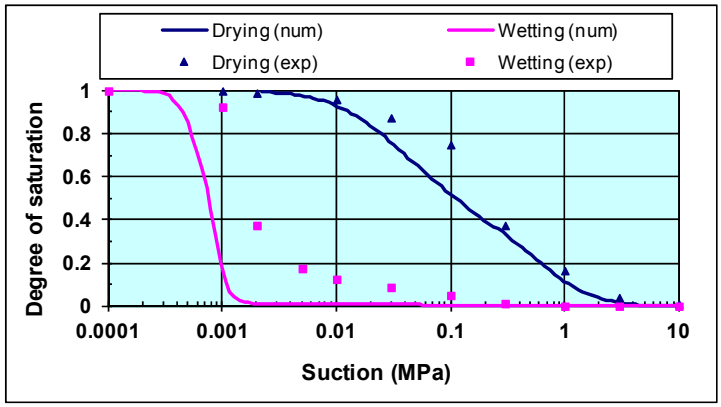

(a)

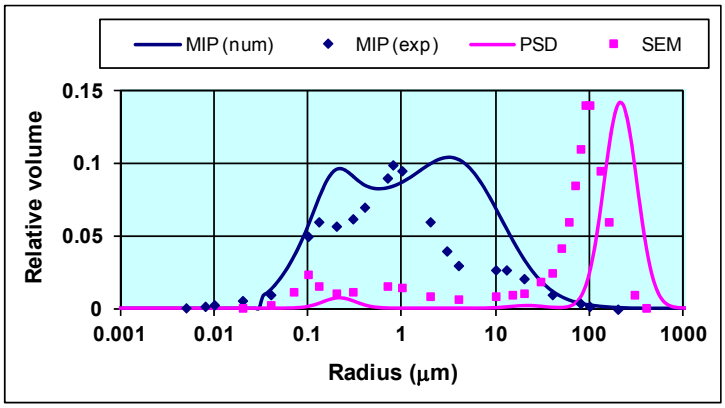

(b)

Figure 13: Comparison between experimental and numerical results for (a) SWRCs and (b) PSD and MIP test for initially proposed parameters.

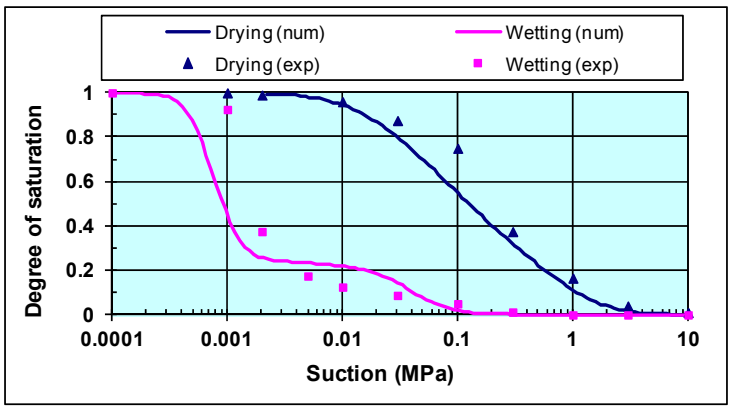

(a)

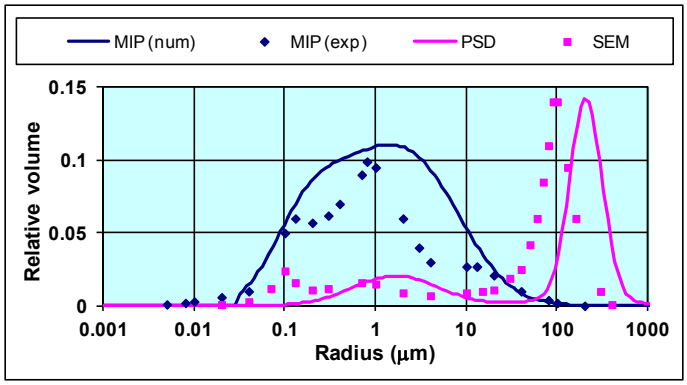

(b)

Figure 14: Comparison between experimental and numerical results for (a) SWRCs and (b) PSD and MIP test. Second try.

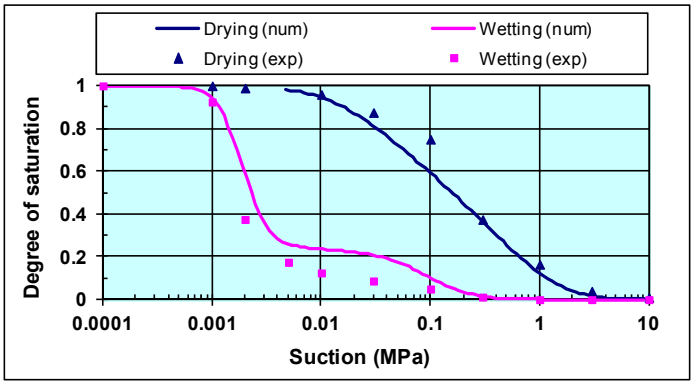

(a)

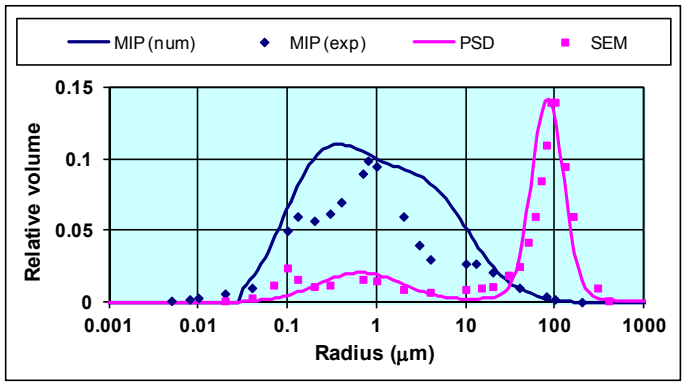

(b)

Figure 15: Comparison between experimental and numerical results for (a) SWRCs and (b) PSD and MIP test. Third try.

Send Orders of Reprints at reprints@benthamscience.net

CHAPTER 6

Compression Strength of Soils

Abstract: In this chapter, the probabilistic porous-solid model is used to determine the mean effective stress of soils at failure. The plot of the deviator stress against the mean effective stress shows a unique failure line for a series of triaxial tests performed at different combinations of the confining net stress and suction for both wetting and drying paths. This result confirms that the proposed effective stress equation is adequate to predict the shear strength of unsaturated soils. It also results in different strengths for wetting and drying paths as the experimental evidence indicates.

Keywords: Shear strength, effective stress, net stress, triaxial tests, confining stress, axis translation technique, constant volume test, friction angle, wetting path, drying path, porous-solid model, soil-water retention curve, logarithmic normal distribution, critical state, pore size distribution, grain size distribution.

6.1. INTRODUCTION

The probabilistic porous-solid model can be used to obtain the mean effective stress at failure for a soil following any stress path. These results can be plotted against the deviator stress to determine the failure surface of the material. In this chapter, the experimental results of the Speswhite kaolin as reported by Wheeler and Sivakumar [83] are used. These researchers performed a series of triaxial tests with different stress paths. With these results, some points of the SWRC at wetting could be obtained. Also the PSDs of samples statically compacted at different vertical pressures and water contents have been reported by Thom, Sivakumar, Sivakumar, Murray and Mackinnon [84]. Finally, the GSD of this material was reported by Espitia [85]. Because at its present stage the probabilistic model does not consider volume changes, only those paths involving no volume change of the sample during shearing were considered for the numerical comparisons. For the same reason, the experimental results were considered in three different groups depending on the confining stress applied to the sample. These groups correspond to the confining pressures of 0.1 (three tests), 0.2 (two tests) and 0.3MPa (one test). Each group corresponds to a different PSD resulting in three different sets of SWRCs and three different groups of curves for parameters f^s, f^d and S_w^u. Accordingly, numerical and experimental comparisons were made independently for each group.

Eduardo Rojas

6.2. NUMERICAL AND EXPERIMENTAL COMPARISONS

All samples used for the determination of the PSD, the SWRC and tested in triaxial tests were prepared by static compaction at a water content of 25% (4% less than the optimal). These samples were compacted in nine layers at a constant displacement of 1.5mm/min and a maximum vertical total stress of 0.4MPa. This procedure provided samples with dry density of 1.2g/cm^3, specific volume of 2.21 and 54% degree of saturation. Prior to the loading stage all samples were subject to an isotropic net stress of 0.05MPa with suctions ranging from 0 to 0.3MPa in the triaxial cell. At these levels of suction all samples increased their water content. In addition, those samples subject to suctions of 0 and 0.1MPa experienced volumetric collapse. Once equilibrium was accomplished, the isotropic net stress was increased to reach a final value ranging between 0.1 and 0.3MPa. Because all samples increased their water content during the equilibrium stage it is considered that all these results correspond to the wetting branch of the SWRC.

The GSD of the Speswhite kaolin reported by Espitia [85] is shown in Fig. **1**. The same figure shows the adjusted numerical curve obtained from a double logarithmic normal distribution. Even though, small differences between these two curves exist, the numerical fitting is sufficiently accurate.

The experimental points of the SWRCs for the confining pressures of 0.1, 0.2 and 0.3MPa are shown in Fig. **2**. These points were obtained from the results of controlled suction triaxial tests at no volume change performed by Sivakumar [86]. They correspond to the value of the degree of saturation at the critical state for those tests performed at the same confining pressure but different suction. This figure also shows the numerical SWRCs at wetting for the different confining pressures. The numerical curves were fitted to the experimental points by successively modifying an initially proposed PSD according to the procedure outlined in the previous chapter. In order to produce complete curves, it was necessary to estimate the value of the residual and the saturated degree of saturation according to the tendency of the experimental points. The first parameter was assessed as 0.05 for all tests while the second was estimated in 0.91, 0.96 and 0.97 for the confining pressures of 0.1, 0.2 and 0.3MPa, respectively.

Fig. **3** shows the PSD obtained from MIP tests carried out on a sample prepared according to the aforementioned procedure. This curve shows a bimodal distribution with two peaks: one at approximately 0.45μm and the other at approximately 4.5μm corresponding to the size distribution of mesopores and macropores, respectively. The same figure shows the PSDs obtained by fitting the numerical and the experimental SWRC at wetting for the three different confining stresses. Although the experimental and the numerical curves show similar shapes, two main differences between them become apparent: the first one is that the numerical PSD is displaced to the left with respect to the experimental results. The second one is that the numerical maximum relative volume of macropores is much smaller than the experimental value. The reason for these differences can be explained by the fact that MIP tests were performed in"as compacted" soil samples before the equalization stage where the confining pressure and the increase in water content produced a volumetric reduction in the sample which affects mainly the size of macropores as has already been discussed in chapters 3 and 5. This same deviation of the numerical PSD with respect to the experimental results was observed when a computational model was used to simulate the SWRC of this material [87].

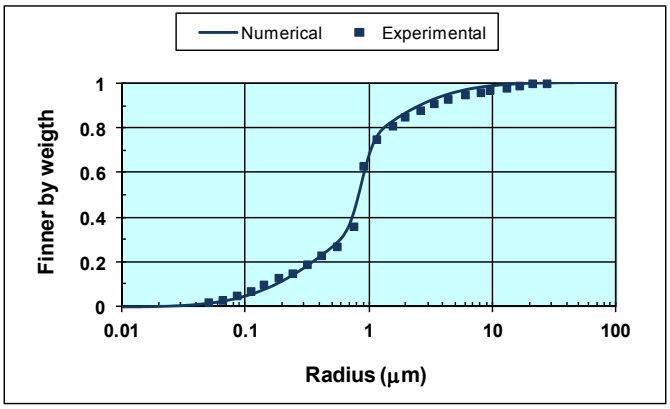

Figure 1: Numerical and experimental GSD.

Once the PSD for each confining pressure has been established, the determination of the parameters of the porous-solid model is completed. Table **1** shows the parameters obtained for a confining pressure of 0.1 MPa. Notice that the bonds needed a double logarithmic distribution (B_1 and B_2) to better simulate the SWRCs.

Table 1: Parameters of the model for a confining pressure of 0.1MPa

Parameter	**M**	**S**	**B_1**	**B_2**	**Sol_1**	**Sol_2**
Mean size $\overline{R}$ (μm)	0.8	0.05	0.13	.008	1.1	.02
Standard deviation δ	1.4	1.7	1.4	1.7	1.1	3.8
P_{vf}	0.01		0.01		.005	

Notes: M = macropores, S = mesopores, B_1 = Bonds (1), B_2 = Bonds (2), Sol_1 = Solids (1), Sol_2 =Solids (2), P_{vf} = Proportional volume factor.

For the confining pressures of 0.2 and 0.3MPa all parameters included in Table **1** remain the same except for the mean size of macropores which take the value of 0.83μm and 0.75μm, respectively. The connectivity for the porous model was considered to be 4. Finally, a value of 0.25 for the shape factor allowed matching the numerical and experimental voids ratio for the different confining pressures as shown in Table **2**.

Table 2: Experimental and numerical voids ratio for different confining pressures

Confining Stress (MPa)	**0.1**	**0.2**	**0.3**
Experimental voids ratio	1.18	1.13	0.99
Numerical voids ratio	1.17	1.15	1.0

Once all parameters of the porous-solid model have been defined, it is possible to simulate a wetting process and obtain the values of parameters f^s, f^d, S_w^u and χ for the full range of suction and for each confining pressure. These results are presented in Fig. **4**. In Figs. **4**(a) and **4**(c) it can be seen that both parameters f^s and S_w^u increase continuously with the degree of saturation although the first parameter grows at an increasing rate while the second at a decreasing rate. On the contrary, Fig. **4**(b) shows that parameter f^d initially increases up to a maximum and then decreases with the degree of saturation. Fig. **4**(d) shows the numerical end experimental values of parameter χ for each confining pressure. The numerical values were derived from Equation (2.15) whereas the experimental ones were obtained by assuming that the failure surface is represented by a single line in the axes of mean effective stress against deviator stress as expressed by Equation (2.19). It can be observed that the numerical and experimental results lie fairly close for the confining pressures of 0.1 and 0.2MPa. A similar comparison can be made for the matric suction stress σ_s^* as defined in

Equation (2.17). This comparison is presented in Fig. **5** and again experimental and numerical results are quite similar for all confining pressures. The numerical results indicate that the maximum strength of the soil can be reached at a degree of saturation of 0.5 or 0.6 which seems rather low. In order to improve these predictions both branches of the SWRC for the entire range of suction would be required.

It is noteworthy that parameters f^s, S_w^u and χ shown in Fig. **4** vary from zero to one even if the degree of saturation of the material does not reach these values. This happens because it is being considered here that free water is the main responsible for the development of the capillary phenomenon as pointed out before. This is equivalent to consider an effective degree of saturation (S_{we}) for the material defined by the relationship:

$$S_{we} = \frac{S_w - S_{wr}}{S_{ws} - S_{wr}} \tag{6.1}$$

where S_{wr} and S_{ws} represent the residual and saturated degree of saturation of the material. This equation has been proposed as a main parameter to determine the strength of unsaturated soils by Vanapalli, Fredlund, Pufahl and Clifton [21] among others and its performance to this purpose has been evaluated by Garven and Vanapalli [19].

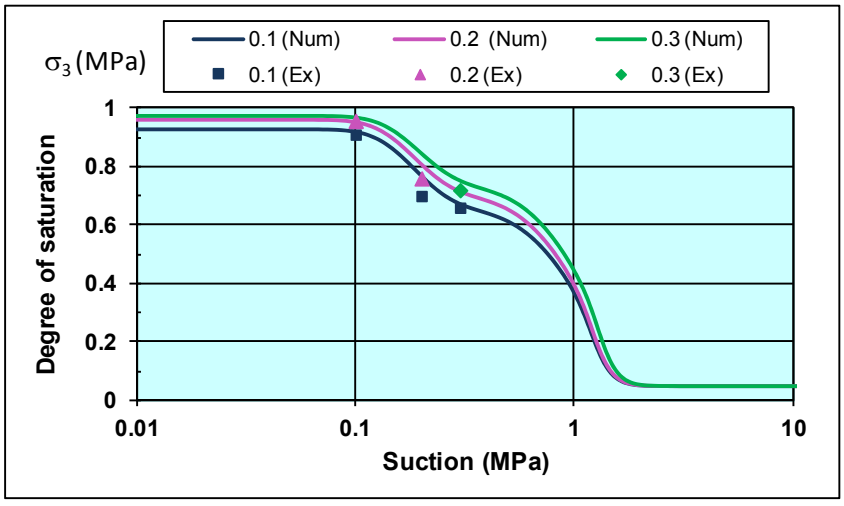

Figure 2: Numerical and experimental SWRCs for different confining pressures.

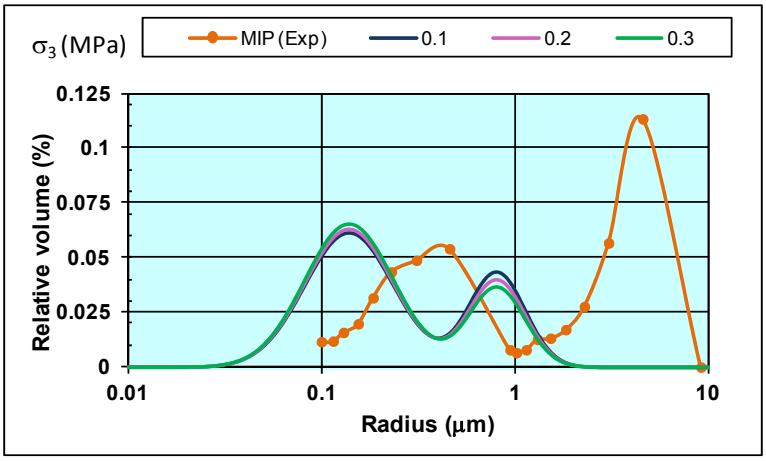

Figure 3: MIP test results and numerical PSDs for different confining pressures.

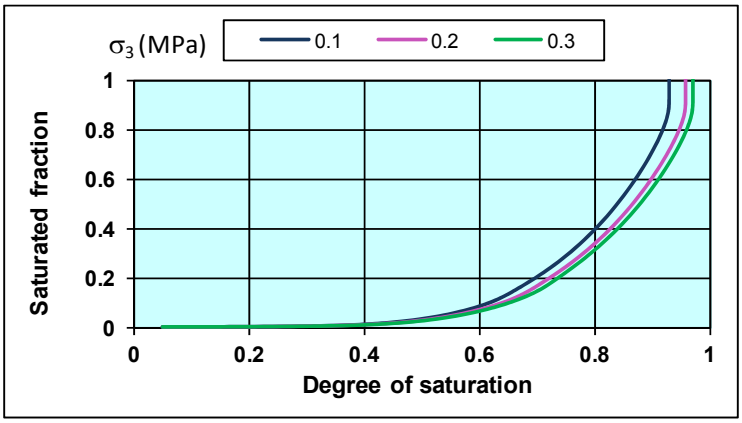

(a)

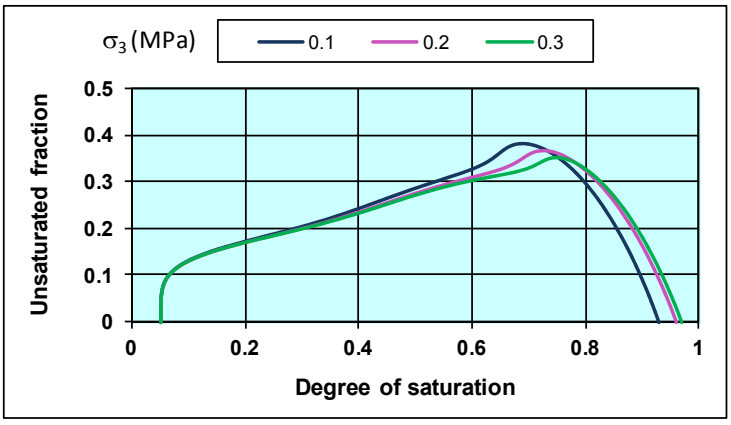

(b)

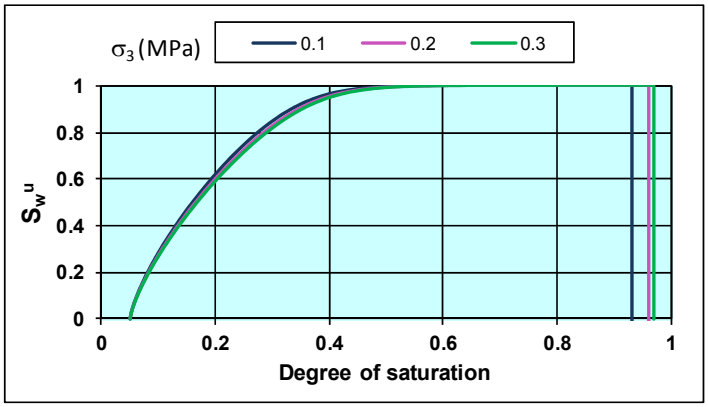

(c)

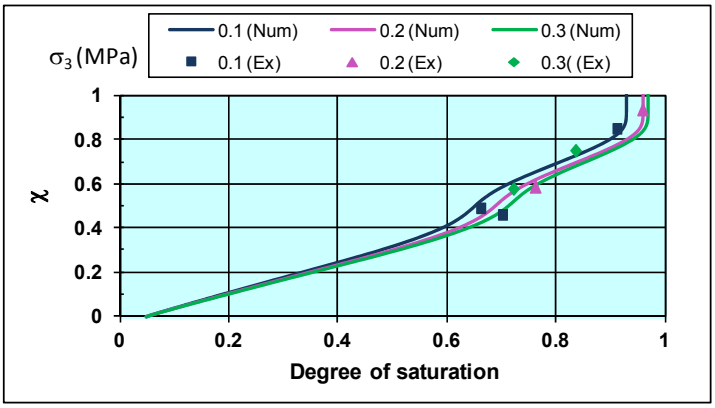

(d)

Figure 4: Parameters derived from the porous-solid model for different confining pressures (a) saturated fraction $f^{\tilde{s}}$, (b) unsaturated fraction f^{u}, (c) degree of saturation of the unsaturated fraction S_w^u and (d) parameter χ.

Finally, Fig. **6** shows the experimental results on the effective stress plane. The effective stress for the experimental points was obtained from Equation (2.14) using the corresponding value of χ for each sample. This value can be obtained from the numerical curves shown in Figs. **2** and **4**(d) according to the suction and confining pressure applied to each sample. It can be observed that tests performed at different suctions and confining stresses align in a single failure surface.

As SWRCs are linked to the current porosimetry of the soil, any action affecting the last modifies the former. Therefore, a porous model intending to represent the

distribution of water into the soil should include the pore size change generated by loading or suction increase. According to Simms and Yanful [46, 78], macropores are responsible for most of the volumetric strain of soils. These results indicate that macropores keep reducing their size with further increments of load or suction up to the point where most of them reach the range of mesopores. Still, most mesopores basically maintain their original size during loading or suction increase. This type of behavior can be introduced into the model by proportionally reducing the size of macropores with the level of loading as proposed by Koliji, Laloui, Cusinier and Vulliet [88]. In such cases the porosimetries of the sample before and after the shear test would be required.

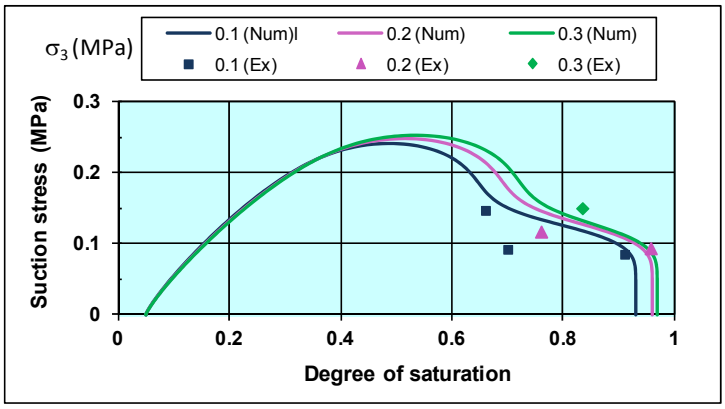

Figure 5: Numerical and experimental matric suction stress for different confining pressures.

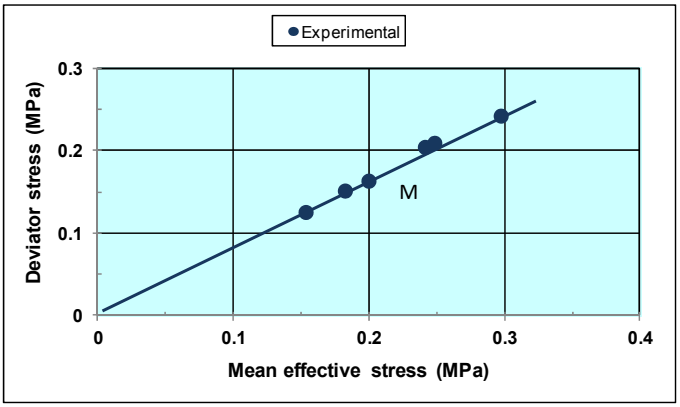

Figure 6: Experimental results on the effective stress plane.

Send Orders of Reprints at reprints@benthamscience.net

CHAPTER 7

Tensional Strength

Abstract: In this chapter, the probabilistic porous-solid model is used to simulate the tensional strength of unsaturated soils tested at different water contents. The strength of unsaturated soils can be split in two parts: one related to the net stress and the other to suction. The strength generated by suction has its origin on the additional contact stresses induced to solid particles by water meniscus. This additional contact stress is called matric suction stress. In that sense, the tensional strength of soils represents the matric suction stress of the material at that particular water content. The numerical and experimental comparisons of the tensional strength of unsaturated soils tested at different water contents show that the probabilistic porous-solid model can simulate this phenomenon with sufficient accuracy.

Keywords: Direct tension test, water meniscus, tension stress, suction, matric suction stress, additional contact stress, tensional strength, probabilistic porous-solid model, effective stress, net stress, suction, cohesion, water menisci, homogenous material, retention curves.

7.1. ITRODUCTION

Equation (2.18) represents the strength of an unsaturated soil subjected to certain suction. This equation can also be rewritten as:

$$\tau = \sigma'_n \tan\phi = \left((\overline{\sigma})_n + \sigma_s^*\right)\tan\phi = \left(\overline{\sigma}\right)_n \tan\phi + c$$

where c represents the cohesion of the soil. If osmotic suction is neglected, the matric suction stress represents an additional contact stress induced by water meniscus to solid particles (Lu, 2008) and is given by the relationship:

$$\sigma_s^* = \chi\, s = \left[f^s + S_w^u f^u \right] s \ldots \tag{7.1}$$

Between the considerations made to obtain this equation is that the soil is considered as a homogeneous isotropic material and in that sense the matric suction stress represents an isotropic stress. During a pure tension test the maximum strength reached by a soil sample represents the linking stress between solid particles and therefore, it also represents the matric suction stress of the

Eduardo Rojas

material at that particular water content [89]. Thus, tension tests can give a direct value of the matric suction stress of soils. In that sense, the probabilistic porous-solid model can be used to determine the matric suction stress of a soil and therefore its tensional strength.

7.2. TENSION TESTS

Vesga and Vallejo [89] performed a series of direct tension tests on kaolin samples with different degrees of saturation following a drying path. At the same time these researchers reported the SWRC of the material.

The tension tests were performed on flat bowtie-shaped samples. In this way, the samples could be fixed at their extremes and failure always occurred at their center. The samples were 7cm long, 2.2cm thick with a central neck 2.5cm wide. These samples were casted in a flat mould where the material was placed at a water content close to the liquid limit (40%). Then a vertical load of 0.03MPa was applied for 24 hours. Once the loading stage was finished, the sample was subjected to a drying process in controlled humidity conditions up to the point where it reached a water content previously specified. Finally the sample was placed in a membrane for 48 hours to allow the homogenization of the humidity before the test was performed.

Unfortunately, all these tests were performed following a drying path and there is no information related to the wetting path. In any case, the porous-solid model was used to simulate the drying branch of the SWRC of the material by successively adjusting an initially proposed PSD as already explained in Chapter 5. Fig. **1**(a) shows the experimental SWRC obtained by Vesga and Vallejo [89] using the filter paper method. This figure also shows the fitted numerical SWRC obtained with the porous model. In this case a single logarithmic normal function was considered for both macropores and mesopores whereas a double logarithmic normal distribution was considered for bonds to achieve the best fit with the SWRC. The required data for each distribution are the mean radius, the standard deviation and the proportional volume factor. These values obtained for these parameters are presented in Table **1**.

Table 1: Parameters of the model

Parameter	**M**	**S**	**B_1**	**B_2**
Mean size $\overline{R}$ (μm)	.075	0.0014	0.0009	.03
Standard deviation δ	1.5	5.1	7	3.5
P_{vf}	0.02			0.1

Note: M = macropores, S = mesopores, B_1 = Bonds (1), B_2 = Bonds (2), Sol_1 = Solids (1), Sol_2 =Solids (2), P_{vf} = Proportional volume factor.

These parameters establish the frequency of the different sizes of pores in the porous network. With this data and the size of the pores, it is possible to determine the numerical relative volume for each size as shown in Fig. **1**(b). Fig. **1**(c) shows the values of parameters f^s, f^u, f^d and S_w^u obtained from the porous-solid model when the sample follows a drying path. Finally, Fig. **1**(d) shows the values for parameter χ *vs.* suction. By comparing Figs. **1**(a) and (d) it can be observed that the values of parameter χ are slightly smaller than those of the degree of saturation. All these parameters were obtained only for the drying condition as no information was provided for the wetting branch of the SWRC.

Fig. **2** shows the comparison between the experimental tensional strength and the matric suction stress obtained from Equation (7.1). Because this last value represents the bonding stress between solid particles, it is equivalent to the tensional strength of the soil.

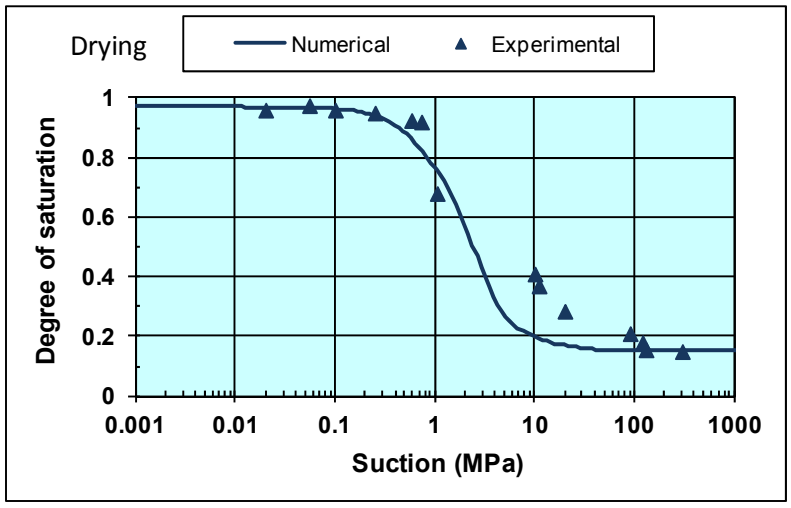

(a)

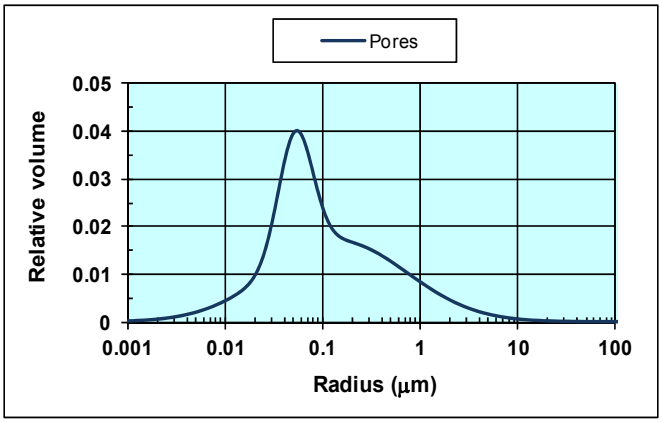

(b)

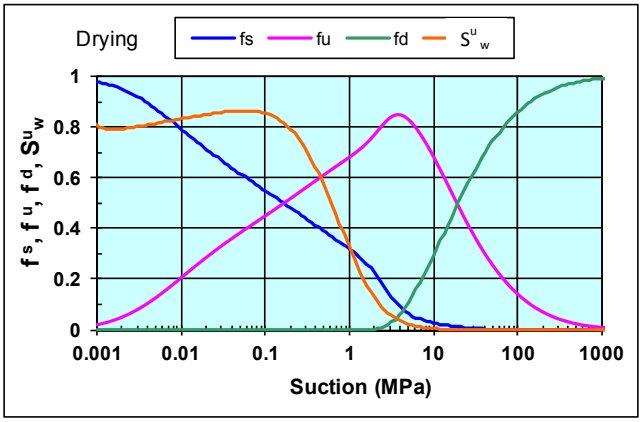

(c)

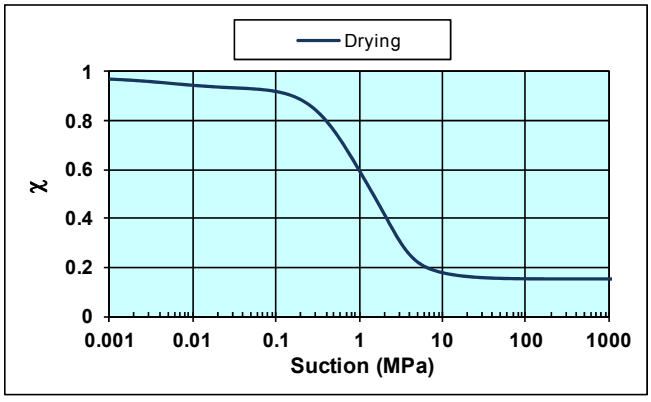

(d)

Figure 1: Results for a kaolin sample: (a) Fit of the experimental SWRC, (b) Numerical PSD, (c) parameters f^s, f^u, f^d and S_w^u and (d) values of χ (experimental data by Vesga and Vallejo [89]).

The numerical and experimental results presented in Fig. **2** show that a maximum tension stress occurs at certain point of the drying process. This maximum is related to a maximum in the matric suction stress represented by Equation (7.1). This maximum can be explained as follows: when an initially saturated soil is subjected to drying, the number of menisci producing the link between solid particles increases at the same rate as the unsaturated fraction increases (see Fig. **1**(c)). Then at certain point, the unsaturated fraction starts decreasing with increasing suction, meaning that the number of menisci decrees at certain point of the drying process. This happens because at this point, a dry fraction develops and progresses with the value of suction as it can be observed in Fig. **1**(c). This reduction in the number of water menisci in the soil sample eventually results in a reduction of the matric suction stress even if suction keeps increasing.

The comparison presented in Fig. **2** shows that the model predicts a maximum tension stress slightly larger than the experimental value. Additionally the numerical maximum stress is displaced to the left hand side with respect to the maximum experimental value, however, the shape and values of the numerical curve correspond well with the experimental results. One problem with these comparisons is that the tension tests were not performed in controlled suction conditions while the numerical results consider that suction remains constant during the test.

In any case and according to these results, it can be said that the probabilistic porous-solid model simulates with fair precision the results of tension tests performed at different water contents.

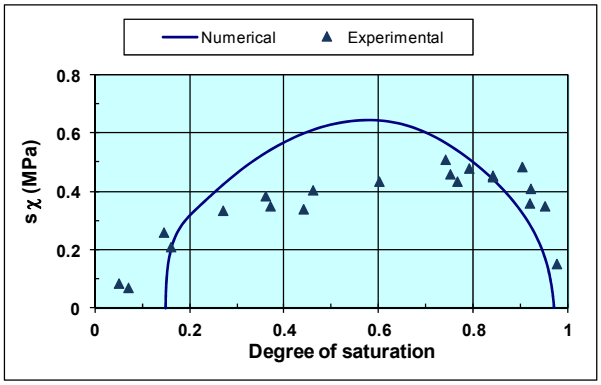

Figure 2: Numerical and experimental results comparison for tension tests (experimental data by Vesga and Vallejo [89]).

Send Orders of Reprints at reprints@benthamscience.net
Towards a Unified Soil Mechanics Theory, 2013, 115-139

CHAPTER 8

Volumetric Behavior

Abstract: An equation to account for the volumetric behavior of unsaturated soils is proposed in this chapter. This equation is based on the effective stress principle and results in a unifying framework for the volumetric behavior for both saturated and unsaturated soils. The results of the proposed equation are compared with experimental results published by different researchers. These comparisons show that the equation is adequate to account for wetting-drying and net stress loading-unloading paths. This analysis confirms that the effective stress principle can be applied to the volumetric behavior of unsaturated soils.

Keywords: Volumetric behavior, effective stress principle, isotropic triaxial test, controlled suction test, effective stress, compression index, unloading-reloading index, unsaturated soils, collapse, elastoplastic framework, hydro-mechanical coupling, water menisci, macropores shrinkage, suction hardening, yield surface.

8.1. INTRODUCTION

Different approaches have been proposed to simulate the volumetric behavior of unsaturated soils. Two of the main trends are the independent stress variables approach and the single stress variable approach. In the first one, two different coefficients are used to account for the contribution of net stress and suction on the volumetric behavior. In the second case, a single volumetric coefficient is related to a single stress variable (in most cases referred as the effective stress) to simulate the volume change.

One of the main advantages in using the single stress approach is that the hydro-mechanical coupling observed in unsaturated soils is implicit into the formulation. On the other hand, the difficulties in finding a correct explanation for the phenomenon of collapse upon wetting were one of the main objections to this approach. However, it is presently acknowledge that the simulation of this phenomenon requires, in addition to the effective stress equation, an appropriate elastoplastic framework. In contrast, the independent stress variables models seem to clearly explain the phenomenon of collapse upon wetting while the implementation of the hydro-mechanical coupling has been included in different degrees [22, 23, 90, 91].

Eduardo Rojas

The first approach has the following general form for the elastoplastic volumetric strain increment $d\varepsilon_v$:

$$d\varepsilon_v = \frac{1}{v}\left(\lambda_{vp}\frac{\bar{p}}{\bar{p}} + \lambda_{vs}\ \frac{ds}{(s + p_{atm})}\right)$$

Where v is the specific volume of the soil, $\bar{p}$ and $d\bar{p}$ represent the apparent preconsolidation mean net stress at the current suction and its increment, respectively, s and ds are the maximum previous suction and its increment, p_{atm} is the atmospheric pressure, λ_{vp} and λ_{vs} are the slopes of the compression curves due to increases of the mean net stress and suction, respectively, in a semilogarithmic plane. Both slopes show negative values meaning that a negative volumetric strain represents a volume reduction. This expression allows great flexibility in the simulation of the volumetric behavior of unsaturated soils. It is common to express λ_{vp} as a function of suction while λ_{vs} is considered constant. However, the experimental results indicate that λ_{vp} must also depend on the mean net stress while λ_{vs} must depend on both the mean net stress and suction (see for example [92] and [93]). In that sense, the above expression becomes more complicated than it seems. Another disadvantage of this expression is that under zero suction the equation for the volumetric behavior of saturated soils is not recovered and therefore there is not a smooth transition between saturated and unsaturated states [94]. Examples of this approach are given in the models developed by Alonso, Gens and Josa [7], Wheeler and Sivakumar [83] and Thu, Rahardjo and Leong [95], among others.

The second approach can be written in the following general form:

$$d\varepsilon_v = \frac{\lambda_v}{v}\frac{dp'}{p'}$$

where p' and dp' represent the preconsolidation effective stress and its increment, respectively and λ_v represents the slope of the compression curve in the axes of the logarithm of the effective stress *versus* specific volume. If parameter λ_v is expressed as a function of suction alone, it shows decreasing values with increasing suction. This, however, contradicts the experimental results [94]. To avoid this inconsistency, λ_v should be written as a function of the mean net stress,

the preconsolidation stress and suction. Another possibility is to write λ_v as a function of the degree of saturation [94]. The effective stress approach has been used in the models proposed by Sheng, Sloan and Gens [25], Sun, Cui, Matsuoka and Sheng [91], Khogo, Nikano and Miyazaky [96], Loret and Khalili [97], Kholer and Hofstetter [98] and Koliji, Laloui and Vulliet [99] among others.

Recently Sheng, Fredlund and Gens [100] proposed a combination of these two trends using two different volumetric parameters in conjunction with a stress parameter that accounts for the effects of both net stress and suction in the form:

$$d\varepsilon_v = \lambda_{vp} \frac{d\bar{p}}{\bar{p}+s} + \lambda_{vs} \frac{ds}{\bar{p}+s} \dots \tag{8.1}$$

Parameter λ_{vs} depends on the value of λ_{vp} according to the following relationship:

$$\lambda_{vs} = \begin{cases} \lambda_{vp} & s < s_a \\ \lambda_{vp} \frac{s_a+1}{s+1} & s > s_a \end{cases} \dots \tag{8.2}$$

where s_a represents the saturation suction [100] (*i.e.* the value of suction at the air entry value). In this case, the volumetric strain by net stress or suction increase depends on both the current net stress and the current suction; therefore, Equation (8.1) can more accurately reproduce the volumetric response of unsaturated soils reported in the international literature.

One of the most important features of this equation is the introduction to some extent of the hydro-mechanical coupling trough parameter s_a. In addition, although the two compression indexes λ_{vs} and λ_{vp} can be related using Equation (8.2), different relationships can be used for more general cases. When plotted in the mean net stress axis against suction, the yield surface generated with Equation (8.1) shows a concavity. In fact most constitutive models for unsaturated soils show a concavity at the transition between saturated and unsaturated states (see for example [101-104]). Although, this concavity poses some difficulties in obtaining a unique response, this can be numerically solved. Moreover, Equation (8.1) cannot be integrated and therefore requires special treatment in the stress integration of the constitutive model.

8.2. PROPOSED EQUATION

Júarez-Badillo [105] and Butterfield [106] proposed the following equation for the volumetric behavior of saturated soils:

$$d\epsilon_v = \frac{dv}{v} = \lambda_v \frac{dp'}{p'}$$

Integration of the above equation results in:

$$\frac{v}{v_0} = \left(\frac{{p_0}'}{p\prime}\right)^{\lambda_v}$$

where $p_0^{'}$ represents the initial effective stress corresponding to a volume v_0 in the virgin consolidation line. For very large values of the mean effective stress $p^{'}$, the specific volume $v=1+e$ tends to zero which is clearly inconsistent. A more likely relationship would involve the void ratio instead of the specific volume, in the form of:

$$\frac{de}{e} = \lambda_e \frac{dp\prime}{p\prime} \ldots \tag{8.3}$$

where λ_e represents the slope of the compression line in a logarithmic plane of effective stress *vs.* void ratio and because the void ratio reduces with increasing effective stress it exhibits negative values. A similar expression was proposed by Sheng, Yao and Carter [107] for the volumetric behavior of sands upon isotropic loading. Integration of the above equation results in:

$$\frac{e}{e_0} = \left(\frac{p'}{p_0'}\right)^{\lambda_e} \ldots \tag{8.4}$$

where e_0 represents the initial void ratio.

Fig. **1** shows the plot of this equation in the axes of the logarithm of the mean effective stress against void ratio for different values of the compression index λ_e and for an initial void ratio of 1.14 at a mean effective stress of 0.02MPa. Most soils show values of the parameter λ_e ranging between -0.05 and -0.3 in which case, the volumetric behavior for stresses in the range of civil engineering interest

(from 0.1 to 10MPa) can be approximated to straight lines, as it is commonly done.

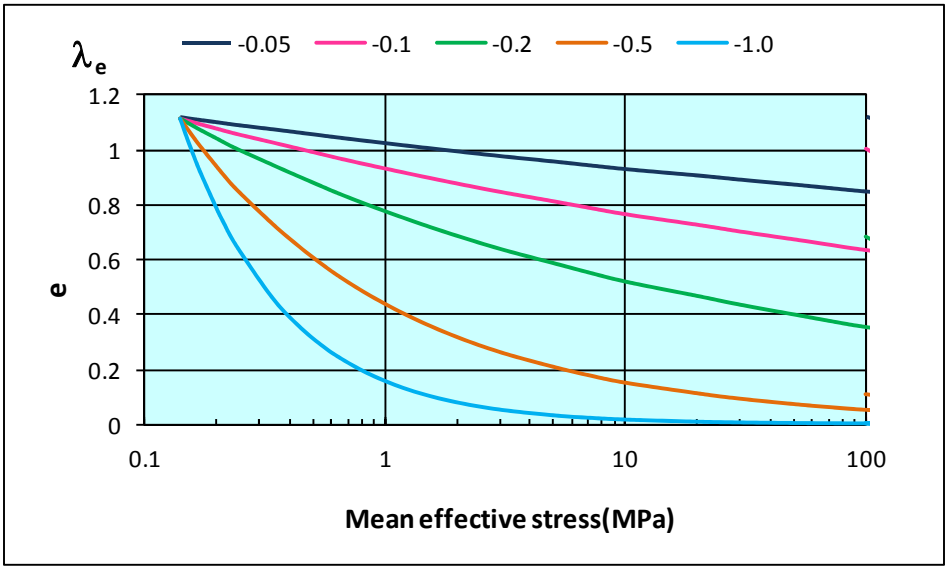

Figure 1: Volumetric behavior of saturated soils for different values of the compression index.

For the case of unsaturated soils, its volumetric behavior can be analyzed through the results of two types of tests: isotropic loading by net stress increase at constant suction and suction increase at constant net stress. The results of the first type of test can be summarized as follows: when suction is below the air entry value, the soil behaves as saturated. However, when suction surpasses the air entry value, water menisci appear among the solid particles. These menisci produce additional contact stresses between the solids increasing the stability of the large pores as if the preconsolidation stress of the soil was increased. Therefore, the shrinkage of these pores can only be produced by applying further increments of the mean net stress. This means that the material experiences suction hardening. The greater the applied suction, the larger the mean net stress required for shrinking these pores and the soil behaves as an overconsolidated material.

For the second type of test, the soil behaves exactly the same as for the first case as long as suction remains below the air entry value. When suction becomes larger than the air entry value a number of pores becomes dry. Under these conditions, when suction increases, all saturated pores tend to shrink following the

same law as for the saturated material. On the contrary, all dry pores show no reaction to suction changes.

According to these descriptions, the evaluation of the volumetric response of unsaturated materials requires the quantification of the menisci of water and the pores that remain saturated at certain suction. For that purpose, the porous-solid model developed in Chapter 4 can be used.

The studies on the PSD of different soils indicate that in some cases these materials show a bimodal distribution meaning that they show two crests [78]: one corresponding to the macropores or large cavities and the other to the mesopores or small cavities. The macropores are cavities that show special arrangements of solid particles in the form of vaults or arches. These pores have the characteristic of being larger than the solid particles forming the pore; therefore, their equilibrium is precarious upon isotropic loading or shearing. This can be confirmed by analyzing the PSD of different soils before and after performing triaxial tests as Futai and Almeida [92] and Simms and Yanful [45] have done. These researchers used the MIP test to compare the PSD before and after testing a soil. They found that most macropores reduce in size and transform into smaller pores at the end of these tests. They concluded that macropores are responsible for most of the volumetric response of soils.

On the other hand, the mesopores have the characteristic of being smaller than their surrounding solids; therefore, they are very stable and in general maintain their size upon isotropic loading or shearing. Sometimes soils show a mono-modal size distribution similar to uniform dense sands. In this case, macropores are absent from the soil and as such all volumetric deformation is generated by the shrinkage of mesopores which in any case is small compared with the shrinkage of macropores in a bimodal structured soil. Mono-modal size distributions can also be obtained from slurries made of soils showing uniform GSD. When slurries start to dry, they adopt well defined structures with diverse PSDs, which depend greatly on the GSD of the material. Bimodal GSDs usually generate bimodal PSDs as it is observed in the experimental results shown in section 4 of this chapter. These bi-modal or mono-modal structures are also reflected on the shape of the SWRCs. Samples with monomodal PSDs show a single inflection point in

their SWRCs. On the contrary, samples with bimodal or trimodal PSD show two or three inflection points in their SWRCs, respectively. In any case, the porous model can simulate any of these cases. In the monomodal case, it is sufficient to consider that macropores do not exist in the porous structure of the material.

The micropores or bonds represent the smallest pores usually found at the contact between solid particles and therefore they are also very stable when the mean net stress or suction increases. All these elements are shown schematically in Fig. **2**.

Now, consider Equation (2.15) representing Bishop's parameter χ. This relationship can be written in the following form:

$$\chi = f^s + S_w^u \, f^u = \sum_f S_w^i \, f^i$$

where superindex i represents the type of fraction: dry (d), saturated (s) or unsaturated (u). In terms of volumetric behavior the above equation can be interpreted as follows: it represents the addition of the product of every fraction by its degree of saturation. This means that for the saturated fraction, the effect of an increment of suction is the same as an increment of the mean net stress (term $s \, f^s$ in Equation (2.14)) because in that case $S_w^s = 1$, whereas for the unsaturated fraction, the effect of an increment of suction is proportional to the degree of saturation of this fraction (term $s \, S_w^u \, f^u$ in Equation (2.14)). Finally, the dry fraction (f^d) shows a nil degree of saturation and therefore does not appear in Equation (2.14). In other words, Bishop's parameter represents the weighted degree of saturation of all three fractions.

Even if the dry fraction does not play any role in the volumetric deformation during suction increase nor appears in the determination of parameter χ, it certainly plays a role during mean net stress increase as in this case all fractions contributes equally to the volumetric deformation of the soil. This means that the term $\bar{p}$ in Equation (2.14) is multiplied by the sum of all fractions which is equal to one. This agrees with the description of the volumetric behavior of unsaturated soils provided before.

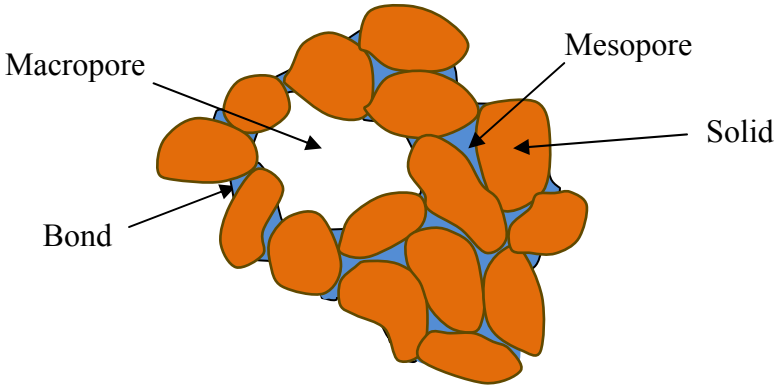

Figure 2: Soil structure: macropores, mesopores, bonds and solids.

It is noteworthy that Equation (8.4) uses the same compressive index λ_e no matter if it corresponds to an increase in mean net stress or suction although, for this last case, the index is affected by parameter χ because it represents the proportion of pores affected by suction changes. In other words Equation (8.4) represents a single compression curve for both net stress and suction increase.

8.3. ELASTOPLASTIC FRAMEWORK

In addition to Equation (8.4), the modeling of the volumetric behavior of unsaturated soils requires an elastoplastic framework. The framework considered herein is sketched in Fig. **3** in the axes of mean net stress (Fig. **3**(a)) and mean effective stress (Fig. **3**(b)). A normally consolidated soil sample exhibits a Loading Collapse Yield Surface (LCYS) represented by a line forming an angle of 135^0 with the mean net stress axis as established by Sheng, Sloan and Gens [25] (Fig 3(a)). When this sample is subjected to a suction s, the drying path (represented by a vertical line in Fig. **3**(a)) crosses the initial yield surface generating a plastic deformation. This plastic deformation produces the hardening of the LCYS which displaces to the right hand side. This displacement depends on the increment of the effective stress applied to the soil and is represented by the value of the matric suction stress χs. In other words, χs represents the increment of the mean net stress that produces the same volumetric plastic deformation generated during the drying of the soil. If at this point the soil is wetted up to saturation, it follows an elastic unloading that does not affect the position of the LCYS. Thus, it can be inferred that the preconsolidation stress in saturated

conditions has also increased in the quantity χs. This means that the LCYS can be represented by a vertical line in the mean net stress plane and therefore, it shows the same shape of the drying path but displaced in the quantity χs. If the intersecting points of this surface with the loadings paths followed by net stress increase at constant suction are linked together by a line (fine dotted line in (8.3a), it adopts the shape of the LCYS that has been experimentally determined by different researchers (see for example [92, 95, 108]). It can be argued (as Sheng [94] does) that the experimental procedure used to obtain the LCYS considers that the soil initially behaves elastically during the loading stage after drying but this could not be the case. Only the analysis of more experimental results would give light to this issue.

In the axis of the mean effective stress, the drying path initially adopts a slope of 45^{o} and then deviates from this direction as the soil becomes unsaturated. Similarly, the LCYS adopts this same shape and displaces the quantity χs on the mean effective stress axis as shown in Fig. **3**(b).

According to this framework, when Equation (8.4) is plotted for a set of tests where the net stress increases while suction remains constant, each sample undergoes a different hardening given by the quantity χs and therefore, the loading paths are represented by a family of curves in the axes of the logarithm of the mean net stress against void ratio as shown in Fig. **4**(a). These curves are similar to the volumetric response of unsaturated soils reported by different researchers (see for example: [83, 92, 107, 109]). When these results are plotted on the axes of the logarithm of the mean effective stress *versus* void ratio, a family of curves, as those shown in Fig. **4**(b), is obtained. In this case, the data reported by Futai and Almeida [92] for a particular soil were used in order to establish the values of Bishop's parameter χ at different suctions. This procedure is shown in the next section of this chapter. In general, these curves can be assimilated to parallel straight lines for small ranges of the mean effective stress. Because parameter χ depends on the SWRCs of the material, the amount of suction hardening also depends on these curves. In general, soils showing large ranges of suction in their SWRCs exhibit large suction hardening. In contrast, suction hardening is difficult to observe in soils showing a small range of suction in their SWRCs.

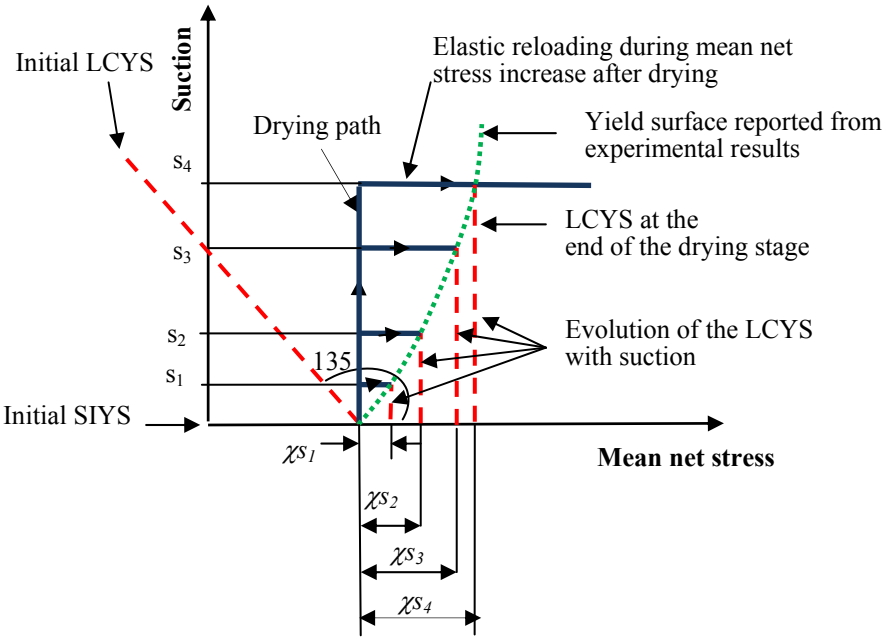

(a)

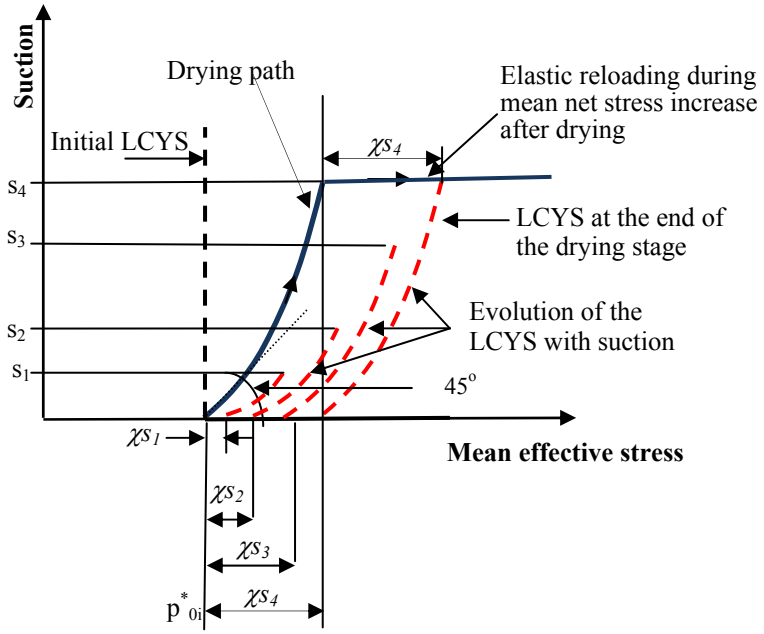

(b)

Figure 3: Evolution of the LCYSs during drying in (a) the mean net stress axis and (b) mean effective stress axis.

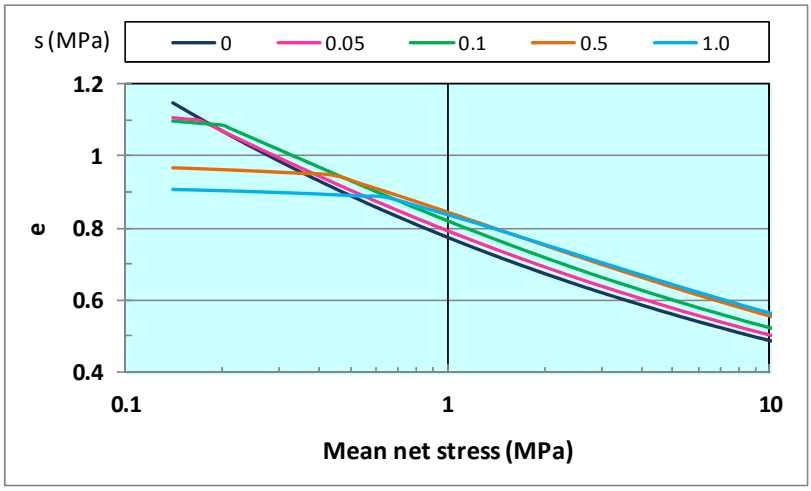

(a)

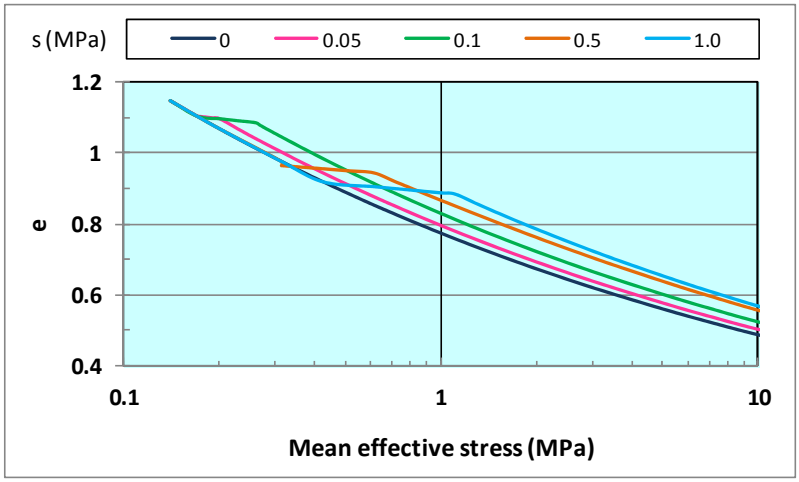

(b)

Figure 4: Numerical volumetric behavior of soils related to (a) mean net stress and (b) mean effective stress.

Elastic behavior of the material occurs when the current mean effective stress is smaller than the maximum mean effective stress experienced by the soil. For such a case, parameter λ_e becomes the slope of the unloading-reloading stress path κ_e, and the relationship (8.4) transforms into:

$$\frac{e}{e_0} = \left(\frac{p_0'}{p'}\right)^{\kappa_e} \ldots \tag{8.5}$$

This behavior happens when the mean net stress applied to the soil reduces while suction remains constant but, this may happen eventually when the soil attains large suctions because the matric suction stress reduces after reaching a maximum as shown in the previous chapter.

8.4. NUMERICAL AND EXPERIMENTAL COMPARISONS

In order to evaluate the proposed framework for the volumetric behavior of unsaturated soils, the results of various tests performed on a variety of materials and for different loading conditions were employed. Fleureau, Kheirbek-Saoud, Soemitro and Taibi [93] prepared different clayey soils at a water content of 1.5 times its liquid limit. This slurry was consolidated in an oedometer cell with vertical stresses ranging between 0.06 and 0.2MPa. Then the samples followed a drying-wetting path where suction was controlled using the axis translation technique for low suctions and the vapor circulation technique for large suctions. With the results of these tests, the variations of the void ratio, the degree of saturation and the water content with the value of suction were determined. Also the GSD and both SWRCs for some of these materials were reported. Here the results of the Sterrebeek loam, Montmorillonite clay and Yelow clay are presented. As the PSD of the soil was not available, it was inferred by fitting the numerical SWRCs with the experimental results according to the procedure outlined in Chapter 5.

The numerical PSD along with the experimental GSD and the void ratio were used to build the porous-solid model from which the value of parameters f^s, f^u and S_w^u were determined as a function of suction for both the wetting and drying paths. This allowed determining the mean effective stress given by Equation (2.14) while the numerical volumetric response of the material was derived from Equation (8.4). Fig. **5**(a) shows the fitting of the SWRCs for the Montmorillonite clay. Fig. **5**(b) represents the numerical PSD obtained at the end of the fitting process along with the experimental GSD of the material in the axes of size *versus* relative volume. The relative volume is the volume of pores (or solids) of certain a size divided by the total volume of pores (or solids) as explained before. Notice the similarity in shape of these two curves as has already been pointed out by Alonso, Rojas and Pinyol [52]. Fig. **5**(c) shows the values of parameters f^s, f^d,

f^u, S_w^u and χ obtained from the porous-solid model during a drying path. It can be observed that the saturated fraction starts reducing at very low suctions while the dry fraction only appears at very large suctions whereas the unsaturated fraction increases up to a certain point and then decreases to become nil at very large suctions. It can also be observed that parameter χ is closely related to the saturated fraction of the soil. In contrast, the degree of saturation of the unsaturated fraction S_w^u shows important fluctuations at low values of suction. This happens because most of the soil is still saturated at these values of suction and the unsaturated fraction (represented by those solids and their surrounding pores showing a combination of saturated and dry pores) is composed of a small number of elements (solids, cavities and bonds). Therefore a small change in the number of saturated elements produces important changes in the value of this parameter.

Only when the number of elements of this fraction is large enough it becomes smooth and shows a continuous increase and, at a certain point it reduces to become nil at large suctions. Finally, the numerical prediction and the experimental results of the volumetric behavior upon drying are compared in Fig. **5**(d). For each increment of suction the value of parameters f^s, f^u and S_w^u are obtained, the value of parameter χ is computed and the new void ratio is calculated. These results were obtained for λ_e = -0.36.

Following the same procedure the results of the Sterrebeek loam were simulated. Fig. **6**(a) shows the fitting of the wetting (W) and drying (D) SWRCs. Fig. **6**(b) shows the values for parameters f^s, f^u, f^d and S_w^u at drying. The values of these same parameters can also be found at wetting using the porous-solid model. With these values parameter χ can be obtained for both conditions: wetting and drying as shown in Fig. **6**(c). Finally, Fig. **6**(d) presents the comparison between numerical and experimental results for the volumetric behavior of this material. In this case, the volumetric response of the slurry following a drying path was determined for two different initial conditions: at zero net stress and at a preconsolidated net stress of 0.2MPa. These results were obtained with λ_e = -0.12. For both cases, it can be said that Equation 8.4 is adequate for simulating the volumetric behavior of the material.

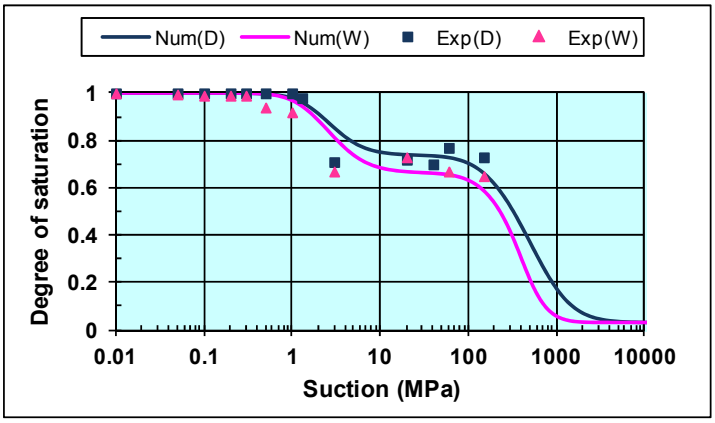
Num(D)
Num(W)
Exp(D)
Exp(W)
Degree of saturation
1
0.8
0.6
0.4
0.2
0
0.01
0.1
1
10
100
1000
10000
Suction (MPa)

(a)

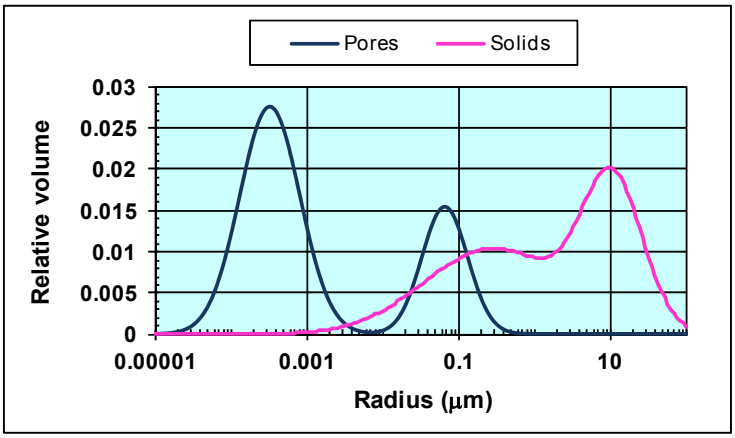
Pores
Solids
Relative volume
0.03
0.025
0.02
0.015
0.01
0.005
0
0.00001
0.001
0.1
10
Radius (μm)

(b)

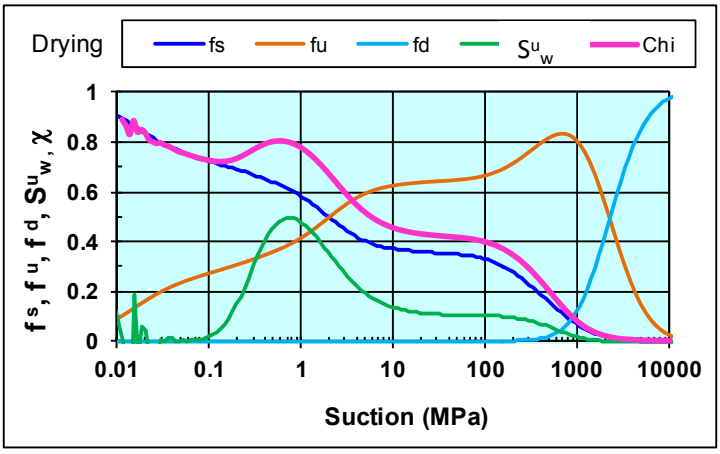
Drying
fs
fu
fd
Suw
Chi
fs, fu, fd, Suw, χ
1
0.8
0.6
0.4
0.2
0
0.01
0.1
1
10
100
1000
10000
Suction (MPa)

(c)

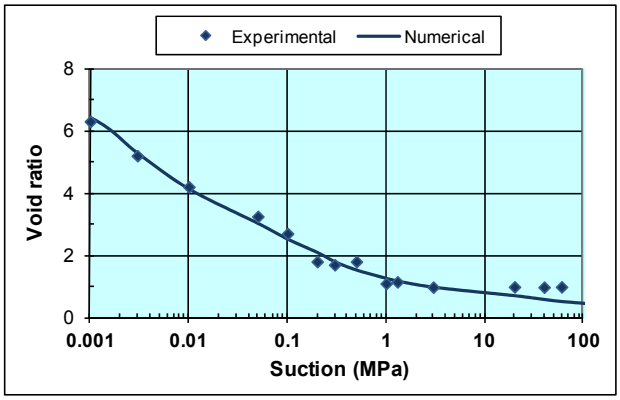

(d)

Figure 5: Results for the Montmorillonite clay: (a) fitting of the SWRCs, (b) numerical PSD and experimental GSD, (c) parameters f^s, f^u, S_w^u and χ and (d) volumetric behavior by suction increase (experimental data by Fleureau, Kheirbek-Saoud, Soemitro and Taibi [93]).

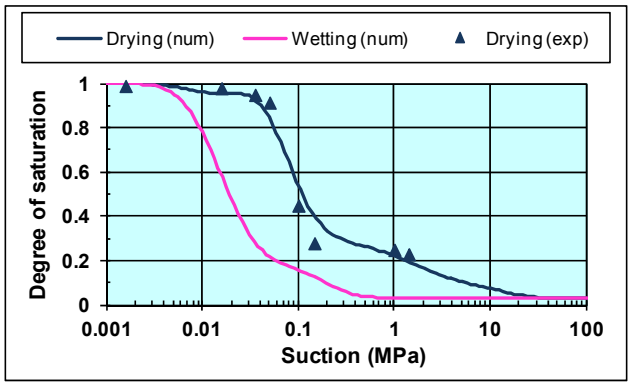

(a)

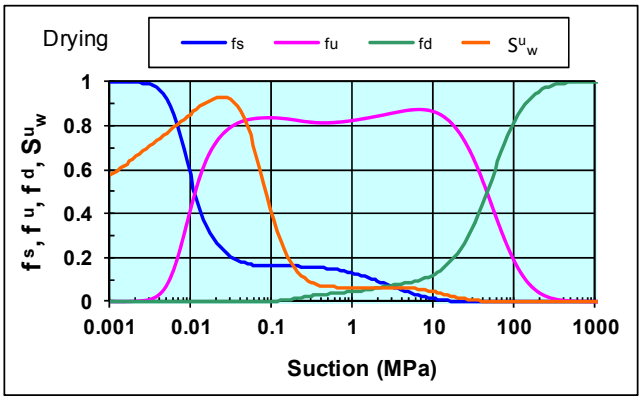

(b)

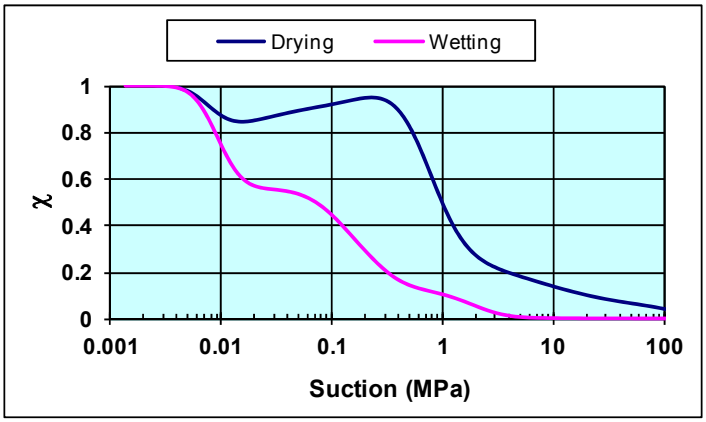

(c)

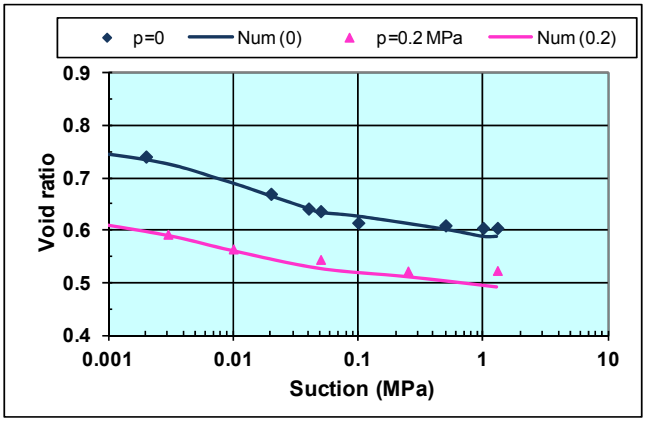

(d)

Figure 6: Results for Sterrebeek loam (a) fitting of the SWRCs, (b) parameters $\boldsymbol{f^s}$, $\boldsymbol{f^u}$ and $\boldsymbol{S_w^u}$ (c) parameter χ and (d) volumetric behavior by suction increase at two different net stresses (experimental data by Fleureau, Kheirbek-Saoud, Soemitro and Taibi [93]).

Fig. **7** shows the results obtained for the Yellow clay. Fig. **7**(a) shows the fitting of the SWRCs at wetting (W) and drying (D). Fig. **7**(b) shows the values for parameters f^s, f^u, f^d and S_w^u at drying. The values for parameter χ at wetting and drying are shown in Fig. **7**(c). Finally, Fig. **7**(d) presents the comparison between numerical and experimental results for the volumetric behavior of this material following wetting and drying paths. These results were obtained for λ_e = -0.13 and κ_e = -0.013. It can be observed that for both stress paths the model adequately simulates the behavior of the material.

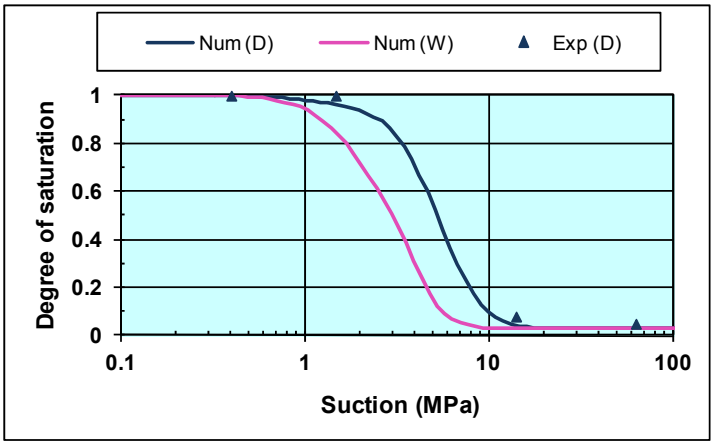
Num (D)
Num (W)
Exp (D)
Degree of saturation
1
0.8
0.6
0.4
0.2
0
0.1
1
10
100
Suction (MPa)

(a)

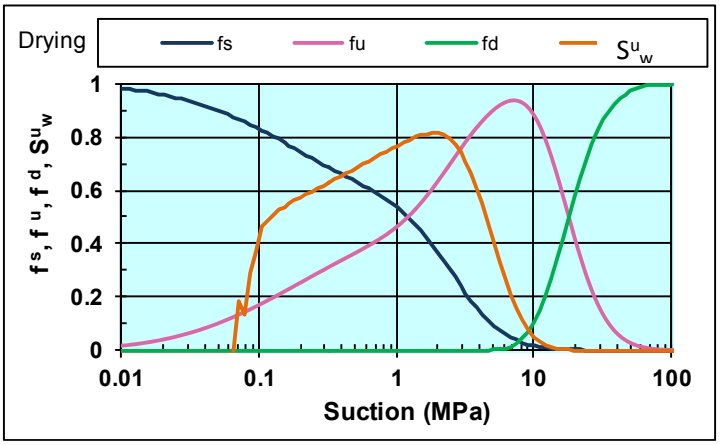
Drying
fs
fu
fd
S^u_w
f^s, f^u, f^d, S^u_w
1
0.8
0.6
0.4
0.2
0
0.01
0.1
1
10
100
Suction (MPa)

(b)

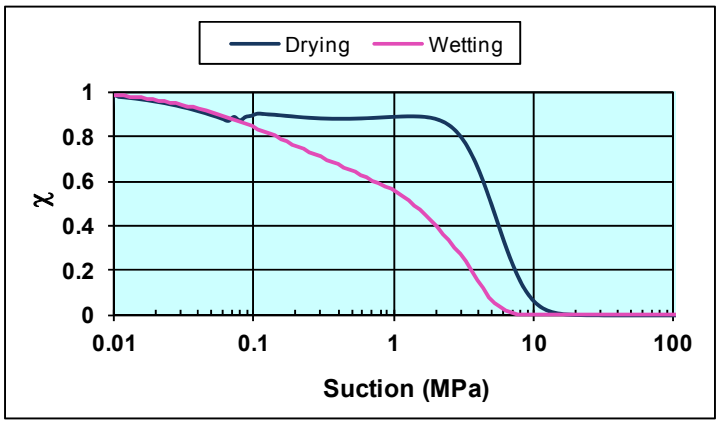
Drying
Wetting
χ
1
0.8
0.6
0.4
0.2
0
0.01
0.1
1
10
100
Suction (MPa)

(c)

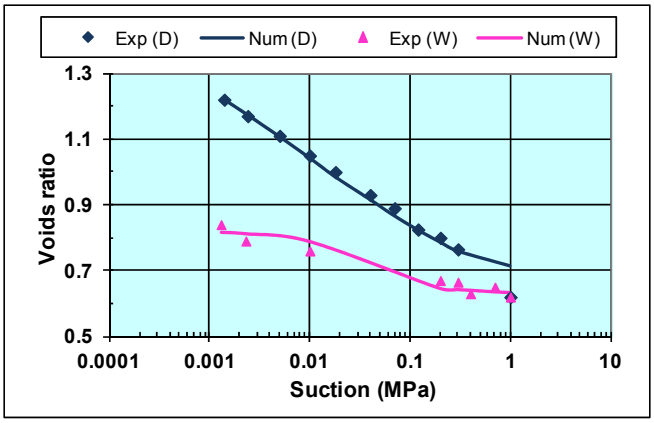

(d)

Figure 7: Results for Yelow clay (a) fitting of the SWRCs, (b) parameters f^s, f^u and S_w^u (c) parameter χ and (d) volumetric behavior by suction increase at two different net stresses (experimental data by Fleureau, Kheirbek-Saoud, Soemitro and Taibi [93]).

Futai and Almeida [92] reported the results of different tests performed on undisturbed samples of a residual soil. Additional data included the GSD, the PSD obtained from MIP tests and both SWRCs obtained by combining the suction plate and the filter paper technique. Fig. **8** shows the results of isotropic compression tests done on gneiss samples subjected to three different suctions.

Fig. **8**(a) shows the fitting of the SWRCs which resulted in the numerical PSD shown in Fig. **8**(b). In this last figure the experimental results of a MIP test are also included and compare well with the numerical results. Fig. **8**(c) shows the values of parameter χ obtained from Equation (2.15). Finally, Fig. **8**(d) shows the comparison between numerical and experimental results of the volumetric behavior during isotropic loading tests on samples subjected to different suctions. It can be noted that although there is some scattering for the sample tested at a suction of 0.3MPa, the proposed framework is able to adequately simulate the volumetric behavior of an isotropically loaded soil subjected to different suctions.

The volumetric strains were determined using Equation (8.5) up to the yield stress generated at the end of the drying stage. From that point, Equation (8.4) was used for the rest of the curve. Because the increase in the yield stress of a saturated

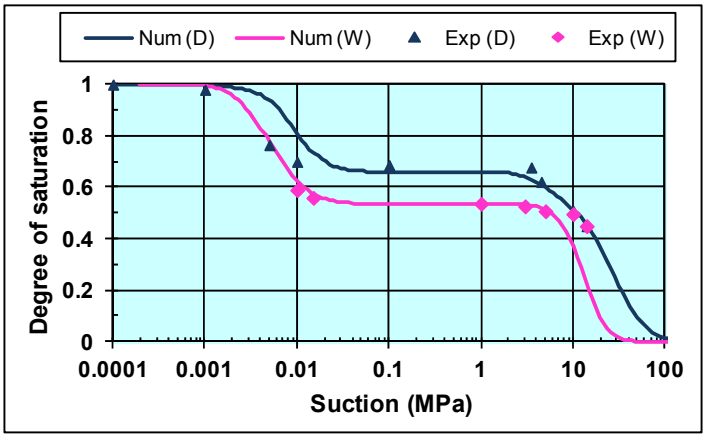
Num (D)
Num (W)
Exp (D)
Exp (W)
Degree of saturation
1
0.8
0.6
0.4
0.2
0
0.0001
0.001
0.01
0.1
1
10
100
Suction (MPa)

(a)

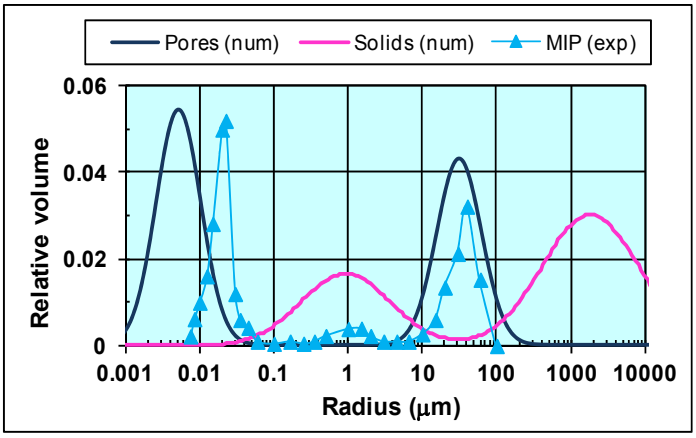
Pores (num)
Solids (num)
MIP (exp)
Relative volume
0.06
0.04
0.02
0
0.001
0.01
0.1
1
10
100
1000
10000
Radius (μm)

(b)

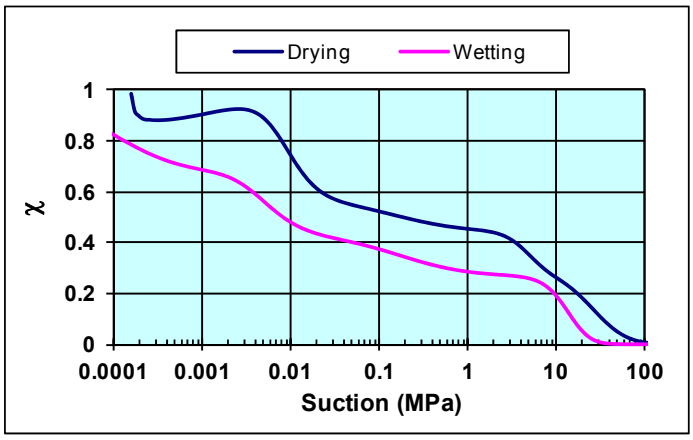
Drying
Wetting
χ
1
0.8
0.6
0.4
0.2
0
0.0001
0.001
0.01
0.1
1
10
100
Suction (MPa)

(c)

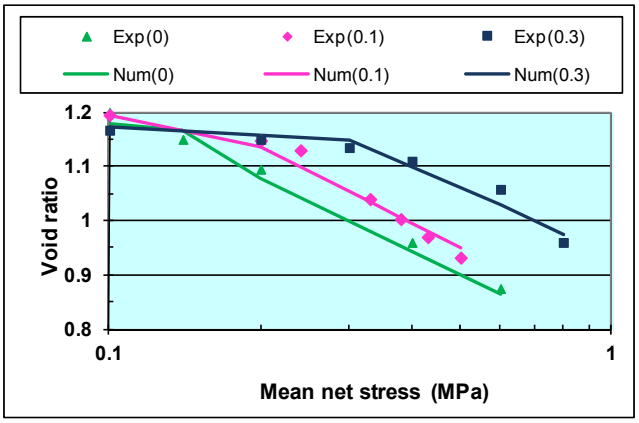

(d)

Figure 8: Results for a residual gneiss (a) fitting of the SWRCs, (b) numerical and experimental PSD, (c) values of parameter χ and (d) volumetric behavior at different suctions (experimental data by Futai and Almeida [92]).

sample generated during the drying stage is given by the quantity χs, the final yield stress is obtained by adding the initial preconsolidation stress of the soil in saturated conditions to the increment of the yield stress during the drying stage. For a small increment of suction (ds), the increase in the yield stress is given by $d\bar{p} = \chi\, ds + s\, d\chi$ where ds represents the increment of suction and $d\chi$ the variation of Bishop's parameter due to that increment. The preconsolidation stress of the material in saturated conditions is around 0.14MPa as can be observed in Fig. **8**(d). The values of parameter χ for the different suctions were obtained from Fig. **8**(c) resulting in: χ = 0.6 for s = 0.1MPa and χ = 0.58 for s = 0.3MPa which produced the following preconsolidation stresses: $\bar{p}_0$ = 0.2 for s = 0.1MPa and $\bar{p}_0$ = 0.31 for s = 0.3 MPa. From the results shown in Fig. **8**(d) it can be noticed that the theoretical preconsolidation stress for the unsaturated samples corresponds well with the experimental results. The considered values for the compression index at loading and reloading were λ_e = -0.25 and κ_e = -0.04.

Similar tests were performed by Cunningham, Ridley, Dineen and Burland [110] in a mixture of 20% speswhite kaolin, 10% of London clay and 70% of silica silt. With this mixture, a slurry was prepared at a water content 1.5 times its liquid limit. Then it was pre-consolidated one-dimensionally in a 20.4cm diameter

oedometer to a maximum vertical stress of 0.2 MPa. The soil samples were then trimmed from this pre-consolidated soil mass to the appropriate size. The tests included the GSD, both SWRCs obtained from the filter paper technique, isotropic loading and shearing tests at constant suction in the triaxial apparatus. For these last tests, suction was controlled using the air circulation technique and was measured directly in the soil samples using two suction probes. Some of the experimental results are shown in Fig. **9**. The experimental SWRCs and the numerical fitting for these curves are shown in Fig. **9**(a). Fig. **9**(b) shows the variation of parameter χ with suction. With these values it is possible to obtain the numerical volumetric response of the material during suction increase as shown in Fig. **9**(c). In this case, the experimental behavior shows a clear elastic rebound (even if there is some scattering) indicating that the effective stress reduces at some stage during the drying process. This happens because as suction increases, the value of the matric suction stress (represented by the product $s\chi$) reaches a maximum and then decreases, as shown in Fig. **9**(d). In this figure, it can be noted that when suction reaches a value slightly greater than 1 MPa, the matric suction stress reaches its maximum and then reduces while suction keeps increasing. When the drying path inverses to wetting, matric suction stress reduces further then increases (but never reaches the drying maximum value) and finally reduces again while suction keeps reducing. Therefore, when the matric suction stress reduces after reaching its maximum value, the numerical response switches from elastoplastic (Equation (8.4)) to purely elastic (Equation (8.5)). The numerical results were obtained with the following parameters λ_e = -0.13 and κ_e = -0.04. The switch from elastoplastic to elastic behavior during suction increase has been well documented by Khalili, Geiser and Blight [111]. Similar results were reported and simulated by Vlahinic, Jennings and Thomas [112] and Blight [113] on different porous materials. This reduction in the effective stress during drying can also be observed in the experimental results reporting the strength of the material with suction. A maximum value and then a reduction of the strength can be observed if suction is increased sufficiently (see for example: [21, 34, 35, 70, 112, 114, 115]). This same behavior is observed in the tensional strength of soils as shown in the previous chapter and also reported by Fredlund, Xing, Fredlund and Barbour [71].

Also, some constitutive models consider this reduction in the strength of soils with suction (see for example [70, 116, 117]). Not all soils show this behavior; for example, soils with large clay contents may show a continuous increase in strength with suction due to the presence of layers of adsorbed water that does not disappear even at very large suctions. On the contrary, the effect of suction on the strength of sandy soils disappears completely at large suctions. Fig. **9**(e) shows the numerical and experimental results for isotropic loading at different suctions on the axis of the mean net stress against void ratio. In this case the materials were dried from slurry and because of that, the preconsolidation stress equals the matric suction stress sχ, where parameter χ was obtained from Fig. **9**(b).

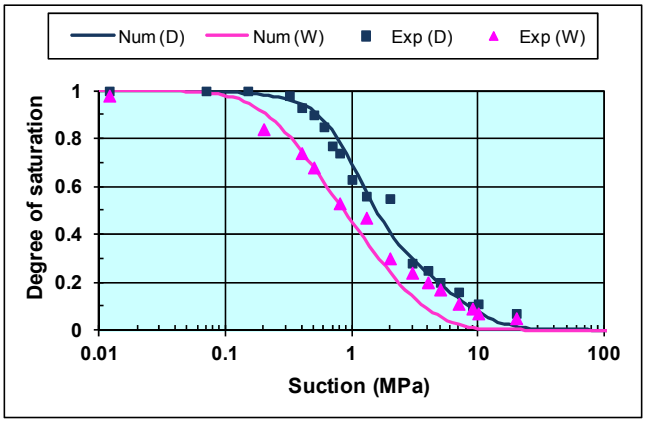

(a)

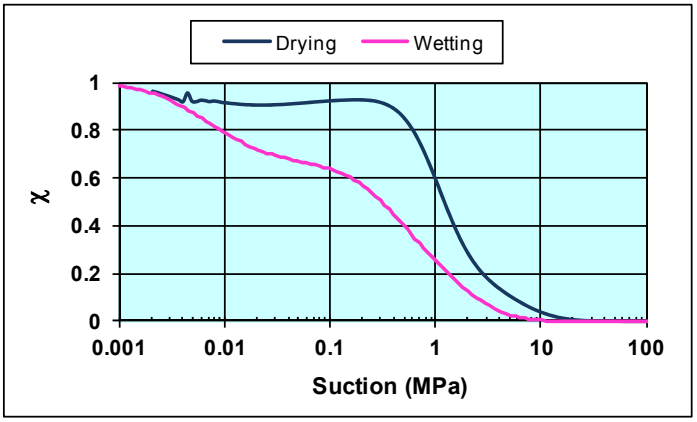

(b)

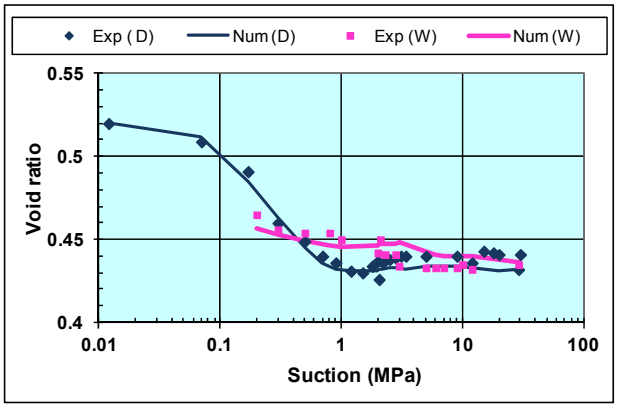

(c)

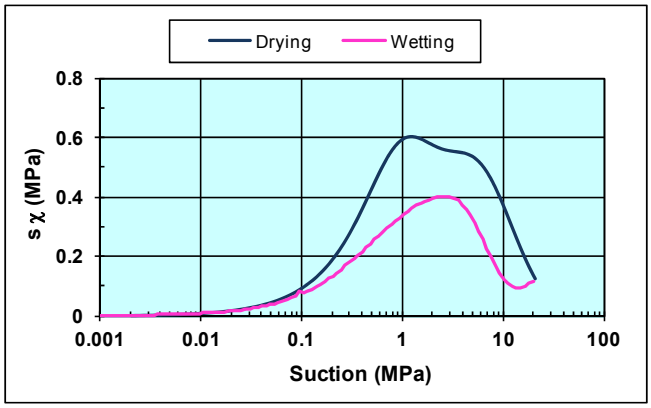

(d)

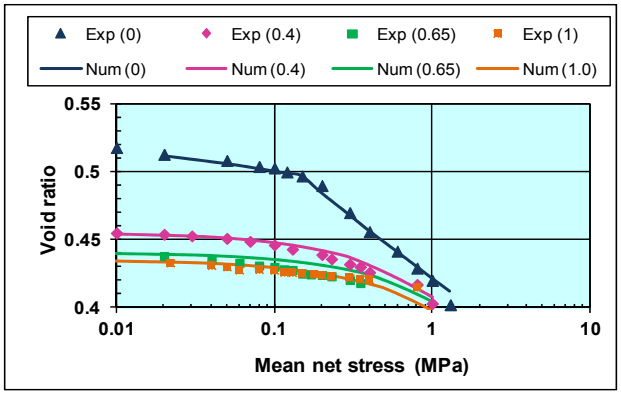

(e)

Figure 9: Results for a soil mixture: (a) fitting of the SWRCs, (b) parameter χ, (c) volumetric response with suction, (d) matric stress sχ and (e) volumetric response with mean net stress (experimental data by Cunningham, Ridley, Dineen and Burland [110]).

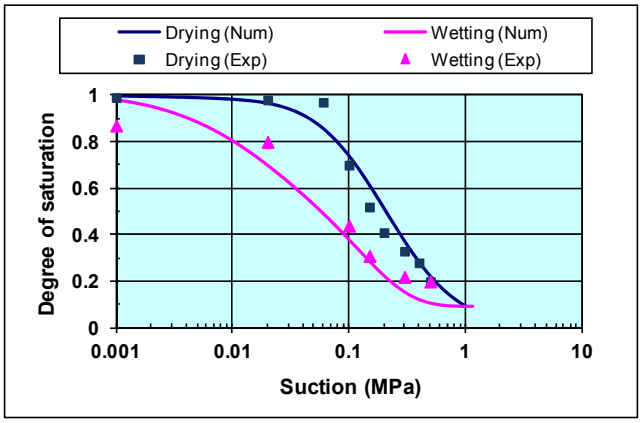

(a)

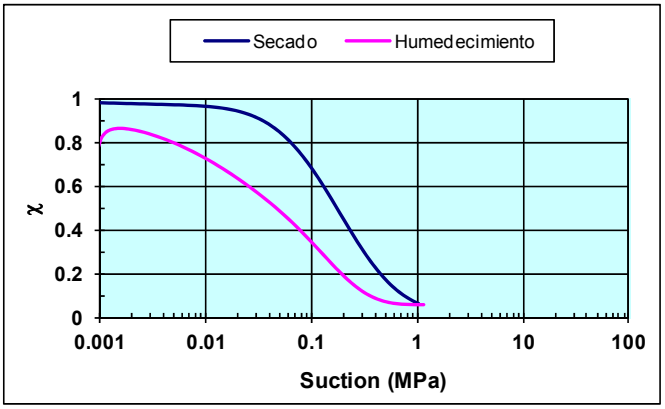

(b)

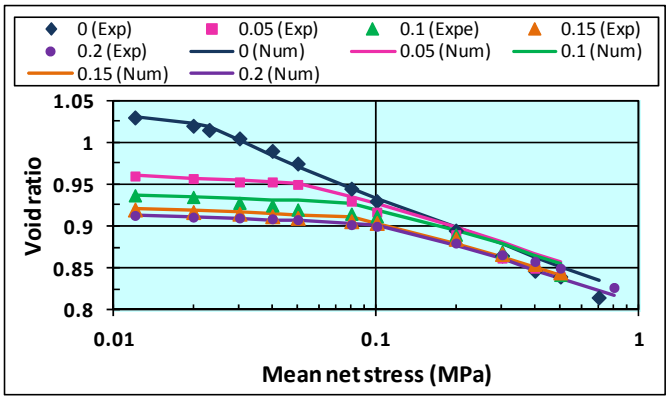

(c)

Figure 10: Results for a coarse kaolin: (a) fitting of the SWRCs, (b) parameter χ in wetting and drying and (c) volumetric behavior (experimental data by Thu, Rahardjo and Leong [95]).

Other tests were conducted by Thu, Rahardjo and Leong [95] on statically compacted samples of industrial coarse kaolin. All samples were compacted at the optimum water content and then saturated using back pressure. Afterwards, all samples were consolidated at an isotropic net stress of 0.01 MPa following a drying stage where suction ranged between 0 and 0.3MPa. Finally, the samples were isotropically loaded up to 0.7MPa in net stress. The fitting of the SWRC in wetting and drying is shown in Fig. **10**(a). The values of parameter χ in wetting and drying are shown in Fig. **10**(b). Finally, Fig. **10**(c) shows the comparison between experimental and numerical results for the isotropic loading tests performed at different suctions. The preconsolidation stress for each test was obtained by adding the matric suction stress χs to the saturated preconsolidation stress (0.025 MPa), resulting in the following preconsolidation stresses: 0.07, 0.09, 0.1, and 0.1 MPa for suctions of 0.05, 0.1, 0.15, and 0.2MPa, respectively. The values of parameter χ for every suction were obtained from Fig. **10**(b). These results show good agreement for both the preconsolidation stress and the overall volumetric behavior of the material.

Send Orders of Reprints at reprints@benthamscience.net

CHAPTER 9

Collapse Upon Wetting

Abstract: This chapter presents the modeling of the phenomenon of collapse upon wetting using the effective stress equation and the elastoplastic framework proposed in the previous chapter. The probabilistic porous-solid model is used to obtain Bishop's parameter χ and then compute the current effective stress. The proposed framework includes the hysteresis of the SWRC and to some extent the hydro-mechanical coupling of unsaturated soils. This model is able to reproduce some particularities of the phenomenon of collapse upon wetting that other models cannot simulate.

Keywords: Collapse upon wetting, unsaturated soils, effective stress, elastoplastic framework, yield surface, suction hardening, soil-water retention curve, hysteresis, hydro-mechanical coupling, porous-solid model, Bishop's effective stress equation, compacted soils, neutral loading, suction controlled tests, preconsolidation stress.

9.1. INTRODUCTION

The Barcelona Basic Model [7] has been able to reproduce the main aspects of the phenomenon of collapse upon wetting using the independent stress variables approach (Fredlund and Morgenstern, 1977). The key point for the simulation of collapse in this model is the consideration that the apparent preconsolidation stress increases with suction (Fig. **1**). This feature is introduced into the model through the Loading Collapse Yield Surface (LCYS) which adopts the geometry shown in Fig. **1**(b). By analyzing the volumetric behavior of a soil sample subject to a drying-wetting cycle, the equation relating the yield stress in unsaturated ($\bar{p}_0$) and saturated ($\bar{p}_0^*$) conditions is obtained as a function of the slopes of the loading ($\lambda(0)$ and $\lambda(s)$) and unloading-reloading (κ and κ_s) curves of the soil in saturated and unsaturated conditions, respectively. This equation writes:

$$\frac{\bar{p}_0}{p^r} = \left(\frac{\bar{p}_0^*}{p^r}\right)^{\frac{\lambda(0)-\kappa}{\lambda(s)-\kappa_s}}$$

where p^r represents a reference pressure. In general, it can be considered that $\kappa = \kappa_s$ as their values are relatively small. In turn, $\lambda(s)$ depends on the values of

Eduardo Rojas

$\lambda(0)$ and suction. This equation represents the shape of the LCYS as shown in Fig. **1**. When an increment of the net stress is applied to an initially saturated sample that has been dried to suction *s* (stress path AA'BD in Fig. **1**), the initial $LCYS_i$ displaces on the mean net stress axis reaching the position $LCYS_f$.

The volumetric compression of the material during a net stress increase (dv_p) beyond the yield stress is given by:

$$dv_p = -\lambda(s)\frac{d\bar{p}}{\bar{p}}$$

In the same way, the volumetric response of the soil during a suction increase (dv_s) beyond the Suction Increase Yield Surface (SIYS) is given by:

$$dv_s = \lambda_s \frac{ds}{s + p_{at}}$$

where λ_s represents the slope of the virgin compression line during suction increase, *ds* is the increment in suction and p_{at} is the atmospheric pressure. When both net stress and suction are increased, the total volumetric response of the material (*dv*) is given by the addition of both terms, in the form:

$$dv = dv_p + dv_s$$

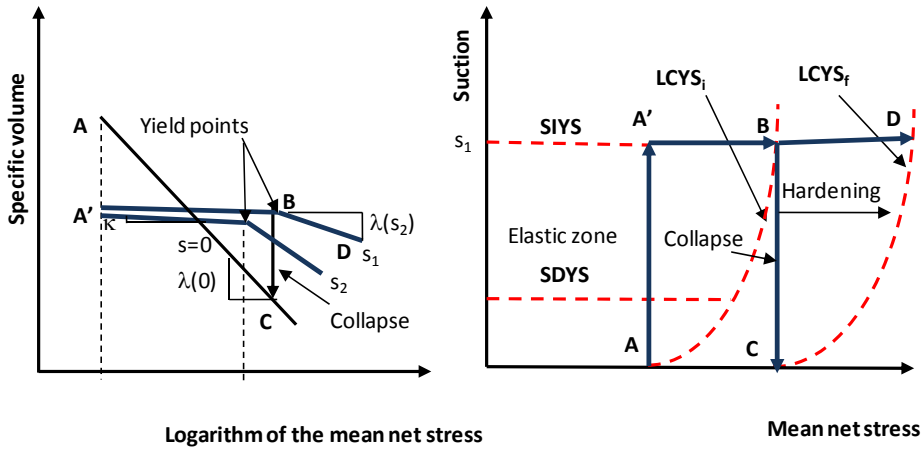

Figure 1: (a) Volumetric behavior and (b) hardening of the LCYS in the BBM.

This model has been widely employed to reproduce the volumetric behavior of unsaturated soils with great success.

Other models use the effective stress approach in their formulations, for example: Bolzon, Schrefler and Zienkiewics [118], Vaunat, Romero and Jommi [90], Loret and Khalili [97], Karube and Kawai [119], Gallipoli, Gens, Sharma and Vaunat [23], Wheeler, Sharma and Buison [22]. These models make use of Bishop's effective stress $\sigma_{ij}^{'}$ (1959):

$$\sigma'_{ij} = \sigma_{ij} - \delta_{ij}[u_a - \chi(u_a - u_w)]$$

The Bishop parameter χ can be written as a function of the degree of saturation, suction or both. For example the model proposed by Gallipoli, Gens, Sharma and Vaunat [23] considers that χ is equal to the degree of saturation. To account for the volumetric behavior of unsaturated soils the model includes the constitutive parameter ξ which represents the bonding and debonding stress produced by water menisci. This parameter is written as a function of the degree of saturation S_r in the form:

$$\xi = f(s)(1 - S_r)$$

where *f(s)* is a function of suction representing interparticle forces. By analyzing the relationship between the ratio e/e_s with parameter ξ, where e and e_s represents the voids ratio in unsaturated and saturated conditions when the soil is subject to the same Bishop stress, the flowing relationship was established:

$$\frac{e}{e_s} = 1 - a[1 - exp(b\xi)]$$

With this model it is possible to model the volumetric response of soils subjected to increments of the mean net stress and wetting-drying cycles including the phenomenon of collapse.

Another variation for the value of parameter χ is presented by Alonso, Pereira, Vaunat and Olivella [120]. In this case the global degree of saturation of the material is split in two parts: one for the macrostructure S_w^M and another for the

microstructure S_w^m in the form $S_w = S_w^M + S_w^m$. Then two possible equations for the value of parameter χ are proposed. The first one is given by the expression:

$$\chi \equiv S_{we} = \langle \frac{S_w - S_w^m}{1 - S_w^m} \rangle$$

where $\langle x \rangle = (x + |x|)/2$ represents the Macauley brackets. The other possibility is given by the expression:

$$\chi = (S_w)^a$$

Where *a* represents a soil parameter which value is larger or equal to 1. With this model the authors have been able to reproduce the strength and volumetric behavior of unsaturated soils.

The model by Della Vechia, Jommi and Romero [121] also uses the concept micro and macroporosity. It includes the evolution of the soil-water retention curve (SWRC) related to the volumetric deformation of the material and the hysteresis of the SWRC. This model is able to reproduce a maximum collapse strain with increasing confining stress.

The model proposed by Wheeler, Sharma and Buison [22] considers a vertical LCYS on the plane of modified suction against mean Bishop's stress. This surface is coupled to the SIYS and the Suction Decrease Yield Surface (SDYS) which are represented by horizontal lines in the same plane. Both the SIYS and SDYS are coupled with the LCYS. For example when a soil dries and suction exceeds the maximum historical value experienced by the soil, plastic strains occur that hardens the SIYS. This hardening is represented by a vertical displacement of the surface that pulls along the SDYS while the LCYS moves outwards. On the contrary, when suction reduces beyond the SDYS this surface is pulled downwards along with the SIYS while the LCYS moves inwards. This coupling between the yield surfaces allows modeling the phenomenon of collapse upon wetting as during the inward movement of the LCYS, the wetting path leaves the elastic zone.

However, these models show deficiencies in reproducing one or more of the following particularities of the phenomenon of collapse upon wetting observed on

compacted materials tested at different densities and loaded at different net stresses: a) In most cases, there is an initial elastic response at the beginning of collapse. The extent of this elastic response depends on the value of the mean net stress applied during the loading stage b) collapse deformation depends on both the density and the stress state before collapse c) For increasing values of the mean net stress applied during the loading stage on samples compacted at the same density, the collapse volumetric strain increases and then decreases (*i.e.,* there is a maximum collapse volumetric strain for samples compacted at the same density). This behavior has been experimentally observed by different researchers, for example: Sun, Sheng, Cui and Sloan [122]; Rodrigues and Volar [123].

This chapter shows the modeling of the phenomenon of collapse upon wetting based on the principle of effective stress resulting in a model able to reproduce the particularities listed above. More importantly, this treatment results in a unifying framework for saturated and unsaturated soils.

9.2. VOLUMETRIC ELASTOPLASTIC FRAMEWORK

Based on the elastoplastic framework developed in the preceding chapter, it is possible to simulate the phenomenon of collapse upon wetting of soils. In that sense, the shape of the LCYS needs to be established. This shape can be determined in a similar way as the usual experimental procedure employed in the laboratory: departing from a previous yield surface, a load is applied to produce plastic deformations that hardens the yield surface, then following an unloading path a new state of stresses is reached inside the elastic zone and finally the sample is loaded until yield is observed. This yielding defines another point on the hardened yield surface. For the numerical case, the same procedure can be applied except that the increment of the plastic deformation should be the same than that obtained with a different combination of stresses. In addition, all these different combinations of stresses need to depart from the previous yield surface and thus they can be reached following a neutral loading along the previous LCYS.

In this case, it is considered that the initial yield surface is the one obtained after the first drying of the sample (dotted line CSD in Fig. **2**). The plastic decrement of the void ratio produced by loading from point C to point E (which represents an increment of the effective stress of $\Delta\bar{p} - \chi_0\, s_0$) is

$$\Delta e^p = e_C(\lambda - \kappa)\left(\frac{\Delta\bar{p} - \chi_0 s_0}{\bar{p}_{0i} + 2\chi_0 s_0}\right)$$

In the same way, the plastic decrement of the void ratio produced by a net stress increase $\Delta\bar{p}_s$ (which is equal to the effective stress increase) departing from point S is:

$$\Delta e^p = e_s(\lambda - \kappa)\left(\frac{\Delta\bar{p}_s}{\bar{p}_{0i} + \chi s + \chi_0 s_0}\right)$$

Because point S is reached by following a neutral loading along the LCYS (red path CD) then, $e_s = e_C$ and, by equalizing the last two equations the following result is obtained:

$$\Delta\bar{p}_s = \left(\frac{\bar{p}_{0i} + \chi s + \chi_0 s_0}{p_0 + 2\chi_0 s_0}\right)(\Delta\bar{\mathrm{p}} - \chi_0 s_0)$$

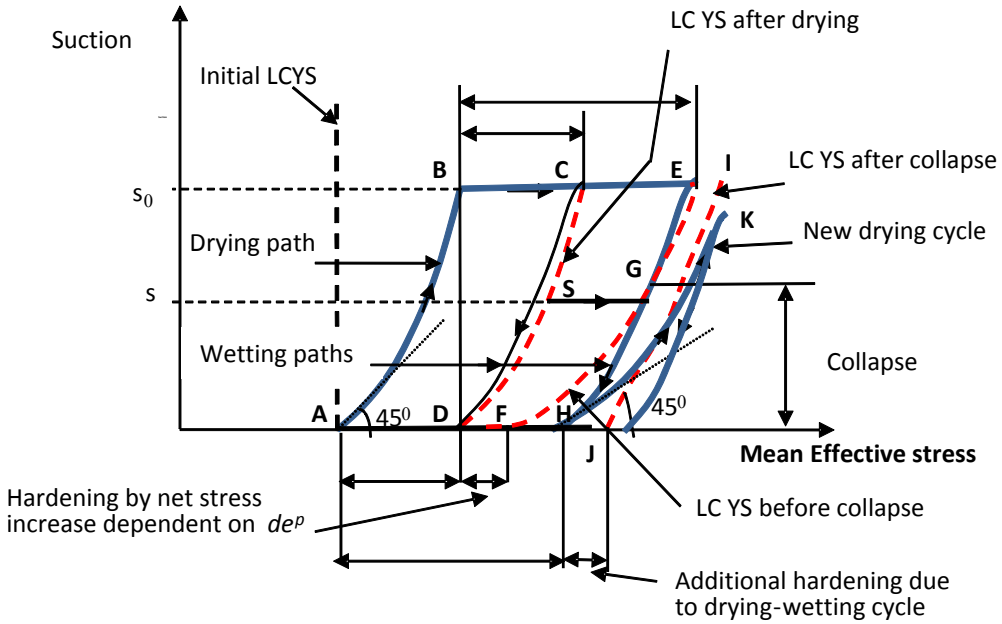

Figure 2: Collapse upon wetting phenomenon.

By adopting different values of suction (s), the corresponding value of $\Delta\bar{\mathrm{p}}_s$ can be obtained and a set of effective stress values defining the LCYS can be plotted. If

$s = 0$ for the new state of stresses then $\Delta\bar{p}_s$ represents the hardening of the yield surface at the effective stress axis ($\Delta\bar{p}_0$ in Fig. **2**). The shape of the LCYS is sketched in Fig. **2** (dotted line EGF). Note that this shape depends not only on the value of the net stress increment $\Delta\bar{p}$ but also on the SWRC of the material trough parameter χ.

When the soil wets after being loaded to point E, it follows a different path to that followed during the drying stage due to the hysteresis of the SWRC, although it intersects the effective stress axis with the same slope of 45^o when the soil fully saturates. Notice that in such a case the soil shows an initial elastic recovery before it collapses (wetting path EG). This is in agreement with the experimental results reported during the collapse of soils (see for example [122, 124]). At the end of collapse (point H) the state of the soil is similar to a saturated slightly preconsolidated material and thus the yield surface is represented by a curved line departing from the preconsolidation stress (dotted line IJ). This preconsolidation stress is given by the addition of the net stress increment ($\Delta\bar{p}$) plus the hardening produced by the wetting-drying cycle. On the other hand, the net stress applied to the material only increases in the quantity $\Delta\bar{p}$ and represents the final position of the wetting cycle (point H) as shown in Fig. **2**. If, at this point, a new drying cycle is applied (stress path HK), the soil initially shows an elastic recovery and then yields again because the stress path crosses the yield surface as it is observed in the same figure.

The proposed framework corresponds well to the experimental results reported by Romero, Gens and Lloret [109]. These researchers performed suction-controlled oedometric tests on samples of Boom clay compacted at different densities and for different vertical stresses (Fig. **3**). It can be observed that the soil initially behaves elastically during the first wetting; the smaller the vertical net stress the larger the elastic response. This occurs because when the mean net stress is large, the yield surface tilts further to the right and the wetting path crosses it earlier (see Fig. **2**). At the end of the elastic behavior, the soil collapses. During the new drying cycle, the soil initially shows an elastic volumetric reduction and then yields. Finally, for the next wetting-drying cycles, the soil behaves elastically. It is noteworthy that some details of the volumetric behavior of unsaturated soils

cannot be captured by a model represented in terms of the independent stress variables approach as the hysteresis of the SWRC cannot be included.

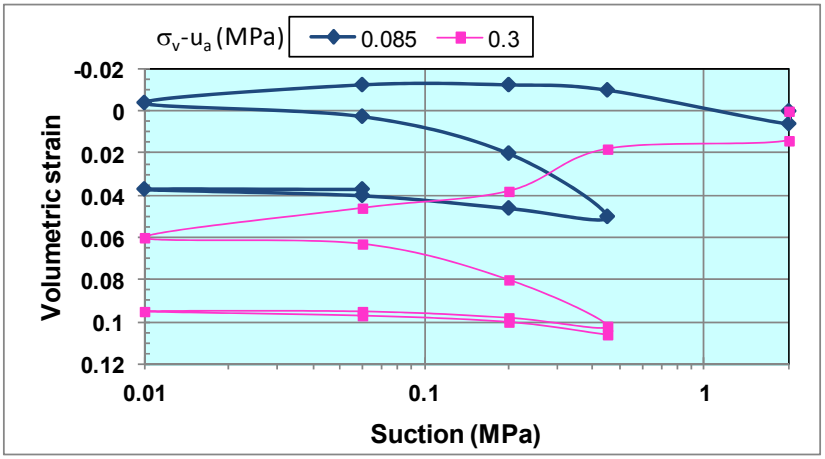

Figure 3: Volumetric behavior of Boom clay during wetting-drying cycles (after Romero, Gens and Lloret [109]).

9.3. COMPACTED SOILS

Now, consider that a soil sample is prepared in different layers by static compaction Because the stress path followed by the soil during compaction cannot be easily determined, it is difficult to establish the initial position of the LCYS even if the applied stresses during compaction and the value of suction in the"as compacted" state are known. Nevertheless, some considerations can be done to establish this initial position. During compaction, stresses are applied on top of a disaggregated material placed inside a mould. These stresses produce the displacement and interlock of solid particles and simultaneously menisci of water distribute mainly at the points of contact between solids. During loading, the solid particles are compressed and then decompressed when unloaded. At the same time, suction decreases during compression and increases during decompression. In that sense, it is possible that at the end of compaction the soil lies closer to the drying branch of the SWRC than to the wetting one. Here it is considered that the process of compaction induces a mean effective stress on the sample that can be decomposed in the addition of a mean net stress called here the interlock or fabric stress p_{fab} and the initial suction s_{00} (point B in Fig. **4**). The fabric stress represents the apparent

mean preconsolidation stress of the compacted sample and can be determined in the same way as the preconsolidation stress for saturated soils. It is also considered that the "as compacted" LCYS initiates at the fabric stress (point A in Fig. **4**) and reaches the point representing the"as compacted" state of stresses of the soil sample (point B in the same figure) following a drying path.

After compaction the soil may be subjected to an equalization stage where a suction s_0 and mean net stress $\bar{p}_0$ are applied to the sample following the stress path BCF shown in Fig. **4**. During the equalization stage, if suction s_0 is larger than the "as compacted" suction (s_{00}), then the LCYS hardens in the quantity $\chi_0 s_0 - \chi_{00} s_{00}$ and displaces to the position given by curve DE. Later, when the soil is loaded to reach the net stress $\bar{p}_0$, the yield surface hardens by displacing and tilting, reaching the position shown by curve FG. If at this point the soil is wetted, the phenomenon of collapse may occur only if $\bar{p}_0 > \chi_0 s_0 - \chi_{00} s_{00}$. If the soil is further loaded by applying a mean net stress increment $\Delta\bar{p}_0$ (path FH) then the LCYS displaces and tilts further reaching the position HJ indicated in Fig. **4**. The suction at which the phenomenon of collapse initiates (point I) depends on both the applied suction s_0 and the total increment of the mean net stress ($\bar{p}_0 + \Delta\bar{p}_0$).

The shape adopted by the hardened LCYS, once the net stress increment $\Delta\bar{p}_0$ has been applied, can be determined using the procedure previously explained. In this case, points D and S located on the LCYS after the equalization stage (dotted line DE) are considered. Let e_D and e_s be the void ratios at points D and S, respectively. Because point S can be reached following a neutral loading from point D, the void ratio at both locations is the same ($e_D = e_s$). Additionally, the plastic decrement of the void ratio produced by loading from point D to point H is:

$$\Delta e^{p} = e_D(\lambda - \kappa)\left(\frac{\bar{p}_0 - \chi_0 s_0 + \chi_{00} s_{00} + \Delta\bar{p}_0}{p_{fab} + 2\chi_0 s_0 - \chi_{00} s_{00}}\right)$$

In the same way, the plastic decrement of the void ratio generated by a net stress increment $\Delta\bar{p}_s$ is:

$$\Delta e^{p} = e_s(\lambda - \kappa)\left(\frac{\Delta\bar{p}_s}{p_{fab} + \chi\, s + \chi_0 s_0 - \chi_{00} s_{00}}\right)$$

By equalizing these two last equations the following result is obtained:

$$\Delta\bar{p}_s = \left(\frac{p_{fab} + \chi s + \chi_0 s_0 + \chi_{00} s_{00}}{p_{fab} + 2\chi_0 s_0 - \chi_{00} s_{00}}\right)(\bar{p}_0 - \chi_0 s_0 + \chi_{00} s_{00} + \Delta\bar{p}_0)$$

By adopting different values of suction, a set of values of $\Delta\bar{p}_s$ can be obtained and the effective stresses defining the LCYS for different values of suction can be plotted according to the following equation:

$$p'_{LCYS} = p_{fab} + \chi s + \chi_0 s_0 - \chi_{00} s_{00} + \Delta\bar{p}_s \ldots \quad (9.1)$$

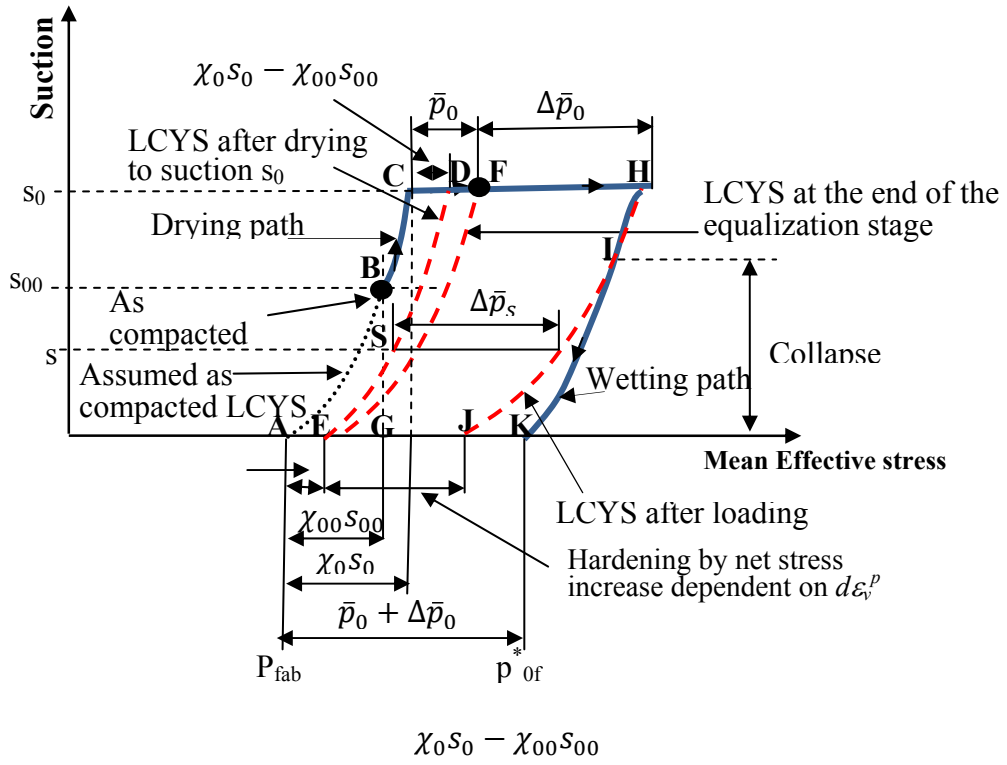

Figure 4: Elastoplastic framework for the volumetric behavior of compacted soils.

Moreover, a Wetting Path (WP) initiating at point H in Fig. **4** is defined by the following relationship:

$$p'_{WP} = p_{fab} + \bar{p}_0 + \Delta\bar{p}_0 + \chi_w s \ldots \quad (9.2)$$

where χ_w represents the values of parameter χ following a wetting path. By solving simultaneously Equations (9.1) and (9.2) it is possible to define the value of suction at which these two curves intersect. This value is called here the collapse suction. For suctions above this value the soil behaves elastically whereas for values bellow the collapse suction, elastoplastic behavior occurs. Once the collapse suction is known, it is possible to compute the void ratio reached at the end of collapse following path ACHK. To that purpose let the void ratio associated to point K be e_4 (see Fig. **4**) and suppose that the WP crosses the LCYS at suction s_c (collapse suction). According to Equations (8.4) and (8.5) the void ratio reached at point K along path ACHK is given by:

$$e_{4\,ACHK} = e_0 \left\{ \left[\frac{\left(p_{fab} + \chi_0 s_0\right)\left(p_{fab} + \chi_0 s_0 + \overset{\blacklozenge}{p}_0 + \Delta \overset{\blacklozenge}{p}_0\right)}{p_{fab} + 2\chi_0 s_0 - \chi_{00} s_{00}} \right]^{(\lambda_e - \kappa_e)} \frac{\left(p_{fab} + \chi_w s_c + \overset{\blacklozenge}{p}_0 + \Delta \overset{\blacklozenge}{p}_0\right)^{(\lambda_e + \kappa_e)}}{\left[\left(p_{fab} + \overset{\blacklozenge}{p}_0 + \Delta \overset{\blacklozenge}{p}_0\right)\left(p_{fab} + \chi_{00} s_{00}\right)\right]^{\lambda_e}} \right\}$$

On the other hand, the void ratio reached at this same point following path AK (normally consolidated line) is:

$$e_{4AK} = e_0 \left(\frac{p_{fab} + \bar{p}_0 + \Delta \bar{p}_0}{p_{fab} + \chi_{00} s_{00}} \right)^{\lambda_e}$$

It can be shown that in general $e_{4AK} > e_{4ACHK}$. This difference happens because the inclusion of the LCYS in the proposed framework produces elastic deformations during the loading and collapse stages along path ACHK. This elastic behavior reduces the final volumetric deformation when compared with that obtained along path AK. Different researchers have reported that the void ratio reached by samples at the end of collapse lie slightly below the normally consolidated line (see for example [122]). This happens because in addition to load increase, the samples have been subjected to a drying-wetting cycle and therefore the LCYS suffers additional hardening as explained in the previous section of this chapter. However as this additional volumetric deformation is small, as a first approach it is considered here that the soil reaches the normally consolidated line at the end of collapse. In that sense, the values of the volumetric deformation occurring during collapse must be corrected. To this purpose, the

difference in the volumetric deformation between both paths has to be added somehow to the computed value of collapse following path ACHK. For simplicity this difference is linearly distributed to the volumetric deformation along the collapse path in the form:

$$\Delta e_{cc} = \Delta e_c \, F_c \ldots \tag{9.3}$$

where Δe_{cc} and Δe_c represent the corrected and uncorrected increment of volumetric deformation during collapse and F_c is the collapse factor given by the relationship:

$$F_c = 1 + \frac{e_{4ACHK} - e_{4AK}}{\Delta e_{cf}}$$

where Δe_{cf} is the reduction in void ratio during collapse and is given by the relationship:

$$\Delta e_{cf} = e_3 \lambda_e \left(\frac{\chi_{wc} s_c}{p_{fab} + \bar{p}_0 + \Delta \bar{p}_0} \right)$$

where e_3 represents the voids ratio at point I in Fig. **4** and χ_{wc} represents Bishop's parameter for suction s_c during a wetting path.

Fig. **5** shows the values of the collapse factor (lines) as a function of the collapse suction and for different densities. It can be observed that this factor shows little variation for values of the collapse suction between 0.15 and 0.05 for the same density. For practical purposes it seems convenient to consider this factor as constant for all suctions and its value can be approached with the following empirical relationship that takes account of the density of the material:

$$F_c = \left(\frac{p_{fab}}{p_{at}} \right)^{(\lambda_e + \kappa_e)} \ldots \tag{9.4}$$

The values of this expression are also indicated in Fig. **5** (symbols). This factor has been used for the comparisons between numerical and experimental results shown in the next section.

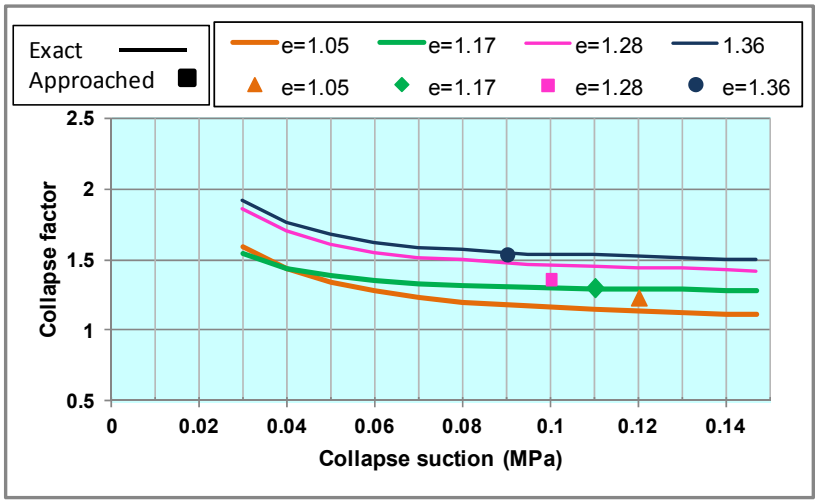

Figure 5: Collapse factor for different densities. Comparison between the exact solution (lines) and the approached value (symbols).

9.4. NUMERICAL AND EXPERIMENTAL COMPARISONS

In this section, the proposed framework for the volumetric behavior of unsaturated soils has been used to simulate the response of samples compacted at different densities and subjected to loading-wetting paths.

Sun, Sheng, Cui and Sloan [122] reported a series of suction controlled triaxial tests to observe the influence of the initial density on the collapse of compacted soil samples of Pearl clay. The specimens were prepared by static compaction in five layers with a vertical stress of 0.3MPa, 0.4MPa or 0.6MPa. This procedure resulted in void ratios ranging from 1.0 to 1.5 and suctions ranging from 0.09 to 0.13MPa. The volumetric deformation of the sample was obtained by measuring its lateral and vertical displacements. The lateral displacements were measured at three different heights of the sample and the volume was obtained by approaching the lateral shape of the sample to a third order polynomial equation. After compaction, all samples were subject to an equalization stage by applying a suction of 0.147MPa and an isotropic mean stress of 0.02MPa. Then the specimens were isotropically loaded to a previously specified net stress under a constant suction of 0.147MPa. Finally, suction was decreased by steps from 0.147 to 0MPa maintaining the nets stress constant. During this wetting stage, the

SWRCs for the different densities and for each isotropic stress were obtained. Finally, the GSD of the material was also reported.

In order to be able to simulate the volumetric behavior of soils within the framework proposed in this paper, the values of parameter χ need to be determined according to the wetting-drying history of the soil. To this purpose the porous-solid model is used along with the SWRC of the material. As explained before, by fitting the main wetting and drying SWRCs of the material it is possible to determine the PSD of cavities and bonds. Then it is possible to simulate any drying-wetting process and define the parameters f^s, f^u and S_w^u required to determine the value of parameter χ. Unfortunately, during the implementation of these tests only the wetting SWRC of the material was obtained. Therefore, only the wetting branch could be fitted with the experimental points while the drying branch was guessed.

Fig. **6**(a) shows the fitting of the wetting branch of the SWRC and the guess made for the drying branch for a sample compacted at a void ratio of e = 1.33. From this fitting, the PSD of cavities and bonds for this specific density of the material could be found. Fig. **6**(b) shows the cavity size distribution of samples compacted at different void ratios (including that for e = 1.36) and their comparison with the GSD of the material. In this figure the reduction in cavity sizes for the different compacted void ratios can be observed.

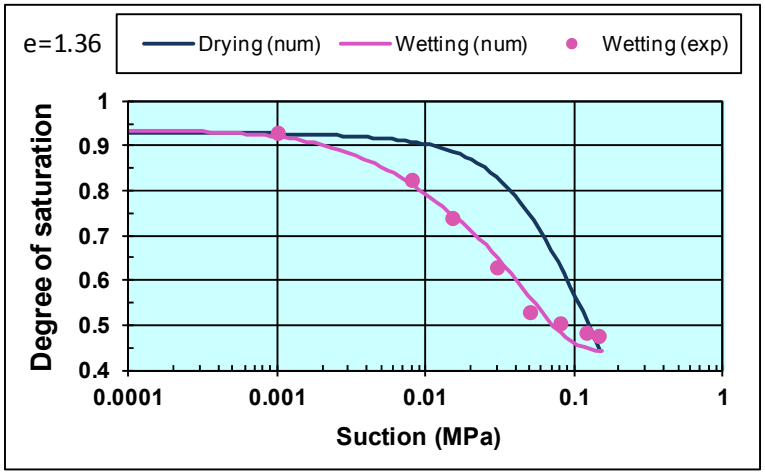

(a)

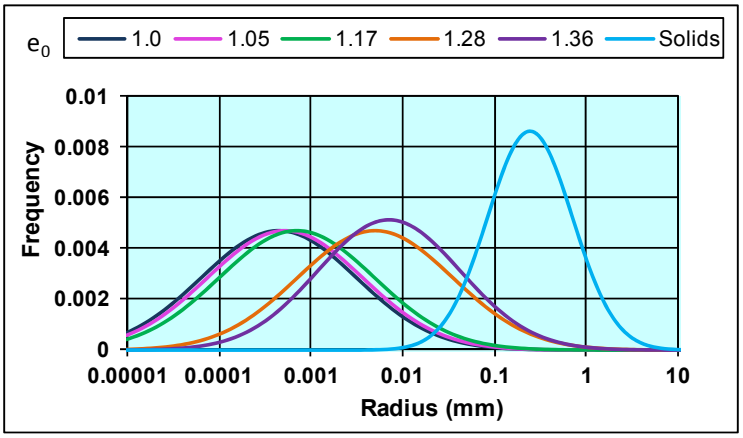
e0
1.0
1.05
1.17
1.28
1.36
Solids
Frequency
0.01
0.008
0.006
0.004
0.002
0
0.00001
0.0001
0.001
0.01
0.1
1
10
Radius (mm)

(b)

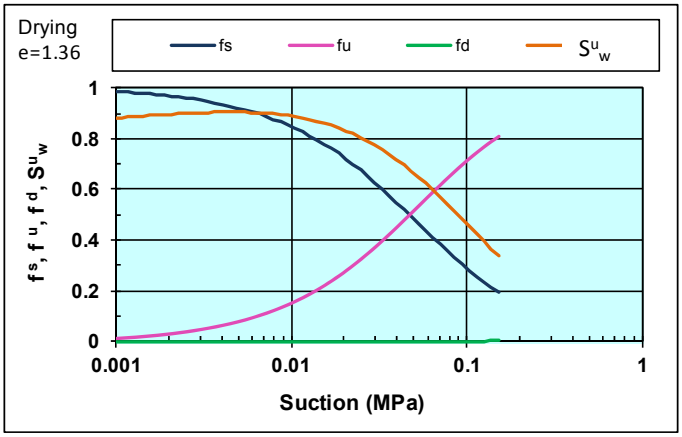
Drying
e=1.36
fs
fu
fd
Suw
fs, fu, fd, Suw
1
0.8
0.6
0.4
0.2
0
0.001
0.01
0.1
1
Suction (MPa)

(c)

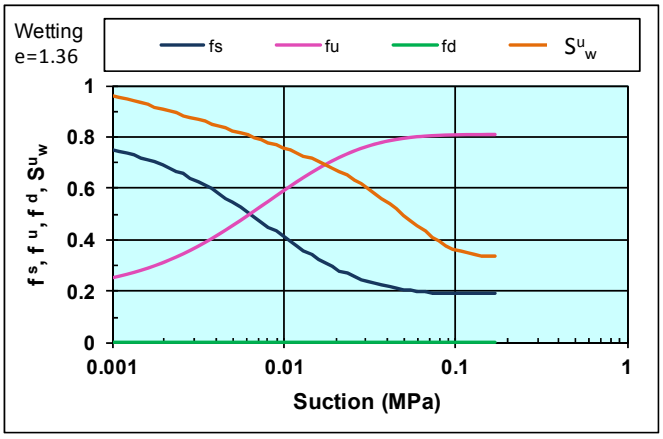
Wetting
e=1.36
fs
fu
fd
Suw
fs, fu, fd, Suw
1
0.8
0.6
0.4
0.2
0
0.001
0.01
0.1
1
Suction (MPa)

(d)

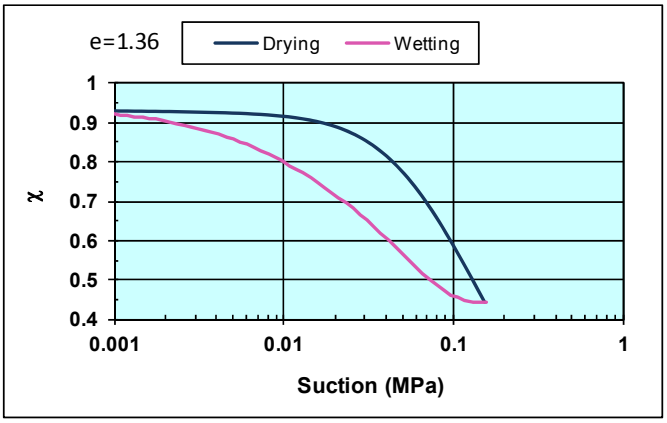

(e)

Figure 6: Numerical simulations obtained with the porous-solid model. (a) Fit of the wetting curve, (b) cavity size distribution for different densities and GSD of the material, (c) and (d) parameters f^s, f^u, f^d and S_w^u at drying and wetting, respectively and (e) values of parameter χ at drying and wetting.

Once the PSD of the material has been established, it is possible to determine the values of parameters f^s, f^u, f^d and S_w^u by simulating the drying and wetting process of the soil. These parameters are shown in Figs. **6**(c) and **6**(d) for the drying stage (reaching a maximum suction of 0.15MPa) and the subsequent wetting stage, respectively. Using Equation (2.15) it is now possible to define the value of parameter χ during the drying and wetting stages. These values are shown in Fig. **6**(e) as a function of suction. Once this parameter has been defined it is now possible to determine the mean effective stress at any stage of the test (Equation (2.14)), simulate the behavior of the material at loading (Equation (8.4)), define the geometries of the LCYS and the WP (Equations (9.1) and (9.2), respectively), define the point at which these curves intersect and finally, determine the volumetric response of the soil during collapse (Equations (8.4), (8.5), (9.3) and (9.4)). This same procedure has to be done for each density of the material and for each value of the mean net stress.

9.4.1. Isotropic Compression

The comparison between experimental and numerical results for samples compacted at different densities and subject to isotropic loading is presented in Fig. **7**. The average initial void ratios of tested samples were: 1.36, 1.28, 1.17 and

1.05. Curves for both unsaturated and saturated conditions are presented. These curves were obtained using Equation (8.4) with λ_e = -0.12. Arrows in this figure indicate the value of the fabric stress for each density. The fabric stress for the samples compacted at void ratios of 1.36, 1.28, 1-17 and 1.05 were 0.03, 0.06, 0.09 and 0.15, respectively. In general, there is good agreement between experimental and numerical results although for samples compacted at a void ratio of 1.28, the results are not as good as for the other samples.

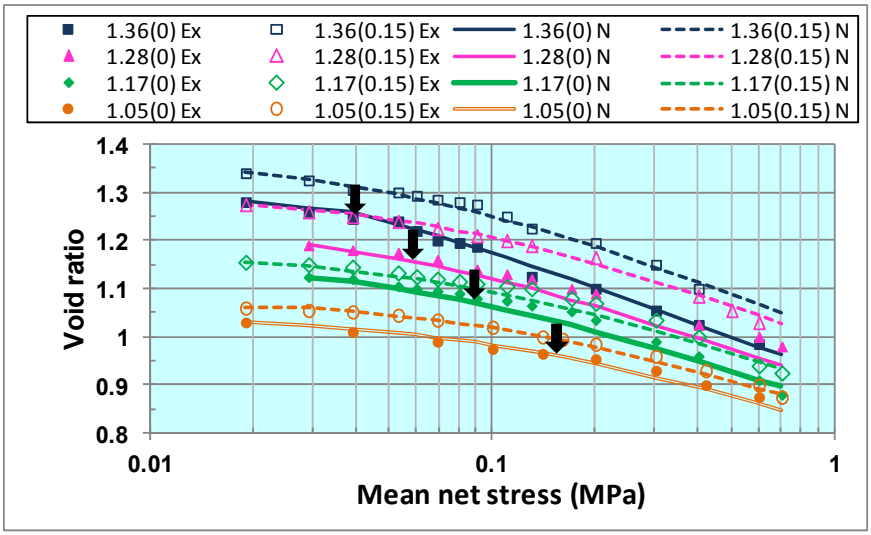

Figure 7: Isotropic loading tests on samples compacted at different densities. The first number identifying the test indicates the "as compacted" void ratio and the number in parenthesis indicates the value of suction during compression in MPa. Ex and N stand for experimental and numerical results, respectively.

9.4.2. Collapse Upon Wetting

Figs. **8-11** show some experimental and numerical comparisons for soils samples compacted at four different densities (e_0=1.05, 1.17, 1.28 and 1.36, respectively) then loaded to different isotropic stresses and finally subjected to wetting. In these figures, plots (a) represent the shapes of both the LCYS and the WP in the axis of effective stress against suction for samples compacted at the same density and loaded at different isotropic stresses (ranging from 0.02 to 0.6MPa). Plots (b) represent the volumetric response of the soil during the wetting stage in the axis of suction against volumetric strain. Finally, plots (c) represent the collapse volumetric strain of the sample against the applied mean net stress. The LCYS

and the WP were obtained from Equations (9.1) and (9.2), respectively. In plots (a) and (b) an initial elastic rebound of the material can be observed followed by the collapse. This type of behavior has also been experimentally observed by Rodrigues and Volar [123]. The value of the unloading-reloading slope considered for these simulations was κ_e = -0.01. It can also be noticed that depending on the isotropic net stress applied to the sample, the WP crosses the LCYS at different stages of the wetting process. The larger the isotropic net stress applied during the loading stage, the earlier the phenomenon of collapse appears during the wetting stage. For sample compacted at a void ratio of 1.05 and loaded to 0.02MPa, collapse never occurs. Instead, for samples compacted at void ratios of 1.17, 1.28 and 1.36 and loaded at the same isotropic stress, collapse occurs close to saturation. This happens because the net stress applied to these samples, $\bar{p}_0 = 0.02$MPa, is close to the value $\chi_0 s_0 - \chi_{00} s_{00}$ representing the hardening of the LCYS during the equalizing stage.

The start of collapse and the evolution of the volumetric deformation of the soil during collapse are correctly simulated by the model (see Figs. **8**(b), **9**(b), **10**(b) and **11**(b)). However, for samples compacted at large void ratios (e = 1.28, 1.36) and subjected to large isotropic stresses, the slope of the numerical volumetric strain against suction remains low compared with the experimental results. This causes under predicted volumetric strains for large values of the mean net stress. In spite of these differences, it can be observed that numerical simulations correctly predict a maximum collapse volumetric strain with increasing mean net stress (Figs. **8**(c), **9**(c), **10**(c) and **11**(c)).

As stated before, this model includes the hysteresis of the SWRC and to some extent the hydro-mechanical coupling of unsaturated soils as the reduction on the size of cavities due to loading or suction increase is still not included in the porous-solid model.

The data required by the model to produce these simulations are: the secondary drying and wetting SWRCs, the GSD of the material, the fabric stress p_{fab}, the slope of both the normally consolidated line (λ_e) and the unloading-reloading line (κ_e) plotted on a logarithmic plane of void ratio *versus* mean effective stress, the initial mean net stress ($\bar{p}_0$), suction (s_0) and voids ratio of the material (e_0) and

the previous loading history or fabrication process in order to define the initial position of the LCYS.

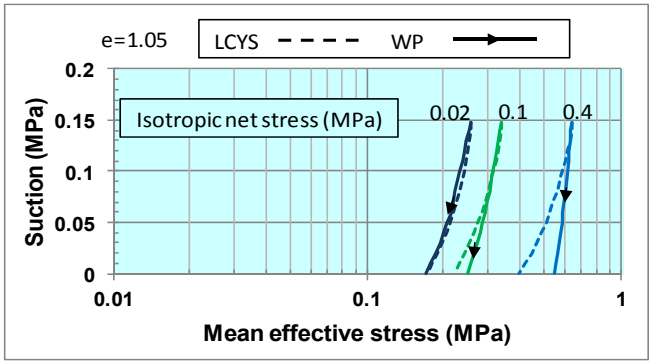

(a)

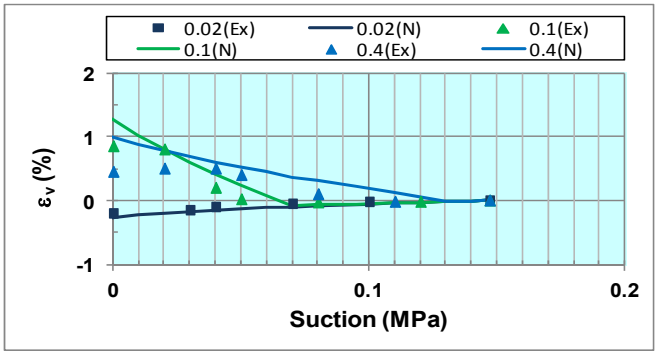

(b)

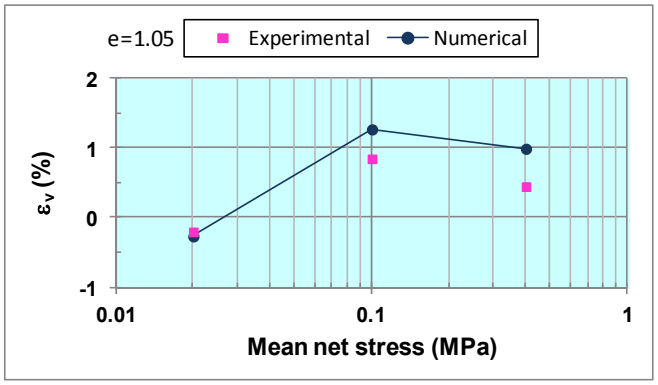

(c)

Figure 8: Samples compacted at an initial void ratio e_0=1.05. (a) LCYSs and WPs, (b) volumetric strain against suction and (c) volumetric strain against mean net stress.

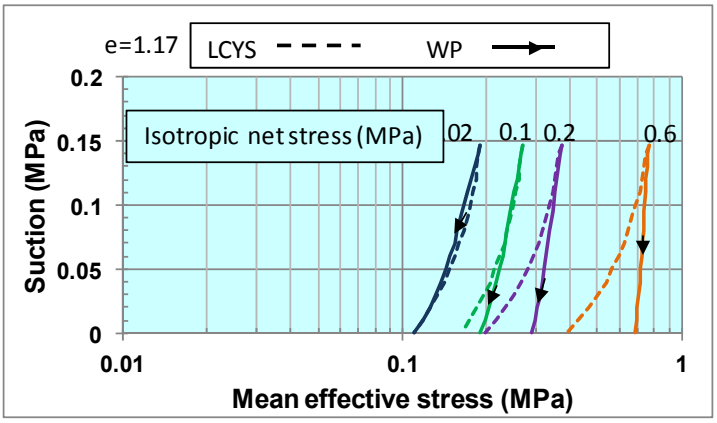

(a)

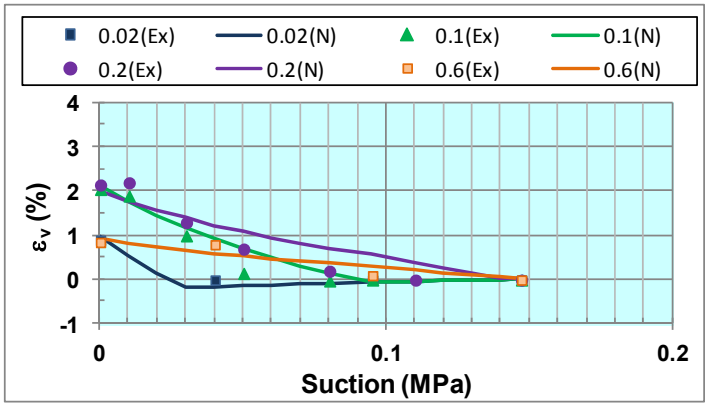

(b)

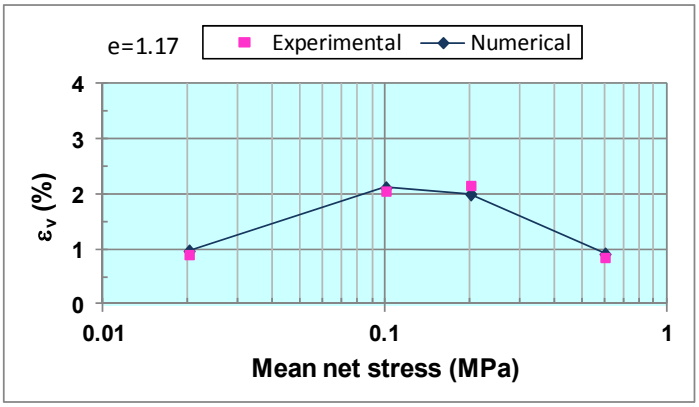

(c)

Figure 9: Samples compacted at an initial void ratio e_0=1.17. (a) LCYSs and WPs, (b) volumetric strain against suction and (c) volumetric strain against mean net stress.

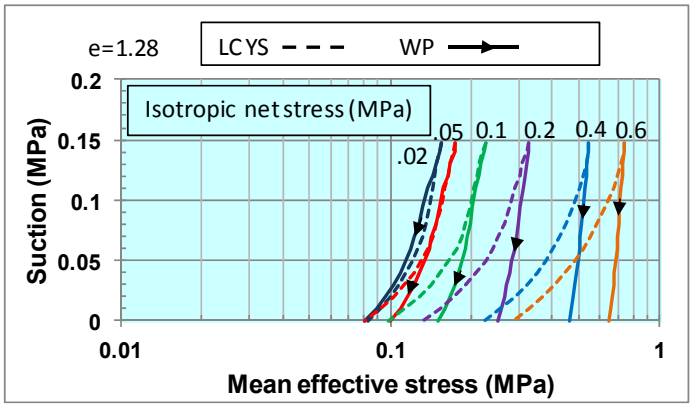

(a)

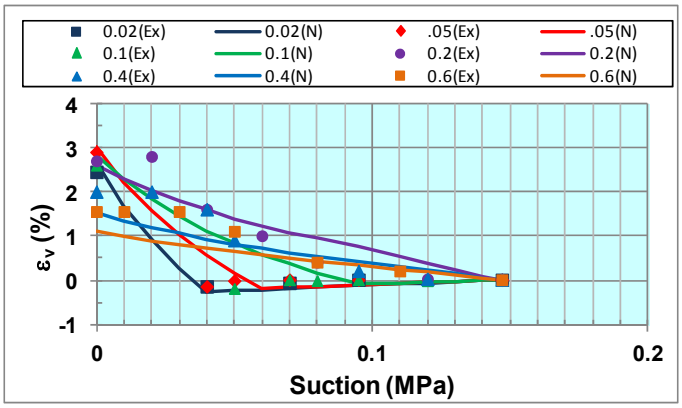

(b)

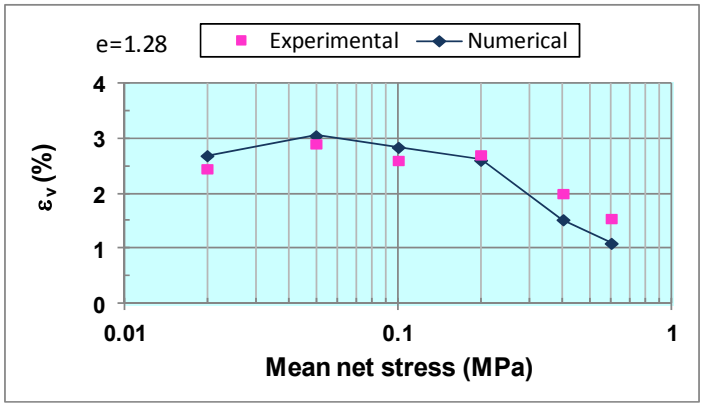

(c)

Figure 10: Samples compacted at an initial void ratio e_0=1.28. (a) LCYSs and WPs, (b) volumetric strain against suction and (c) volumetric strain against mean net stress.

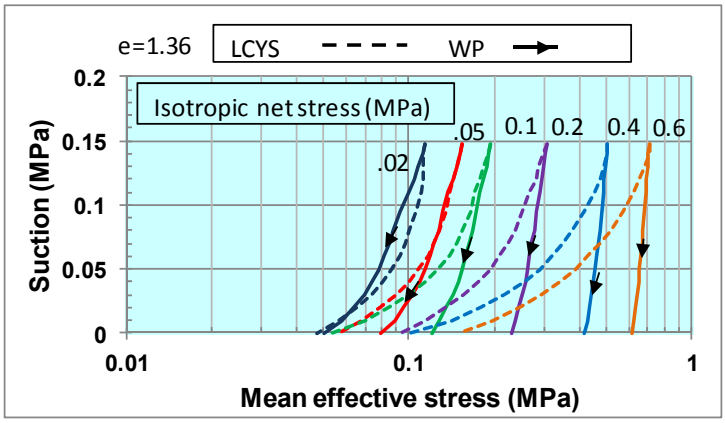

(a)

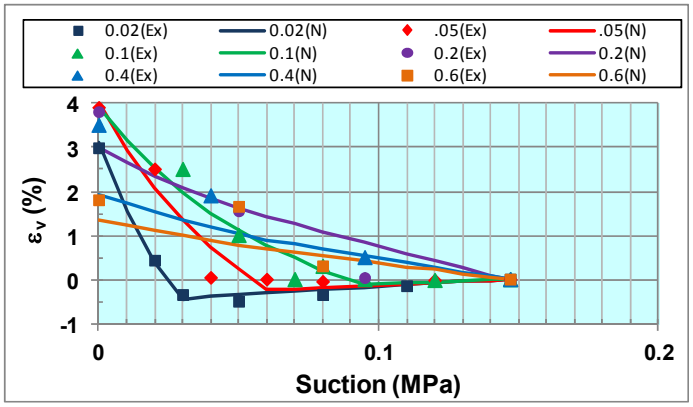

(b)

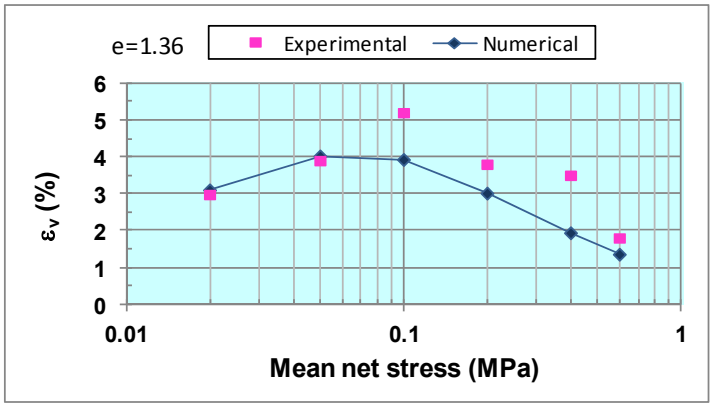

(c)

Figure 11: Samples compacted at an initial void ratio e_0=1.36. (a) LCYSs and WPs, (b) volumetric strain against suction and (c) volumetric strain against mean net stress.

CHAPTER 10

General Elastoplastic Framework

Abstract: In the previous chapters it has been shown that the principle of effective stress can be applied to the shear strength, the tensional strength and the volumetric behavior of unsaturated soils. This chapter shows that the critical void ratio plotted against the mean effective stress for samples tested at different suctions align parallel to the virgin consolidation line of the material. This means that the critical state concept also applies to unsaturated materials. Taking into account all these results, an elastoplastic framework that can be used to develop general constitutive models for soils including saturated, unsaturated and compacted materials is presented.

Keywords: Critical state concept, critical void ratio, effective stress, virgin consolidation line, elastoplastic framework, elastic zone, constitutive models, tensional strength, volumetric behavior, effective stress, yield surface, plastic deformations, suction hardening, failure surface, preconsolidation stress.

10.1. CRITICAL STATE

An aspect that requires reviewing is the critical state concept for soils that are tested at different suctions. Wheeler and Sivakumar [83] performed a series of triaxial tests on samples of unsaturated compacted speswhite kaolin. The samples were prepared by static compaction in a mould at 25% water content. The tests were conducted in double-walled triaxial cells designed to accurately measure the volume change of the samples during the test. In Chapter 6, the strength of unsaturated samples subjected to different suctions was predicted using the concept of effective stress. These simulations showed that a unique failure surface can be obtained when results are plotted on the plane of the mean effective stress against the deviator stress at the critical state. Figs. **1** and **2** shows the void ratio at the critical state against the logarithm of the effective stress for two different types of soil samples tested at different suctions. The effective stresses plotted in Fig. **1** were obtained from data previously reported by Rojas [87]. These results show that the critical void ratio for different suction aligns in parallel curves with the same slope of the virgin consolidation line (VCL). This same result has been found by other researchers in different soils (see for example [117]). This means that the critical state concept can also be applied to the case of unsaturated

materials and this opens the possibility of developing general constitutive models for any type of soil based on the critical state theory.

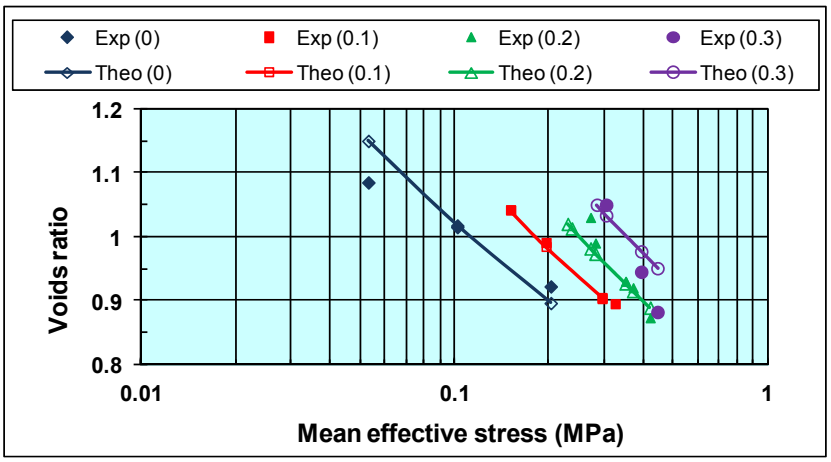

Figure 1: Critical state for speswhite samples tested at different suctions. Experimental data by Wheeler and Sivakumar [83].

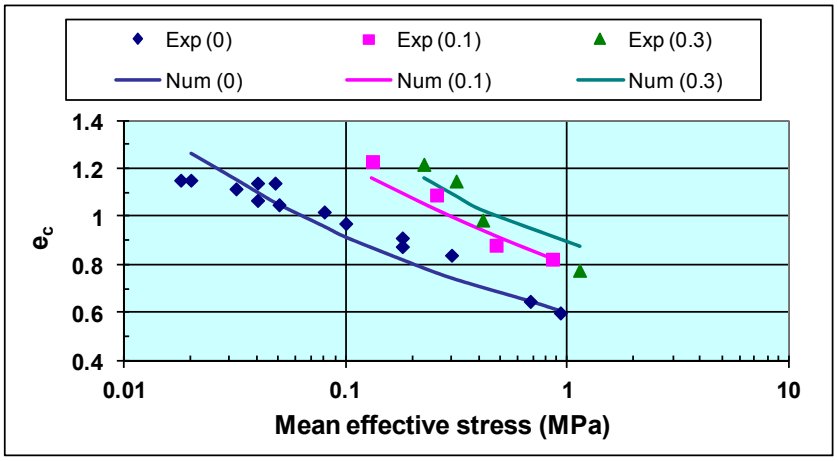

Figure 2: Critical state for residual gneiss samples tested at different suctions. Experimental data by Futai and Almeida [92].

10.2. GENERAL ELASTOPLASTIC FRAMEWORK

For the case of complex stress paths that may include an initial drying followed by net stress increase or decrease ending with further drying, it is possible that the imposed stress path surpasses the maximum historical suction applied to the

sample at different values of the mean net stress. Therefore, in order to complete the elastoplastic framework for the volumetric behavior of unsaturated soils presented in Chapter 8 it is convenient to bound the elastic zone by including the SIYS. For that purpose, the same reasoning used to define the shape of the LCYS can be used for the SIYS. It has been shown that the drying of a soil sample produces suction hardening. This means that in order to produce plastic deformation on an initially saturated sample by increasing the mean net stress after it has been dried by increasing suction up to value s, the mean net stress needs to exceed the yielding value which results from the addition of the preconsolidated mean net stress plus the suction stress χs (see Fig. **3**(a)).

On the contrary, when a sample is loaded by increasing the mean net stress, the suction yield stress is not affected. In other words, there is no mean net stress hardening due to suction increase. Therefore, when a soil has been subjected to a suction s and then the net stress increases or reduces, the yield point for suction does not change. This happens because suction is different in nature to net stress. While suction is an internal stress, the net stress is applied externally to the sample. Then, when a soil dries, additional contact stresses develop mainly at the contact between particles. These additional contact stresses produce the same effect as an increase in the preconsolidation net stress of the sample. In contrast, when the net stress increases while suction remains constant, the additional contact stresses produced by water menisci are not affected and the suction yield stress remains constant.

The influence of the mean net stress on the SIYS has been studied by Thu, Rahardjo and Leong [125] who performed a series of triaxial tests on compacted samples of coarse kaolin subjected to different confining stresses. These results show that the SIYS is only slightly affected by the value of the mean net stress. In brief, when suction increases, the LCYS displaces parallel to the drying path in the quantity χs while the SIYS displaces vertically to the maximum value of suction and remains basically horizontal. Accordingly, the observation made by Nuth and Laloui [126] in the sense that the SIYS can be omitted from the model is valid, as it can be substituted by the maximum historical value of suction. Moreover, even if the intersection between the SIYS and the LCYS is not smooth,

the volumetric strain produced by a combination of net stress and suction increase at the intersecting point is still obtained from Equation (8.3).

Based on these considerations, a general elastoplastic framework for the volumetric behavior of soils in the axes of mean effective stress against suction and under the assumptions of the critical state theory is shown in Fig. **3**. Figs. **3**(a) and (b) represent the volumetric behavior of a soil sample in the axis of the void ratio against the mean net stress and the mean effective stress, respectively. Initially, the sample is saturated (point A) and follows a drying path up to suction s_0 (point B). Then it is subjected to an increment of the mean net stress $\Delta\bar{p}$ (path

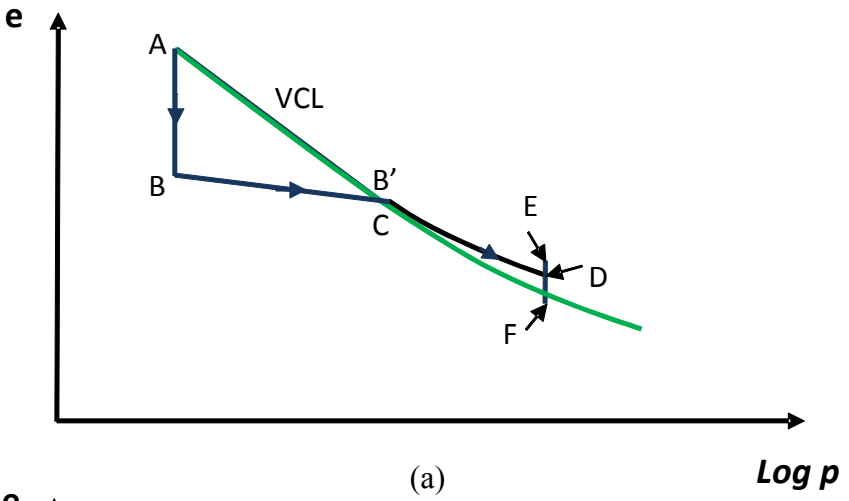

(a)

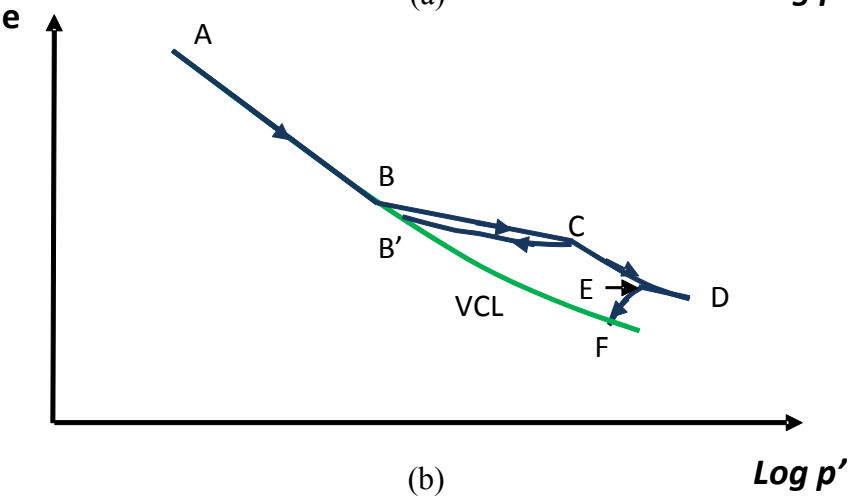

(b)

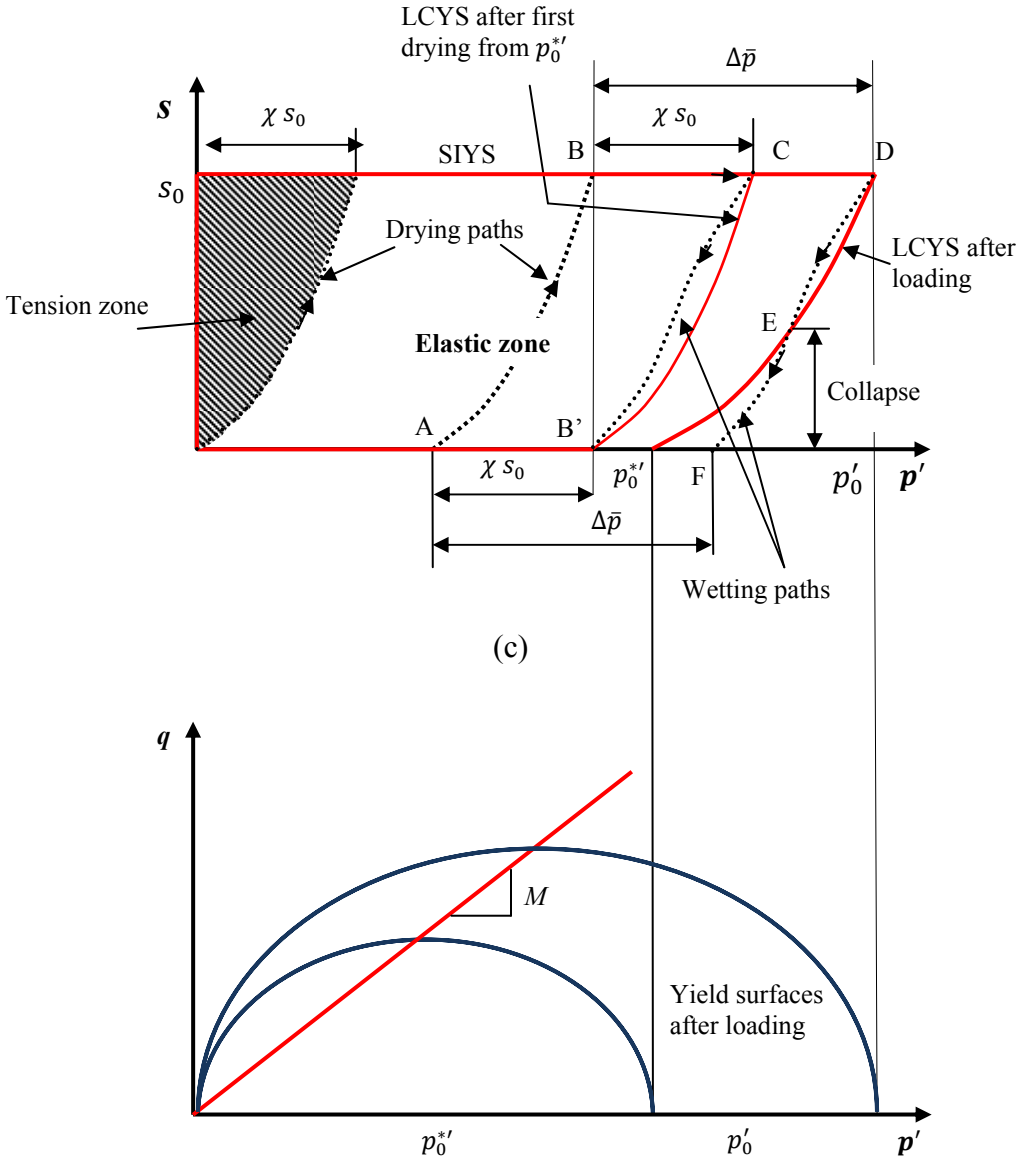

Figure 3: General elastoplastic framework on the mean effective stress-suction plane under the critical state theory.

BCD) and finally, it is wetted up to saturation (point F). During the saturation stage, the sample initially increases its volume as the effective stress reduces inside the elastic zone (path DE) and subsequently it collapses (path EF). These figures also show the Virgin Consolidation Line (VCL) for saturated conditions. Fig. **3**(c) shows the stress path followed by the sample and the evolution of the LCYS in the plane of mean effective stress against suction. It is noteworthy that at point C (Figs. **3**(a) and (b)), the soil will not collapse upon wetting because it remains inside the elastic zone (see Fig. **3**(c)). Therefore, when the sample is re-saturated it moves from point C to B' in Figs. **3**(a), (b) and (c). The drying-wetting path in Fig. **3**(b) shows the loop BDB´ because of the hysteresis of the SWRC. Only when the state of stresses surpasses point C, the material will be able to show some irreversible deformation upon wetting. Finally, Fig. **3**(d) represents the yield surface in the plane of mean effective stress against the deviator stress. In this figure $p_0^{*\prime}$ and p_0' represent the mean effective preconsolidation stress in saturated conditions and the yield mean effective stress at suction s_0, respectively, both considered at the end of the loading stage. This framework is based on the critical state theory and can be used to develop a complete and general elastoplastic models that account for the behavior of saturated, unsaturated and compacted materials.

A drawback to this approach is that the constitutive model should be coupled with a reliably porous-solid model able to simulate the distribution of water in the pores of the material. On the other hand, a phenomenon that has not been included in the above simulations is the effect of the progressive change of the PSD and its influence on the SWRCs due to the volumetric deformation of the soil during shearing or suction increase. Another aspect that needs to be reviewed in the model is the influence of the adsorbed water layer for the case of clays.

REFERENCES

[1] E.L. Matyas and H.S. Radhakrishna, "Volume change characteristics of partially saturated soils", *Géotechnique,* vol. 18, pp. 432-448, 1968.

[2] V.Q. Hung, D.G. Fredlund and J.H.F. Pereira, "Coupled solution for the prediction of volume change in expansive soils", in Proceedings of the Third International Conference on Unsaturated Soils, Recife Brazil, vol. 1, pp. 181-186, 2002.

[3] J.A. Jiménez, "Hacia una mecánica de suelos no saturados", Décima Conferencia Nabor Carrillo, Sociedad Mexicana de Mecánica de Suelos, México, 1990.

[4] X. Zhang and R. L. Lytton, "Modified state-surface approach to the study of unsaturated soil behavior. Part I: Basic concept", Can. Geotech. J., vol. 46, pp. 536-552, 2009.

[5] D.G. Fredlund and N.R. Morgenstern, "Stress state variables for unsaturated soils", *J. Geotech. Engrng. Div*., vol. 103, pp. 447-466, 1977.

[6] A.W. Bishop and I.B. Donald, "The experimental study of partly saturated soil in the triaxial apparatus", in Proc. 5th Int. Conf. Soil Mech., Paris, 1961, vol. I, pp. 13-21.

[7] E.E. Alonso, A. Gens and A. Josa, "A constitutive model for partially saturated soils", *Géotechnique*, vol. 40, pp. 405-430, 1990.

[8] K.H. Roscoe and J.B. Burland, "On the generalized stress-strain behavior of wet clay", Engineering Plasticity, De Heyman and Leckie, Cambridge University Press, pp: 535-609, 1968.

[9] K. Terzaghi, "The shearing resistance of saturated soils and the angle between the planes of shear", in Proc. 1st Int. Conf. Soil Mech., Int. Soc. Soil Mech. Found. Engrng, vol. 1, pp. 54-56, 1936.

[10] A.W. Skempton, "Terzaghi's discovery of effective stress", *From theory to practice in soil mechanics*, John Wiley, New York, USA, 1960.

[11] P.V. Lade P.V and R. De Boer R., "The concept of effective stress for soil, concrete and rock", *Géotechnique*, vol. 47, pp. 61-78, 1997.

[12] J.E.B. Jennings, "Discussion on M.S. Youssef's paper, " *Proc. 4th Int. Conf. on Soil Mech., Int. Soc. Soil Mech. Found. Engrng.* vol. 3, pp. 168, 1957.

[13] D. Croney, J.D. Coleman and W.P.M. Black, "Movement and distribution of water in soil in relation to highway design and performance", *Highway Research Board,* Spec. Report No. 40, 1958.

[14] A.W. Bishop, "The principle of effective stress", *Teknisk Ukeblad*, vol. 39, pp. 859-863, 1959.

[15] G.D. Aitchison, "Relationships of moisture stress functions in unsaturated soils*", Conf. Pore Pressures*, Institution of Civil Engineering, Buttherworths, London, U.K., 1960.

[16] G.E. Blight, "Effective stress evaluation for unsaturated soils", *J. Soil Mech. Div*., vol. 93, pp. 125-148, 1967.

[17] N. Khalili and M.H. Khabbaz, "A unique relationship for χ for the determination of the shear strength of unsaturated soils"*, Géotechnique*, 48, 681-687, 1998.

[18] A.-L. Öberg and Sällfors G., "A rational approach to the determination of the shear strength parameters of unsaturated soils", in Proceedings 1st Int. Conf. on Unsaturated Soils, Alonso & Delage eds., Paris, France, vol. 1, pp. 151-158, 1995.

[19] E.A. Garven and S.K. Vanapalli, "Evaluation of empirical procedures for predicting the shear strength of unsaturated soils", in proceedings 5th International Congress on Unsaturated Soil Mechanics, Arizona, USA, 2006.

Eduardo Rojas

[20] J.E.B. Jennings and J.B. Burland, "Limitations to the use of effective stress in partly saturated soils". *Géotechnique*, vol. 12, pp. 125-144, 1962.

[21] S.K. Vanapalli, D.E. Fredlund, D.E. Pufahl and A.W. Clifton, "Model for the prediction of shear strength with respect to soil suction", *Can Geotech. J*. vol. 33, pp. 379-392, 1996.

[22] S.J. Wheeler, R.S. Sharma and M.S.R. Buisson, "Coupling hydraulic hysteresis and stress-strain behavior in unsaturated soils", *Géotechnique*, vol. 53, pp. 41-54, 2003.

[23] D. Gallipoli, A. Gens, R. Sharma and J. Vaunat, "An elasto-plastic model for unsaturated soil incorporating the effects of suction and degree of saturation on mechanical behavior", *Géotechnique*, vol. 53, pp. 123-135, 2003.

[24] R. Tamagnini, "An extended Cam-clay model for unsaturated soils with hydraulic hysteresis", *Géotechnique,* vol. 54, pp. 223-228, 2004.

[25] D. Sheng, D.G. Sloan and A. Gens, "A constitutive model for unsaturated soils: thermomechanical and computational aspects", *Computational Mechanics*, vol. 33, pp. 453-465, 2004.

[26] C.S. Desai and Z. Wang, "Disturbed state model for porous saturated materials", *International Journal of Geomechanics*, vol. 3, pp. 260-265, 2003.

[27] A. Sridharan, A.G. Altschaeffl and S. Diamond, "Pore size distributions studies". *J. Soil Mech. Found. Div*., vol. 97, pp. 771-787, 1971.

[28] W. B. Haines, "The hysteresis effect in capillary properties and the mode of moisture distribution associated therewith", *J. Agric. Sci*., vol. 20, pp. 7, 1929.

[29] E.J. Murray, "An equation of state for unsaturated soils", *Can. J. Geotech*., vol. 39, pp. 125-140, 2002.

[30] C.S. Desai and Z. Wang Z., "Disturbed state model for porous saturated materials", *Int. J. Geomech.*, vol. 3, pp. 260-265, 2003.

[31] A.-L. Öberg, "Stability of sand and silt slopes". *Internal report*. Department of Geotechnical Engineering, Chalmers University of Technology, Gothenburg, Sweden, 1995.

[32] M.A. Biot, "Theory of elasticity and consolidation for a porous anisotropic solid". *J. Appl. Physics*, vol. 26, pp. 182-185, 1955.

[33] W.B. Haines, "A note on the cohesion developed by capillary forces in an ideal soil", *J. Agric. Sci*., vol. 15, pp. 529-535, 1925.

[34] V. Escario, J.F.T. Jucá and M.S. Coppe, "Strength and deformation of partly saturated soils", in Proceedings of the 12th International Conference of Soil Mechanics and Foundation Engineering, Rio de Janeiro, International Society of Soil Mechanics and Foundation Engineering, Río de Janeiro, Brazil, vol. 1, pp. 43-49, 1989.

[35] J.K. Gan and D.G. Fredlund, "Shear strength characteristics of two saprolitic soils". *Can. Geotech. J.*, vol. 25, pp. 500-510, 1996.

[36] A.W. Bishop and G.E. Blight, "Some aspects of effective stress in saturated and partly saturated soils", *Géotechnique*, vol. 13, pp. 177-197, 1963.

[37] M.M. Allan and A. Sridharan, "Effect of wetting and drying on shear strength", *J. Geotech. Engrng. Div*., vol. 107, pp. 421-438, 1981.

[38] T. Nishimura, Y. Hirabayashi, D.G. Fredlund and J. Gan, "Influence of stress history on the strength parameters of an unsaturated statically compacted soil", *Can Geotech. J*. vol. 36, 251-261, 1999.

[39] V. Sivakumar and S.J. Wheeler, "Influence of compaction procedure on the mechanical behavior of an unsaturated compacted clay (Part 1 and 2)", *Géotechnique*, vol. 50, pp. 359-376, 2000.

[40] G. Klubertanz, L. Laloui, L. Vulliet and P. Gachet, "Experimental validation of the hydromechanical modeling of unsaturated soils", Proceedings Workshop Chemo-mechanical coupling in clays, 2002, pp. 223-230.

[41] V. Mayagoitia, F. Rojas and I. Kornhauser, *J. Chem. Soc., Faraday Trans.*, vol. 84, pp. 785, 1988.

[42] V. Mayagoitia and I. Kornhauser, Fundamentals of adsorption IV, Suzuki M. ed., The engineering foundation, New York, USA, 1990.

[43] D.G. Fredlund and A. Xing, "Equations for the soil-water characteristic curve", *Can. Geotech.* J., vol. 31, pp. 521-532, 1994.

[44] P.H. Simms and E.K. Yanful, "Pore network modelling for unsaturated soils", in Proceedings the 56th Can. Geotech. Conf., Winnipeg, Canada, 2003, (Electronic proceedings).

[45] P.H. Simms and E.K. Yanful, "Measurement and estimation of pore shrinkage and pore distribution in a clayey till during soil-water characteristic curve tests". *Can Geotech. J.* vol. 38, pp. 741-754, 2001.

[46] P.H. Simms and E.K. Yanful, "A discussion of the application of mercury intrusion porosimetry for the investigation of soils, including an evaluation of its use to estimate volume change in compacted clays", *Géotechnique*, vol. 54, pp. 421-426, 2004.

[47] N.R. Morrow, "Physics and thermodynamics of capillary action in Porous media", *Ind. Eng. Chem.*, vol. 62, pp. 32, 1970.

[48] D.H. Everet, "The solid–gas interface", E. Edisson Flood, Dekker, New York, USA**,** vol. II; 1005-1010, 1967.

[49] R. P. Ray and K.B. Morris, "Automated laboratory testing for soils-water characteristic curves", in Proc. 1st Int. Conf. Unsat. Soils, Elsevier ed., Paris, France, vol. 1, pp. 547-552, 1995.

[50] P.A. Cundall and O.D.L. Strack, "The development of constitutive laws for soil using the Distinct Element Method, *Proceedings Int. Conf. Num. Meth. Geomech*., vol. 1, pp. 289-298, 1979.

[51] J.A. Gili and E.E. Alonso, "Microstructural deformation mechanisms of unsaturated granular soils", *Int. J. Num. Anal. Methods in Geomech*., vol. 26, pp. 1-36, 2002.

[52] E.E Alonso, E. Rojas and N.M. Pinyol, "Unsaturated soil mechanics", *Reunión Nacional de Mecánica de Suelos*, Aguascalientes, Mexico, Especial Volume, 117-205, 2008.

[53] G.A. Leonards, A. Alarcon, J.D. Frost, Y.E. Mohamedzein, J.C. Santamarina, S. Thevanayagam, J.E. Tomaz and J.E. Tyree, "Dynamic penetration resistance and the prediction of the compressibility of a fine-grained sand-A laboratory study" Discussion, Géotechnique, vol. 36, pp. 275-279, 1986.

[54] J. Horta, E. Rojas, M.L. Pérez, T. López-Lara and Hernández J.B, "A random porous model to simulate the retention curve of soils" *Int. J. Num. Anal. Meth. Geomech.*, 2012 DOI: 10.1002/nag.1133.

[55] F.A.L. Dullien, *Porous media, fluid transport and pore structure*, Academic Press, USA, 1992.

[56] D.W. Taylor, *Fundamentals of soil mechanics*, John Wiley ed., New York, USA, 1954.

[57] K. Collins and A. McGown, "The form and function of microfabric features in a variety of natural soils", *Géotechnique*, vol. 24, pp. 223-254, 1974.

[58] M. He, A. Szuchmacher, D.E. Aston, C. Buenviaje, R. Overney and R. Luginbuhl, "Critical phenomenon of water bridges in nanoasperity contacts" *J. Chem. Phys*., vol. 114, pp. 1355-1360, 2001.

[59] E. Rojas and F. Rojas, "Modeling hysteresis of the soil-water characteristic curve", *Soils and Foundations*, vol. 45, pp. 135-146, 2005.

[60] W.B. Haines, "Further contribution to the theory of capillary phenomena in soil", *J. Agric. Sci.* vol. 17, pp. 264-290, 1927.

[61] M.T. van Genuchten, "A closed form equation for predicting the hydraulic conductivity of unsaturated soils". *Soil Sci. Soc. Am. J.*, vol. 44, pp. 892-898, 1980.

[62] A.J. Brown, "The thermodynamics and hysteresis of adsorption", PhD thesis, University of Bristol, England, 1963.

[63] B.V. Enustun and M. Enuysal, "Determination of the Pore Size Distribution by Direct Methods", *Middle East Tech. Univ. J. Pure Applied Sci.*, vol. 3, pp. 81-88, 1970.

[64] G. Mason, "Determination of the Pore Size Distribution and Pore-Space Interconnectivity of Vycor Porous Glass from Adsorption-Desorption Hysteresis Capillary Condensation Isotherms", *Proc. of the Royal Society*, U.K., vol. A 415, pp. 453-486, 1988.

[65] D. Penumadu and J. Dean, "Compressibility effect in evaluating the pore-size distribution of kaolin clay using mercury intrusion porosimetry", *Can. Geotech. J.*, vol. 37, pp. 393-405, 2000.

[66] E. Romero, A. Gens and A. Lloret, "Water permeability, water retention and microstructure of unsaturated compacted Boom clay", *Engrng Geol.*, vol. 54, pp. 117-127, 1999.

[67] A.B. Abell, K.L. Willis and D.A. Lange, "Mercury intrusion porosimetry and image analysis of cement-based materials", *J. Colloid Interface Sci.*, vol. 211, pp. 39-44, 1999.

[68] S. Roels, J. Elsen, J. Cermeliet and H. Hens, "Characterization of pore structure by combining mercury porosimetry and micrography". *Materials and Structures*, vol. 34, pp. 76-82, 2001.

[69] A. Sawangsuriya, T.B. Edil and P.J. Bosscher, "Modulus-suction-moisture relationship for compacted soils in postcompaction state", *J. Geotech. Geoenviron. Engrng*, vol. 135, pp. 1390-1403, 2009.

[70] L.F. Vesga, "Equivalent effective stress and compressibility of unsaturated kaolinite clay subjected to drying", *J. Geotech. Geoenviron. Engrng*., vol. 134, pp. 366-378, 2008.

[71] D.G. Fredlund, A. Xing, M.D. Fredlund and S.L. Barbour, "The relationship of unsaturated soil shear strength to the soil–water characteristic curve", *Can. Geotech. J.*, vol. 33, pp. 440–448, 1996.

[72] M. Fredlund, D.W. Fredlund and G. Wilson, G., "Prediction of the soil-water characteristic curves from grain-size distribution and volume-mass properties", in Proc. Third Brazilian Symp. Unsat. Soils, Rio de Janeiro, Brazil, vol. 1, pp. 13-23, 1997.

[73] M. Aubertin, J.F. Richard and R.P. Chapuis, "A predictive model for the water retention curve: Applications to tailings from hard rock mines", *Can. Geotech. J.*, vol. 35, pp. 55-69, 1998.

[74] J.S.C. Mbagwu and C.N. Mbah, "Estimating water retention and availability in Nigerian soils from their saturation percentage", *Communications in Soil Science and Plant Analysis*, vol. 29, pp. 913-922, 1998.

[75] L.M. Arya and J.F. Paris, "Physicoempirical model to predict the soil moisture characteristic from particle-size distribution and bulk density", *Soil Sci. Soc. Am. J.*, vol. 45, pp. 1023-1030, 1981.

[76] L.M. Arya and T.S. Dierolf, "Predicting soil moisture characteristics from particle size distributions: an improved method to calculate pore radii from particle radii", *Proc. Int.*

Workshop Indirect Meth. Estim. Hydraulic Prop. Unsat. Soils, University of California, Riverside, pp. 115-124, 1992.

[77] A. Basile and G. D'Urso, "Experimental corrections of simplified methods for predicting water retention curves in clay-loamy soils from particle size determination" *Soil Technology*, vol. 10, 261-272, 1997.

[78] P.H. Simms and E.K. Yanful, "Predicting soil-water characteristic curves of compacted plastic soils from measured pore-size distributions", *Géotechnique*, vol. 52, pp. 269-278, 2002.

[79] P.H. Simms and E.K. Yanful, "A pore network model for hydromechanical coupling in unsaturated compacted clayey soils", *Can Geotech. J*., vol. 42, pp. 499-514, 2005

[80] G.P androutsopoulos and R. Mann, "Evaluation of mercury porosimeter experiments using a network pore structure model", *Chem. Engrng Sci.*, vol. 34, pp. 1203-1212, 1979.

[81] L.M. Zhang and X. Li, "Microporosity structure of coarse granular soils", *J. Geotech. Geoenviron. Engrng.*, vol. 136, pp. 1425-1436, 2010.

[82] J. Bear, "Hydraulic of Groundwater". McGraw-Hill, *Series of Water Resources and Environmental Eng*., 1979.

[83] S. Wheeler and V. Sivakumar, "An elasto-plastic critical state framework for unsaturated soils", *Géotechnique*, vol. 45, pp. 35-53, 1995.

[84] R. Thom, R. Sivakumar, V. Sivakumar, E.J. Murray and P. Mackinnon, "Pore size distribution of unsaturated compacted kaolin: the initial states and states following saturation", *Géotechnique*, vol. 57, pp. 469-474, 2007.

[85] J. Espitia, "Micromechanical model to reproduce the soil-water retention curve of soils", Master thesis, University of Queretaro, Mexico, 2005

[86] V. Sivakumar, "A critical state framework for unsaturated soils", PhD thesis, University of Sheffield, UK, 1993.

[87] E. Rojas, "An Equivalent stress equation for unsaturated soils, II: Porous-solid model", *Int. J. of Geomech.*, vol. 8, pp. 291-299, 2008.

[88] A. Koliji, L. Laloui, O. Cusinier and L. Vulliet, "Suction induced effects on the fabric of a structured soil", *Transport in Porous Media*, vol. 64, pp. 261-278, 2006.

[89] L.F. Vesga and L.E. Vallejo, "Direct and indirect tensile tests for measuring the equivalent effective stress in a kaolinite clay", in Proceedings Fourth Int. Conf. Unsat. Soils, Arizona, USA, vol. 1, pp. 1290-13, 2006.

[90] J. Vaunat, E. Romero and C. Jommi, "An elastoplastic hydromechanical model for unsaturated soils". *Experimental Evidence and Theoretical Approaches in Unsaturated Soils*, Balkema Rotterdam, 121-138, 2000.

[91] D.A. Sun, H.B. Cui, H. Matsuoka and D. Sheng, "A three-dimensional elastoplastic model for unsaturated compacted soils with hydraulic hysteresis". *Soils and Found.* Vol. 47, pp. 253-264, 2007.

[92] M.M. Futai and S.S. Almeida, "An experimental investigation of the mechanical behavior of an unsaturated gneiss residual soil", *Géotechnique,* vol. 55, pp. 201-213, 2005.

[93] J.M. Fleureau, S. Kheirbek-Saoud, R. Soemitro and S. Taibi, "Behavior of clayey soils on drying-wetting paths", *Can. Geotech. J.*, vol. 30, pp. 287-296, 1993.

[94] D. Sheng, "Review of fundamental principles in modeling unsaturated soil behavior". *Computers and Geotechnics,* vol. 38, pp. 757-776, 2011.

[95] T.M. Thu, H. Rahardjo and E.-C. Leong, "Elastoplastic model for unsaturated soil with incorporation of the soil-water characteristic curve", *Can. Geotech. J.*, vol. 44, pp. 67-77, 2007.

[96] Y. Khogo, M. Nikano and T. Miyazaky, "Theoretical aspects of constitutive modeling for unsaturated soils", *Soils & Foundations*, **33**: 49-63, 1993.

[97] B. Loret and N. Khalili, "A three phase model for unsaturated soils". *Int. J. Num. Anal. Methods Geomech.*, vol. 24, pp. 893-927, 2000.

[98] R. Kholer and G. Hofstetter, "A cap model for partially saturated soils", *Int. J. Num. Anal. Meth. Geomech.*, vol. 32, pp. 981-1004, 2008.

[99] A. Koliji, L. Laloui and L. Vulliet, "Constitutive modeling of unsaturated aggregated soils", *Int. J. Num. Anal. Meth. Geomech*., vol. 34, pp. 1846-1876, 2010.

[100] D. Sheng, D.G. Fredlund and A. Gens, "A new modelling approach for unsaturated soils using independent stress variables", *Can. Geotech. J.*, vol. 45, pp. 511-534, 2008.

[101] D. Sun, D. Sheng and Y. Xu, "Collapse behavior of unsaturated compacted soil with different initial densities", *Can. Geotech. J.*, vol. 44, pp. 673-686, 2007.

[102] R.I. Borja. Cam clay plasticity, Part V: "A mathematical framework for three phase deformation and strain localization analysis of partially saturated porous media", *Computer Methods in Applied Mechanical Engineering*, vol. 193, pp. 5301-5338, 2002.

[103] L.R. Hoyos and P. Arduino, "Implicit algorithms in modeling unsaturated soil response in three-invariant stress space" *Int. J. Geomech.*, vol. 8, pp. 266-273, 2008.

[104] H.W. Zhang and L. Zhou, "Implicit integration of chemo-plastic constitutive model for partially saturated soils", *Int. J. Num. Anal. Meth. Geomech.*, vol. 32, pp. 1715-1735, 2008.

[105] E. Juárez-Badillo, "Constitutive relationships for soils", in Proceedings of the Symposium on Recent Developments in the Analysis of Soil Behavior and their Application to Geotechnical Structures, University of New South Wales, NSW, Australia, pp. 231-257, 1975.

[106] R. Butterfield, "A natural compression law for soils (an advance on e-log p')", *Géotechnique*, vol. 29, pp. 469-480, 1979.

[107] D. Sheng, Y. Yao and J.P. Carter, "A volume-stress model for sands under isotropic and critical stress states", *Canadian Geotechnical Journal*, vol. 45, pp. 1639-1645, 2008.

[108] J.A. Infante Sedano and S.K. Vanapalli, "The relationship between the critical state shear strength of unsaturated soils and the soil-water characteristic curve", in Proceedings of the Fifth International Conference on Unsaturated Soils, Barcelona, Spain, vol. 1, pp. 253-258, 2010.

[109] E. Romero, A. Gens and A. Lloret, "Suction effects on a compacted clay under non-isothermal conditions", *Géotechnique*, vol. 53, pp. 65-81, 2003.

[110] M.R. Cunningham, A.M. Ridley, K. Dineen and J.B. Burland, "The mechanical behavior of a reconstituted unsaturated silty clay", *Géotechnique*, vol. 53, pp. 183-194, 2003.

[111] N. Khalili, F. Geiser and G.E. Bligth, "Effective stress in unsaturated soils: review with new evidence", *Int. J. Geomech.*, vol. 4, pp.115-126, 2004.

[112] I. Vlahinic, H.M. Jennings and J.J. Thomas, "A constitutive model for drying of partially saturated porous materials", *Mech. Mat.,* vol. 41, pp. 319-328, 2009.

[113] G.E. Blight, "Shrinkage during wetting of fined-pored materials. Does this accord with the principle of effective stress?", in Proceedings of the fifth International Conference on Unsaturated Soils, vol. 1, pp. 205-209, 2010.

[114] A. Pereira, C. Feuerharmel, W.Y.Y. Gheling and A.V.D. Bica, "A study on the shear strength envelope of an unsaturated colluviums soil", in Proceedings of the Fourth International Conference on Unsaturated Soils, Arizona, USA, vol. 1, pp. 1191-1199, 2006.

[115] D. Sheng, A. Zhou and D.G. Fredlund, "Shear strength criteria for unsaturated soils", *Geotech. Geol. Engrng*, vol. 29, pp. 145-159, 2009.
[116] D.G. Toll and B.H. Ong, "Critical state parameters for an unsaturated residual sandy clay", *Géotechnique*, vol. 53, pp. 93–103, 2005.
[117] J.C.B. Benatti, M.G. Miguel, R.A. Rodriguez and O.M. Vilar, "Collapsibility study for tropical soil profile using oedometric tests with controlled suction", In Proceedings of the fift*h* International Conference on Unsaturated Soils, Barcelona, Spain, 2010, vol. **1,** pp. 193-198.
[118] G. Bolzon B.A. Schrefler and O.C. Zienkiewics, "Elastoplastic soil constitutive laws generalized to partially saturated states", *Géotechnique* vol. 46, pp. 279-289, 1996.
[119] D. Karube and K. Kawai, "The role of pore water in the mechanical behavior of unsaturated soils", *Geotech. Geol. Engrng*., vol. 19, pp. 211-241, 2001.
[120] E.E. Alonso, J.-M. Pereira, J. Vaunat and S. Olivella, "A microstructurally based effective stress for unsaturated soils", *Géotechnique*, vol. 60, pp. 913-925, 2010.
[121] G. Della Vechia, C. Jommi and E. Romero, "A fully coupled elastic-plastic hydromechanical model for compacted soils accounting for clay activity", *Int. J. Num. Anal. Meth. Geomech.*, vol. 37, pp. 503-535, 2012.
[122] D.A. Sun, D. C. Sheng, H.B. Cui and S.W. Sloan, "A density-dependent elastoplastic hydro-mechanical model for unsaturated compacted soils", *Int. J. Num. Anal. Meth. Geomech.*, vol. 31, pp. 1257-1279, 2007.
[123] R.A. Rodrigues and O.M. Volar, "Experimental study of the collapsible behavior of a tropical unsaturated soil", in Proceedings 5th Int. Conf. Unsat. Soils, Barcelona, Spain, vol. 1, pp. 353-357, 2010.
[124] Q. Wang, D.E. Pufahl and D.G. Fredlund, "A study of critical state on an unsaturated silty soil", *Can. Geotech. J.,* vol. 39, pp. 213-218, 2002.
[125] T. M. Thu, H. Rahardjo and E.-C. Leong, "Soil-water characteristic curve and consolidation behavior for a compacted silt", *Can. Geotech. J.*, vol. 44, pp. 266-275, 2007.
[126] M. Nuth and L. Laloui, "Effective stress concept in unsaturated soil: Clarification and validation of a unified framework", *Int. J. Num. Anal. Meth. Geomech.*, vol. 32, pp. 771-801, 2008.

BIBLIOGRAPHY

THIS EBOOK HAS BEEN PREPARED USING MATERIAL FROM THE FOLLOWING PUBLICATIONS

E. Rojas and F. Rojas, "Modeling hysteresis of the soil-water characteristic curve", *Soils and Foundations*, vol. 45, pp. 135-146, 2005. With permission from Elsevier.

E.E. Alonso, E. Rojas, and N.M. Pinyol, "Unsaturated soil mechanics", *Reunión Nacional de Mecánica de Suelos*, Aguascalientes, Mexico, Especial Volume, pp. 117-205, 2008. With permission from Sociedad Mexicana de Ingeniería Geotécnica.

E. Rojas, "Equivalent stress equation for unsaturated soils, I: Equivalent stress", *International Journal of Geomechanics*, vol. 8, pp. 285-290, 2008. With permission from ASCE.

E. Rojas, "Equivalent stress equation for unsaturated soils, II: Porous-solid model", *International Journal of Geomechanics*, vol. 8, pp. 291-299, 2008. With permission from ASCE.

E. Rojas., J. Horta, T. López-Lara and J.B. Hernández, "A probabilistic porous-solid model to determine the shear strength of unsaturated soils", *Probabilistic Engineering Mechanics*, Elsevier, vol. 26, pp. 481-491, 2011. With permission from Elsevier.

E. Rojas, A. Zepeda, M.L.Pérez-Rea, J. Leal and F. Gallegos, "A four elements porous model to estimate the strength of unsaturated soils", *Geotechnical and Geological Engineering*, vol. 29, pp. 193-202, 2011. With permission from Springer Science.

E. Rojas, D. Hurtado, A. Zepeda and M.L. Pérez-Rea, "Modeling the tensile strength of Soils", in Proceedings 5th Int. Conf. Unsat. Soils, Barcelona, Spain, vol. 2, pp. 933-938, 2010. © Taylor and Francis Group. London, UK. Used with permission.

E. Rojas, G. Gallegos and J. Leal, "A porous model based on porosimetry to simulate retention curves", in Proceedings 5th Int. Conf. Unsat. Soils, Barcelona, Spain, vol. 2, pp. 927-932, 2010. © Taylor and Francis Group. London, UK. Used with permission.

J. Horta, E. Rojas, M.L. Pérez-Rea., T. López-Lara and J.B. Hernández, "A random porous model to simulate the retention curve of soils" *International Journal of Numerical and Analytical Methods in Geomechanics*, vol. 37, pp. 932-944, 2012, With permission from John Wiley and Sons.

E. Rojas, J. Horta, T. López-Lara and J.B. Hernández, "A porous-solid model to simulate the retention curves of soils", *Journal of Geotechnical and Geoenvironmental Engineering,* vol. 139, pp. 320-329, 2013. With permission from ASCE.

E. Rojas and O. Chávez, "Volumetric behavior of unsaturated soils", *Canadian Journal of Geomechanics*, vol. 50, pp. 209-222, 2013. Reproduced with permission © 2013 Canadian Science Publishing or it licensors.

GLOSSARY

A = total area of a cross section of an unsaturated soil

A_a = total area of the cross section where air reacts

A_w = total area of the cross section where water reacts

$A_{\tilde{s}}$ = total area of the cross section where solids react

A^s = area of the saturated fraction

A^u = area of the unsaturated fraction

A_a^u = area of the unsaturated fraction where air reacts

$A_{\tilde{s}}^s$ = area of solids of the saturated fraction

$A_{\tilde{s}}^u$ = area of solids of the unsaturated fraction

$A_{\tilde{s}a}^u$ = horizontal projection of the peripheral area of solids in contact with air in the unsaturated fraction

$A_{\tilde{s}w}^{\tilde{s}}$ = horizontal projection of the peripheral area of solids subject to water pressure in the saturated fraction

$A_{\tilde{s}w}^u$ = horizontal projection of the peripheral area of solids in contact with water in the unsaturated fraction

A_v^u = area of voids in the unsaturated fraction

A_w^s = area of the saturated fraction where water reacts

A_w^u = area of the unsaturated fraction where water reacts

a = contact area between solid particles per unit area of material

$B(R_C)$ = probability function of the relative volume of bonds

Eduardo Rojas

$B_A(R_C)$ = adjusted probability function for bonds

C = connectivity (number of bonds converging at one site)

C_c = cluster coefficient

C_e = compressibility of the solid structure of the soil

$C_{\tilde{s}}$ = compressibility of the solid material comprising the particles

C_{SB} = fraction of sites and bonds in closed clusters

c = soil cohesion

D = diameter of a spherical particle

D_e = equivalent diameter of clay particles

d = diameter of a pore

e = void ratio

f^d = dry soil fraction

f^s = saturated soil fraction

f^u = unsaturated soil fraction

F_{BD}^s = saturation factor for bonds during drying

F_{BI}^s = saturation factor for bonds during wetting

F_{BID}^s = saturated wetting factor for bonds after a drying inversion

F_{SD}^s = saturated darying factor

F_{SDI}^s = saturated wetting factor for sites after a drying inversion

F_{SD}^d = dry factor for cavities in the solid unit during a drying process

F_{SI}^{S} = saturation factor for cavities during wetting

F_{SID}^{S} = drying saturation factor for cavities after drying inversion

G_{BDR} = bonds invaded by gas at the end of a drying inversion

G_{BD_1} = probability of an external bond to be filled with gas during drying

G_{BI} = probability of the bond to be filled with gas

G_{PD} = probability of a solid to be surrounded exclusively by pores filled with gas during drying

G_{PI} = probability of a solid to be surrounded exclusively by pores filled with gas during wetting

G_{SDR} = sites invaded by gas at the end of a drying inversion

G_{SI} = probability of a cavity to be filled with gas

k = parameter related to the effective stress for saturated soils

L_{BD} = probability of a bond to be liquid-filled

L_{BDR} = probability of a bond to be liquid-filled at the moment of a drying inversion

L_{BDI} = probability of a bond to be liquid-filled after an inversion in drying

L_{BD_1} = probability of an external bond to be filled with liquid

L_{BI} = probability of a bond to saturate during a wetting process

L_{BID} = probability of a bond to be liquid-filled at drying after a wetting inversion

L_{BIR} = probability of a bond to be liquid-filled at the moment of a wetting inversion

L_{BI_1} = probability of an external bond to be saturated

L_{SD} = probability of a cavity to saturated during a drying process

L_{SDI} = probability of a cavity to be liquid-filled after an inversion in drying

L_{SDR} = probability of a site to be liquid-filled at the moment an inversion in drying

L_{SD_1} = probability of surrounding sites to be liquid filled during a drying process

L_{SI} = probability of a cavity to saturate during a wetting process

L_{SID} = probability of a site to be liquid-filled at drying after a wetting inversion

L_{SIR} = probability of a site to be liquid-filled at the moment of a wetting inversion

L_{SI_1} = probability of a surrounding site to be liquid filled

$L_{\tilde{s}D}$ = probability that all pores surrounding a solid are saturated during a drying process

$L_{\tilde{s}I}$ = probability that all pores surrounding a solid are saturated during a wetting process

n = soil porosity

P_{vf} = Proportional volume factor

$\overline{p}$ = mean net stress

p' = mean effective stress

p = mean total stress

P_{atm} = atmospheric pressure

q = deviator stress

$\overline{R}$ = mean size

$\overline{R}_B$ = mean size for bonds

R_c = critical radius or maximum size of a pore to be filled with water at certain suction

$\overline{R}_S$ = mean size for sites

r_B = radius of a bond

$r_{\tilde{s}}^s$ = ratio of the volume of saturated solids to the total volume of solids

r_v^s = ratio of the volume of saturated voids to the total volume of voids

r_S = radius of a site

$S(R_C)$ = probability function of the relative volume of cavities

$S_A(R_C)$ = adjusted probability function for sites

S_f = shape factor for the solid particles

S_w = degree of saturation

S_{we} = effective degree of saturation

$S_{wD}(R_C)$ = degree of saturation at drying

$S_{wI}(R_C)$ = degree of saturation at wetting

S_w^u = degree of saturation of the unsaturated fraction

s = soil suction

s_m = suction in a pore filled with mercury

s_w = suction in a pore filled with water

T_s = liquid-gas interfacial tension

T_{sm} = superficial tension for mercury

T_{sw} = superficial tension for water

u = pore pressure for saturated soils

u_a = air pressure

u_w = water pressure

V = total volume of a portion of soil

V_a = air volume

V_B = volume of bonds

V_{BI}^s = volume of saturated bonds during wetting

V_{BID}^s = volume of saturated bonds during drying after a wetting inversion

V_{BR} = volume of all bonds of size R

V_B^d = voluem of bonds of the dry fraction

V_B^s = volume of saturated bonds

$V_{\tilde{s}}$ = volume of solids

$V_{\tilde{s}}^d$ = volume of solids of the dry fraction

V_S = volume of cavities

V_S^d = volume of cavities of the dry fraction

V_S^S = volume of saturated cavities

V_{SI}^S = volume of saturated cavities during a wetting process

V_{SID}^S = volume of saturated sites during drying after a wetting inversion

$V_{SR}(R)$ = volume of all sites of size R

V_B^d = volume of dry bonds

$V_{BD}^S(R_C)$ = volume of saturated bonds during drying

$V_{BDI}^S(R_C)$ = volume of saturated bonds at wetting after a drying inversion

$V_{BI}^S(R_C)$ = volume od saturated bonds at wetting

$V_{BR}(R)$ = volume of bonds of size R

$V_{\tilde{s}I}^S$ = volume of saturated solids

$V_{RB}(R)$ = relative volume of bonds of size R

$V_{RS}(R)$ = relative volume of cavities of size R

$V_{SR}(R)$ = volume of all sites of size R

$V_{SD}^S(R_C)$ = volume of saturated sites at drying

$V_{SDI}^S(R_C)$ = volume of saturated sites at the end of a drying inversion

$V_{SI}^S(R_C)$ = volume of saturated cavities during wetting

V_v = volume of voids of the soil sample

V_w = water volume

V^s = volume of the saturated fraction of the sample

V^u = volume of the unsaturated fraction of the sample

V_a^u = volume of air of the unsaturated fraction

$V_{\tilde{s}}^s$ = volume of solids of the saturated fraction

$V_{\tilde{s}}^u$ = volume of solids of the unsaturated fraction

$V_{\tilde{s}a}^u$ = volume of solids influenced by the pressure of air in the unsaturated fraction

$V_{\tilde{s}w}^u$ = volume of solids influenced by the pressure of water in the unsaturated fraction

V_v^s = volume of voids of the saturated fraction

V_v^u = volume of voids of the unsaturated fraction

V_w^s = volume of water of the saturated fraction

V_w^u = water volume of the unsaturated fraction

v = specific volume

χ = Bishop's effective stress parameter

δ_{ij} = Kronecker's delta $\left(\delta_{ij}=1, i=j;\ \delta_{ij}=0, i\neq j\right)$

θ_m = contact angles of mercury with the minerals of soil

θ_w = contact angles of water with the minerals of soil

κ = fitting parameter

σ = total stress

δ = standard deviation

δ_B = standard deviation for bonds

δ_S = standard deviation for sites

σ' = effective stress

σ_s^* = matric suction stress

σ_i = principal total stress in direction *i*

σ_i' = principal effective stress in direction *i*

σ_{ij} = total stress tensor

σ_{ij}' = effective stress tensor

$\overline{\sigma}$ = net stress

τ = shear stress internal friction angle

ψ = friction angle of the material comprising the solid particles

SUMMARY

When Karl von Terzaghi applied the effective stress principle in the soil mechanics theory, the strength and volumetric behavior of saturated soils could be clearly understood and general constitutive models for these materials could be developed. This eBook shows that the principle of effective stress can also be applied to unsaturated soils and that the same equations used to determine the strength and volumetric behavior of saturated soils can be applied to unsaturated materials. These developments open the door for general constitutive models that include saturated, unsaturated and even compacted materials leading to a unified soil mechanics theory.

Eduardo Rojas

INDEX

Eduardo Rojas